

SUBJ
MNG
TBFI

SOCIETY OF MINING ENGINEERS of AIME

540 ARAPEEN DRIVE — SALT LAKE CITY, UTAH 84108

PREPRINT
NUMBER

78-AS-112



UNIVERSITY OF UTAH
RESEARCH INSTITUTE
EARTH SCIENCE LAB.

A TEST BLAST FOR IN SITU COPPER LEACHING

Dennis V. D'Andrea
Geophysicist

Peter G. Chamberlain
Geophysicist

Jon K. Ahlness
Mining Engineer

Bureau of Mines
U. S. Department of the Interior
Minneapolis, Minnesota

For presentation at the 1978 AIME Annual Meeting
Denver, Colorado - February 28 - March 2, 1978

Permission is hereby given to publish with appropriate acknowledgments, excerpts or summaries not to exceed one-fourth of the entire text of the paper. Permission to print in more extended form subsequent to publication by the Institute must be obtained from the Executive Secretary of the Society of Mining Engineers of AIME.

If and when this paper is published by the Society of Mining Engineers of AIME, it may embody certain changes made by agreement between the Technical Publications Committee and the author, so that the form in which it appears here is not necessarily that in which it may be published later.

These preprints are available for sale. Mail orders to PREPRINTS, Society of Mining Engineers, 540 Arapeen Drive, Box 8800, Salt Lake City, Utah 84108.

PREPRINT AVAILABILITY LIST IS PUBLISHED PERIODICALLY IN
MINING ENGINEERING.

Abstract The Bureau of Mines and Cyprus Mines Corp. conducted a cooperative research program to investigate the in situ leaching potential of copper ore along the fringes of the open pit Johnson mine near Willcox, Ariz. A test blast was detonated in August 1977 to evaluate blast design, solution flow rate, and solution containment. Thirteen 9-7/8-inch-diameter blastholes were spaced 14 feet apart and drilled to depths ranging from 185 to 224 feet. A total of 51,500 pounds of ANFO was detonated with an average of 56 feet of stemming in each hole. Core drilling, permeability testing, and water circulation tests were used to evaluate the results of the blast.

Introduction

The Johnson mine, located 17 miles west of Willcox, Ariz., is operated by Cyprus Johnson Copper Co., a division of Cyprus Mines Corp. This oxide copper deposit is mined by open pit-heap leach methods, and the leach solutions are created by solvent extraction and electrowinning. About 4,000 tons of ore are mined to produce 25,000 to 30,000 pounds of cathode copper each day. The grade of the deposit averages about 0.5 pct acid-soluble copper.

The projected life of this mine is about another 8 years depending on mining costs and the price of copper. In situ leaching is being considered by Cyprus in combination with heap leaching or as a final phase for this operation. The Bureau of Mines entered into a cooperative agreement with Cyprus in June 1976 to investigate the in situ leaching potential of ore along the fringes and beyond the proposed final limits of the open pit. Research on this problem is of general interest to the mining industry, and the results can be applied to other similar mining operations.

A program of core drilling and permeability testing was begun to establish the initial characteristics of the ore. The ore being considered for in situ leaching at the Johnson mine is above the water table, which is located about 600 feet below the surface. In-place testing showed that permeabilities ranged from 50 to less than 10 millidarcys (md) as one proceeded away from the pit in the down-dip direction. These permeability values indicated that blasting would be required for successful leaching and that solution containment should not be a problem.

A test blast, based on previous Bureau research (1, 2, 3, 4, 5), was designed to fracture an area for water circulation tests and hopefully a pilot in situ leaching test. This paper presents the details of the August 1977 blast and the preliminary evaluation of the blast results.

Johnson Mine Deposit

A cross section through the Johnson mine deposit looking northwest is shown in figure 1. The present pit, along with the proposed final pit limits, is shown. The test blast area was 56 feet below the surface and extended from 185 to 224 feet deep. The metashale ore is in the lower member of the Abrigo formation and is underlain by the Bolsa quartzite. The principal copper mineral in the lower Abrigo is chrysocolla

with minor amounts of malachite and azurite. The impervious Bolsa quartzite is about 150 feet thick in the area. The Johnson mine operation has been previously described (6).

The physical properties of the Johnson mine ore as determined from laboratory tests on drill core samples are listed in table 1. The rock has very low tensile strength (24 psi), a porosity of 11 pct, and permeability of 1.7 md. Field permeabilities were higher, ranging from 5 to 50 md, because of fluid flow through natural fractures which are not present in laboratory test specimens.

Test Blast

Figure 2 shows the test blast design. Thirteen 9-7/8-inch-diameter blastholes were spaced 14 feet apart in an equilateral triangle pattern. The pattern was elongated in the down-dip direction, and the blasthole depths varied with the deepest blastholes on the northeast end. The pattern was elongated because it was felt that solutions would tend to flow along bedding plane fractures and migrate down dip. Blasthole depths ranged from 185 to 224 feet, and a constant stemming height of 56 feet was maintained. Blastholes were drilled with an air-flushed rotary system. Six of the blastholes were surveyed for deviation, and the maximum hole deviation was only 3 feet. A total of 51,500 pounds of ANFO was loaded into the 13 blastholes. The blast was delayed as shown in figure 2 with 18-millisecond (msec) (two 9-msec) detonating cord delays between each row. The blast was bottom-primed with two 0.4-pound cast primers, for protection against cutoffs, two cast primers were placed at the top of the powder column with an 18-msec delay to the top primer. A summary of the test blast data is listed in table 2. A powder factor of 2.2 lb/ton (for ore in the powder column zone only) fractured about 19,700 tons of ore, assuming a 4-foot overbreak. Ore in the stemming region was not included in the 19,700-ton estimate. The powder factor was higher than that normally used in bench blasting but was considered necessary to break ore in a confined situation.

Blast Results

Topographic surveys were run before and after blasting to determine elevation increases on the surface (figure 3). The surface rose over a broad area with significant displacement along a north-south-trending fault. Because of the unusual geometry of this blast and resulting surface rise, no attempt was made to calculate a swell factor. However, a volume increase at the surface of 1,500 yd³ was produced.

The core and permeability test holes are shown in figure 4. The core holes were drilled with water only and no drilling mud to minimize plugging of the formation. Table 3 lists the data for the preshot and postshot core holes. The postshot core was very highly fractured with only 23 pct of the core recovered and an RQD of 2 pct. Most of the core recovered after the shot came from the stemming region or in the area below the blast. Figure 5 shows core

recovery versus depth for the two core holes. The powder column region is very obvious from the postshot core hole recovery.

Constant-head permeability tests (7) run before and after blasting are listed in table 4. These permeability test holes are shown in figure 4. Preshot permeabilities ranged from 15 to 43 md, while postshot values ranged from 180 to 8,500 md. The postshot permeability values are considered adequate for successful leaching.

Blast vibration data recorded for six production blasts in the pit and the test blast are listed in table 5. Blast vibrations were recorded with a portable three-component seismograph. Figure 6 shows peak particle velocity versus scaled distance for the data listed in table 5. Vibrations from the test blast were higher than vibrations from pit production blasts at similar scale distances but were generally within the scatter of the production blast data. The test blast produced vibration levels of 2.0 to 4.0 in/sec at mine surface facilities such as the truck shop, office, and solvent extraction and electrowinning plant. These levels were not high enough to cause any damage to surface facilities.

Initial water circulation tests were run by injecting water into holes IH-1 and IH-2 and by monitoring the water in IH-3 (figure 4). During this test 300,000 gal of water was injected at 35 gpm in an attempt to fill the bottom of the fractured zone. However, very little water was observed in the 224-foot-deep IH-3 hole. The water may be escaping from the fractured zone along the Bolsa quartzite contact, or the IH-3 hole may not be deep enough and insufficient water was injected to fill all the void spaces created at the bottom of the fracture zone. Further testing may involve deepening the observation hole; if that fails, a program of grouting along the ore-quartzite contact will be considered.

Conclusions

The test blast at the Johnson mine was considered a success in terms of fracturing the ore body and creating permeability for in-place leaching. Blast vibration levels were not high enough to damage surface mine facilities or cause annoyance to neighbors. The major problem with this test blast in ore above the water table is ensured solution containment. Preliminary water circulation tests did not build up significant water levels at the bottom of the fractured zone. A deeper recovery well hole and a grouting program are being considered.

References

1. D'Andrea, D. V., R. A. Dick, R. C. Steckley, and W. C. Larson. A Fragmentation Experiment for In Situ Extraction. Proc. Solution Mining Symposium, 103d Ann. Meeting, AIME, Dallas, Tex., Feb. 25-27, 1974 (ed. by F. F. Aplan, W. A. McKinney, and A. D. Pernicchia). American Institute of Mining, Metallurgical, and Petroleum Engineers, Inc., New York, 1974, pp. 148-161.
2. D'Andrea, D. V., W. C. Larson, P. G. Chamberlain, and J. J. Olson. Some Considerations in the Design of Blasts for In Situ Copper Leaching. Proc. 17th U.S. Symposium on Rock Mechanics, Snowbird, Utah, Aug. 25-27, 1976 (pub. as Site Characterization, compiled by W. S. Brown, S. J. Green, and W. A. Hustrulid). Utah Engineering Experiment Station, University of Utah, Salt Lake City, Utah, 1976, pp. 5B1-1 to 5B1-4. Also published in Monograph 1 on Rock Mechanics Applications in Mining (ed. by W. S. Brown, S. J. Green, and W. A. Hustrulid), SME of AIME, New York, 1977, ch. 24, pp. 201-204.
3. D'Andrea, D. V., W. C. Larson, L. R. Fletcher, P. G. Chamberlain, and W. H. Engelmann. In Situ Leaching Research in a Copper Deposit at the Emerald Isle Mine. BuMines RI 8236, 1977, 43 pp.
4. D'Andrea, D. V., and S. M. Runke. In Situ Copper Leaching Research at the Emerald Isle Mine. Proc. Joint MMIJ-AIME Meeting, Denver, Colo., Sept. 1-3, 1976 (pub. as World Mining and Metals Technology, ed. by A. Weiss). American Institute of Mining, Metallurgical and Petroleum Engineers, New York, 1976, v. 1, pp. 409-419.
5. Steckley, R. C., W. C. Larson, and D. V. D'Andrea. Blasting Tests in a Porphyry Copper Deposit in Preparation for In Situ Extraction. BuMines RI 8070, 1975, 47 pp.
6. Argall, G. O., Jr. Copper Oxide to Copper Cathode--New Cyprus Johnson Operation. World Mining, August 1976, pp. 48-51.
7. O'Rourke, J. E., R. J. Essex, and B. K. Ranson. Field Permeability Test Methods With Applications to Solution Mining. Woodward-Clyde Consultants (San Francisco, Calif.), Final Report for BuMines Contract J0265045, July 1977, 180 pp.; BuMines Open File Report 136-77, available for consultation at the Bureau of Mines libraries in Minneapolis, Minn., and Denver, Colo.; at the Central Library, U.S. Department of Interior, Washington, D.C.; and from National Technical Information Service, Springfield, Va., PB 272 452/AS.

TABLE 1. - Physical properties of Johnson mine ore

Property	Value	number of tests
Compressive strength, psi	2,800	12
Tensile strength, psi	24	10
Young's modulus, psi x 10 ⁵	8.9	12
Specific gravity	2.34	22
Density, tons/yd ³	1.97	—
Porosity, pct	11.4	12
Permeability, md	1.7	11
Sonic velocity, ft/sec	12,000	—

TABLE 2. - Test blast summary

Quantity	Value
Number of blastholes	13
Blasthole diameter, in	9-7/8
Blasthole spacing, ft	14
Range of blasthole depths, ft	185 to 224
Average blasthole depth, ft	209
Average subdrilling, ft	7
Total drilling, ft	2,717
Explosive	ANFO
Average powder column depth, ft	202
Average stemming, ft	56
Average powder column length, ft	146
Average explosive/hole, lb	3,960
Average loading density, lb/ft	27.2
Total explosive, lb	51,500
Powder factor, lb	2.2
Assumed overbreak, ft	4
Ore volume, yd ³	9,850
Ore weight, tons	19,700

TABLE 3. - Drill core data

Quantity	Value	
	Preshot	Postshot
Total recovery, pct	87	23
Recovery > 1 in, pct	79	10
RQD, pct	51	2
Average size > 1 in, in	4.1	2.3
50 pct passing, in	3.9	< 0.5

TABLE 4. - Constant head permeability measurements
test blast area

Location	Description	Permeability, md
PRESHOT		
CH-1	NX core hole	15
BH-9	9-7/8-in blasthole	43
BH-7	9-7/8-in blasthole	35
POSTSHOT		
IH-1	60 ft deep, 6-3/4-in air rotary, up dip	8,500
IH-2	188 ft deep, 6-3/4-in air rotary, up dip	1,500
IH-3	244 ft deep, 6-3/4-in air rotary, down dip	180

TABLE 5. - Blast vibration data

Shot	Date	Distance, ft	Charge weight total, lb	Charge weight per delay, lb	Scaled distance, ft/lb ^{1/2}	Peak particle velocity, in/sec
1	05-24-77	1,270	6,850	6,850	15.3	1.4
2	05-26-77	1,450	10,750	5,400	19.7	.6
3	05-31-77	490	15,500	6,825	5.9	2.4
4	08-12-77	850	15,500	3,750	13.9	1.0
5	08-16-77	420	6,900	6,900	5.1	2.2
6	08-17-77	1,850	4,850	2,425	37.6	.28
Test blast	08-18-77	780	51,500	19,950	5.5	4.7

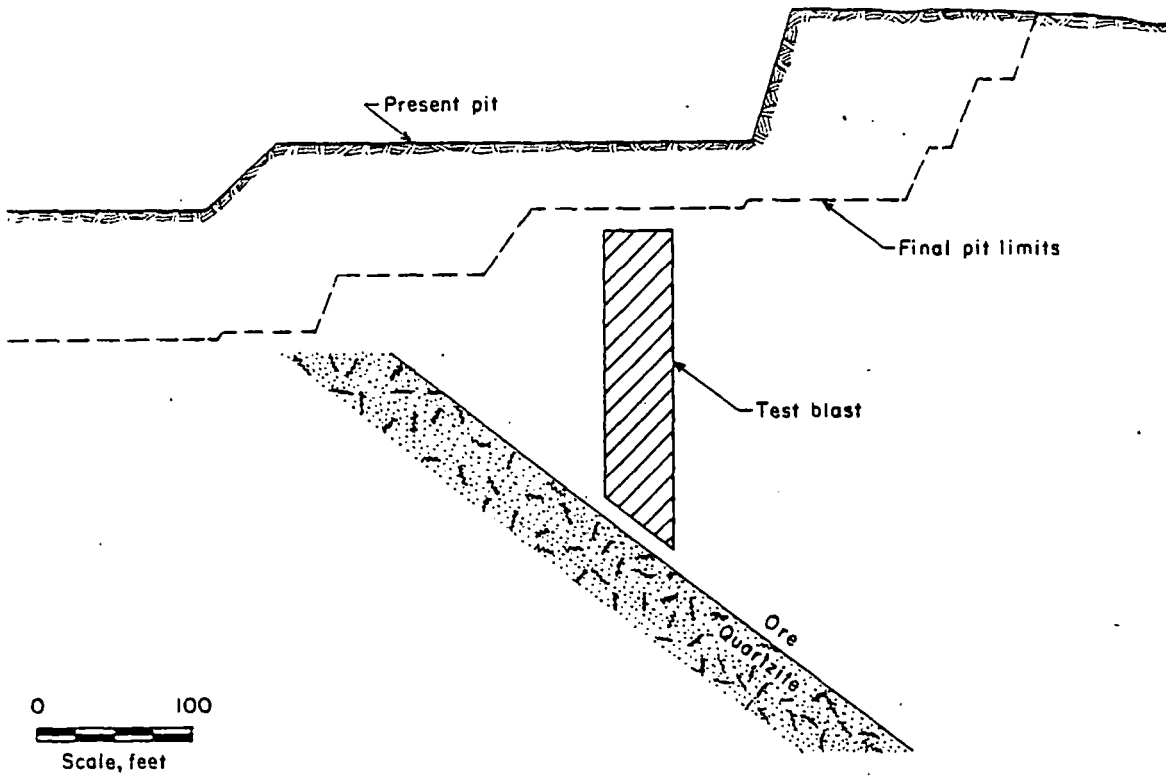


FIGURE 1. - Cross section of Johnson mine deposit looking northwest.

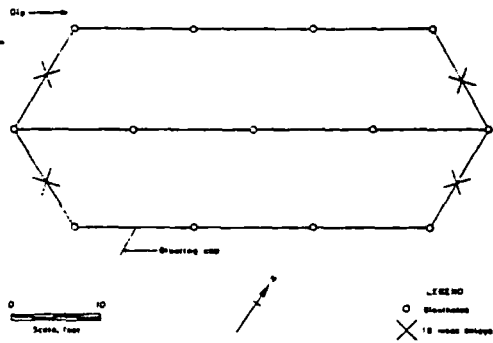


FIGURE 2. - Test blast design.

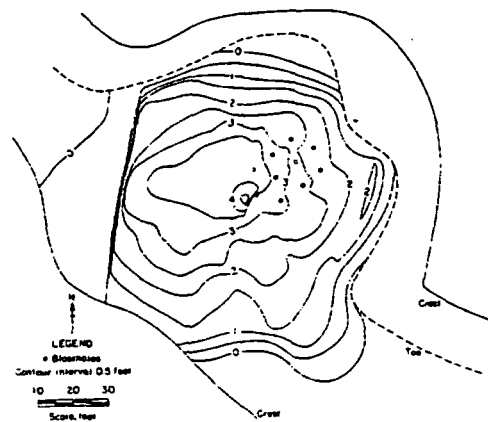


FIGURE 3. - Elevation increases after blasting.

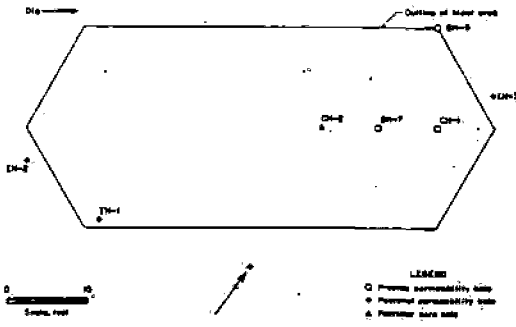


FIGURE 4. - Core hole and permeability test hole locations.

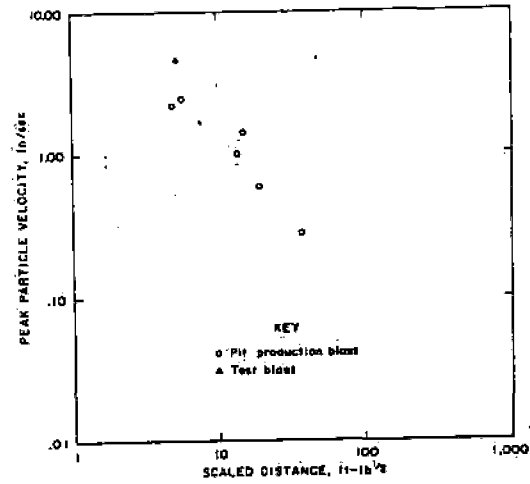


FIGURE 6. - Peak particle velocity versus scaled distance.

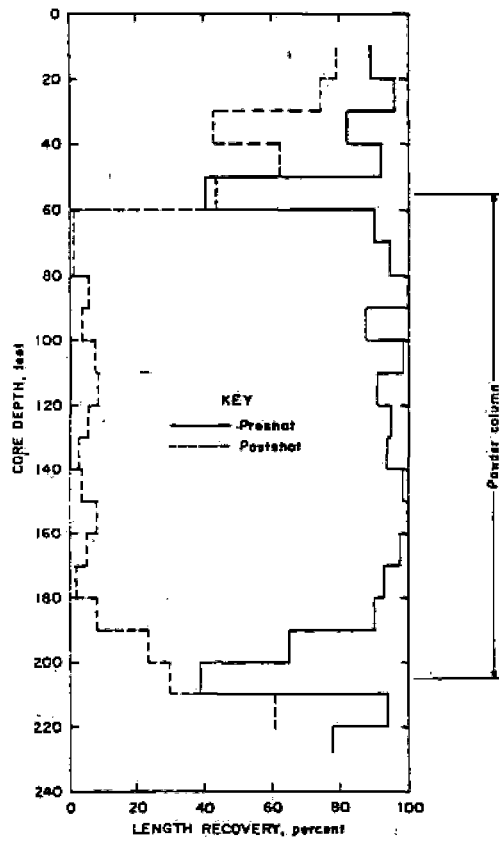
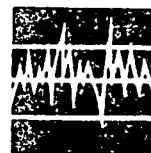


FIGURE 5. - Drill core length recovery versus depth.

THE BACTERIAL LEACHING OF URANIUM

R. A. MacGREGOR *Stanrock Uranium Mines Limited, Elliot Lake, Ontario*



Received July 15, 1968
Revised October 14, 1968

KEYWORDS: uranium ores, uranium, production, leaching, economics, bacteria, uses

SUBJ
MNG
TBLU

UNIVERSITY OF UTAH
RESEARCH INSTITUTE
EARTH SCIENCE LAB.

Bacterial leaching of uranium ores in the Elliot Lake area has been used as a production method since 1962. Minor amounts were recovered from mine waters prior to this. Uranium in a pyritized quartz pebble conglomerate is oxidized from the tetravalent to the hexavalent state in the presence of bacteria. The bacteria are naturally occurring autotrophs of the Ferrobacillus-Thiobacillus group. The solubilized uranium is then dissolved with water or acid solution and pumped to surface for treatment. Recovery of ammonium diuranate from the resulting acid mine water is carried out in a conventional uranium ion exchange plant. The method produces uranium at low cost from abandoned or caved mine workings. Recovery of thorium and rare earths by the same method is limited only by market conditions.

INTRODUCTION

The bacterial leaching of ores, particularly copper, has been used for centuries, although the role of bacteria has come to be recognized only much more recently.¹ Production of uranium by bacterial leaching in the Elliot Lake area, and Stanrock Mine in particular, has been carried on as a small but profitable adjunct of conventional mining since 1960. As the sole means of recovery, it has been in use by Stanrock since October 1964 and was used experimentally by Milliken Mine of the Rio Algom group in the period July 1964 to August 1965.² Nordic Mine, also of the Rio Algom group, is expected to convert to leaching as the sole means of recovery in

1968. Discovered as a result of naturally occurring phenomena, it is now an established practice. This paper describes its development, present practice, and some of the possible future applications to which it may be put.

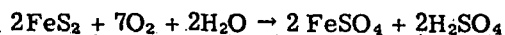
DEVELOPMENT

The Elliot Lake area is a short distance north of the north channel of Lake Huron approximately equidistant between Sudbury and Sault Ste. Marie, Ontario. The ore bodies are extensive quartz pebble conglomerate beds from 6 to 40 ft in thickness dipping from 5° to a maximum of 40°. There are also thinner uneconomical beds. Depths of the mines vary from near surface to 3000 ft. The ore consists of quartz pebbles in a pyritized sericitic matrix. Uranium minerals are chiefly brannerite, frequently intergrown with anatase or rutile, uraninite, some monazite, and minor coffinite and thucolite. The sulfides are pyrite, which constitutes 5 to 10% of the ore, and minor pyrrhotite, chalcopyrite, and galena.³ Mining is by room and pillar with 65 to 80% extraction.

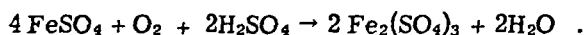
As the ore body was exposed by mining, there was a gradual decrease in pH of mine waters to 4.5, followed by a more rapid decrease to 3.0 to 2.3. Steps were taken to neutralize the water before pumping to surface in order to prevent corrosion of the pumps and pipelines. With the decrease in pH, a small but significant amount of uranium was noted in the water as well as a high ferric-to-ferrous iron ratio. Treatment of the water for uranium recovery was started in 1960 to recover the small amount of uranium present and to control pollution. Investigations into the causes of acid mine water led to the conclusion that bacterial action was converting pyrite to sulfuric acid and ferric sulfate.^{4,5} Bacteria of the *Ferrobacillus-Thiobacillus* group were later identified.⁶

Bacteria of this group are unicellular organisms, 0.25 μ in diameter and 1 μ long.⁶ They reproduce by simple division and thrive in acid iron-bearing media. Their energy source is derived from the oxidation of ferrous iron and/or sulfides and sulfur. They require fixed nitrogen and gaseous carbon dioxide and oxygen from the air. Optimum conditions for growth are a pH range of 1.8 to 3.5 and temperatures of 25 to 40°C. Outside these limits, their growth tends to be inhibited. They will survive under adverse conditions in a dormant or semidormant state provided that the changes occur gradually. They are sensitive to metal ion concentration, but can be bred to high tolerance levels if the concentration of ions is increased gradually.

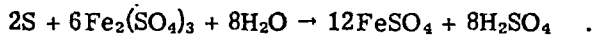
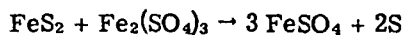
Several chemical changes take place in the leaching action.⁷ Under ordinary conditions, pyrite is slowly oxidized to ferrous sulfate and sulfuric acid:



In the presence of bacteria, the ferrous sulfate is oxidized to the ferric state:



The reaction appears to be strongly catalyzed by bacteria.⁶ Ferric sulfate will attack pyrite to form more ferrous sulfate by the proposed reactions:



These reactions may also be catalyzed by similar strains of bacteria. Researchers at Kennecott⁸ claim experimental evidence of bacteria that will act directly upon pyrite, producing ferric sulfate and an excess of H_2SO_4 .

Uranium, which occurs in the insoluble tetravalent state, is oxidized to the soluble hexavalent state in ferric sulfate solutions by ferric sulfate,



provided the ferric-to-ferrous ratio is kept high enough to maintain a redox potential ≥ 410 mV.

As mining progressed, worked out stopes became coated with a brown iron oxide; yellow uranium salts were also noted. The uranium content of the mine water continued to increase gradually. While the original treatment of mine water was primarily for the control of pollution in the watershed, the increased acidity and consequent uranium content motivated research into means for increasing the recovery by leaching methods. Various types of sprays were tried, as well as a fast, high-pressure (80 to 100 psi) washing with hand-held hoses. The fast, high-pressure washing

of stopes on a cyclical basis proved the most effective. Optimum cycle time was determined as three months.⁹ Water for washing is drawn from Quirke Lake at a pH of 5.0 by Stanrock and Denison mines. Milliken Mine used water drawn from a drill hole to the adjoining Lacnor Mine, having a pH of 3.5 and a uranium content of 0.14 lbs/ton.² Nordic Mine, which began leaching more recently, is using mine water for stope washing.

Laboratory tests have demonstrated the effectiveness of bacteria in leaching uranium from crushed samples of ore.² The extraction rate appears to be a function of the exposed mineral surface. Almost 80% extraction was achieved in 67 days on a -6-mesh + 20-mesh sample. A $-\frac{1}{2}$ -in. + 4-mesh sample gave an extraction of only 54% in the same period of time. Extraction in the absence of bacteria was only 10%. Tests during stope washing at Stanrock indicated a 75% recovery of uranium in the fines on the first wash.⁹

The effects of nutrient on bacterial leaching has also been investigated. The standard "9K formula" has the following composition¹⁰:

	g/liter
Ammonium sulfate	3.0
Potassium chloride	0.1
Potassium acid phosphate	0.5
Magnesium sulfate	0.5
Calcium nitrate	0.015
Ferrous sulfate	44.2
Sulfuric acid	1.0 cm ³
Distilled water	1000 cm ³

Although controlled laboratory tests show a definite advantage in the use of nutrient, its use in underground washing has been only partially successful. Tests at Stanrock showed no appreciable increase in recovery for stopes where nutrient was spread after washing and the stopes then re-washed on the regular 3-month cycle. Drying out of the stopes is probably the difficulty.

Milliken Mine reported an increase in yield and a decreased cycle time from the use of nutrient with a wetting down procedure between cycles.⁸ However, when the increase in recovery is balanced against the cost of nutrient plus additional manpower for spreading and wetting down, it is not considered to be economical.

At Stanrock, washing has been carried on continuously since December 1962. Economic values are still being obtained from some stopes washed 15 to 18 cycles. Beginning in late 1966, a progressive decrease in recovery was noted, especially in stopes containing lower grade ore. Stopes giving consistently poor recoveries are dropped from the washing program. Withdrawal of stopes from cyclical washing has gradually reduced the extent of washing activity.

The depth of penetration of bacteria into the rock is still a matter of conjecture. Studies of polished sections of ore show a very low penetration rate. Production results obtained from bacterial leaching would indicate a penetration of at least an inch or two. Stanrock's production from leaching at over 650 000 lbs U_3O_8 is 6.5% of the total mine recovery.

To maintain production, certain sections of the mine are being flooded according to a program. By this method, it is hoped to recover the maximum amount from stopes too low in grade to warrant the cost of high-pressure hosing. Recovery of uranium from extensive caved areas that are inaccessible to washing is anticipated. Flooding will also reduce the open area of the mine to be supplied with fresh air for ventilation. (Good ventilation is important in uranium mines to control the buildup of radon daughter products in breathing air.) Filling of the west part of the mine began in late 1966. When flooded to its full extent, this area will contain $1\frac{1}{4}$ million tons of water or 250 million gallons. No recovery from the area, which is now only about half filled, has been made yet. A smaller area in the east end of the mine, containing 100 to 150 thousand tons of water, has been filled and partially recovered. Grade has exceeded expectations by ~10 to 20%.

The use of low pH barren solution from the mill was tried in 1964 for the washing down of stopes. It was found that this water would give recoveries in recently mined stopes, where bacteria had obviously not yet been active. Barren solution also speeded up bacterial activity so that recently mined stopes could be successfully included in the leaching program after 3 to 6 months instead of the usual 1 year. However, the highly corrosive nature of this solution precluded its use on any large scale because of distribution problems.

Flooding permits use of a large volume in a relatively confined area. The flooding area was designed to introduce water into the uppermost workings of the mine, allow it to flow over the greatest possible area, and withdraw it at a lower level for pumping to surface for treatment.

To discharge the barren solution into this area, four 2-in. polyethylene plastic lines were run 1000 ft from the mill to No. 2 shaft, then 3000 ft down the shaft to a sump at the bottom. A stainless steel, 420 gal/min, 4-stage transfer pump moves the barren solution through 3000 ft of 6-in. acrylonitrile-butadiene-styrene (ABS) plastic pipe to the flood area.

RECOVERY

Water from the east-end flood area, together with water from high-pressure hosing, is pumped

by stainless steel secondary pumps to a settling sump (Fig. 1). Water from the west end will flow to the settling sump by gravity through 1300 ft of 6-in. ABS pipe now being installed. This water flows by gravity to a clear-water sump from where it is moved by three 8-stage pumps and one 4-stage pump to the mill through 5000 ft of 6-in. rubber-lined steel pipe against a vertical head of 3500 ft. Conversion of the pumping system to stainless steel pumps and rubber-lined pipe in 1966 made it possible to dispense with neutralizing the water before pumping.

Treatment of the water on surface uses a section of the conventional mill. Mine water discharges on surface into a 90- \times 12-ft rubber-lined thickener tank that acts as a surge tank for the clarifiers. After clarification, the water is pumped to ion exchange. The mine water was formerly pumped to ion exchange at the normal mine water pH of 2.3 to 2.4. However, with the implementing of a closed system in which barren solution is recirculated, pH adjustment to 2.0 is being made before treatment. Lower pH barren is expected to be beneficial to leaching. Ion exchange columns are eluted with a 20-g/liter nitric acid solution. The high-grade eluant is pumped to the precipitation circuit where the pH is raised to 3.8 with lime and ammonia, iron being precipitated and settling out in a thickener. The thickener overflow is pumped to the second stage of precipitation, where the pH is increased to 7.0 with ammonia to precipitate the uranium as ammonium diuranate or yellow cake. This yellow cake, containing 80% U_3O_8 , is filtered, dried, and packed in drums of 500 lbs.

Barren solution from ion exchange is returned underground by the plastic lines previously mentioned. At some time in the future, it is proposed to bleed off a portion of the barren solution to prevent a buildup of metal ions that might be deleterious to the bacteria. Thorium or rare earths could be recovered from the barren bleed if a suitable market should develop.

COSTS

Bacterial leaching costs are generally lower than conventional recovery methods. Direct operating costs of bacterial leaching at Stanrock were 31¢/lb in the first year of operation,⁷ and subsequently were lowered to <25¢/lb while operated as an adjunct to a conventional mining operation. Only those costs that were additional because of leaching were included. Costs of pumping, recovery, overhead, etc., did not change appreciably and were charged to the conventional operation. As the sole means of recovery, total operating

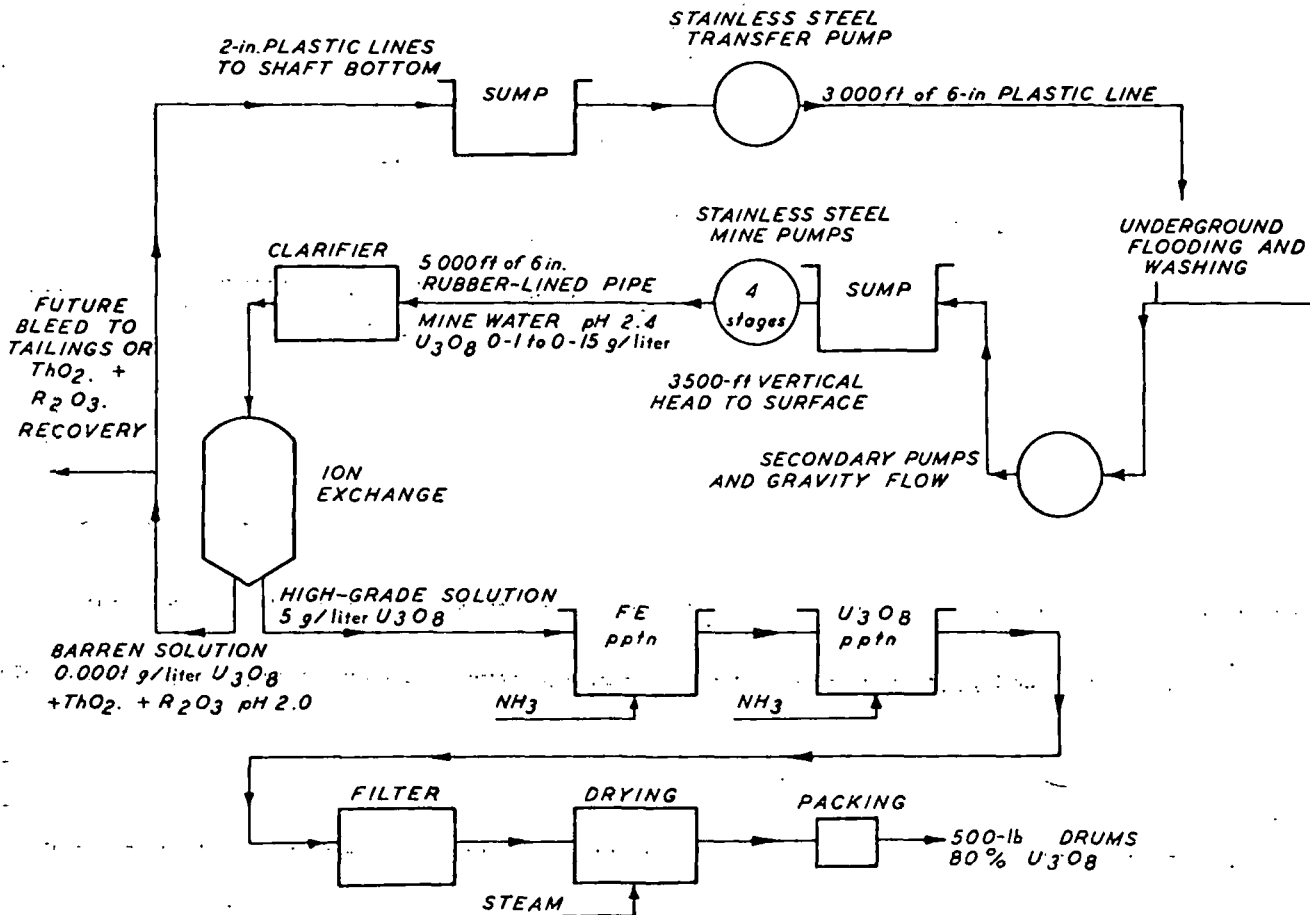


Fig. 1. Flow sheet.

costs have averaged \$3.50/lb. The costs in a flooding operation are expected to be comparable.

FUTURE USES

Conventional mining and milling methods are unlikely to be superseded by bacterial leaching. The method does, however, provide a means of scavenging worked-out mines, caved areas, or low-grade material inaccessible or uneconomical to treat by conventional recovery methods. It holds promise for the recovery of uranium from material rejected by flotation, heavy media, electronic sorting, or other upgrading procedures. Tests in South Africa have shown that tailings dumps are amenable to bacterial leaching.¹¹ If required, it could be used to recover thorium and rare earths from the Elliot Lake area tailings dumps. Research on the use of bacteria as the oxidant in uranium mill leach circuits has shown promise.¹² Although recoveries are lower, and retention times somewhat higher, reductions in

capital and operating costs might make the method attractive under certain economic conditions.

The mechanisms of bacterial leaching are still relatively new and not fully understood; further research will undoubtedly result in improvements in operating and cost-saving techniques.

REFERENCES

Specific

1. P. C. TRUSSELL, D. W. DUNCAN, and C. C. WALDEN, "Biological Mining," *Can. Min. J.*, 85, 46 (1964).
2. S. M. ROSCOE, "Geology and Uranium Deposits, Quirke Lake-Elliot Lake, Blind River Area, Ontario," Paper 56-7, Geological Survey of Canada (1957).
3. J. R. FISHER, "Bacterial Leaching of Elliot Lake Uranium Ore," *Trans. Can. Inst. Min. Metall.*, LXIX, 167 (1966).
4. A. R. COLMER and M. E. HINKLE, "The Role of Micro-Organisms in Acid Mine Drainage," *Science*, 106, 253 (1947).

5. K. L. TEMPLE and E. W. DESCHAMPS, "Autotrophic Bacteria and the Formation of Acid in Bituminous Coal Mines," *Appl. Microbiol.*, 1, 255 (1953).

6. V. F. HARRISON, W. A. GOW, and K. C. IVARSON, "Leaching of Uranium from Elliot Lake Ore in the Presence of Bacteria," *Can. Min. J.*, 87, 64 (1966).

7. S. R. ZIMMERLY, "Cyclic Leaching Process Employing Iron Oxidizing Bacteria," U.S. Patent 2,829,964 (April 8, 1958).

8. R. P. MILLER, E. NAPIER, R. A. WELLS, A. AUDSLEY, and G. R. DABORN, "Natural Leaching of Uranium Ores," *Bull. Inst. Min. Metall., London*, 674, 217 (1963).

9. R. A. MacGREGOR, "Recovery of U_3O_8 by Underground Leaching," *Trans. Can. Inst. Min. Metall.*, LXIX, 162 (1966).

10. M. P. SILVERMAN and D. G. LUNDGREN, "Studies

on the Chemoautotrophic Iron Bacterium *Ferrobacillus-Ferrooxidans*," *J. Bacter.*, 77, 642 (1959).

11. M. MATIĆ and M. MROST, "In Situ Leaching of Uranium from Gold Mine Residue Dams," *South African Ind. Chem.*, 127 (October 1964).

12. V. F. HARRISON and W. A. GOW, "Progress Report on Bacterial Leaching of Uranium-Bearing Ore from an Elliot Lake Mine," Department of Mines and Technical Surveys, Ottawa (November 1966).

General

a) M. P. SILVERMAN and H. R. EHRlich, "Microbial Formation and Degradation of Minerals," *Advan. Appl. Microbiol.*, 6, 153 (1964).

b) S. I. KUZNETSOV, M. V. IVANOV, and N. N. LYALIKOVA, *Introduction to Geological Microbiology*, McGraw-Hill, New York (1963).

An all new rig for Magmont shaft would have cost twice as much as new and used parts

Component part	New	Up-graded	Cost
Engines (3 @ \$30,000.00)	\$ 90,000.00	—	\$ 90,000.00
Drawworks	—	\$20,000.00	20,000.00
Mud pumps			
1—1,000	60,000.00	—	60,000.00
1— 850	—	—	—
Power transmission	—	20,000.00	20,000.00
Substructure	—	15,000.00	15,000.00
Derrick	—	3,000.00	3,000.00
Blocks, hook, etc.	40,000.00	—	40,000.00
Miscellaneous	—	5,000.00	5,000.00
Drill string	134,000.00	—	134,000.00
Choke manifold (10,000 psi)	25,000.00	—	25,000.00
Total	\$349,000.00	\$63,000.00	\$412,000.00

All new rig	Cost
Engines (3)	\$ 90,000.00
Drawworks	20,000.00
Mud pumps (2) 1—1,000	115,000.00
1— 850	—
Power transmission	20,000.00
Substructure	15,000.00
Derrick	3,000.00
Blocks, hook, etc.	40,000.00
Miscellaneous auxiliary equipment	5,000.00
Drill string	134,000.00
Choke manifold (10,000 psi)	25,000.00
Total	\$309,000.00

Estimated cost of a nuclear leaching experiment on copper ore

SUBJ
MNG
TCOL

loop, a proposal by Kennecott Copper Corp. and the Atomic Energy Commission, would provide for a million contained 20-kiloton nuclear blast and mining experiment at its Safford, Ariz., copper porphyry. If the project is approved by Congress and proceeds as planned, it should go a long way in proving or disproving the feasibility of nuclear blasting for the preparation of an oxide zone of low-grade deposit for in-situ recovery of copper. After the blast, the recovery would be made possible by using solution recovery holes and piping and access drifts below the chimney created by the blast. The pregnant solution would be pumped to the surface precipitator (see E/MJ, November 1967, p 116).

Some comparisons of the nuclear shot with other big blasts in mining indicate that more rock has been broken with conventional blasts than the estimated 1.3-million tons that the proposed 20-kiloton nuclear device would break. Other production blasts, however, have broken to one or more free faces, while the proposed nuclear shot would be a contained experiment. Other large blasts in the recent past include:

- 1) International Nickel Co.—Frood mine—5.25-million tons with 464 tons of powder.
- 2) Climax Molybdenum—1.25-million tons in a glory hole blast with 208 tons of explosives.
- 3) Minnesota taconite mine—broke 1.3-million tons using 850 tons of high energy slurry (Hercules Powder Co, report).

Cost estimates for Project Sloop

Phase 1	
Field start-up and initial support facilities	
Pre-shot sampling holes	
Site safety studies	
Total Phase 1	\$750,000
Phase 2	
Project start-up and support facilities	
Rehabilitation of existing workings	
Scientific program and explosive diagnostics	
Emplacement hole	
Emplacement, stemming	
Operational support	
Communications	
Post-shot drilling, re-entry and testing	
Miscellaneous construction	
Engineering inspection	
Total Phase 2	\$5,750,000
Phase 3	
Underground re-entry and rehabilitation	
Leach solution and recovery system	
Post-shot sample and solution input holes	
Underground process piping and pumping system	
Copper precipitation plant	
Process water supply	
Leach plant operating costs—one year	
Public and industrial safety monitoring	
Project evaluation	
Total Phase 3	\$6,675,000
Total Project Sloop	\$13,175,000

The cost of leaching U₃O₈ in stopes and pumping solution to the surface

The economic advantages of microbiological processing have given new life to some mines and, in other cases, will allow the leaching of low-grade ore (see E/MJ, October 1967, p 75). At Stanrock Uranium Mines Ltd., Stanrock, Ontario, Canada, the use of bacteria leaching provided the answer to the question of "how to stay in business," in the face of skyrocketing costs by conventional mining methods.

The high-pressure washing of stopes at Stanrock, beginning in 1963, increased production from 27,100 lb of U₃O₈ in 1962 to 105,300 lb in 1963. Uranium recovery from mine water at that time was 7% of total production.

Between July and October of 1964, mining costs increased to \$5.09 per lb of U₃O₈ recovered. This allowed only 41¢ per lb profit. As a result of the high costs the

entire mine was converted to bacteria operation at the end of October 1964. By the summer of 1965, bacterial leaching was credited with lowering production costs to \$3.30 per lb of U₃O₈. Heating of mine intake air during the winter added 50¢ to total U₃O₈ costs. The conversion to corrosion-resistant materials in the mine solution circuit resulted in a 50¢ per lb U₃O₈ direct savings in chemicals and pump maintenance supplies.

Stanrock is recovering 15,000 to 16,000 lb of U₃O₈ monthly from 1,200 stopes having an average floor area of 6,000 sq ft each.

To eliminate the need of neutralizing mine solutions, 316 stainless steel pump components, rubber-lined solution lines in the shaft, and plastic distribution lines were installed in the mine.

Years
1923-34
1928
1929-34
1928-30
1928
1928
No significant
1930
1929-34
1928-32
1928-29

• U.S. = U

Some

In COM
producti
the fol
meeting.

The l
to be f
short ac
that nee
\$300 to
\$30,000

Cap
mine pi
shaft in
length.
balance
and hau

The
to devel
lished tr
by deep
produce
ment in

A nu
these ci
cost car
daily cr
ably nee
spent fo
ing unit
items of
ton of

Labor p

Some
undergr
bourow.
of nine
bined st

Increa
open stu
longwall
hole) c
order. C
of a ge
other m

sociation, which occurred in the plasma, is maintained. According to equilibrium phase diagrams, the zirconium oxide phase should contain 3-5% silica, but the Ionarc process produces a zirconia containing only about 0.5% silica. This phenomenon is thought to be the result of ultra-high temperature and rapid cooling. After plasma treatment, sodium hydroxide is used to leach out the silica (Fig. 4). Depending on the number of leaches,

various grades of zirconia ranging up to 99+ % purity are produced.

Plasma processing may also be applicable to many other materials, such as complex silicate or oxide minerals. The upgrading of ilmenite to rutile, the direct reduction of iron ore, and the chlorination of various ores (in a chlorine plasma) are only a few of the possibilities that have been suggested.

Trends in chemical processing and hydrometallurgy

Developments in hydrometallurgical approaches to minerals processing continued to receive the lion's share of research throughout 1971. This trend became more pronounced during the year for a number of reasons: production cutbacks at copper smelters unable to meet pollution regulations; smelter closures in the zinc industry; and reduced shipments of sulphide concentrates—especially to the Japanese, who have their share of domestic problems in complying with pollution control requirements.

R&D in copper hydrometallurgy keeps growing

The copper industry, more so than others, continues to focus its efforts on developing pollution-free hydrometallurgical processes for metal recovery.

Here is a brief rundown of recent developments:

- Haver and Wong, at the US Bureau of Mines (USBM), have reported on a new study for the use of ferric chloride as a leaching reagent for chalcopyrite. In this method, copper concentrates are leached at relatively low temperature and atmospheric pressure with ferric chloride solution. Copper is recovered by cementation with iron, and elemental sulphur may be recovered or removed from the leach residue by solvent extraction with perchloroethylene. The ferric chloride solution is recovered and recycled. The sulphur-stripped leach residue may then be cyanided to recover precious metal values. Recoveries of 99.9% of the copper values have been obtained, together with 70.5% of the sulphur in elemental form.

- Another USBM development is a process to leach oxide copper ores with chelating agents. Bauer and Lindstrom report that a solution of the trisodium salt of ethylenediamine tetra-acetic acid (EDTA) is highly effective in leaching copper from ores containing large amounts of calcite or dolomite. (Acid leaching of these high-carbonate ores is usually not feasible because of excessive acid consumption.) In studies on an oxide ore from Utah containing 40% calcium carbonate, 3.7% copper and 1.9% zinc, copper was recovered as the hydroxide by lime addition and the EDTA solution was recycled.

- Inspiration Consolidated Copper Co., in collaboration with researchers from the University of Arizona, has developed a new process for chalcopyrite concentrates. The technique involves dissolution of the sulphide in an acid solvent at atmospheric pressure and 95°C, and copper

separation from iron, followed by copper recovery via electrowinning. The process is said to be applicable also to the winning of zinc and nickel from their sulphides.

- At the industrial level, there has been further expansion of proven chemical processing routes for copper ores. Nchanga Consolidated Copper Mines announced plans for the world's largest metallurgical liquid ion exchange plant at Chingola, Zambia. Power Gas Corp. is designing the plant to produce 12 million lb per month of copper from a leach liquor flow rate of 15,000 gpm. This represents an impressive scale-up in the size of facilities from the first commercial liquid ion exchange plant for copper, that of Ranchers Exploration and Development Corp. Ranchers' plant at Miami, Ariz., now in its fourth year of operation, currently produces copper at a monthly rate of about 1 million lb. Liquid ion exchange technique has also been used in a unique operation combining pollution control and metal recovery at the El Paso, Tex., plant of the SEC Corp. This plant treats a copper-nickel stream from a copper refinery containing about 80 grams per liter of copper and 25 gpl of nickel. Copper is separated by liquid ion exchange using General Mills' LIX-64N[®] reagent, and the copper is then electrowon after the loaded organic is stripped (Fig. 1). After pH adjustment to remove iron and aluminum, nickel is similarly separated by liquid ion exchange and electrowinning. Daily production rate is 4,000 lb of copper and 1,000 lb of nickel.

- An innovation in copper electro-refining has been introduced at the Mufulira copper refinery in Zambia. After extensive pilot investigations, periodic current-reversal facilities will be put in the refinery extension due on stream in 1973. This permits cell operation at considerably higher levels than conventional current densities (up to 30 amp per sq ft) with considerable savings in capital investment.

Nickel and cobalt developments

Hydrometallurgical developments in nickel processing have generally represented expansions of current proven technology. Marinduque Mining and Industrial Corp. for example, has announced the successful completion of an 11-month pilot plant test run on laterite nickel ore from the Surigao Mineral Reservation in the Philippines, at Sherritt Gordon Mines Ltd. facilities at Fort Saskatchewan, Canada. During this period, 18,000 lb of nickel was produced from 5,000 tons of Surigao ore utilizing

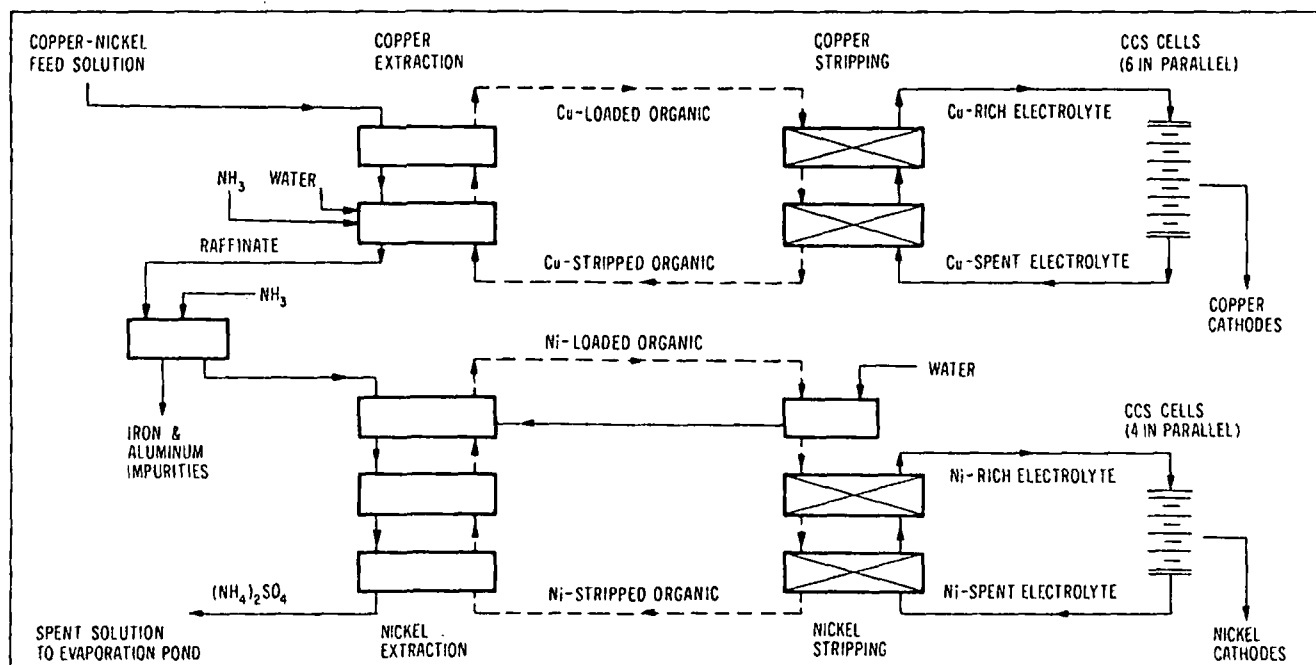


Fig. 1—SEC nickel recovery process. Through solvent extraction of an impure copper-nickel feed solution, the process first strips copper from solution and recovers it

by electrowinning—while the copper-free solution undergoes pH treatment ahead of solvent-extraction of nickel. Nickel is then recovered in a separate bank of cells.

the Sherritt Gordon process. Nickel recovery is said to be 82.2% on feed assaying 1.33% nickel during one 28-day run. Sherritt will assist in construction of a nickel refinery and has licensed Marinduque to use its hydrometallurgical processes for the recovery of nickel and other metals from laterites.

In another related development, PT Pacific Nickel has announced that it will ship 12,000 tons of laterite nickel ore from Indonesia to Sherritt Gordon's demonstration pilot plant for process test work.

In a somewhat similar project, jointly sponsored by American Metal Climax Inc. (Amax) and Societe Miniere et Metallurgique de Penarroya SA, bulk samples of lateritic nickel from deposits in New Caledonia are shipped to the Amax Extractive Metallurgical Laboratory at Golden, Colo. (Fig. 2). Certain slurry pumpings and other tests at Golden have been performed with satisfactory results, and further pilot testings are being conducted to determine the economic feasibility of nickel and cobalt recovery on a commercial scale. Amax, which recently purchased the Port Nickel refinery in Braithwaite, La., is also conducting pilot plant studies to evaluate refining improvements at Port Nickel.

Nickel recovery via leaching and solvent extraction

Details of the copper-nickel matte process used by Falconbridge at its Kristiansand, Norway, nickel refinery reveal an interesting chemical processing technique coupled with extensive use of a digital computer control system to provide the plant with a high degree of automatic operation. Copper-nickel matte, shipped from Canada, is leached with concentrated hydrochloric acid to affect only the nickel solution in the primary leaching operation. This permits a neat separation of nickel from copper, cobalt, and precious metals. The nickel solution

is purified by a two-stage solvent extraction process, which removes first the minor amounts of iron dissolved in the leach, and then any cobalt and copper present. After crystallization of nickel chloride from the purified solution, 99.7+ % nickel metal is recovered by hydrogen reduction of the oxide produced by thermal decomposition of the chloride salt. Copper is recovered from the hydrochloric acid leach residue by a combination of roasting, sulphuric acid leaching, and electrowinning.

The high strength of the hydrochloric acid used (275 gpl) is such that Falconbridge can carry out the leaching operation at fairly low temperature (70°C) and atmospheric pressure, thus overcoming the need for high-pressure equipment required in other processes. The computer is used for overall control functions as well as supplying an automatic printout at the end of each shift of key average readings and a solution balance.

Winning metal values from ocean nodules

Hydrogen chloride is also the solubilizing reagent used in a process for winning metal values from ocean nodules announced by Deepsea Ventures Inc., Gloucester Point, Va., a Tenneco Inc. subsidiary. This company is piloting the recovery of nickel, cobalt, copper, and manganese from ocean nodules obtained from a site in the Pacific, which typically analyze 26-27% manganese, 1.3% nickel, 1.0% copper, and 0.2% cobalt. The pilot plant, designed to process about 80 lb per hr of nodules, involves hydrochlorination of dried and crushed nodules with hydrogen chloride gas in a multihearth furnace at temperatures above 120°C to convert the metal oxides into their water-soluble chlorides. After countercurrent water leaching to dissolve the chlorides, the pregnant leach liquor is separated from the solid residue by filtration. Separation of nickel, cobalt, copper, and manganese values is done by

three separate liquid ion exchange steps, leaving the manganese in the final solution. Manganese chloride is then recovered by crystallization, and manganese metal can be produced by one of several conventional routes. The reagent used in the liquid ion exchange step is an unidentified proprietary substance dissolved in a kerosine diluent.

Ultimate recovery of nickel, copper and cobalt values is by conventional electrowinning cells.

Deepsea Ventures feels that its process is economically feasible and that metal recoveries are satisfactory. The company, in fact, has already spent some \$20 million on exploration and development work—which culminated in the selection of the hydrochlorination solvent-extraction route, a selection made after investigating more than 100 different processes.

As far as commercialization is concerned, Deepsea hopes to achieve full production of metals from nodules within the next three or four years.

Fluid bed roasting

Outokumpu Oy metallurgists have revealed details of their process for the sulphatizing roasting of nickel-, copper-, and zinc-bearing cobaltiferous pyrite concentrates at their Kokkola works in Finland. They utilize a fluid bed sulphatizing roast technique to convert nickel, cobalt, and other valuable metals into water-soluble forms for subsequent recovery. The process involves the feeding of a mixture of green concentrate and precalcined concentrates together with sodium sulphate into a fluid bed roaster. The fine mixture (60%, minus 200 mesh) is roasted at 650°C and, after cooling, is magnetically separated: the incompletely sulphatized fraction of the product is magnetic and can be recycled to the fluid bed reactor. The success of the scheme rests in large part upon its ability to convert the valuable metals to water-soluble form, while rendering the iron insoluble as ferric oxide. Iron sulphate formation is eliminated by rapid product cooling in fluidized bed coolers, where the fluidizing air also purges the sulphatizing gases from the bed. Nickel and cobalt recovery from the product is effected by multi-stage countercurrent-leaching with water.

New alumina process

An interesting process for production of alumina from a formerly valueless aluminum-containing mineral, alunite (sometimes known as alum stone) has been developed by workers at the University of Guanajuato in Mexico. Alunite, a hydrated potassium sulphate, $KAl_3(OH)_6(SO_4)_2$, has not heretofore been of commercial significance as a source of alumina due to its low Al_2O_3 content (25-39% in US deposits), especially when compared with the only other aluminum ore, bauxite, which generally contains 50-55% Al_2O_3 .

The ore, after crushing and sizing to 1 in. and dehydroxylation in a rotary kiln at 750°C to remove all bound water, is then ball-milled to minus 20 mesh and pulped with water (Fig. 3). This slurry, transferred to a stainless steel reactor, is reacted with ammonia gas to break down alunite into ammonium and potassium sulphates in solution, together with a slurry of alumina and silica. After filtration, the mixed sulphate solution is taken to a crystallizer to produce a byproduct fertilizer. The alumina-silica filter cake is repulped and reacted with SO_2 gas at a temperature of 80°C to form a soluble acid aluminum sulphite.

After the solid-liquid separation, alumina-containing sludge is pumped to another reactor and treated with sulphuric acid to solubilize the balance of the aluminum values as aluminum sulphate. Insoluble silica and other impurities are filtered off and the two solubilized alumina streams are combined in a fourth reactor. As this mixture is boiled, SO_2 gas released from the acid aluminum sulphite is then recycled. Under the low pH condition maintained in the reactor, the aluminum precipitates as a basic sulphate, or a mixture of basic sulphate and alumina hydrate. Iron, titanium, and other soluble impurities remain in solution. After thickening and filtration, aluminum sulphate is recovered and calcined to yield alumina and sulphur trioxide for acid production and recycle.

Electro-oxidation technique for gold

Gold hydrometallurgy advanced in 1971 when USBM published details of a process it had developed to over-

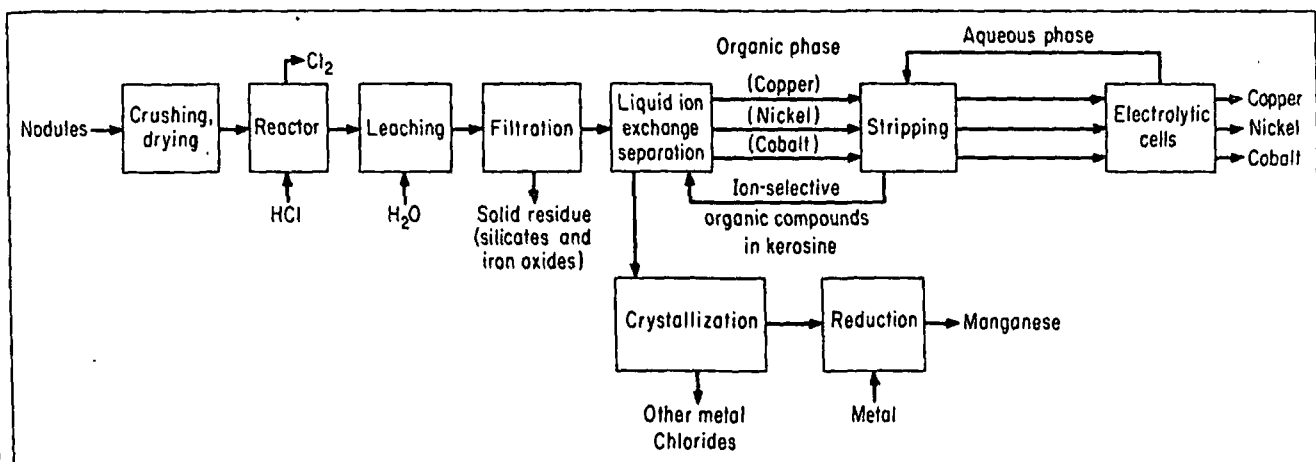


Fig. 2—Metals recovery from ocean nodules in this hydrometallurgical route, developed by Deepsea Ventures Inc., begins with a hydrochlorination step at 120°C to convert manganese, copper, nickel and cobalt into water-soluble

chloride compounds. Leached out with water, these metal values are then recovered by ion-exchange adsorption and stripping, followed by conventional electrowinning (for copper, nickel and cobalt), and crystallization.

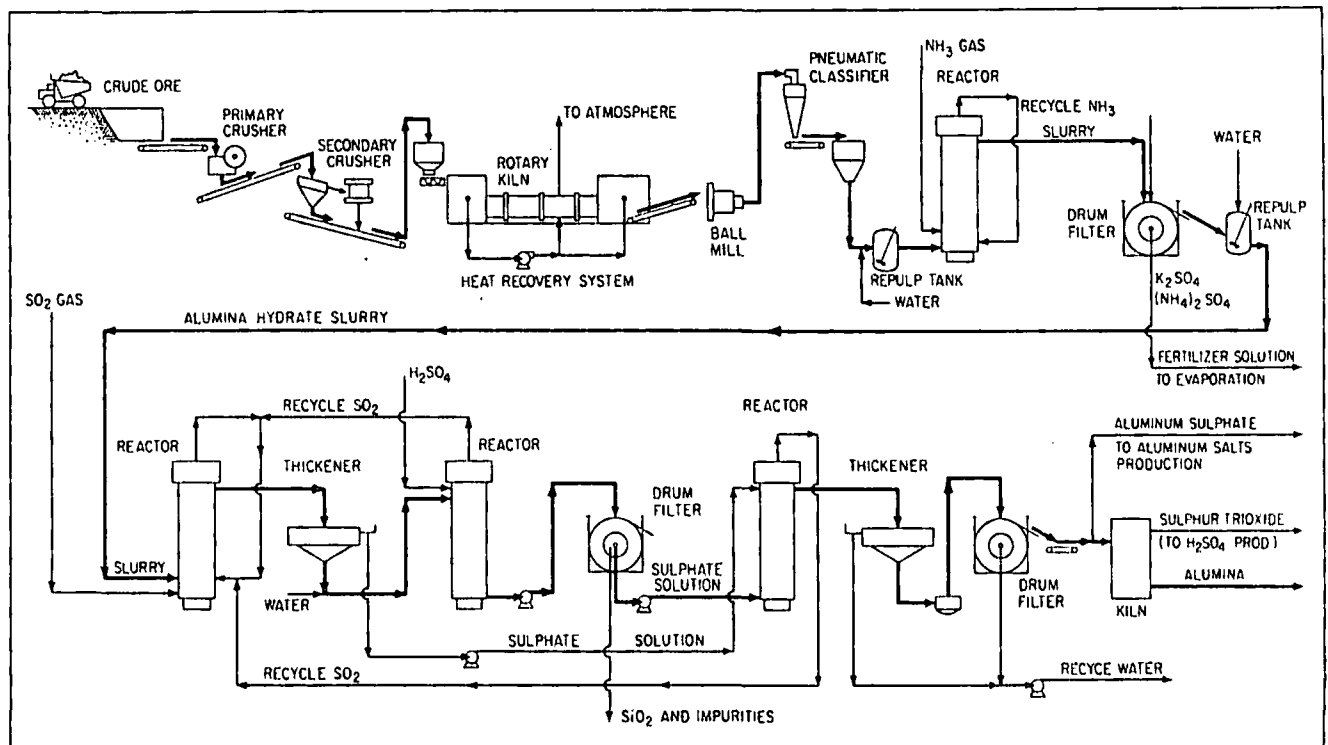


Fig. 3—This new route to alumina, developed in Mexico, is based on alunite—formerly considered intractable.

come problems in processing "carbonaceous" gold ores. The ores studied originated from various locations in northern Nevada. The process developed involves an electro-oxidation treatment of the ore prior to cyanidation, to either destroy or render innocuous the organic components present in the ore feed—thus permitting the gold to be recovered by the conventional cyanide process. Pre-treatment technique involves the addition of sodium chloride to the water-pulped ore and in-situ generation of sodium hypochlorite in the slurry using a plate-type graphite-graphite electrode system. Oxidation of the organic compounds by the sodium hypochlorite results in an improvement in gold recovery from 0.018-0.096 oz per ton without electro-oxidation, to better than 0.27 oz per ton on ores assaying 0.3 oz gold per ton. The optimum addition rate of sodium chloride is about 10% relative to the weight of ore processed. At this sodium chloride level, power consumption per ton of ore is about 70 kwh. Brine from the barren solution is recycled to the electro-oxidation cells, thus minimizing reagent consumption.

Electro-oxidation for molybdenum and rhenium

The electro-oxidation technique has also been examined by USBM to solubilize metal sulphides. At the Reno Metallurgy Research Center, studies on the recovery of molybdenum and rhenium from molybdenite concentrates have given encouraging results in small scale pilot tests. Recoveries of molybdenum and rhenium from a molybdenite concentrate obtained as a byproduct of porphyry copper ores were 95% and 97%, respectively. These results were obtained by electro-oxidation in a 10% brine solution at 30°-40°C, with power consumption in the range of 16 to 24 kwh per lb of molybdenum extracted. Since present techniques for molybdenum-rhenium con-

centrate processing are all pyrometallurgical, requiring the handling of sulphur oxides as byproducts, electro-oxidation shows great promise as a new candidate in mineral processing.

Uranium from phosphate by SX

Workers at Oak Ridge National Laboratory have announced the development of a new solvent extraction (SX) process to recover uranium from wet-process phosphoric acid produced from Florida phosphate rock. This material commonly analyzes 90-200 mg of U_3O_8 per liter, and at present day production levels of acid, several thousand tons of byproduct U_3O_8 are potentially available from phosphoric acid. The new process reagent costs are estimated to be less than \$1.00 per lb of recovered U_3O_8 and the solvent extraction reagent is said to consist of a mixture of 0.5 Molar di(2-ethylhexyl) phosphoric acid and 0.125 Molar trioctylphosphine oxide in an aliphatic diluent. Overall recoveries of 95% of uranium have been obtained with a purity of 97+ %.

Progress in leaching methodology

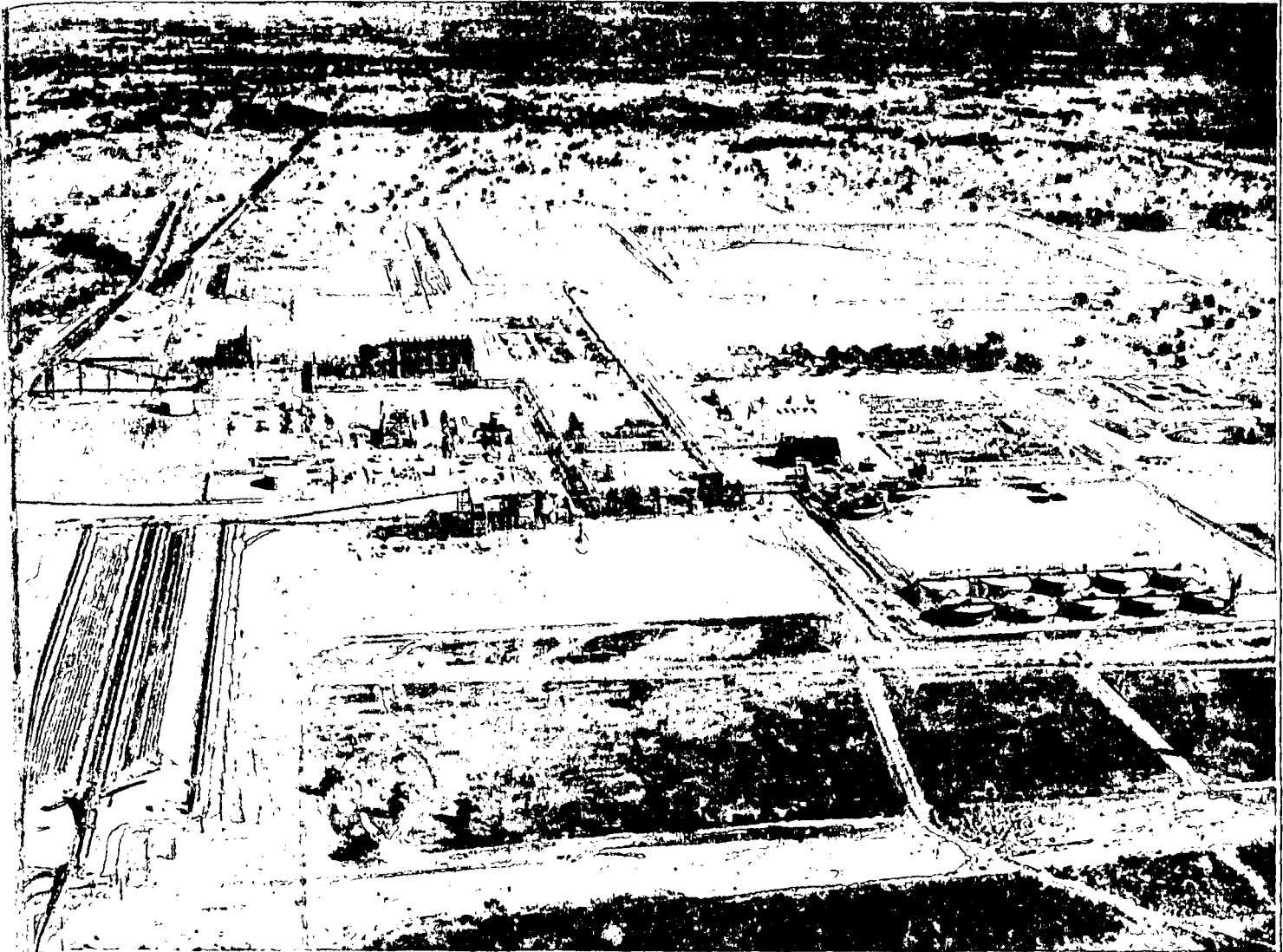
In-situ leaching of minerals, particularly base metals, continues to attract a good deal of interest. To be a workable mineral deposit, within the context of in-situ leaching, a deposit should possess three major characteristics: 1) technical response to a low-cost lixiviant; 2) reasonable degree of permeability; and 3) ability to confine liquor circulation to the zone of metallurgical interest.

Several pilot operations were reported during 1971, among which are Kennecott's in-situ copper leaching operation at its Nevada Mines Div. in the Robinson Mining district in eastern Nevada. The site chosen for the pilot

study was a worked-out open pit, the Kimbley pit. A bench some 250 ft above pit bottom was selected and five holes 9 in. in diameter and 40 ft deep were drilled on this mining level. (These holes, spaced 50 ft apart and 25 ft back from the edge of the level, are used to pump acid into the test area.) After an examination of the flow pattern through the structure had been made by means of a tunnel drifted 175 ft beneath the bench, sufficient information was obtained concerning flow and liquid distribution to develop a pilot plant operation nearby. This project involves leaching of a mineralized area east of the Kimbley pit said to contain some 5 to 6 million lb of copper in place. If successful, the operation will have saved stripping some 7.25 million tons of the over-burden which caps the mineralized zone.

Development of techniques for practical microbiological leaching of sulphide concentrates continues to make progress. One of the leading exponents of the technique, the British Columbia Research Council of Vancouver, Canada, outlined a proposed copper sulphide concentrate

leaching process utilizing a bacterium named *Thiobacillus ferro-oxidans* to solubilize the copper. The feasibility study for a plant to process 100 tpd of chalcopyrite proposes the use of 20-sq-ft x 16-ft-deep agitated concrete leaching vessels to contain the concentrate and leach liquor. The leach liquor would be nothing more than a mixture of water, bacteria, oxygen, and carbon dioxide, together with minor amounts of nutrients necessary for life-support of the bacteria. Since studies have shown that the rate of leaching is inversely proportional to particle size of the concentrate, the pregnant liquor (25-28 gpl Cu concentration) and unreacted material are separated and the residual concentrate is sent to a regrind circuit and then back to leaching. Sludge formed containing minor elements such as gold, silver, and molybdenum is thickened and the copper sulphate solution is transferred to conventional electro-winning cells. Operating costs are estimated at 6¢ per lb of copper produced for a 100-tpd plant and about 4¢ per lb of copper at a 1,000-tpd level.



The Pinjarra alumina refinery, built by Alcoa of Australia Ltd. 55 mi south of Perth, Western Australia, was officially opened on May 3. Its initial capacity is in excess of 200,000

mtpy. Nearly 30% of production from the new Pinjarra refinery will be sold to Japan; some alumina will also go to customers in the Middle East.

Taking a new approach to the study of chemical reactions in a well-known process, Asarco researchers have uncovered valuable data in a . . .

UNIVERSITY OF UTAH
RESEARCH INSTITUTE
EARTH SCIENCE LAB.

SUBJ
MNG
TCS

Thermoanalysis of Copper Segregation

EDWARD MARTINEZ

Although the copper segregation process has been known as a method for treating oxide copper ores since the 1920's, the reactions involved in this process are still a matter of conjecture. However, the evidence turned up in a recent series of experiments at Asarco's Central Research Laboratories strongly indicates that some of the proposed reactions may not be occurring.

Experimental work on oxide copper ores from the Sagasca mines in Chile led to the discovery of the copper segregation process in 1923. It was found that the reduction of the copper with coal at about 700°C occurred on the surface of the coal instead of remaining disseminated in the ore. The unusual behavior of the copper, which caused it to migrate from the ore particles to the coal, was traced to the presence of a small quantity of sodium chloride occurring in the ore. Further experiments with oxide copper ores proved that the presence of a halide, either occurring naturally or admixed with the ore, caused the copper to migrate from the ore particles and to segregate in the charge.

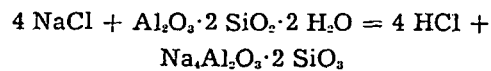
The ratio of salt to reducing agent may vary somewhat, but in general 0.5% to 1.5% sodium chloride and 0.5% to 1.0% coal or coke have been mixed with the ore. Less than stoichiometric amounts of salt are required to convert all the oxide copper to a chloride, so that a cycle of reactions appears to be occurring. Several investigations reported in the literature have proposed reactions to explain the mechanism of the process.³⁻⁶ There appears to be general agreement that water is necessary for the reactions to occur; that once the sodium chloride reacts with silica or silicates in the ore, the hydrochloric acid formed will convert the cupric oxide in the mineral structure to cuprous chloride. However, there appears to be a conflict of opinion on the reactions involved in the reduction of the cuprous chloride to metallic copper on the surface of the carbon.

Rey³ has indicated that salt, water vapor, and silica in the ore react to produce hydrochloric acid, as follows:

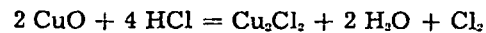


SME Member EDWARD MARTINEZ is a Research Engineer at the Central Research Laboratories of American Smelting and Refining Co. in South Plainfield, N. J.

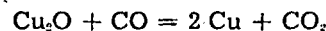
U.S. Bureau of Mines investigators^{3,4,6} believe that the salt reacts with hydrous clay minerals in the ore, such as montmorillonite and kaolinite:



The hydrochloric acid formed attacks the cupric oxide in the mineral structure to form a cuprous or cupric chloride, probably the former since cupric chloride is unstable at the elevated temperatures involved. Both Rey and the Bureau of Mines agree that the chlorination and partial reduction of the cupric oxide take place as follows:

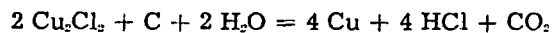


Rey⁴ states that the cuprous chloride vapors are reduced to copper in the following manner:



The reduction of the copper oxide takes place on the carbon particles because the latter are the sites of carbon monoxide production. Note that the chloride decomposition reactions are the inverse of the chlorination reactions.

The Bureau of Mines^{3,4,6} believes that many side reactions are occurring, but that the principal one is the reduction of the cuprous chloride vapor directly to copper upon coming into contact with the hot carbon particles and water vapor:



Kellogg⁷ states that, although carbon is one of the most useful reducing agents for metallic oxides, it is useless as a reducing agent for chlorides. However, carbon can react with water vapor to form hydrogen which will reduce copper chlorides at segregation temperatures. In an interesting experiment with cuprous chloride and graphite held in separate boats, Diaz² found that a thick deposit of copper formed on the graphite at 800°C only when water vapor was present in the system.

Chrysocolla, a hydrated copper silicate, is one of the principal copper minerals found in oxide ores. It is known that chrysocolla undergoes several reactions, both endothermic and exothermic, as it is heated to 750°C.^{8,9,10} The present investigation of

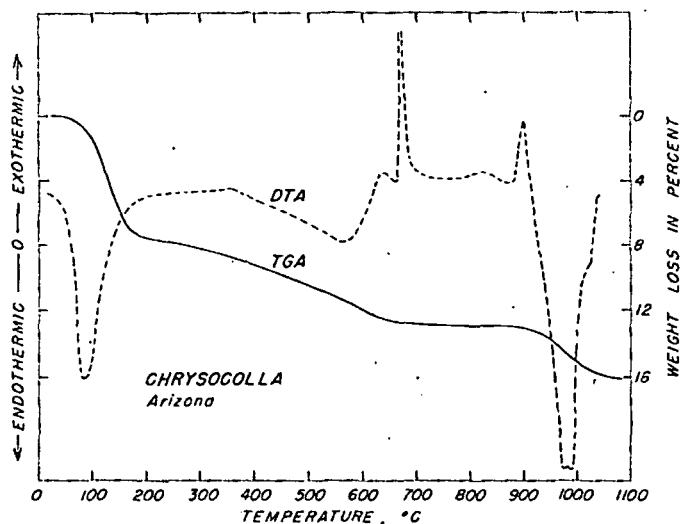


Fig. 1:—DTA and TGA of chrysocolla from Inspiration, Ariz., in nitrogen atmosphere. Sample weights were 500 mg in the TGA and 200 mg in the DTA. Sensitivity in DTA was $10 \mu\text{v}$ per in.

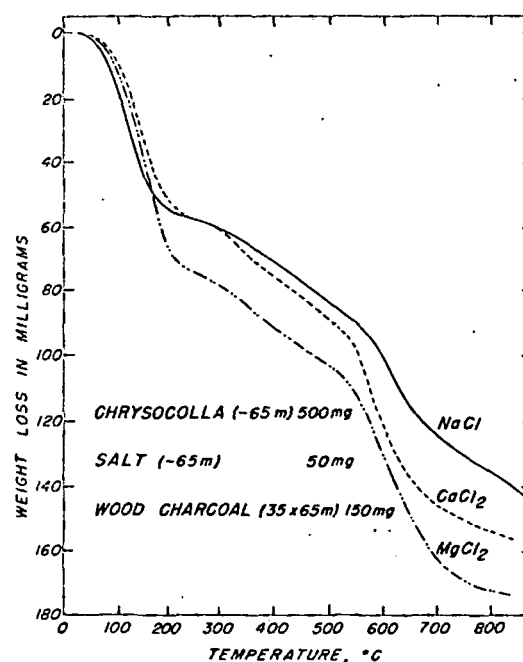


Fig. 2:—TGA of chrysocolla, wood charcoal, and salt mixtures. Heating rate was 5°C per min; nitrogen was streamed through furnace tube.

reactions occurring between chrysocolla, salt, and a reducing agent was undertaken to seek further information that might provide a better understanding of the segregation process. Differential thermal analysis (DTA) and thermal gravimetric analysis (TGA) were the main techniques used in this study.

EQUIPMENT AND TEST PROCEDURES

Differential thermal analysis (DTA) and thermal gravimetric analysis (TGA) involve raising the temperature of the sample at a uniform rate. DTA detects, amplifies, and records enthalpic changes occurring in the sample as it is heated; changes in weight are measured in TGA.¹¹ A DTA manufactured by the Robert L. Stone Co. having a heating rate of 10°C per min and a Chevenard thermobalance converted electronically for graphic recording were used. The heating rate can be varied in the thermobalance, but in general a 5°C per min temperature rise was used. Most runs were stopped at temperatures from 500° to 850°C .

In nearly all tests the DTA and TGA were run with the samples in a nitrogen atmosphere. However, in some of the special tests with reagent grade chemicals the nitrogen was bubbled through a water saturator at room temperature to provide water vapor in the sample atmosphere.

Mixtures of chrysocolla, salt, and reducer were run in the DTA-TGA. A typical segregation charge to the TGA was 500 mg of chrysocolla, 50 mg of salt, and 150 mg of wood charcoal. Decreased weights with the same ratios were run in the DTA. A procedure described by Rey¹ was modified in some of the tests so that a concentrate of the segregated copper could be easily obtained. The chrysocolla and salt were reduced to -65 mesh and the charcoal was 35x65 mesh. At the end of a run, the coarser copper-coated charcoal was separated from the residue by screening on a 65 mesh sieve.

TEST RESULTS

Thermal Analysis of Chrysocolla: Investigations of the thermal properties of chrysocolla, $2 \text{CuO} \cdot 2 \text{SiO}_2 \cdot \text{H}_2\text{O}$, using DTA and TGA have been reported in the literature.^{9,9,20} Since chrysocolla is used as the oxide copper source in most of the tests in this investigation, the DTA and TGA of a sample of chrysocolla from Inspiration, Ariz., are shown in Fig. 1. The weight loss and endotherm below 200°C are due to loss of absorbed water. The broad endotherm and weight loss from 300° to 650°C are caused by the loss of hydroxyl groups bound in the structure. The exotherm at 680°C has been ascribed to the crystallization of tenorite (CuO)⁹ and to changes in the Si-O bonds.⁹ The high temperature exotherm is believed to be due to further changes in the Si-O structure. The weight loss and endothermic reactions from 900° to 1000°C are caused by the reduction of cupric oxide to cuprous oxide.

Chrysocolla-Charcoal Reactions: The addition of charcoal to chrysocolla produced some modification of the chrysocolla thermograms. The sharp exotherm at 680°C with chrysocolla alone (Fig. 1) was considerably decreased in peak height and occurred at a lower temperature with charcoal.

The TGA revealed a larger weight loss between 300° and 650°C with charcoal than with chrysocolla alone. In addition, the loss of weight continued above 650°C . Microscopic examination of the residue from the DTA run, which was stopped at 700°C , revealed no evidence of copper on the surface of the charcoal. A small amount of copper was noted in some of the chrysocolla particles, but most of the chrysocolla remnants were black with some yellow to green portions.

Chrysocolla-Salt Reaction: In these experiments, 50 mg of each of the three salts, NaCl , CaCl_2 , and MgCl_2 , were mixed with 500 mg of -65 mesh chrysocolla and run in the thermobalance. The ad-

diti
the
incl
was
wit
T
dec
per
(Fi
elin
deto
C
and
Mg
bala
tair
Fig
mes
A
cur
all
550
red

dition of a salt to the chrysocolla caused a break in the weight loss curve at approximately 550°C. The increased weight loss, starting at this temperature, was considerably greater with CaCl₂ and MgCl₂ than with NaCl.

The DTA of similar mixtures revealed that NaCl decreased the peak height and lowered the temperature of the chrysocolla exotherm noted at 680°C (Fig. 1). The other two salts caused the complete elimination of the exotherm. In addition, the DTA detected a small endotherm between 525° and 590°C.

Chrysocolla-Charcoal-Salt Reactions: Chrysocolla and wood charcoal, to which either NaCl, CaCl₂, or MgCl₂ had been added, were run in the thermobalance to approximately 850°C. The curves obtained with the three chloridizers are shown in Fig. 2. The chrysocolla and salt were finer than 65 mesh and the charcoal 35 by 65 mesh.

A striking feature is the break in the weight loss curve at approximately 550° to 575°C obtained with all three salts. It appears that the weight loss from 550°C to 850°C is the result of the volatilization and reduction of the copper chloride. A similar but less

pronounced break in the weight loss curve was obtained at about this same temperature when mixtures of chrysocolla and a salt were heated.

Examination of the -65 mesh residues from the CaCl₂ and MgCl₂ runs showed that in general the chrysocolla remnants were colorless, with an occasional pale green particle. When NaCl was used, however, there were many red to pink particles remaining, which indicated an incomplete removal of the copper from the chrysocolla structure. This was confirmed by copper analyses of the +65 mesh fractions, which all weighed approximately 250 mg. The MgCl₂ and CaCl₂ tests assayed 48% and 46% copper, respectively, compared to 38% for the NaCl run.

Polished briquettes of the +65 mesh copper-charcoal from the three runs were examined. Microphotographs of the NaCl and MgCl₂ tests are shown in Fig. 3. The segregation product obtained with CaCl₂ was in general similar to that obtained with MgCl₂, but the briquettes from the NaCl run revealed a basic difference in the distribution of the copper throughout the charcoal. With NaCl, the copper was almost wholly on the outer surface of

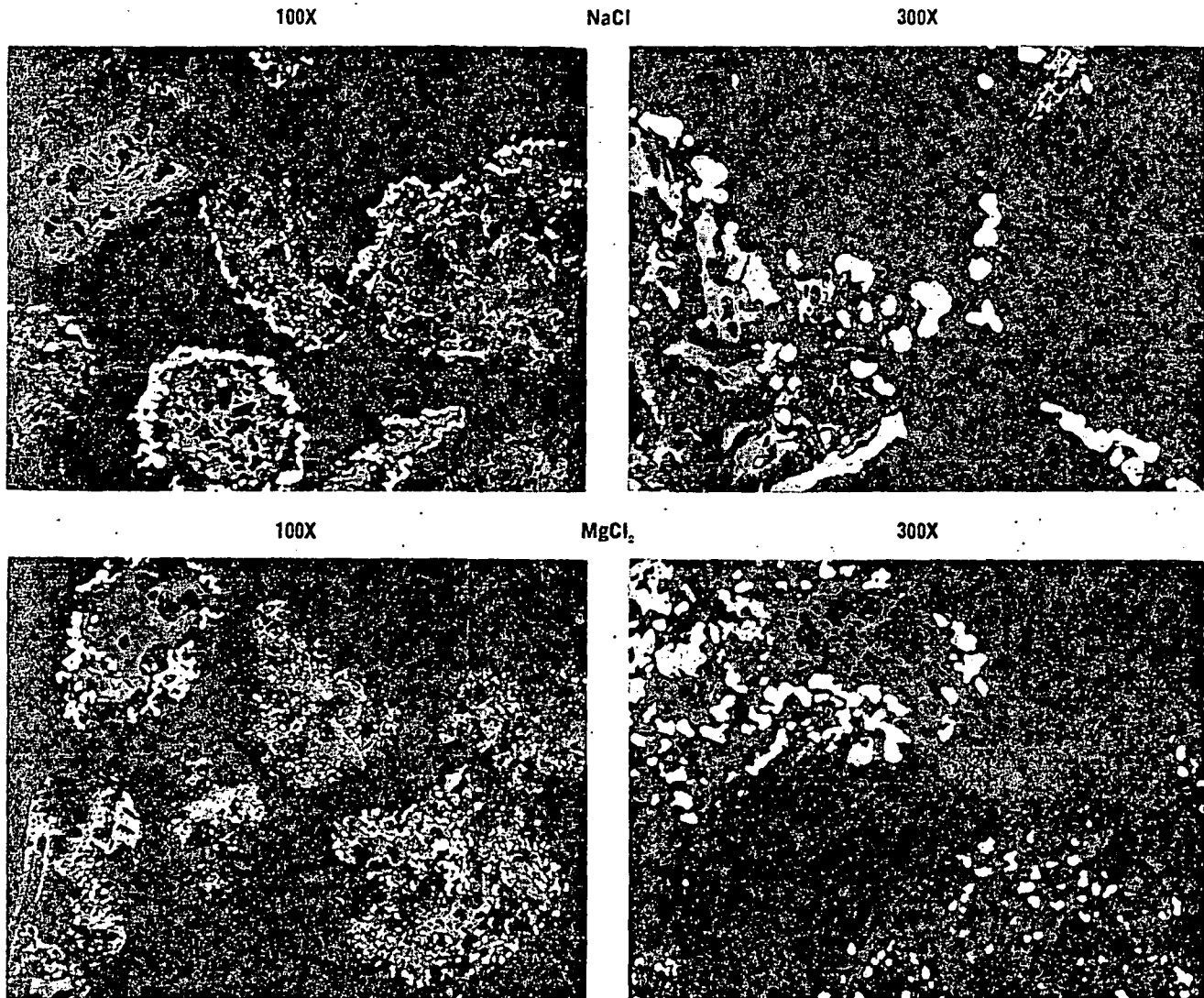


Fig. 3.—Microphotographs of charcoal-copper concentrates from segregation tests run in TGA with chrysocolla, wood charcoal, and salt (Fig. 2) showing results with NaCl and MgCl₂. The copper distribution with CaCl₂ was similar to that obtained with MgCl₂. The white phase is copper; the gray and black portions are charcoal.

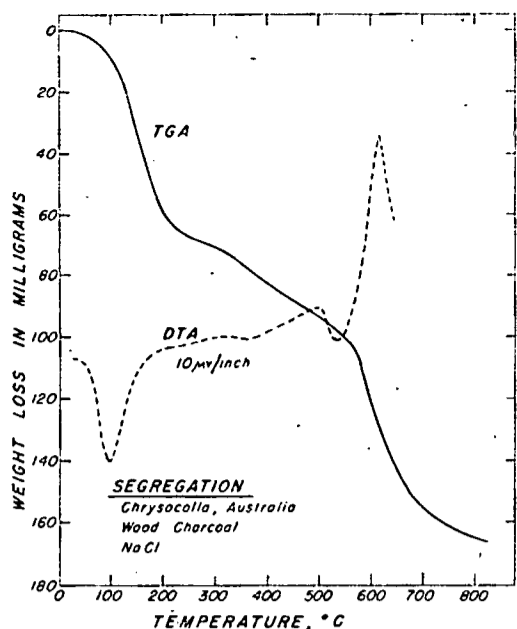


Fig. 4.—DTA-TGA of mixtures of chrysocolla, wood charcoal, and sodium chloride run in nitrogen atmosphere.

the charcoal and a relatively thick deposit was formed. On the other hand, with either $MgCl_2$ or $CaCl_2$ as the chloridizer, the copper was largely in the form of small specks throughout the interior of the charcoal. In an occasional particle of charcoal that appeared to lack porosity, the copper also formed on the surface with $MgCl_2$.

The microphotograph (magnified 300X) of the copper obtained with $NaCl$ shows that it appears to extend out from the surface of the charcoal. This is confirmation of a general impression obtained from examining products from numerous runs with the stereoscopic binocular microscope at much lower magnification. Note the copper on the charcoal particle on the right. The copper does not appear to have been formed by replacement of the charcoal, but rather extends out from the surface.

During this investigation, chrysocolla samples from many different sources including Arizona, Nevada, and Australia were tested. In all cases segregation was obtained and the thermograms were quite similar. Fig. 4 is the DTA and TGA of a segregation mixture with a chrysocolla sample from Australia. The endotherm detected above $500^\circ C$ is believed to be due to the volatilization of the copper chloride; the exotherm following is undoubtedly caused by the reduction reactions leading to the weight losses above $550^\circ C$ noted in the TGA.

A series of tests were run with mixtures of chrysocolla, $CaCl_2$, and petroleum coke or wood charcoal in which the DTA was stopped at 500° , 550° and $625^\circ C$. Although the best segregation occurred with the $625^\circ C$ run, copper was observed coating the reducer even at $500^\circ C$. X-ray diffraction of products from the $550^\circ C$ test indicated a few weak lines. The strongest lines of quartz were identified, and one of the few remaining lines matched the strongest line for $CuCl_2 \cdot 2H_2O$. Examination with a stereoscopic binocular microscope revealed the presence of a pale

green phase on the surface of the reducer. Furthermore, it was observed that the color of some of the chrysocolla remnants, as well as the green phase on the reducer, turned a deep green on exposure to the atmosphere.

Cupric Oxide-Salt-Reducer-Quartz Reactions: Interpretation of the results obtained with chrysocolla as the oxide copper source is difficult because chrysocolla itself undergoes many reactions as it is heated. Furthermore, it is a silicate with which the salt may be reacting, as previous investigators have proposed.¹⁻⁶ To obtain data on a somewhat less complex system, several TGA tests were run with various mixtures of cupric oxide, sodium chloride, charcoal, and quartz. The nitrogen was bubbled through a water saturator at room temperature.

Fig. 5(a) is the TGA of a mixture of cupric oxide, charcoal, and quartz. It was noted that the cupric oxide was reduced to some extent in place and little copper was on the surface of the charcoal. When sodium chloride was added to a similar mixture, the charcoal was coated with copper, i.e., segregation had occurred. The TGA of this run is shown in Fig. 5(b). Note the break in the weight loss curve between 500° and $600^\circ C$, and the larger loss of weight obtained when salt was added.

A test with cupric oxide, sodium chloride, and charcoal, but no quartz, also produced segregation. The thermogram is shown in Fig. 5(c) and appears to be quite similar to the one in Fig. 5(b).

A synthetic ore was prepared by mixing 100 mg each of cupric oxide, sodium chloride, and petroleum coke with 1700 mg of quartz. The sample, containing approximately 4% copper, was run in the thermobalance to $900^\circ C$ and segregation occurred. The break in the weight loss curve at about $550^\circ C$, as shown in Fig. 5(b), was evident in this run also.

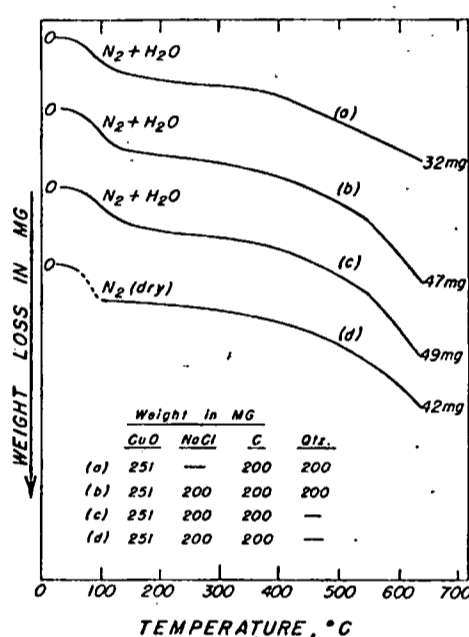


Fig. 5.—TGA of various mixtures of CuO , $NaCl$, charcoal, and quartz. In runs (a), (b), and (c), nitrogen was bubbled through a water saturator prior to entering furnace. In (d) the nitrogen was passed through Anhydron to remove water vapor.

The recovery of copper that migrated was lower in tests with $NaCl$ than in similar tests with $MgCl_2$ or $CaCl_2$. The larger weight losses obtained with the latter in the 550° to $850^\circ C$ range (Fig. 2) are probably indicative of the effectiveness of the chloridizer. In addition, the chrysocolla remnants were mainly colorless with $MgCl_2$ or $CaCl_2$, but contained many pink and red particles with $NaCl$ owing to incomplete removal of copper. The effect of the salts on the chrysocolla exotherm at $680^\circ C$ may indicate the extent of the chloridizing. The peak height and temperature of the exotherm were decreased by the addition of $NaCl$, but with $MgCl_2$ the exotherm was completely eliminated.

The TGA of the chrysocolla-salt mixtures each showed a break in the weight loss curve at approxi-

One of the postulated reactions in the segregation process is between the salt and a silicate or quartz. The silicate may be present either in the chrysocolla structure or in other minerals present in an ore. The products of this reaction are a sodium silicate and hydrochloric acid. The mechanisms proposed involve a solid-solid reaction between $NaCl$ and the silica or silicate, since water would be the only vapor phase present initially. Although solid-solid contact may occur between the 1% to 2% salt and silica in highly siliceous ores, good segregation is possible in ores containing very little SiO_2 . Therefore, it is improbable that a solid-solid contact can occur to any large extent in these ores. The DTA did not detect any reaction that could be attributed to the forma-

References

- 1 Rey, M.: The Segregation Process for Low-Grade Copper Oxide Ores. 7th Int. Cong. Min. Met. & Appl. Geol., Met. Sec., Vol. II-3. Paris, Oct. 20-26, 1935. pp. 55-62; Rev. Met., 33, 1936, pp. 295-302.
- 2 Diaz, C. M.: Mechanism for the Segregation Process, M.S. Thesis, Dept. of Mineral Eng., Columbia Univ., 1958, pp. 1-59.
- 3 Rampacek, C., W. A. McKinney, and P. T. Waddleton: Treating Oxidized and Mixed Oxide-Sulfide Copper Ores by the Segregation Process. USBM Rep't of Invest. No. 5501, 1959, pp. 1-28.
- 4 Anon.: USBM Charts Segregation Process, Eng. and Min. Jnl., 160, Nov., 1959, pp. 98-99.
- 5 Rampacek, C., and W. A. McKinney: The Copper Segregation Process, Paper presented at AIME meeting in N. Y., Feb., 1960.
- 6 Pollandt, F., and M. E. Pease: Extraction of Copper and Silver by the Segregation Process in Peru, Inst. of Min. and Met. Trans., 69, Sept., 1960, pp. 687-697. Discussions: ibid., 70, Dec., 1960, pp. 143-156; March, 1961, pp. 390-396.

- 7 Kellogg, H. H.: Thermodynamic Relationships in Chlorine Metallurgy, Jnl. of Metals, June 1950, AIME TRANSACTIONS, 188, 862-872.
- 8 Sun, M. S.: The Nature of Chrysocolla from Inspiration Mine, Arizona, Am. Mineral., 48, 1963, pp. 649-658.
- 9 Martinez, E.: Chrysocolla Studied by Differential Thermal Analysis, Thermal Gravimetric Analysis and Infrared Spectrophotometry, AIME TRANSACTIONS, 226, 1963, pp. 424-427.
- 10 Prosser, A. P., A. J. Wright, and J. D. Stephens: Physical and Chemical Properties of Natural Copper Silicates which Resemble Chrysocolla, Inst. of Min. & Met., Trans., 74, Feb. 1965, pp. 233-258; Discussion: April, 1965, pp. 393-401.
- 11 Gordon, S.: Thermoanalysis, Encyclopedia of Science and Technology, McGraw-Hill, New York, 1960, pp. 556-559.
- 12 Sutulov, A.: Evaluating Copper Segregation Results by Screen Sizing Analysis, AIME TRANSACTIONS, 226, March, 1963, pp. 17-20.
- 13 McKinney, W. A., and P. T. Waddleton: Use of Various Salts as Copper-Volatilizing Agents in the Segregation Process, USBM Rep't of Invest. No. 6044, 1962, pp. 1-17.

SUBJ
MNG
TEAF

TECHNICAL, ECONOMIC, AND ENVIRONMENTAL EVALUATION
OF IN SITU COAL GASIFICATION

Thomas F. Edgar
Department of Chemical Engineering
The University of Texas at Austin
Austin, TX 78712

ABSTRACT

Underground coal gasification is a process which should be considered as a competitor on an economic basis with shaft mining of coal. However, not all coal seams and locations are viable candidates for the application of this technology. The important factors in site evaluation, including coal properties, geological conditions, and operating parameters, as well as the economics of underground coal gasification, are discussed. Specific reference to the Soviet system of underground gasification is given.

INTRODUCTION

Underground coal gasification (UCG) has as its objective the recovery of the energetic and chemical content of coal without mining. A gaseous mixture composed of nitrogen, oxygen, and steam in variable proportions is introduced in a coal seam prepared for gasification; combustion and gasification reactions occur in situ. The products, carbon monoxide, carbon dioxide, hydrogen, water vapor, methane, nitrogen and other hydrocarbons are obtained in a readily usable form for the production of electric power or the manufacture of chemicals.

In situ coal gasification is a process which should be considered as a competitor on an economic basis with shaft mining but not with surface mining. The successful application of this method would provide a low Btu gas (100-300 Btu/SCF) which can be readily cleaned for sulfur compounds and at the same time eliminate many

UNIVERSITY OF UTAH
RESEARCH INSTITUTE
EARTH SCIENCE LAB.

UNIVERSITY OF UTAH LIBRARY

of the health, safety, and environmental problems associated with conventional deep mining of coal. The in situ method also has the potential to recover the energy from deep coal deposits which are not economic to mine using conventional schemes.

A review of the Soviet work in UCG makes it abundantly clear that the Russian gasification effort far surpasses that of all other countries combined. The first field tests were performed in 1933, and their efforts peaked in the late 1960's. The Soviets arrived at a UCG system design that could be operated successfully in a predictable manner, and they were able to transfer the method successfully from one geological area to another (and from one coal type to another). They developed a large quantity of field data for all coal types, strata, and operating conditions, as recently discussed by Gregg et al.¹

TECHNICAL FEATURES OF THE RUSSIAN UCG SYSTEM

The Soviet system of UCG is based on two steps: pregasification and gasification. The pregasification step is probably the most critical one, since proper seam preparation allows successful gas production. The main step in the preparation of the coal seam is the "linking" of definable points within the coal deposit. Initially air is injected under pressure and passes through the natural cleat system; however, most coals require a better link than the natural permeability provides for gasification to proceed successfully.

In the Soviet approach, two steps are undertaken to insure the success of gasification. The first step is drying of the seam (with heated air or combustion gas) to further enhance the seam permeability. This process is usually only recommended for so-called "shrinking" coals, such as found in the western United States. The second step is to increase the permeability of the

air path by burning part of the coal, using an approach called reverse combustion or backward burning. Reverse combustion involves the injection of the oxidant blast in a direction counter-current to the movement of the combustion front; this method is contrasted to that of forward burning, where the gases and combustion front move co-currently. Linking between boreholes is achieved after reverse combustion.

The effect of volatiles from the coal and allowable operating pressures are two of the important reasons why backward burning is utilized for permeability enhancement prior to application of forward combustion. In forward burning, volatiles are produced ahead of the combustion front; these volatiles are cooled with the product gases and begin to condense at about 150°C, according to Soviet experience. However, in backward burning the volatiles must pass through the flame front, thus cracking many of the components. The volatiles then pass through the path of high permeability already created, which minimizes the potential of plugging. This path of high permeability also allows operation at high flow rates and low pressures during gasification.

In UCG it is important to minimize the loss of both the injected blast and the product gas, which can leak through cracks to surrounding formations as the roof collapses due to removal of the coal. By operating the system at the lowest possible pressure, gas leakage can be minimized. Low pressure operation can only be facilitated through permeability enhancement of the coal seam, which usually entails backward burning.

One other crucial element in the Soviet design for UCG is to form the linkage at the bottom of the seam. The flame front undercuts the coal at the bottom of the seam, and the overlying coal falls into the void. This occurrence promotes efficient gas-solid contact and thus has desirable reaction properties. Another

reason for establishing the reaction at the bottom of the seam is to prevent the flame front from moving to the top of the seam. Liquids (water and pyrolysis products) would tend to force the reaction upwards if the permeable path were established in a higher position in the seam. Once a channel is allowed to form across the top of the seam, the slagged coal ash tends to seal the bottom of the channel, preventing further combustion of coal. This can result in very poor resource utilization. Because of the liquid movement and collection, gasification in the updip direction is preferred over the downdip direction.

The Soviets used a linear well pattern, where two rows of wells are simultaneously linked prior to the gasification process. They also sequenced the operations so that a consistent heating value was produced. Once the product gas reaches a low heating value, as it inevitably will at some point in the operation, that production hole is capped off and the product gas is then forced to pass through the seam to the next production borehole, some 75 feet away. This new path has already been prepared by previous drying and backward burning operations. Schematics of this approach have been presented by Elder².

RECENT FIELD TESTING RESULTS

The most advanced field test in the U.S. is being operated by the Laramie Energy Research Center of ERDA at Hanna, Wyoming on sub-bituminous coal. Over a four month period in 1974, an average yield of 130 Btu/SCF was produced from a two hole (inlet/outlet) system. The linked vertical borehole method was used, and forward burning was found unworkable without prior backward burning; due to tars plugging up the porous media. Estimates of coal recovery efficiency ranged from 30 to 50 per cent for the 30-foot seam. A second Hanna experiment was performed in 1975, and over 38 days

the heating value averaged 152 Btu/SCF (higher heating value). The Russian percolation design for UCC was essentially used in this test. The UCC system was operated at relatively high flow and production rates compared to previous tests, which aided in the high yields (Fischer and Schrider³). The test was terminated before the combustion front reached the production well. A typical composition for the product gas is shown in Table 1, and for the purposes of comparison, the composition from a surface gas producer (Lurgi) is also shown.

TABLE 1
Typical Gas Yields (Water-Free) from In Situ and
Conventional Gasifiers

	<u>UCC</u>	<u>Lurgi</u>
Hydrogen	18.6	23.1
Methane	3.6	4.1
Nitrogen and argon	47.5	42.1
Carbon monoxide	16.5	15.1
Carbon dioxide	13.1	15.1
Hydrogen sulfide	0.1	0.1
Ethane +	0.6	0.6
Higher heating value, Btu/SCF	161.0	175.0

It is also of interest to calculate the thermal efficiency of this UCC test facility and compare it with results from a Lurgi gasifier; these data are shown in Table 2. The thermal efficiency is defined as the heating value of the "cold" gas recovered divided by the heating value of the coal reacted. Energy used for air compression or seam preparation (linking) is not included in this comparison. It is clear that the in situ thermal efficiency

(cold gas) is significantly higher than that for the Lurgi system (83% vs. 63%). One reason for this is that the Lurgi gasifier often uses excessive steam/air ratios in order to prevent slagging of the ash. Also higher production of tars and oils are experienced in the Lurgi gasifier. Other advantages to the UCG system include the natural insulation provided by the overburden, which yields lower sensible heat losses than for the cooling system used in a conventional gasifier. The process heat from a Lurgi gasifier can be re-used above ground, however. The fact that only a two-hole test system was used affected the reported efficiency for the Hanna test, since no significant gas leakage was experienced. Leakage problems will become more severe for a commercial-scale operation.

TABLE 2

Comparison of Heat Balances for In Situ and Conventional Gasifiers

<u>in situ</u>		<u>conventional</u>	
<u>in</u> coal (no air preheating or steam injection)	100.0%	<u>in</u> coal steam (air 250°F)	96.2% 3.7 <u>0.1</u> 100.0%
<u>out</u> produced gas (cold)	82.9%	<u>out</u> produced gas (dry, cold)	62.6%
tars and oils	5.0	sensible heat (1200°F)	10.3
sensible heat (512°F)	7.0	steam	1.9
hot ash	2.1	bottom ash (combustion + sensible)	1.1
heat loss to rock	<u>3.0</u>	dust, fines	3.2
	100.0%	tar and oils	12.9
		water jacket	3.4
		agitator cooling	1.5
		ambient losses	<u>3.1</u>
			100.0%

Typical efficiency data for a Russian commercial system are given in Table 3, showing a cold gas efficiency more comparable to conventional gasifiers⁴. Note that nearly ten per cent heat losses occur due to leakage; this figure is characteristic for steeply dipping seams. Gasification of horizontal seams exhibited less leakage, on the order of three to five per cent.

TABLE 3

Thermal Balance of the Gasification Process in Generator 5a-b In Seam IV Interior (9m Thickness) at Yuzhno-Abinsk from January 12, 1961 to January 31, 1961

Calorific value of the gas Q = 1300, to 1196 kcal/m³
 Gas Leakage = 10%
 Gas water content = 290 g/m³
 Relative blast intensity = 17 m³/hour per m²

- 1 - Heat of combustion of the dry gas = 69.9%
- 2 - Heat of combustion of leakage gas = 7.8%
- 3 - Heat content of the gas = 4.2%
- 4 - Heat content of leakage gas = 0.5%
- 5 - Heat content of water in the gas = 9.2%
- 6 - Heat content of humidity in gas leakage = 1%
- 7 - Heat content of the ash residue = 0.1%
- 8 - Losses to the surrounding medium = 7.3%
- 9 - Heat content of the dry coal
- 10 - Heat content of water in the coal
- 11 - Heat content of dry air blast
- 12 - Heat content of water introduced = 0.5%

} 0.1%

(Kreinin⁴)FAVORABLE TECHNICAL FACTORS FOR UCG

A number of factors which are conducive to application of UCG from a technical standpoint can be identified. In general it can

be remarked that the Western U.S. coals appear to be the most suitable coals for application of UCG. Unfortunately, most Western coals, e.g., those in Wyoming, while very attractive from a technical viewpoint, are hampered by their location. The utilization of Wyoming coal will depend upon development of suitable schemes for production of synthetic natural gas through UCG or in the production of petrochemicals such as ammonia or methanol. More efficient long distance transmission of electricity may also stimulate development.

The technical criteria for the successful utilization of a coal by UCG are listed below. These criteria can be grouped into three categories: those dealing with characteristics of the coal, those dealing with the overburden and other geological considerations, and those based on desirable operating conditions for the process.

Shrinking Coal

Most Western coals are shrinking coals in that they do not expand upon heating; this is extremely important in terms of maintaining a high flow rate at low pressures throughout the coal bed. For example, as these coals are heated, cracks open up and the structural integrity of the material is decreased, thus causing a large amount of reaction area to be exposed. On the other hand, most Eastern caking coals first expand upon heating, causing the internal pore structure to remain rather tight. In the presence of a confining pressure such as is experienced by coal at depth, crack formation due to gasification is restricted.

Highly Permeable Coal/Well Established Cleat System

Since it is necessary to establish air flow underground prior to gasification, a well developed cleat system will allow an air

path to be formed over reasonably long distances in order to link injection and production wells. As the coal is dried due to gas flow, the change in the matrix permeability significantly affects the flow characteristics through the bed. The removal of water by drying with heated air causes the coal permeability to increase, for example, from 10 millidarcies to 10 darcies. If the coal sample is heated further and partially devolatilized, then an increase in the matrix permeability by another factor of 100 to 1000 can be obtained. This latter permeability will be obtained after the backward burning step in UCG.

Reactive Coal

It is important that ignition be maintained in the system for high sweep efficiency and that the coal be susceptible to gasification. Lower rank coals are already partially oxidized; hence their gasification rates are higher at low temperature. Minimum temperatures for burning vary from 1100°F (lignite) to 1350°F (sub-bituminous) to 1550°F (bituminous).

The next three factors deal with the geology of the system. It should be recognized that there are some trade-offs involved in each of these factors.

Thick Seams

Data from Russian operations indicates that the thermal efficiency of the process is significantly affected by the seam thickness variable, due to varying rates of heat loss to the overburden. Figure 1 shows the combined effects of seam thickness and water influx on the heating value of the gas produced. Note that the heating value tends to level off at about a 5-foot seam thickness. Based on these data, a minimum seam thickness of 5 feet appears to

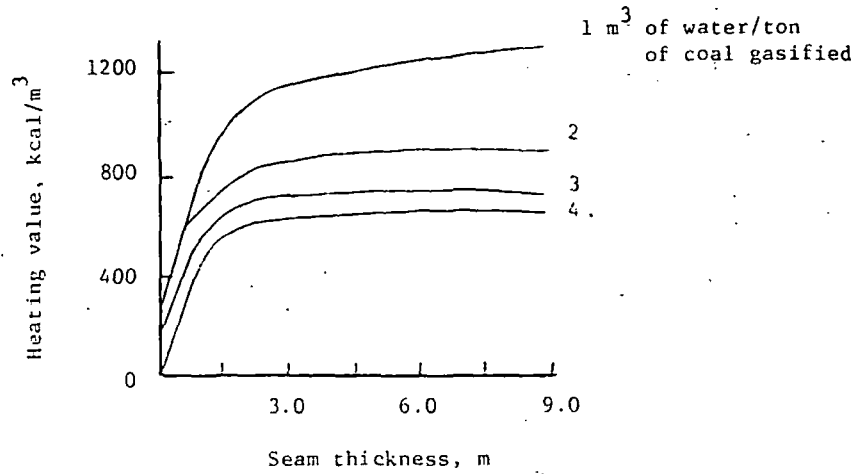


FIG. 1: Effect on Seam Thickness and the Specific Water Inflow into Gasification Zones on the Calorific Value of Gas Obtained by Underground Gasification

Source: Gregg et al.¹

be desirable for application of UCG. A maximum seam thickness might be dictated by the effects of large surface subsidence, which would cause excessive gas leakage and possible borehole damage. The effect of seam thickness on economics is discussed in a later section.

Water Influx

Water influx, if abnormally high, can be extremely detrimental to the operation of an UCG system. In the extreme, the reaction can be extinguished. Usually a significant degradation in the overall thermal efficiency of the process results from water intrusion. Figure 2 shows the typical relationship among thermal efficiency, water influx, and air injection rate. In each case, there is an optimum water/air ratio; for water influxes larger

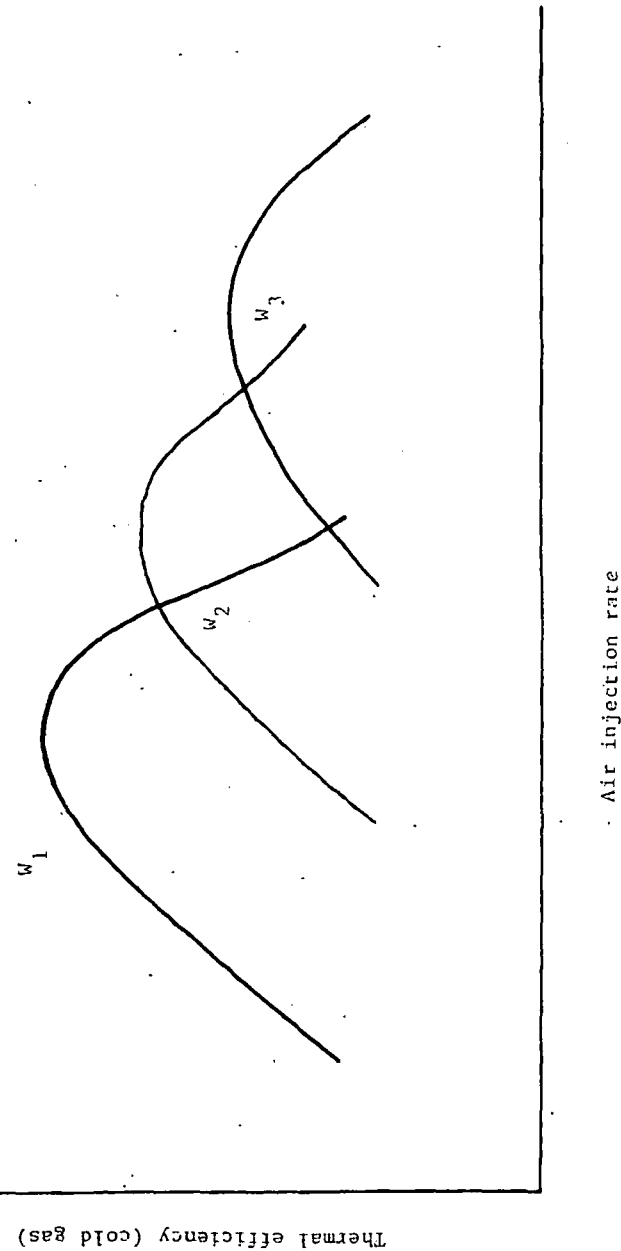


FIG. 2: Typical Variation in Cold Gas Thermal Efficiency with Air Injection Rate for Various Water Influx Rates; $W = \text{water influx rate } (W_1 < W_2 < W_3)$

than optimal, a large amount of energy is expended in vaporization and heating the water to the outlet gas temperature. As mentioned earlier, the Lurgi gasifier suffers from this inefficiency. The recent ERDA field tests in Wyoming have operated at nearly optimum water influxes, thus allowing that test to realize extremely high yields (as high as 175 Btu/SCF) and high thermal efficiencies. However, tests in the same location six months later experienced much higher water intrusion rates and hence lower product gas heating values (and thus thermal efficiencies). For extremely wet seams, it may be that gasification with oxygen is warranted simply as a way of minimizing the water intrusion rate relative to the gasification rate. Use of oxygen rather than air will result in higher gasification rates, and it is expected that water influx rate will be independent of the gasifying medium.

The water influx is also important from an environmental standpoint. In most underground systems, there is significant ground water, which, during gasification, intrudes into the seam. Therefore the possible environmental impact of subjecting this water to high temperatures and organic products from the gasification reaction must be considered. However, by operating the in situ gasifier at lower pressure than the hydrostatic pressure, some investigators believe that water will seep into the gasifier, carrying organic materials. In the gasifier, these organic materials are cracked to other hydrocarbons in the reaction zone and collected at the production well. The quantity of tars and oils collected during UCC tests is significantly lower than that from a Lurgi gasifier, indicating a thermal decomposition phenomenon.

Roof Collapse without Surface Subsidence

Roof collapse is at the same time beneficial and detrimental. As mentioned previously, increases in water influx and gas leakage can result from the collapse of the roof. On the other hand, roof collapse is desirable from the standpoint of having a thermally efficient operation, thus filling in any voids in the in situ

gasifier. This is because the presence of void space underground encourages the phenomenon of oxygen bypassing, in which carbon monoxide is oxidized to carbon dioxide. This results in a decrease in the heating value and a substantial increase in the outlet temperature of the gas, especially in thin seam gasification. The nature of the roof collapse depends upon the mechanical properties of the overlying strata and the geometry of the cavity. The collapse of the roof can lead to the formation of channels by-passing the gasification area. In addition, communication can be established with highly permeable or water bearing strata, which can lead to considerably higher losses of blast and gas from the in situ generator, or to a higher influx of ground water.

According to Skafa⁵ three types of changes in the state of the roof rock are distinguished:

The first type is represented by a sagging of the roof rocks without any substantial break in continuity. The gasified space is thus filled in, maintaining an approximately constant specific reaction surface of the coal in the gasification channel. This helps keep the characteristics of the blast and gas flow constant (Figure 3).

The second type is represented by collapse of the roof rocks with partial filling of the gasified space, due to the fragmentation of the roof rocks during their collapse. As a result, part of the gasified space is filled with rock rubble which divert the gas flow. This effect may have a favorable effect on the course of the gasification process, as in the case of the sagging roof (Figure 4), since the fragmentation and bulking of the rock yields an effective increase in volume of this material.

The third type is represented by a collapse of the roof rocks in which the specific reaction surface of the coal in the gasification channel is not kept at an approximately constant value. This gives rise to bypass channels for the blast and the gas (Figure 5), when successively larger surface area of the overburden is exposed to the hot gas. This type of collapse is undesirable.



FIG. 3: Character of the Filling of the Gasified Space due to Sagging of the Roof Rocks



FIG. 4: Character of the Filling of the Gasified Space by the Collapse of the Roof Rocks

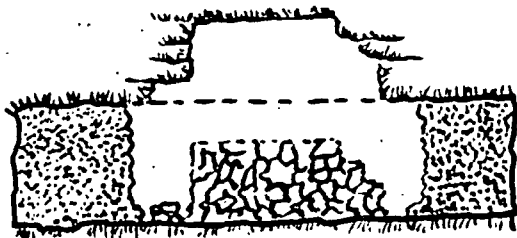


FIG. 5: Scheme of the Collapse of the Roof Rocks into the Gasified Space without Considerable Breakdown of these Rocks.

Surface subsidence is not desirable, but in unpopulated areas, this is not a serious problem. The scale of subsidence depends upon seam thickness and depth. Thick seams at reasonably shallow depths below the surface should exhibit some surface subsidence

eventually. For small scale field tests, the effect of surface subsidence should be negligible.

The final four factors deal with operational parameters for the process.

High Throughput

It is desirable to maximize the gas production rate from a given in situ gasifier. In previous field tests and in the Russian literature, it has been shown that high throughput can ameliorate the negative effects caused by water influx, as shown previously in Figure 2. High throughput is made possible by proper seam preparation, i.e., thorough drying and reverse combustion.

Low Pressure Operation

Previously it has been pointed out that low pressure operation reduces gas leakage and also minimizes the potential of groundwater contamination by organics. On the other hand, low pressures result in higher water intrusion rates. Hence for a given location, the operating pressure and flow rate must be balanced against gas leakage and water influx, and ultimately thermal efficiency. The allowable pressures are a function of the depth and hydrostatic pressure at that point. Pressures must be elevated above 300 psi before significant amounts of methane can be produced through gasification (this does not rule out production of methane by coal pyrolysis). Therefore, if low Btu gas is the desired final product, high pressure operation does not appear to be justified. However, another consideration is the ultimate use of the gas, e.g., if it is to be burned in a gas turbine, the gas pressure can be an important determinant of conversion from thermal to electrical energy.

Maximum Sweep Efficiency

Historically, sweep efficiencies during UCG have varied from 10% to nearly 90% (sweep efficiency is defined as the coal contacted or reacted over a large area of operation). The Russians appear to have achieved almost complete contacting of the coal, and they did not leave any coal underground deliberately. Another factor to consider here is the recovery per hole drilled, i.e., what is the region of influence for a given set of injection and production holes. A maximum sweep efficiency corresponds to a minimum cost operation. Russian experiments with borehole spacing indicated that it affected sweep efficiency. For example, for 25 meter spacing, a coal recovery of 83 per cent resulted, while for a 40 meter spacing the fractional recovery dropped to 63 per cent. It is interesting to note, however, that experiments with oxygen enrichment gave higher sweep efficiencies than those obtainable with air injection (Gregg et al.¹). This indicates that the extra capital and operating costs incurred by an oxygen plant may be offset by higher sweep efficiencies and higher product gas heating values (but not higher thermal efficiencies).

Consistent Gas Production

Historically, a declining heating value has been a recurrent problem in many field tests. Relatively uniform heating values are required for utilization of the gas. The Russians developed a system which gave consistent heating value for the gas produced; this consistency was due to the well sequencing used¹ and the initiation of gasification at the bottom of the seam, which creates a rubble zone of coal particles, much as in a surface coal gasifier.

ULTIMATE, PROXIMATE ANALYSES

In Table 4 is a list of typical physical and chemical properties for a Western lignite. Possibly the most significant physical property of lignite is the relationship between its heating value and the per cent moisture. As is well known, lignite has a fairly low heating value and is a low rank coal; however, if all the

TABLE 4

Representative Composition of Western Lignite (As Received)

<u>Proximate Analysis</u>		<u>Ultimate Analysis</u>	
Fixed carbon	27.2%	Carbon	44.9%
Ash	11.7%	Hydrogen	3.4%
Water	25.4%	Oxygen	13.2%
Volatiles	34.5%	Nitrogen	.2%
Sulfur	1.2%	Sulfur	1.2%
Heating value	7500 Btu/ll	Ash	11.7%
		Water	25.4%

moisture were removed from the lignite, then a significant upgrading of the heating value would result. Usually, moisture from the coal is removed downstream from the gasification area, and this removal of water results in a lowering of the temperature of the exit gas. Therefore, the thermal efficiency of in situ gasification will be lowered somewhat by the natural water content, although the precise amount depends upon the water influx to the gasifier. Based on the heat of vaporization of water, a reduction in thermal efficiency of 3 to 4 per cent would be expected for the lignite composition shown in Table 4.

The ash components in lignite are also reasonably high compared to other U.S. coals; however, ten per cent ash does not pose any particular problem from the standpoint of underground gasification. Usually the ash of Western coals does have a relatively low ash fusion point, and thus it is expected that some of the ash will be slagged during gasification due to the high temperatures involved.

The Russians found that coals with ash contents varying from zero to 50 per cent could be successfully gasified. They found in

some cases the optimum ash content to be about 40 per cent. The occurrence of an optimum is due to several competing effects:

- (1) the existence of less void space underground for higher ash coals, which minimizes oxygen bypassing.
- (2) the catalytic effect of ash as a function of the actual amount.
- (3) inhibition of gas-solid contacting for high ash contents, yielding lower reaction temperatures.
- (4) heat loss due to hot ash left underground.

Some Western lignites and sub-bituminous coals contain a low to moderate sulfur content and will not satisfy the new source performance standards for stack gas emissions when burned in a boiler, except when some means of sulfur dioxide control is exercised. Because of the low heating value of this particular lignite, an apparently low percentage of sulfur actually corresponds to a somewhat higher value on the basis of pounds of sulfur per million Btu of coal to the boiler. One of the advantages of underground coal gasification is that it operates in a reducing atmosphere, i.e., the sulfur is converted to hydrogen sulfide (H_2S) and carbonyl sulfide (COS), both of which can be readily removed from the gas stream upon cooling using commercially proven technology. This, however, is not true when the coal is combusted in an oxidizing atmosphere, and the sulfur is produced as sulfur dioxide, which has been proven to be very difficult to separate from other gas constituents. There is also evidence from the Hanna UCG experiment that approximately one-half of the sulfur is left underground, indicating that the ash retains a significant amount of sulfur during gasification.

The per cent volatiles is a measure of the amount of hydrocarbons which are trapped in the coal matrix. If coal is heated in the absence of air, hydrocarbons such as methane, ethane, and

A recent study (Edgar et al.⁶) at The University of Texas at Austin has evaluated the economics for in situ gasification of Texas lignite. A UCG facility capable of servicing a 1,000 MW generating plant was assumed, using a forty per cent gas to electric conversion (combined cycle power plant). The "quick" cost estimation procedure given by Peters and Timmerhaus⁷ has been used for preliminary cost estimates. This procedure involves ratios of total capital investments to purchased process equipment costs, using past experience with these ratios. The accuracy of these estimates varies from approximately 20 to 30 per cent. This costing scheme has been found to be successful for estimating economics of coal gasification plants. The chemical engineering plant construction cost index was used to escalate published process equipment costs to 1976.

The sizing of the linkage compressor units was based upon an average depth (1,000 feet deep and a six foot coal seam). Operating cost of linkage is basically the power charge for air compression. The pressure required for linkage is estimated to be one-half psi per foot of overburden. This is based on the assumption that a static column of groundwater is present above the air injection horizon up to the surface and sufficient pressure is to be applied to permit air flow through the wet seam. The total cost of linking increases with an increase in overburden height because of the increased air pressures required for linking. It decreases with increasing seam thickness. This is because of the reduction in the size of the operation field for thicker seams. The capital investment for linking compressors, computed at an average seam thickness of 6 feet and a depth of 1,000 feet is \$2.5 million and operating costs vary from \$0.35 to \$7.0 million per year, depending upon depth and seam thickness.

Gasification air to the generators is supplied by centrifugal compressor units at a pressure of 50 psig. The sizing of the

aromatic compounds are produced. This carbonization behavior is important not only in predicting the yield which will be obtainable from underground coal gasification, but also in assessing the types of hydrocarbons produced underground and how they might affect the subsurface environment. The 30% figure given in Table 4 is rather high in comparison with other U.S. coals. In UCG pyrolysis generally occurs downstream from gasification, and the pyrolysis products are essentially additive with gasification. Pyrolysis can thus enhance gas heating values by as much as 50 Btu/SCF.

In the ultimate or atomic analysis of Western coal, one important factor is the per cent oxygen. It should be recognized that the lignite described in Table 4 contains a rather high per cent oxygen, which is indicative of its high reactivity as well as the fact that it is already partially oxidized and extremely susceptible to further oxidation or gasification. It is well known that lignite, upon drying, can undergo spontaneous combustion without external ignition. This high reactivity is a tremendous advantage in terms of operating an in situ gasifier, as discussed earlier.

FAVORABLE ECONOMIC FACTORS IN UCG

The economics of in situ gasification depend primarily on the thermal efficiency of the process and the fractional recovery of the coal seam. A high recovery efficiency increases the net value of the low Btu gas by making more efficient use of the holes drilled. Other factors can be cited:

- (1) A high natural coal permeability would yield significant cost savings in two areas. Fracturing is obviated, and the well density can be much lower, thus lowering the drilling costs tremendously.
- (2) Thick seams and the existence of multiple seams would

yield a high energy content per well drilled, thus saving drilling costs and making the necessary operating field much smaller in size. On the other hand, the magnitude of subsidence for very thick seams may result in increased drilling cost per foot of depth.

- (3) Above ground coal processing equipment and gasifiers, which contribute one-fourth of the total costs of the produced gas in the Lurgi process, would be eliminated.

The depths at which in situ gasification can be applied are dependent upon drilling costs and technology. Current drilling and completion costs probably limit its application to less than 2,000 feet. For a 1,000 MW plant, a six foot coal seam, and a fifty per cent recovery of coal as low Btu gas, an areal extent of 1.0 to 1.5 square miles per year would need to be gasified, depending upon the conversion efficiency of the electric plant.

There appear to be several modes of utilization for low Btu gas produced by UCG:

- (1) Direct combustion to produce electricity: Projected improvements in gas turbine generators (combined cycle) would yield efficiencies approaching 50% (compared with 37% in conventional power plants) with low Btu gas from UCG.
- (2) Direct heating in industrial processes: Low Btu gas could replace natural gas for direct firing of industrial processes.
- (3) Chemical feedstock: Much of the petrochemical industry now requires liquid petroleum or natural gas as a starting point for the manufacture of chemicals. The low Btu gas could serve as a basic building block for the production of organics. Gasification with pure oxygen is a necessity in this application.

A recent study (Edgar et al.⁶) at The University of Texas at Austin has evaluated the economics for in situ gasification of Texas lignite. A UCG facility capable of servicing a 1,000 MW generating plant was assumed, using a forty per cent gas to electric conversion (combined cycle power plant). The "quick" cost estimation procedure given by Peters and Timmerhaus⁷ has been used for preliminary cost estimates. This procedure involves ratios of total capital investments to purchased process equipment costs, using past experience with these ratios. The accuracy of these estimates varies from approximately 20 to 30 per cent. This costing scheme has been found to be successful for estimating economics of coal gasification plants. The chemical engineering plant construction cost index was used to escalate published process equipment costs to 1976.

The sizing of the linkage compressor units was based upon an average depth (1,000 feet deep and a six foot coal seam). Operating cost of linkage is basically the power charge for air compression. The pressure required for linkage is estimated to be one-half psi per foot of overburden. This is based on the assumption that a static column of groundwater is present above the air injection horizon up to the surface and sufficient pressure is to be applied to permit air flow through the wet seam. The total cost of linking increases with an increase in overburden height because of the increased air pressures required for linking. It decreases with increasing seam thickness. This is because of the reduction in the size of the operation field for thicker seams. The capital investment for linking compressors, computed at an average seam thickness of 6 feet and a depth of 1,000 feet is \$2.5 million and operating costs vary from \$0.35 to \$7.0 million per year, depending upon depth and seam thickness.

Gasification air to the generators is supplied by centrifugal compressor units at a pressure of 50 psig. The sizing of the

units is based upon the air flow rates used in the Hanna field tests. The compressor capital investment and operating cost for gasification were assumed to be independent of depth and seam thickness. Installed costs of the centrifugal compressors were estimated to \$3 million and operating costs to be \$3.6 million. Gas cleanup (hydrogen sulfide and particulates) costs are estimated to be \$48 million.

The annual cost of drilling varies from about \$25 to \$30 per foot drilled, depending upon the depth. Capital costs vary from \$5.5 million to \$97 million, depending upon the depth of drilling and the seam thickness. Working capital is assumed to be 2.5 per cent of total property, plant, and equipment, including startup. Startup is estimated as 25 per cent of the total annual operating costs plus \$1.5 million for drilling materials for initial operation. Total capital investment for 6 foot or thicker seams for the delivery of clean low Btu gas from UCG is on the average about \$200 million. Note that this capital investment is much lower than that required for comparable surface gasification plants. The trade-off in this case is the higher operating costs per year, due to drilling costs.

Figure 6 shows the projected cost in cents per million Btu of a clean low Btu gas (hydrogen sulfide and particulates removed) as a function of seam thickness and depth beneath the surface of the earth. The utility financing method was used. As can be seen from the figure, the cost of the gas produced appears to level off at approximately a six-foot seam thickness, which is mainly due to a diminishing of relative drilling costs. It is apparent from the figure that for underground coal gasification a low Btu gas can be produced competitively for overburden to seam thickness ratios approaching 150 to one and possibly even higher. For strip mining, one might forecast that the economic overburden to seam thickness ratio might approach fifteen to one in the future. Thus a tenfold

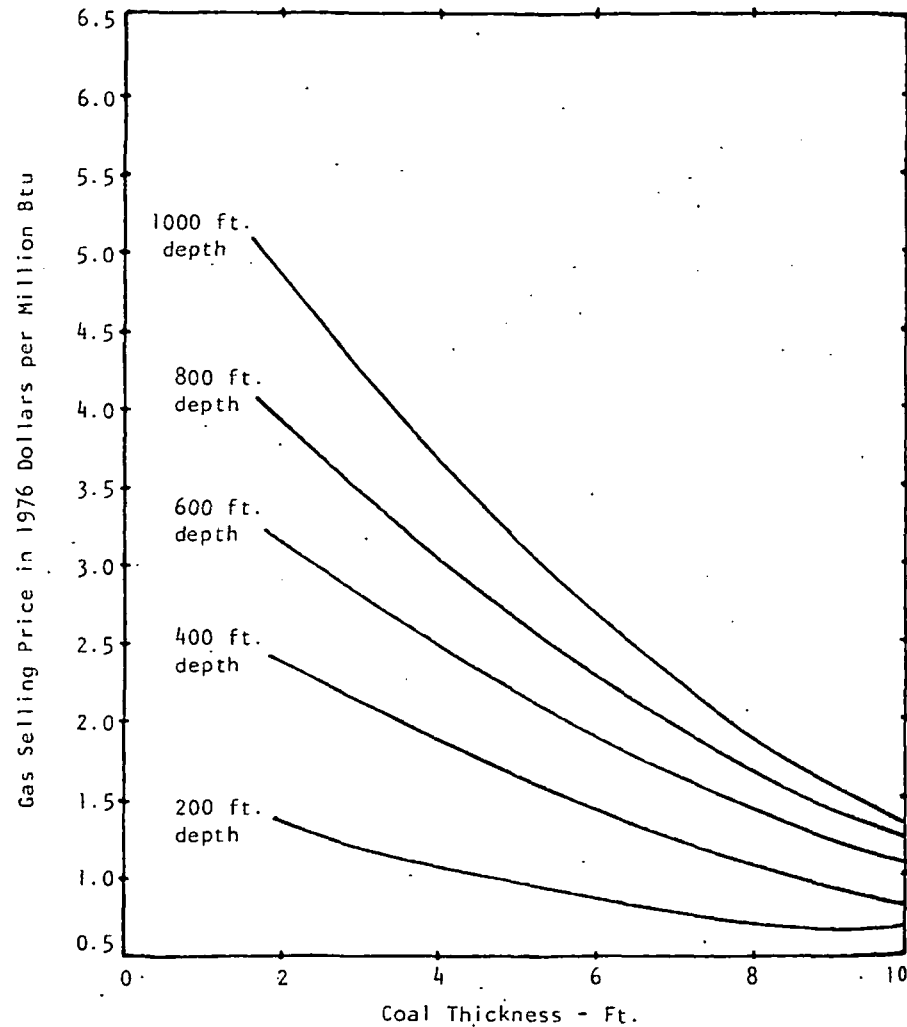


FIG. 6: Gas Selling Prices with Height of Overburden as a Parameter

enhancement in economic recovery potential is offered by in situ gasification. A key assumption in the development of these curves is the borehole spacing of 75 feet by 75 feet, which is that normally used in the Russian operations. It is obviously desirable to maximize the borehole spacing, since the amount of energy recovered per hole drilled is the most significant economic factor in underground coal gasification. A number of other economic studies^{8,9,10,11} on underground coal gasification have been performed and are in general agreement with the above data.

Other assumptions made in the economic analysis include a gasification efficiency of 60 per cent and a contact efficiency of 80 per cent, thus giving an overall resource recovery of 48 per cent. This means that 48 per cent of the latent energy available in the coal underground is recovered in the form of a low Btu gas. These data are representative of the Russian commercial operations. The heating value of the gas produced during underground coal gasification is directly related to the thermal efficiency of the process and varies with the moisture content, heating value, and volatile content of the coal gasified, water influx, and gas leakage, as discussed earlier.

ENVIRONMENTAL ASPECTS OF UCG

In situ gasification overcomes many of the objectionable environmental features of strip and deep mining. As previously mentioned, the sulfur in the lignite is principally converted to hydrogen sulfide, which is readily removed from the product gas stream. Pollution by solid waste is reduced, since inert ash material is left underground. Massive excavation of the overburden is avoided, although the close well spacing does create some surface damage. On the other hand, UCG does present water pollution problems in the subsurface environment.

Because gasification will sometimes be carried out in a fresh water environment, the potential threat of ground water contamination is the environmental aspect of greatest concern. Possible pollutants freed during gasification include phenols, tars, ammonia, and sulfur compounds. Russian field data has indicated the presence of these compounds in produced water from the gasification area, especially in steeply dipping seams. However, little is known at this time about the potential accumulation of pollutants underground.

Important hydrologic parameters in site evaluation include transmissivity, hydraulic conductivity and gradient, water chemistry, sand grain size and sorting, and porosity. Regional areas where water productivity (transmissivity) and mobility (hydraulic conductivity) are relatively low appear to be attractive. A hydrologically ideal site is characterized by coal seams roofed and floored by thick mud, a low sand environment, saline waters, and a strike oriented depositional system. Potential sites, upon evaluation of exploratory drilling and hydrologic testing, can be compared with the ideal site.

Low values of transmissivity and hydraulic conductivity will correlate with low sand environments. Low sand environments will give decreased rates of gas leakage and water influx. For Texas lignite, both the Wilcox Group and Yegua Formation, at exploitable depths, are dip-oriented channel systems. Transmissivity and hydraulic conductivity of channel sands parallel to regional flow vary directly with thickness. Thick, coarse-grained, areally extensive channel sands are found in the Wilcox. Transmissivities range from 30 to 2,000 $m^3/day/m$; conductivities 1 to 20 $m^3/day/m^2$. Average ground water velocities, calculated using Darcy's law divided by porosity, range from 0.3 to 49 m per year. Obviously, values at the low end of the ranges cited are desired for aquifers subject to the greatest impact from gasification, that is, those

immediately overlying lignite. At the maximum velocity, the most mobile toxic species would take 200 years to travel 10 km.

Yegua sands are thinner, finer-grained, poorer sorted, and less areally extensive. Because permeability in unconsolidated sediments is largely a function of grain size and sorting, Yegua permeabilities are considerably less than those of the Wilcox. For these reasons the Yegua is only locally an aquifer. From a hydrologic standpoint, therefore, Yegua lignite is superior to Wilcox lignite for gasification. Overall ground water productivity and mobility are low for the Yegua. Lower mobility means pollutants would be localized and more easily treated. Furthermore, because the Yegua has some strike oriented elements, ground water movement is further restricted. In sands normal to regional flow, movement is greatly impeded and there is much less flushing by fresh water.

It should be emphasized that there is very little quantitative data on the generation of pollutants underground and the potential dispersion of the various species present. The potential of natural cleanup by the subsurface and dilution of the pollutants by ground water is still unknown. Therefore, procedures for the a priori environmental evaluation of potential UCG sites are still ill-defined.

ACKNOWLEDGMENTS

Financial support for the study of underground gasification of Texas lignite has been provided by the National Science Foundation (RANN Program) and private industry (ARCO, Conoco, Dow Chemical, E. I. Du Pont de Nemours, Enserch, Mobil, Shell, and Texas Utilities.)

REFERENCES

1. Gregg, D. W., Hill, R. W., and Olness, D. N., "An Overview of the Soviet Effort in Underground Gasification of Coal," UCRL-52004, Lawrence Livermore Laboratory, January, 1976.

2. Elder, J. L., "The Underground Gasification of Coal," in Chemistry of Coal Utilization, Lowry, N. N. (Ed.), Wiley, New York, 1963.
3. Fischer, D. D., and Schrider, L. A., "Comparison of Results from Underground Coal Gasification and from a Stirred-Bed Producer," National AIChE Meeting, Houston, March, 1975.
4. Kreinen, E. V., "Various Factors Affecting the Calorific Value of Gas Produced by Underground Gasification of Coal," Tr. Vses. Inst. Podz. Gazif. Uglei (UCRL-Trans-10802), 12, p. 3, 1964.
5. Skafa, P. V., "Underground Gasification of Coal," Gosudarstvennoe Nauchno-Tekhnicheskoe Izdatel'stvo Literaturny Po Gornomu Delu (UCRL-Trans-10880), Moscow, 1960.
6. Edgar, T. F., Kaiser, W. R., Thompson, T. W., Humenick, M. J., and Gray, K. E., "In Situ Conversion of Texas Lignite to Synthetic Fuels," Semi-Annual Report, The University of Texas, Austin, January, 1977.
7. Peters, M. S., and Timmerhaus, K. D., Plant Design and Economics for Chemical Engineers, McGraw-Hill, New York, 1968.
8. Jennings, J. W., "Some Economic Considerations of Underground Coal Gasification," SPE 5429, presented at the Northern Plains Section Regional Meeting of the SPE of AIME, Omaha, Neb., May 15-16, 1975.
9. Moll, A. J., "The Economics of Underground Coal Gasification," presented at the Second Underground Coal Gasification Symposium, Morgantown, W. Va., Aug. 10-12, 1976.
10. Garon, A. M., "An Economic Evaluation of Underground Coal Gasification," presented at the Second Underground Coal Gasification Symposium, Morgantown, W. Va., Aug. 10-12, 1976.
11. Buder, M. K., Fisher, R. A., McCone, A. I., Terichow, O. N., and Wong, M. J., "Factors Influencing the Economics of Large-Scale In Situ Coal Gasification Operations," presented at the Second Underground Coal Gasification Symposium, Morgantown, W. Va., Aug. 10-12, 1976.

IN SITU HIGHLIGHTS

THE VAIL CONFERENCE ON IN-SITU LEACHING OF URANIUM

D. A. Shock
233 Virginia
Ponca City, OK 74601

A significant conference on in-situ uranium leaching was held August 24-27, 1976, at the Manor Vail Lodge, Vail, Colorado, under the joint sponsorship of the AAPG, SME, and SPE. Approximately 100 attendees gathered to hear and discuss the following papers:

1. Hunkin, G. G., "Review and Status of Technology of In-Situ Leaching of Uranium."
2. Frank, J. N., and Klemenic, John, "Economics of Producing Uranium by Solution Mining."
3. Potter, R. W., III, and Brooks, R. A., "The Geological and Geochemical Parameters Affecting In-Situ Leaching of Uranium Deposits."
4. Olson, J., and Tweeton, D., "Mining Research for Improved In-Situ Extraction of Uranium."
5. McKee, C. R., and Hanson, M. E., "Predicting and Controlling Fluid Movement During In-Situ Uranium Extraction."
6. Sissler, F. D., "Geomicrobiological Leaching Processes for Uranium Ores."
7. Coode, A., "Recovery of Uranium by Bacterial Leaching of Broken Ore In-Situ."
8. Oakes, A., "Recovery of Uranium by Bacterial Leaching of Broken Ore In-Situ."
9. Buma, G., "Case History of In-Situ Leaching Field Testing."
10. Jacobson, R. H., and Hutterer, G. W., "Development of the Pawnee Ore Body."

SUBJ
MNG
TGCB

The Gabon and Congo Basins Salt Deposits

P. A. C. DE RUITER

Abstract

The Lower Cretaceous salt deposits of the Gabon basin and Congo basin were laid down on top of an Early Cretaceous-Late Jurassic, continental graben fill that represents the rifting phase of the Afro-American continent. The salt is characterized by high percentages of potash and magnesium salts and a scarcity of sulfates and carbonates. The salt probably originated from a brine that was already enriched in highly soluble salts before entering the Gabon-Congo basins. Their low-solubility equivalents are found in the Cuanza basin of Angola. Commercial mining of the potash salt is only possible in those onshore areas where it is essentially undisturbed, shallow, and of the right chemical composition. These conditions are met in the Congo where the Holle mine production comes from rich sylvinitic deposits.

Introduction

CRETACEOUS salt deposits were discovered in Gabon in 1935 by one of the earliest oil exploration wells. The first potash salt was encountered in 1948 and a systematic search was launched by a French consortium in 1954. However, the Gabon basin proved disappointing because of the very high degree of salt doming and in 1960 a new company started to look for the same salts in a more favorable area, the Congo basin, where oil exploration wells had also given good potash shows. An extensive shallow drilling campaign confirmed that exploitable sylvinitic deposits were present and production started in 1969. The present paper intends to sketch the geologic setting of the Gabon-Congo salt basins and to describe the interesting salt section in some detail.

Apart from a comprehensive review of the salt basin by Belmonte et al. (1965) and a description of the Holle salt mine in the Congo by Lambert (1967) and Depege (1967), there is no specifically salt-oriented literature available on this area. In fact most of the geological data are provided from the results of the exploration for oil; the most recent general description was given by Brink (1974). Fortunately the salt was extensively logged in a few oil exploration wells to which the author has had access; this allows a reasonably accurate description and discussion of the origin of the salt deposits.

Regional Geological Setting

The Lower Cretaceous salt deposits of the western continental margin of Africa are confined to the Douala basin (Cameroun), the Gabon basin, the Congo basin (Congo, Zaïre, Angola), and the Cuanza basin (Angola). These four basins together make a mega-unit which was described by Lehner and de

Ruiter (1977) as the area bounded to the north by the Cameroun slope anomaly and to the south by the Walvis Ridge (Fig. 1).

The present-day salt distribution (Fig. 2) indicates that these basins were connected at the time of salt deposition. The wide extent of the salt deposits oceanward was first suggested by Baumgartner and van Andel (1971) and was confirmed by later seismic surveys. Some high-quality data even suggest that the salt may not be confined to areas of continental crust only but may also overlie oceanic basement.

The salt separates an underlying continental sequence from an overlying marine section. The pre-salt continental clastics were deposited prior to and during the rifting phase of the Afro-American continent. The post-salt marine units accumulated during the general subsidence of the continental margin of Africa.

Stratigraphy (Figs. 3 and 4)

Pre-rift sediments: Permian to Middle Jurassic, continental clastics were found in outcrop in the northeastern part of the Gabon sedimentary basin and were described by Jeardine et al. (1968). These deposits can be considered to represent the remains of a pre-rift sequence laid down on a stable shield then embracing Africa and South America.

Rift sediments: Loosely called the "Cocobeach Group," these sediments are continental clastics of greatly varying depositional environment. Fault-controlled thickness differences and synsedimentary tilting is characteristic. Their fresh-water environment is indicated by the ostracod faunas. The "Lower Cocobeach" (Upper Jurassic-Neocomian) consists largely of relatively deep-water, lacustrine shales with occasional turbiditic sands. It is in places underlain by a sandy unit that overlies basement rock.

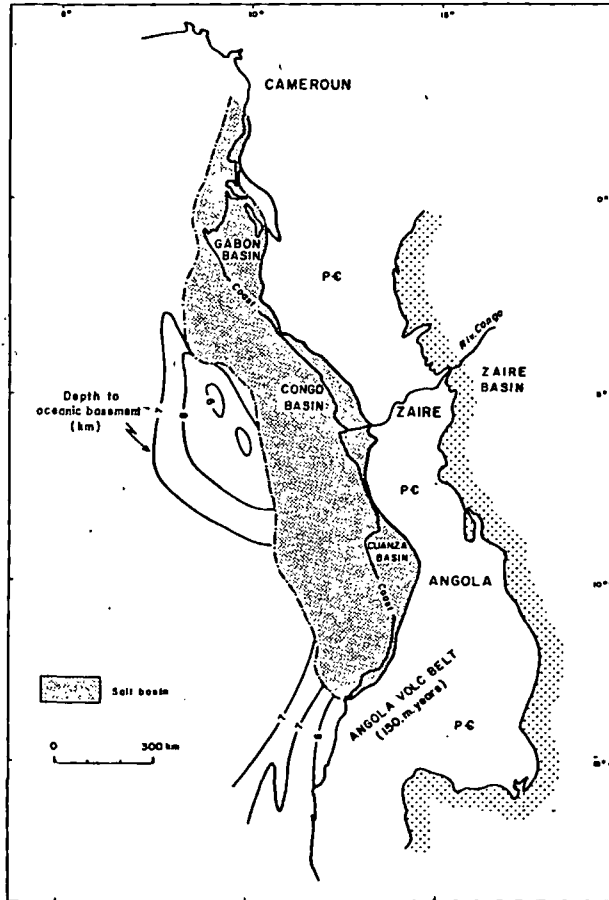
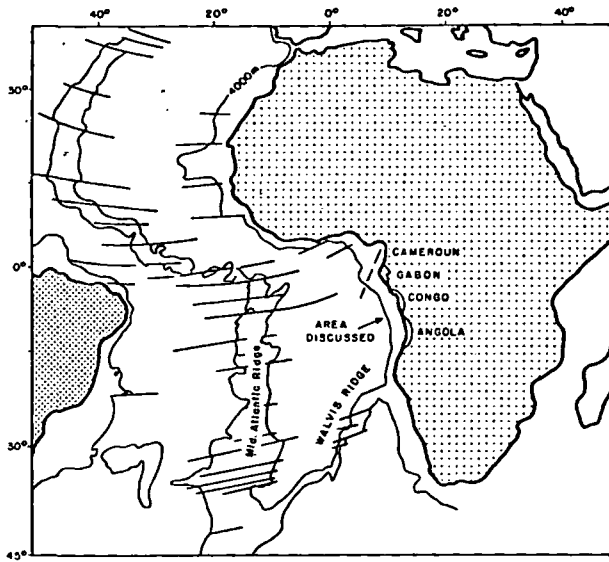


FIG. 2. Outline of the Cameroun-Gabon-Angola salt basin. The shape of the depth contours of the oceanic basement suggests that the outer portion of the salt basin may be underlain by oceanic basement.

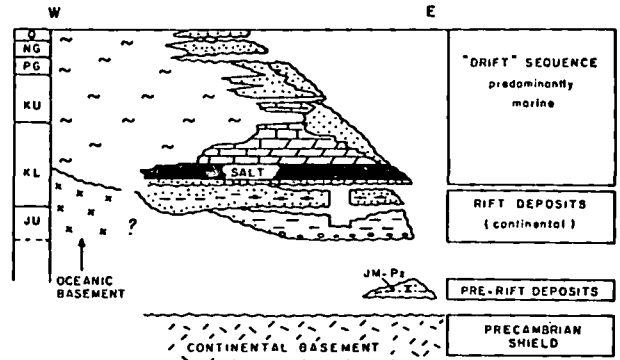


FIG. 3. Stratigraphy of the Gabon sedimentary basin.

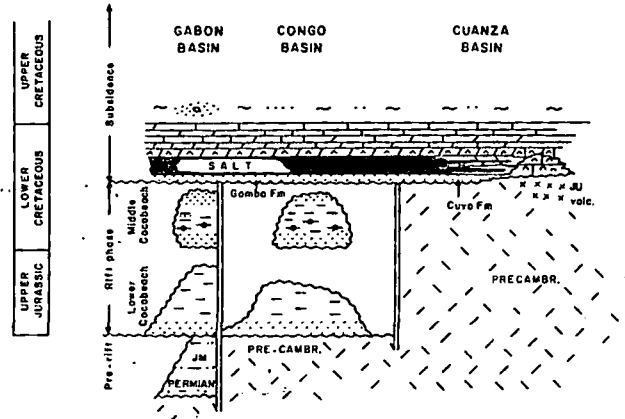


FIG. 4. Comparison of the Mesozoic stratigraphy of the Gabon, Congo, and Cuanza basins (Angola). It appears that the Cuanza basin developed only after the rift phase, whereas in the Gabon and Congo basins several thousands of meters of continental clastics were deposited during the rift phase.

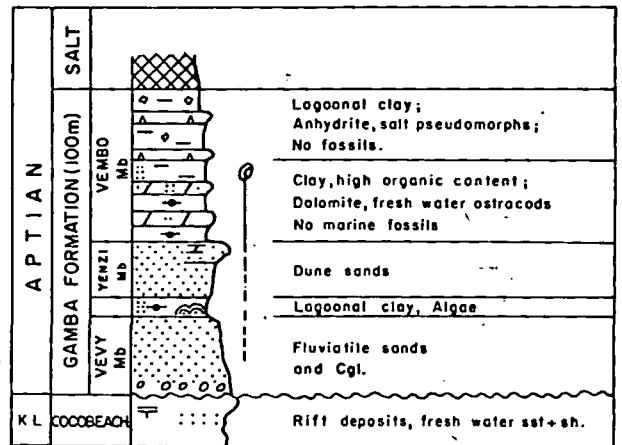


FIG. 5. The Gamba Formation in the Gabon basin. The unit represents the first postrift deposits. The upper part of the Vembo Member is transitional toward the overlying Salt Formation, but restricted conditions set in earlier (oil shales).

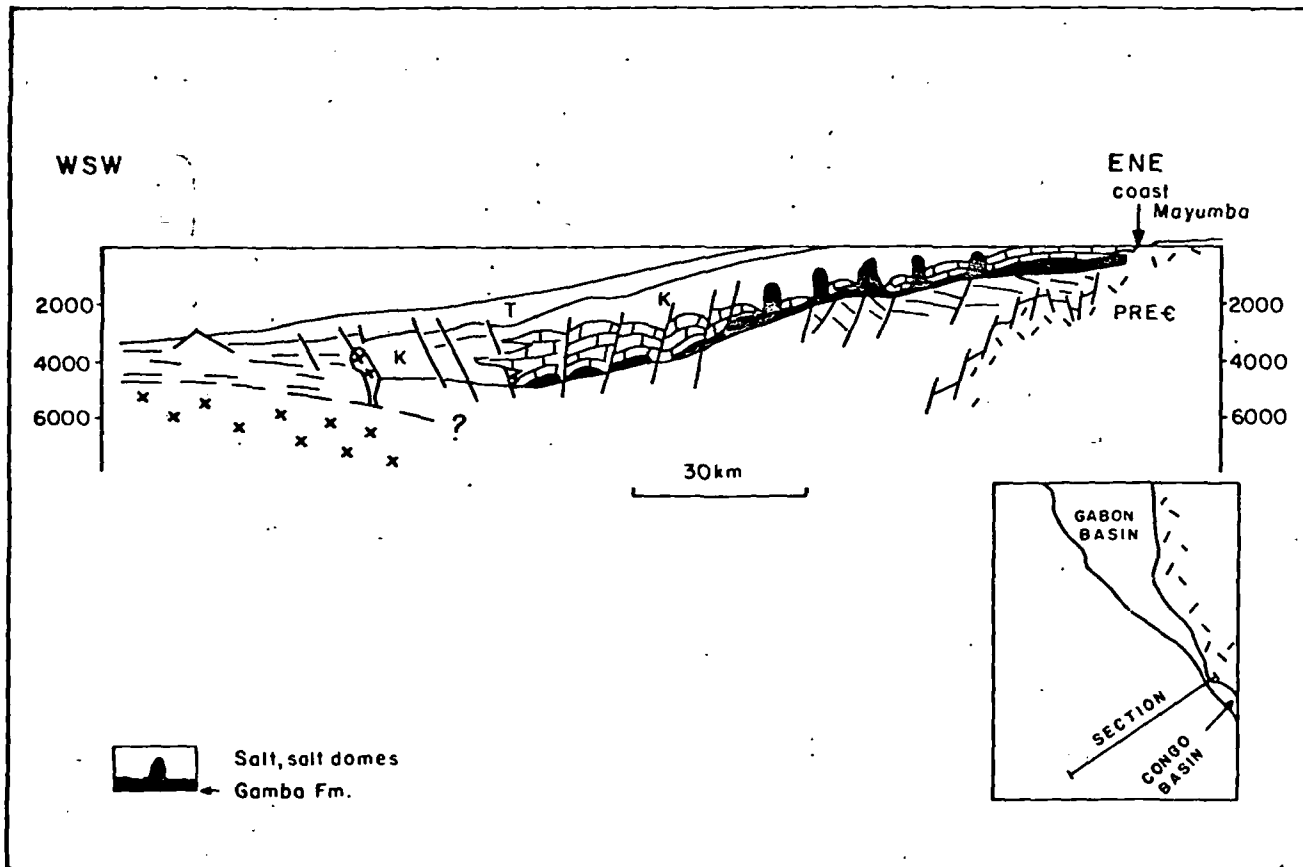


FIG. 6. Cross section through the Gabon-Congo basins. Note the eastern part of the salt which is nearly undisturbed as is the case over most of the Congo basin.

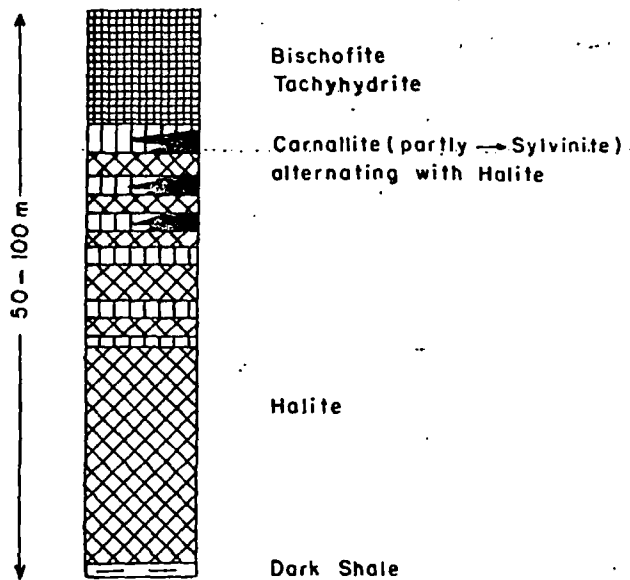


FIG. 7. The salt cycle as described by Belmonte et al. (1965). This cycle is "normal" in the sense that it shows a gradual increase upward of salts of high solubility.

The "Middle Cocobeach" is made up of a thick sedimentary cycle with sandstones at the bottom and at the top. These high-energy environments are separated by a thick shale section containing up to 100 meters of oil shale, deposited in a restricted and clastic-starved environment. The top and bottom of this cycle are marked by a regional unconformity.

Post-rift sequence: The rifting phase was concluded by a phase of faulting, tilting, and subsequent peneplanation. A new cycle of deposition commenced during the Aptian. Its development was governed by two dominating factors: the gradual appearance of salt water by the newly established connection with the oceans and subsidence along the continental margin. A salt formation, together with the underlying transgressive Gamba Formation, makes up the basal part of the post-rift sequence. The salt is overlain by an increasingly fully marine sequence of Albian-Cenomanian carbonates (Madiela Formation of Gabon) and Cenomanian to Recent clastics. A major regional break is recorded at the base of the Miocene.

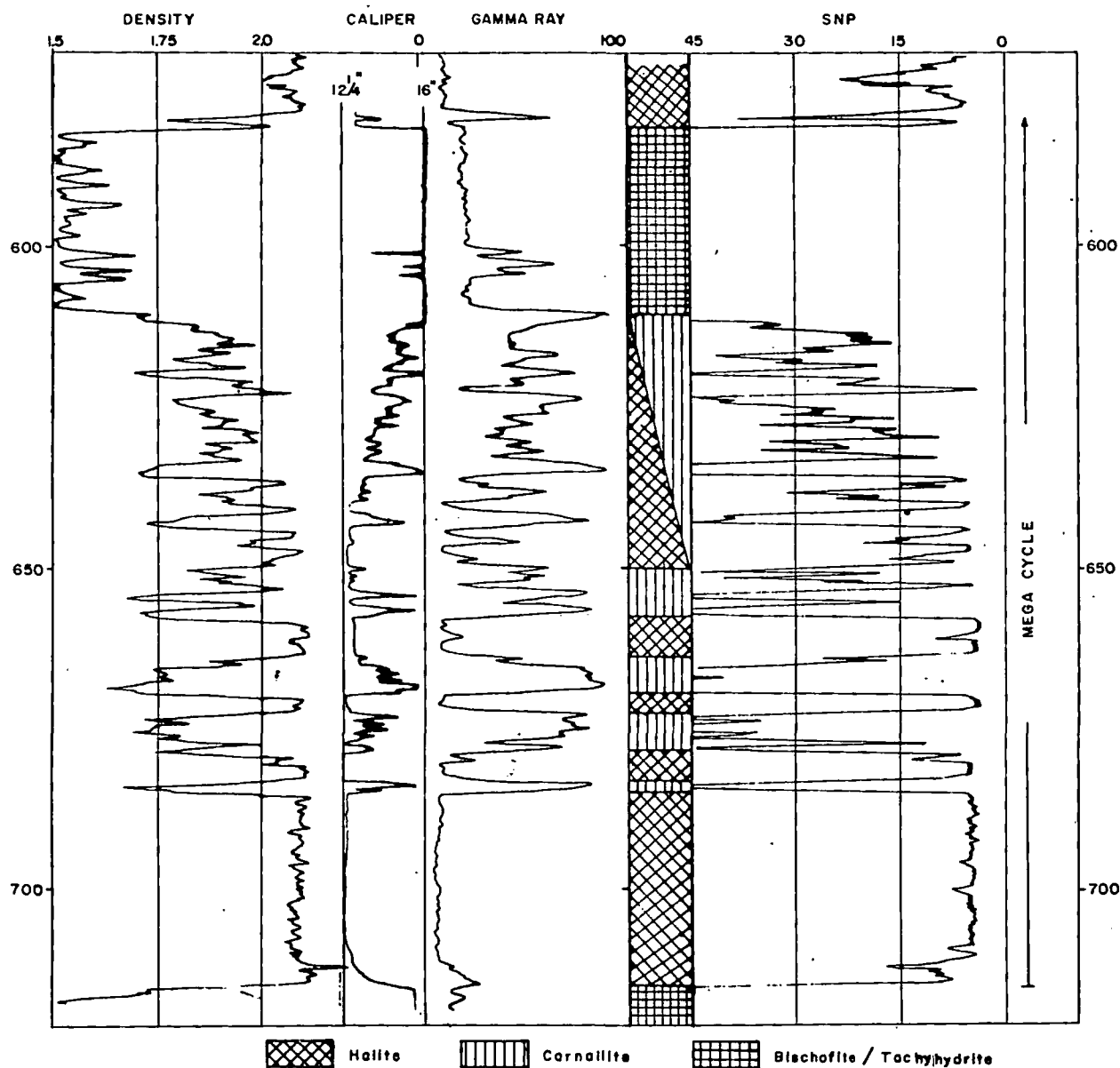


FIG. 8. A normal salt cycle. The cycle stands out clearly on the caliper log. Note that the logs probably read irrelevant values opposite the large washout over the bischofite interval. SNP = standard neutron porosity.

The Salt Basins

Transitional deposits

The salt deposits of the Gabon and Congo basins separate two essentially different phases: a terrestrial clastic graben fill (rifting phase) and a stage of regional subsidence under marine conditions. The earlier phase of the regional subsidence can be studied in detail by examining the well-known Gamba Formation (Aptian). This clastic unit, less than 100 m thick, grades upward into salt, and its upper part can be considered as the basal part of the lowest salt

cycle (Fig. 5). In structural style it differs from the rift sediments (Fig. 6); it is essentially a westward-dipping monocline, occasionally interrupted by reactivated horst blocks of the rift phase. The Lambaréné horst and the Gamba horst are examples of such reactivated horst blocks.

The Gamba Formation may rest on basement or any of the rift phase sediments. The lower fluviatile sands may be absent over paleohighs, but by the time the Vembo Shales were deposited the area was remarkably flat. This Vembo Shale consists of dolomitic shale, dolomite, and, toward the top, layers of an-

hydrite and salt pseudomorphs. The high organic content of the lower shales indicates very restricted conditions in the absence of salt water. Fresh-water ostracods occur up to the level of the first anhydrite and then die out. It is remarkable that no marine fossils replaced the extinct fresh-water fauna. This suggests that the first salt water that invaded the Gabon basin was already supersaline.

Salt deposits

The salt can only be studied in proper detail in the Congo basin where it is largely undisturbed in the land area and under part of the continental shelf. Data from Belmonte et al. (1965) and Lambert (1967) indicate that the chemical composition of the salt is exceptional by the virtual absence of sulfates and carbonates and the high proportion (15%) of carnallite ($\text{KCl} \cdot \text{MgCl}_2 \cdot 6\text{H}_2\text{O}$). Moreover, in several wells the extremely soluble bischofite ($\text{MgCl}_2 \cdot 6\text{H}_2\text{O}$) was found in thicknesses of several tens of meters.

Normal or regressive salt cycle

According to Belmonte et al. (1965) the basic salt cycle of the Congo basin is made up from bottom to top by (1) a thin black shale, (2) a layer of halite, (3) a mixture of halite and carnallite, sometimes with (4) an end member of bischofite or tachydrate ($\text{CaMg}_2\text{Cl}_6 \cdot 12\text{H}_2\text{O}$). This cycle is schematically illustrated in Figure 7. Figure 8 shows how such a cycle is expressed on the logs of a well in the northern part of the Congo basin. This well, situated in southernmost Gabon, was drilled with salt-saturated mud and was particularly generously logged. This cycle stands out quite well.

The halite beds can be identified from the logs by their low gamma-ray response, low neutron porosity, and the 2.10-g/cc density. The carnallite beds are characterized by relatively high radioactivity, very high neutron porosity reflecting the high percentage of molecular water, and a density of 1.60 g/cc. Moderate washouts of the bore hole are also typical.

The main criterion for distinguishing bischofite is

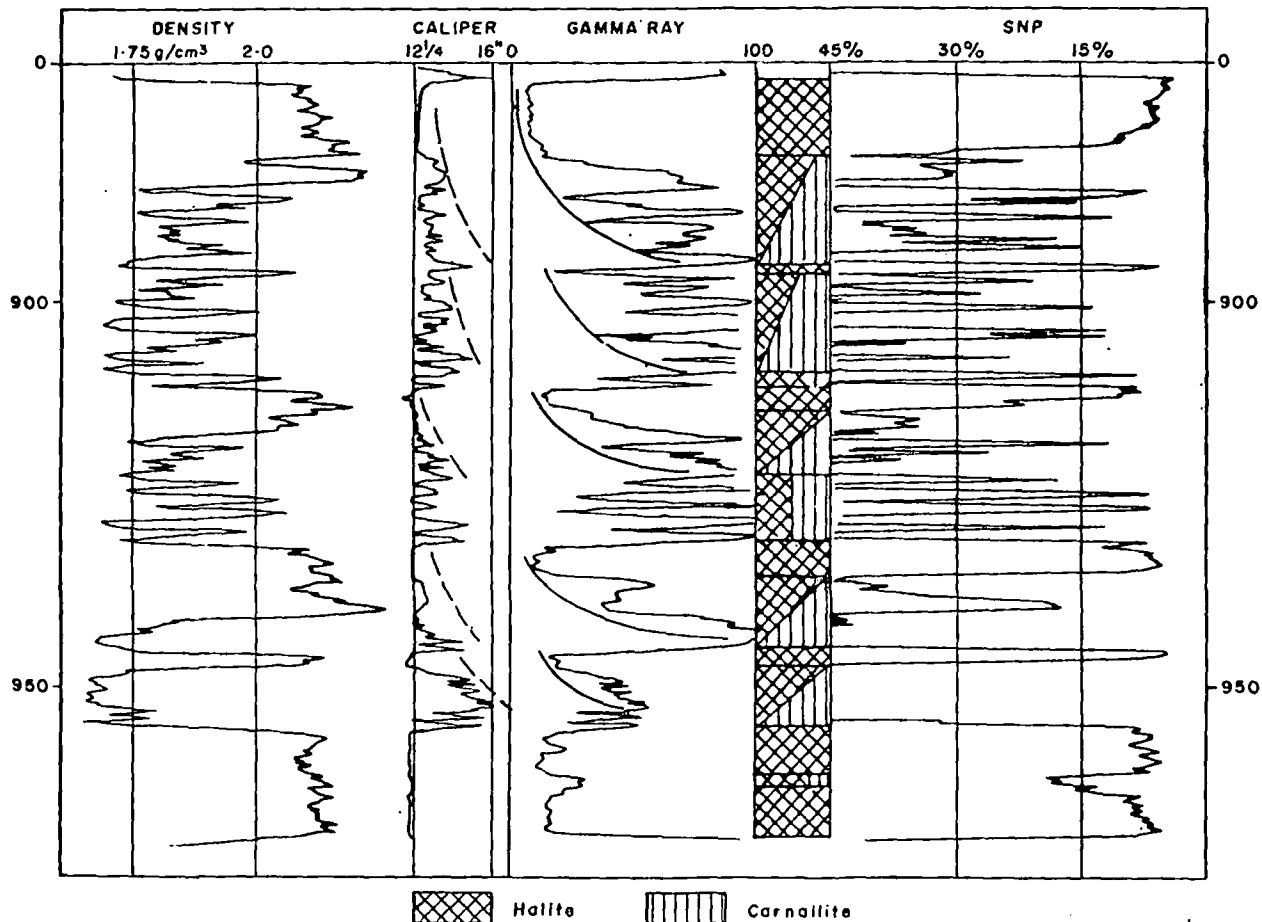


FIG. 9. Inverse salt cycles. A stack of thin cycles, characterized by decreasing solubility upward, is found above the basal halite unit. SNP = standard neutron porosity.

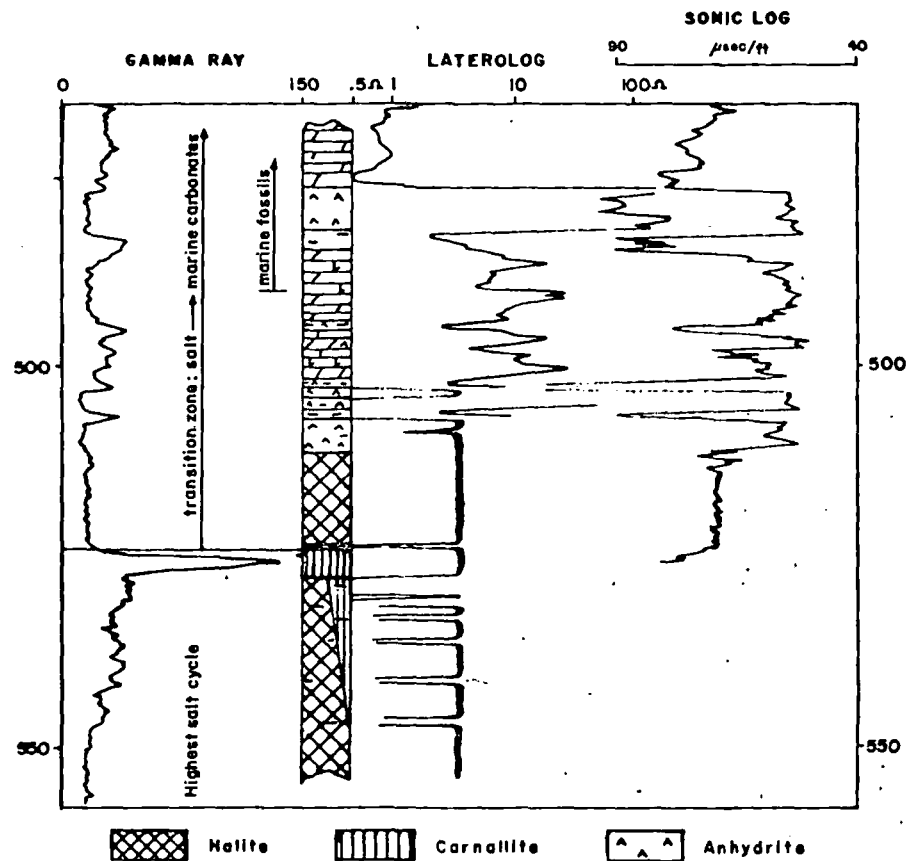


FIG. 10. Terminal cycle of evaporite deposition, Congo basin. The transition toward normal marine conditions, reflecting an uninhibited connection with the oceans, is marked by the first appearance of marine microplankton.

the hole size. The very severe washouts, beyond the measuring capacity of the caliper tool, indicate salts of significantly higher solubility than carnallite. The data on known salt minerals, as given by Lotze (1957), for instance, seem to leave only bischofite or tachydrate as possible contenders. Belmonte et al. (1965) and Lambert (1967) mention the occurrence of bischofite from core data and this lends support to the log interpretation. It is to be noted that the other log measurements opposite the bischofite washouts are totally unreliable.

The three normal salt cycles that can be easily recognized and correlated in the wells of the Congo basin occur in the middle part of the salt section (Fig. 11). The lower and upper parts of the salt section show a different cyclical development.

The inverse or transgressive salt cycle

Up to five relatively thin inverse salt cycles can be recognized in our key well just above the basal halite bed (Fig. 9). These cycles are made up of a nearly pure carnallite layer at the base, overlain by an increasingly halitic section capped by a pure halite.

The inverse cycle unit can be correlated over a large part of the Congo basin.

The uppermost salt unit consists of halite at the base, overlain by shale, anhydrite, and dolomite and is a cycle of decreasing solubility (Fig. 10). The first marine microplankton are found above the highest halite occurrence but below the last anhydrite bed. Fully marine conditions took over gradually at the end of salt deposition. The lower part of the Madiela Carbonates (Albian) is largely composed of restricted marine dolomites which could be seen as the end member of the salt formation.

Origin of the Congo basin salt

The chemical composition of the salt section of the Congo basin strongly suggests that the salt water that reached the basin during Aptian times was already much enriched in highly soluble components (Evans, 1978). In contrast, the Angola salt section (Fig. 11) has a more balanced composition of halite, anhydrite, and dolomite. The Angola salt section could represent the first phase of evaporites that occurred when the South Atlantic opened and allowed

normal sea water into basins that were bounded by the remaining tectonic high elements of the rift phase. Some of these high elements are still known (Fig. 12), like the Cabo Ledo High described by Brognon and Verrier (1966). Other bounding elements, especially those which one has to assume west of the present-day salt basin, were lost during the birth of the Atlantic Ocean or may still be present on the eastern margin of South America. At any rate, it

appears likely that in the different basins and sub-basins the composition of the saline water which entered differed as a function of the precipitations that had taken place already in the neighboring basins and of the relative elevation of the barriers separating these basins.

The two different types of mega-cycles described above cannot be explained satisfactorily since we have no data on the details of the mineral composition.

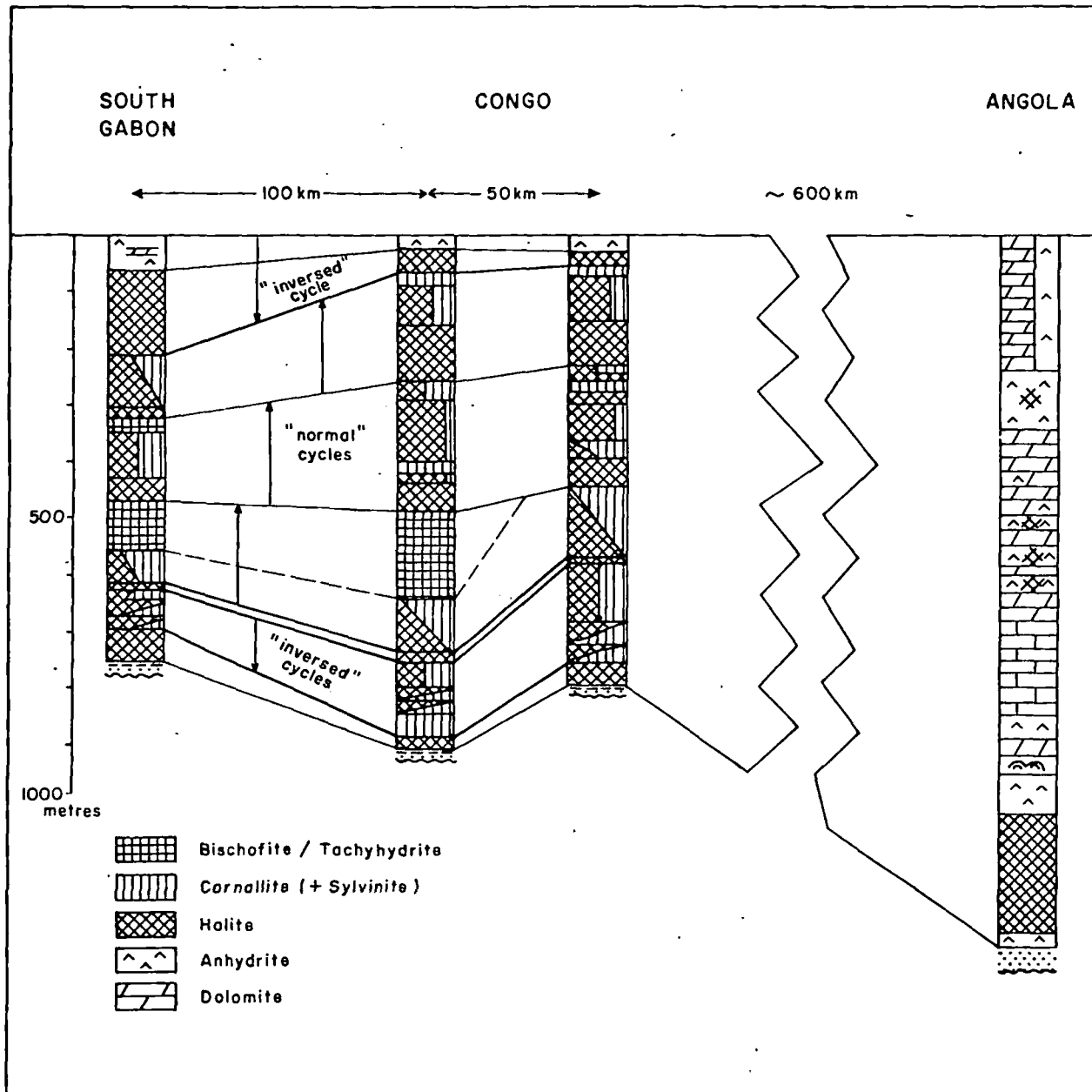


FIG. 11. Correlation of salt sections of the Gabon-Congo basins. The Angola salt section is not correlatable with the Congo sections; it represents a totally different facies.

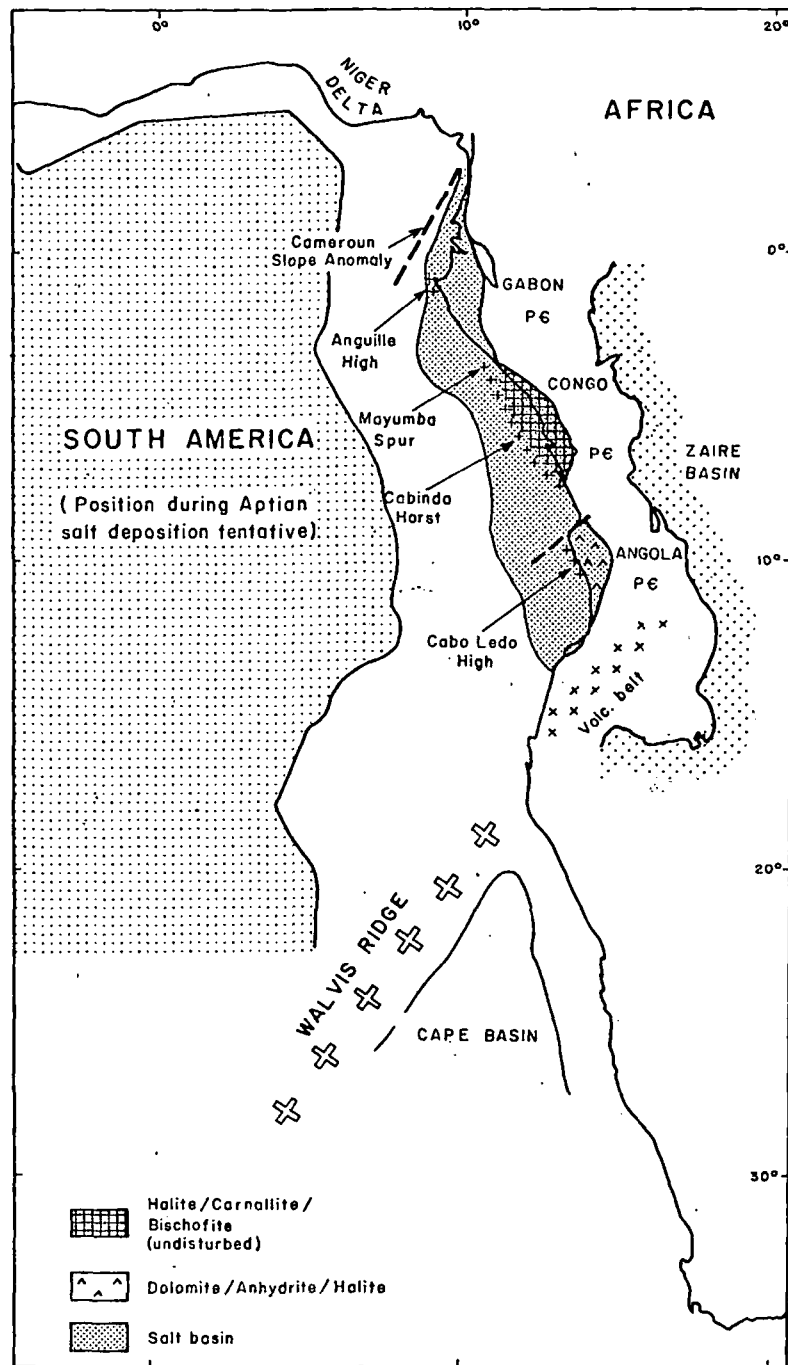


FIG. 12. Tectonic highs that may have had influence on salt deposition. At the time of salt deposition, the South American continent was close to Africa and this was a major restricting factor, possibly in conjunction with the Walvis Ridge.

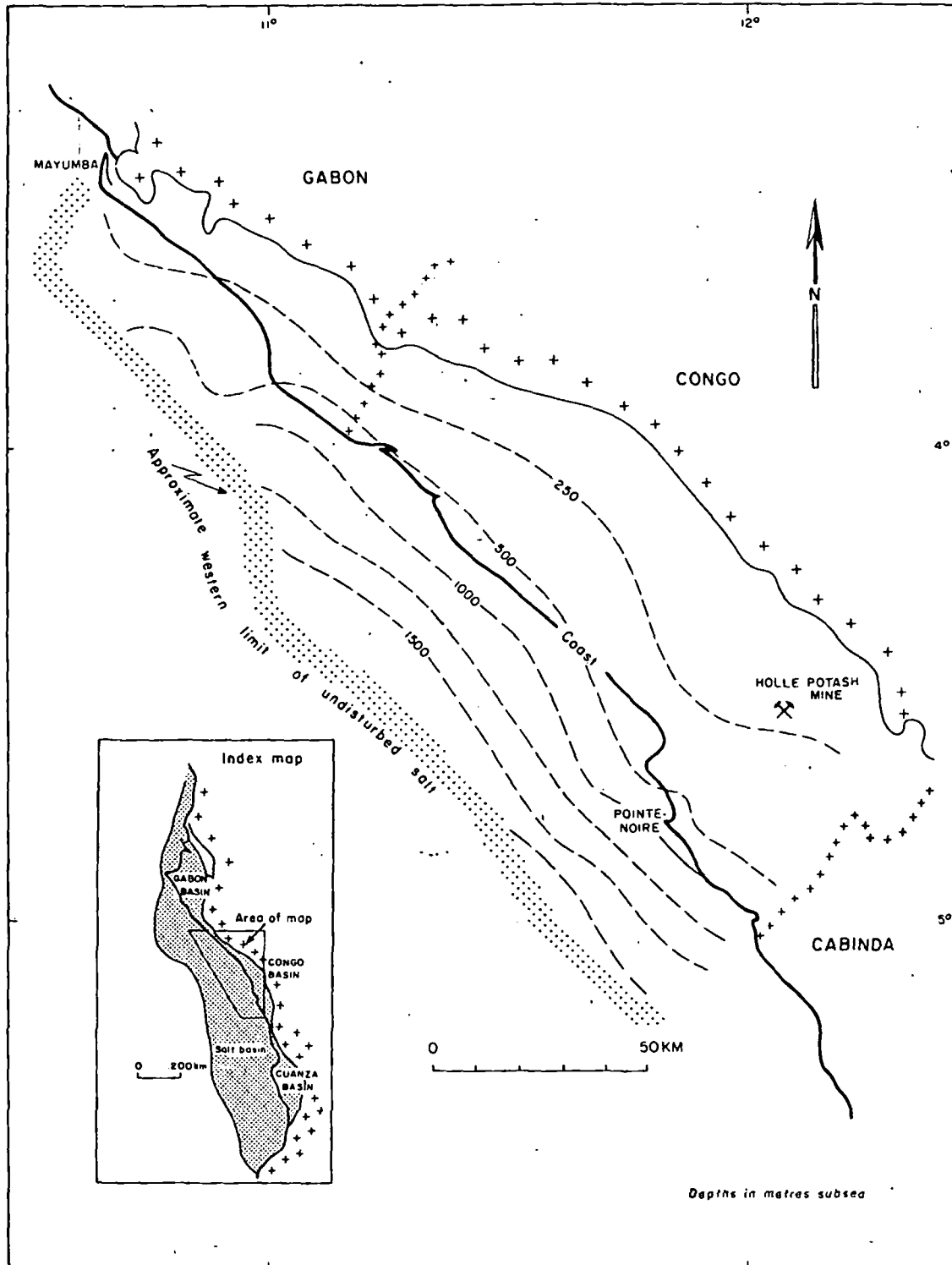


FIG. 13. Tentative isobaths of the top salt in the Congo basin.

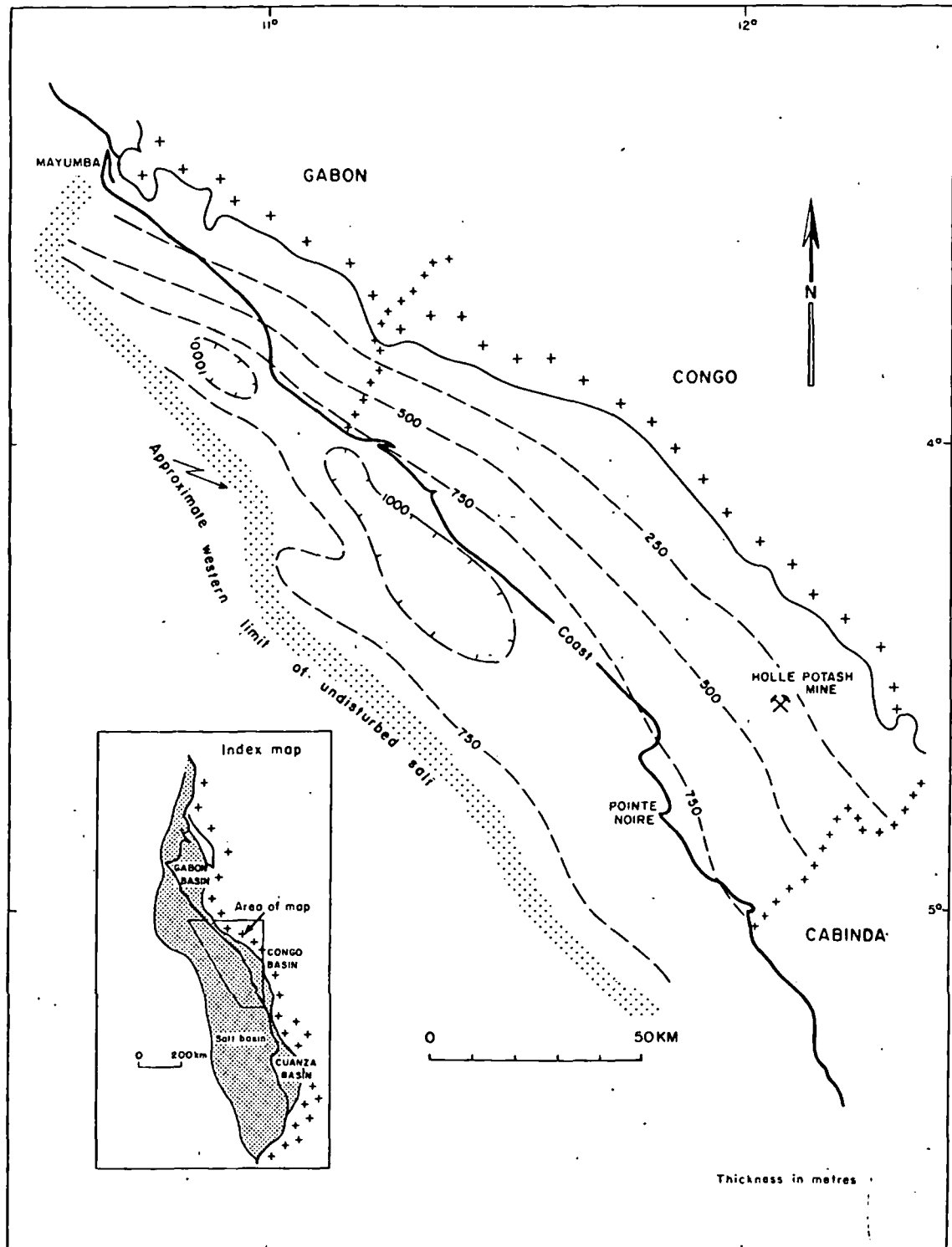


FIG. 14, Tentative isopachs of salt in the Congo basin.

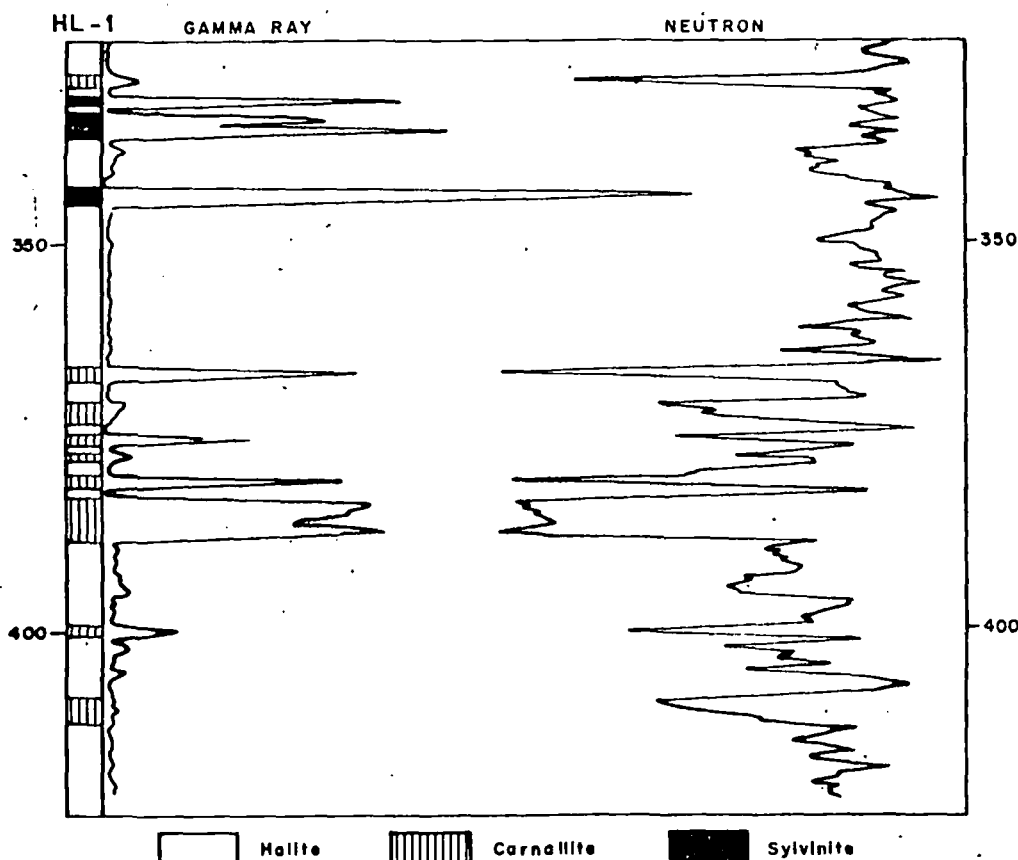


FIG. 15. Gamma-ray-neutron response opposite the Holle salt section (no horizontal scale available). The highest gamma-ray readings are derived from a sylvinite layer containing 38 percent K_2O .

These mega-cycles are apparently composed of stacks of thinner units, an analysis of which cannot be made with log data only.

Commercial Salt Deposits

The Congo basin contains a thick layer of almost undisturbed salt (Figs. 13 and 14) and is the only part of the Gabon-Congo-Angola salt basin where commercial salt exploitation has taken place. The Holle potash mine, described by Lambert (1967), has been operating since 1969.

Lambert noticed that the salt of the Congo basin is very rich in carnallite; the in situ reserves of potash and magnesium are estimated to be several billions of tons. However, for reasons of practicality, the only salt that has been mined is the sylvite (KCl) contained in the relatively rare sylvinite layers. This sylvinite is a secondary mineral derived from carnallite and laterally a sylvinite bed may be of limited extent.

Figure 15 illustrates the log expression in an oil exploration well, Holle-1, of the salt mined. The sylvinite stands out by its high radioactivity and its low neutron porosity. Core drilling around this well

confirmed these sylvinite layers to be of semiregional extent. The sylvinite is, however, far less continuous than the carnallite from which it was derived. Its composition and microfacies are variable. In some places it is made up of imbricated sylvite and halite crystals, elsewhere it consists of sylvite laminated with halite.

In the area of Holle four sylvinite layers were found in the second highest salt cycle. Only rarely do all four layers occur in one well (Fig. 16). Two layers, 3 and 7/8, were selected for exploitation (Fig. 17).

The highest, 7/8, occurs between 288 and 380 m and extends over an area of 28 km². Its average net thickness is 1.9 m; its K_2O content is 18 percent. It is thought to contain mineable reserves of 17 million tons K_2O . Layer 3, some 10 to 20 m below 7/8, has an average thickness of 3 m and its K_2O content may reach 38 percent, which classes it among the richest deposits in the world. It contains some 26 million tons of mineable reserves.

Apart from some less well explored and deeper layers, it was thought, prior to actual mining operations, that a production of 500,000 metric tons per

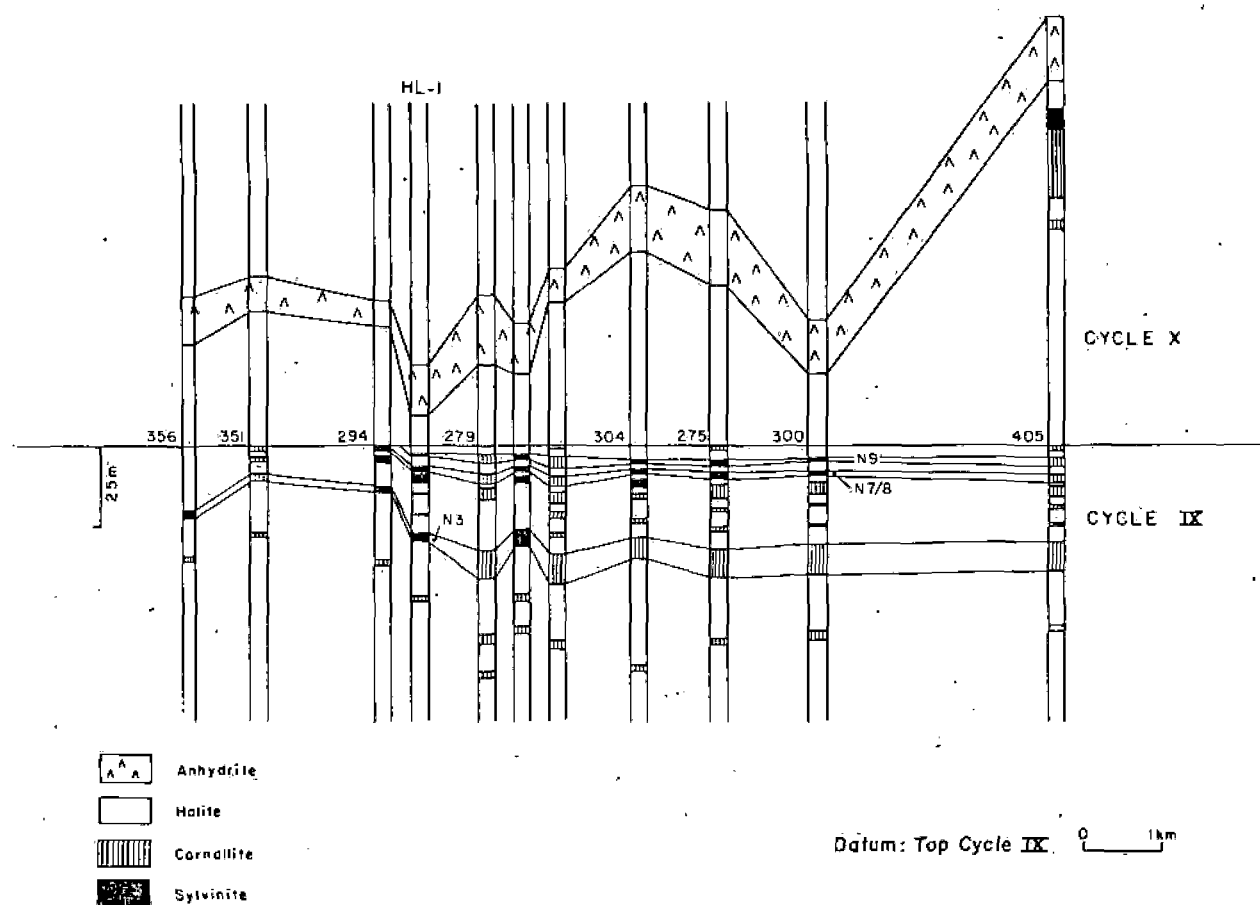


Fig. 16. Correlations, from core hole data, of wells of the Holle potash mine (after Lambert, 1967). The layers 3 and 7/8 are being exploited.

annum of K_2O could be maintained for 35 years, allowing for a high (60%) percentage of losses during mining and treating operations. The target of 500,000 metric tons per annum or more has, however, never been reached. This is largely due to the fact that the sylvinitite layers are more irregularly developed than was foreseen: their composition and thickness is more unfavorable and variable and their dip higher and more unpredictable than had been deduced from the exploration and appraisal drillings.

The following production levels have been obtained:

1969	66,900	metric tons	KCl
1970	205,049	"	"
1971	429,736	"	"
1972	473,771	"	"
1973	463,911	"	"
1974	475,279	"	"
1975	461,892	"	"
1976	435,131	"	"
1977 (first half only)	172,934	"	"
Total	3,184,603	"	"

The very expensive mechanical production method, coupled with the relatively low market price that could be realized, has resulted in a poor economical return. The mine has run continuously at a loss; only during one year have the operating costs been recovered from the proceeds.

After extensive studies it was considered attractive to attempt to mine carnallite as well; from late 1976 pilot galleries were bored. The great thickness and continuity of the carnallite layers and the possibility of using the entire infrastructure of the sylvinitite mine would, together, compensate for the more expensive treatment needed to extract potash from the carnallite. An economically viable project of 1,000,000 metric tons of KCl per annum was visualized.

By mid-1977, during the boring of one of the carnallite trial galleries, a few drops of water appeared through the roof of the gallery. The high solubility of the salt led to a rapid increase of water influx and within 36 hours the entire mine was flooded; the mine and most of the subsurface equipment were lost. The decision was taken to abandon the project.

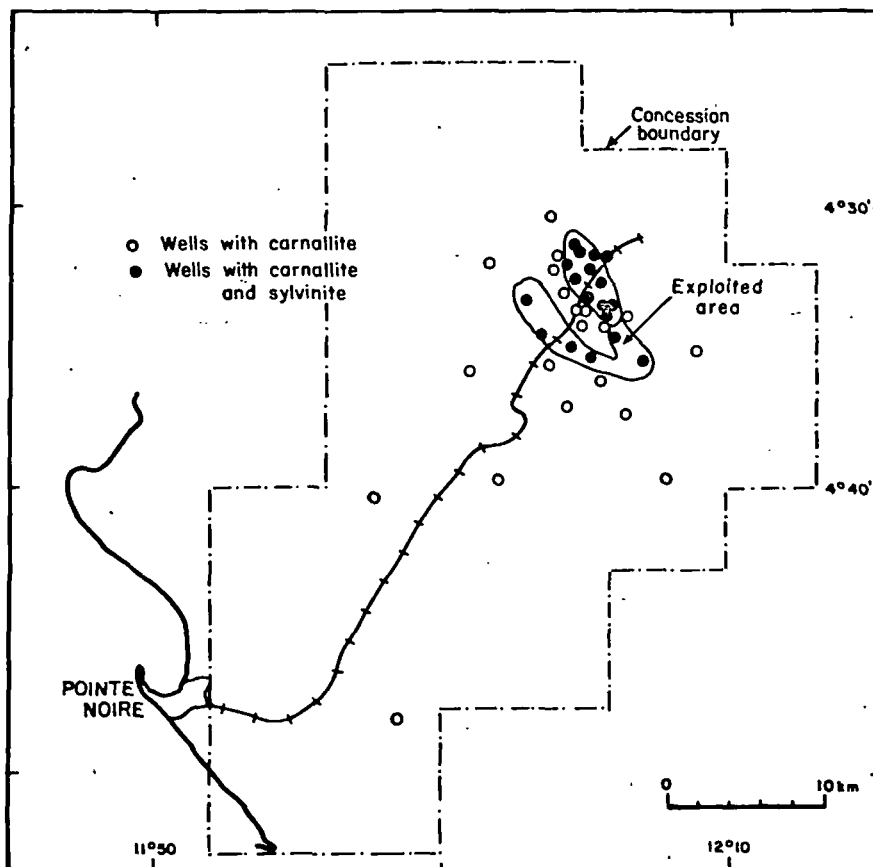


Fig. 17. Map of the Holle potash mine. Note that sylvanite was encountered only over a relatively small area, whereas carnallite is present in all the wells.

Acknowledgments

The author thanks Robert Evans for critically reading and correcting the first version of this paper, which was presented at the 1978 AIME/SEG annual meeting.

KONIGE JULIANAWEG 45
LEIDSCHENDAM 2264 BB, NETHERLANDS
November 13, 1978

REFERENCES

- Baumgartner, T. R., and Andel, Tj. H. van, 1971, Diapirs of the continental margin of Angola, Africa: *Geol. Soc. America Bull.*, v. 82, p. 793-802.
- Belmonte, Y., Hirtz, P., and Wenger, R., 1965, The salt basins of the Gabon and the Congo (Brazzaville), in *Salt basins around Africa*: London, Inst. Petroleum, p. 55-74.
- Brink, A. H., 1974, *Petroleum geology of the Gabon basin*: *Am. Assoc. Petroleum Geologists Bull.*, v. 58, p. 216-235.
- Brognon, G. P., and Verrier, R., 1966, Oil and geology in the Cuanza basin of Angola: *Am. Assoc. Petroleum Geologists*, v. 50, p. 108-158.
- Depege, V., 1967, La mise en exploitation du bassin potassique Congolais; *Annales des Mines*, v. 11, p. 724-734.
- Evans, R., 1978, Origin and significance of evaporites in basins around the Atlantic margin: *Am. Assoc. Petroleum Geologists Bull.*, v. 62, p. 223-234.
- Jeardine, S., Micholet, J., Molinas, E., and Penet, B., 1968, Présence de Permien au Gabon: identification stratigraphique et sédimentologique du Groupe de l'Angola: *Soc. Géol. France Compte rendu*, pt. 8, v. 8, 17.11.68, p. 1-3.
- Lambert, R., 1967, Esquisses géologiques du bassin potassique Congolais: *Annales des Mines*, v. 11, p. 709-723.
- Lehner, P., and Ruitter, P. A. C. de, 1977, Structural history of the Atlantic margin of Africa: *Am. Assoc. Petroleum Geologists Bull.*, v. 61, p. 961-981.
- Lotze, F., 1957, *Steinsalz und kalisalze*; Berlin, Bornträger, 477 p.

SUBJ
MNG
TIH

Theoretical investigations in the hydrometallurgy of noble metals

I A Kakovskii (Urals Polytechnical Institute)

The beginning of the hydrometallurgy of noble metals can be considered to be the establishment of the fact, observed by Lomonosov in the middle of the eighteenth century, that gold dissolves in solutions which release chlorine. However, on account of the low level of technology at that time this process, subsequently called hydrochlorination, only obtained practical application in 1848 (its introduction by Percy and Plattner). In 1843 Bagration published his investigation¹⁾ into the dissolution of gold in cyanide solutions, thereby formulating the main principles of the modern cyanide process, i.e., the use of dilute solutions of cyanide and the need for an oxidizing agent (oxygen). The cyanide process only obtained practical application more than three decades after the work of McArthur and the Forrest Brothers, but in all literature sources of those times Bagration has always been named "the father of the cyanide process". The advantages of cyaniding as a chemical method for the extraction of gold soon gave rise to its widespread use. The first cyanide plant in Russia at Kochkar' was constructed in 1896. The first investigations into the theoretical principles of the cyanide process²⁻⁴⁾ and the kinetics of the process appeared at the end of the nineteenth and the beginning of the twentieth centuries. However, the level of the experimental work at that time remained low, and much remained unclear. The serious investigations of I I Andreev⁵⁾ on the effect of oxygen and hydrogen peroxide on the dissolution rate of gold and silver stood out particularly well against this background; he was the first to use a rotating plate to investigate the dissolution rate. In the second quarter of the twentieth century Mostovich and Plaksin and other investigators studied the processes of the extraction of gold from ores in greater detail. [A summary of the work can be found in the brochure "I N Plaksin", Izd. Akad. Nauk SSSR, Moscow (1962)]. This made it possible to create the theoretical principles of the processes involved in the extraction of noble metals from ores and concentrates and to secure the vigorous development of the Soviet gold industry.

In 1952 Frumkin⁶⁾ described the rotating disc method, which was first used to study the kinetics of the dissolution of noble metals and proved very effective. The dissolution of gold, silver, or copper in cyanide solutions with oxygen as oxidizing agent is heterogeneous and is a three-component process. On account of the limited solubility of oxygen in water, it can be divided into two regions, i.e., the preliminary region in which the process rate is determined by the diffusion of cyanide and the translimiting region controlled by diffusion of oxygen. When the rotating disc method is used, the theoretical rate constant of the reaction occurring under diffusion control can be calculated from the following equation

$$k = \frac{6.18 \cdot 10^{-5} (2\pi)^{1/2} D^{2/3}}{m \cdot \nu^{1/6}}$$

where D is the diffusion coefficient of the reagent, cm²/sec; ν is the kinematic viscosity, cm²/sec; m is the stoichiometric coefficient of the reaction. n is the number of moles or ions of the diffusing reagent reacting with 1 g-atom of the metal. The constant has the dimensions litre · cm²/sec^{1/2} · rev^{1/2}. The following equation is used to calculate the dissolution rate:

$$V = Q \cdot \tau = k \cdot S \cdot C \cdot n^{1/2}$$

where: S = the surface area of the disc cm²
C = the concentration of the reagent mole/l
n = the number of revolutions of the disc per second
 τ = the dissolution time sec

We give the calculation of the rate constant of the cyaniding reaction (25°C potassium cyanide):

$$k = \frac{1.55 \cdot 10^{-5} (1.84 \cdot 10^{-4})^{2/3}}{2 \cdot (8.93 \cdot 10^{-3})^{1/6}} = 1.18 \cdot 10^{-6} \text{ l/cm}^2 \cdot \text{sec}^{1/2} \cdot \text{rev}^{1/2}$$

For the translimiting region $k = 1.0 \cdot 10^{-6}$. Further data on the experimental procedure and the calculations can be found in the literature⁷⁾. During investigation of reaction kinetics by the rotating disc method the effect of four main factors is usually determined, i.e., the concentrations of the reagents, the number of revolutions of the disc, and the temperature, and this is supplemented where necessary by other methods of investigation.

During investigation of the kinetics of the dissolution of gold, silver, and copper in cyanide solutions⁸⁾ the following characteristics of the process were found. Copper and silver dissolve in the diffusion region with almost any degree of agitation, whereas gold behaves differently, and with a disc rotation rate of more than 150 rpm the process moves into the kinetic region (non-dependence on the intensity of agitation). This is usually considered to be the main criterion for determination of the process regime, but it can also sometimes be observed when the surface is passivated by very compact films⁹⁾. In the text, however, the term "kinetic control" will be used for the present. The dissolution of gold under diffusion control occurs with incomplete utilization of the oxidizing potentialities of the oxygen (its reduction to hydrogen peroxide), i.e., the process only occurs according to the first stage of the Bodalender equation: $2\text{Au} + 4\text{CN}^- + \text{O}_2 + 2\text{H}_2\text{O} = 2\text{Au}(\text{CN})_2^- + 2\text{OH}^- + \text{H}_2\text{O}_2$. The second stage $2\text{Au} + 4\text{CN}^- + \text{H}_2\text{O}_2 = 2\text{Au}(\text{CN})_2^- + 2\text{OH}^-$ hardly occurs at all in spite of the very high thermodynamic probability ($\Delta G^\circ = -68.786 \text{ kcal}$). The dependence of the dissolution rate of gold on the pressure of oxygen above the solution also differs [it is proportional to $P_{\text{O}_2}^{1/2}$, and this was confirmed by experimental methods of investigation¹⁰⁾].

A second feature of the dissolution of noble metals in cyanide solutions was the fact that the experimental dissolution rate was lower than the calculated rate. For gold (under diffusion control), silver, and copper the experimental rate amounted to 70.3, 57.6, and 87.7% respectively of the theoretical rates. The reason for this is the formation of films of intermediate reaction products on the reaction surface, as demonstrated by investigations with labelled cy-

nide¹¹). Fairly thick films of simple copper and silver cyanides are formed on the surface of copper and silver. On the surface of gold, however, only a film of gold oxides was found¹²). Potentiostatic investigation and the corresponding calculations confirmed these data¹³ and the active passivation of gold in the cyanide solution by oxygen. For silver a scheme of successive stages was proposed with the formation of the oxide and simple cyanide, and this supplements the Bodlaender equation and makes it possible to determine certain details of the mechanism and the stoichiometry of the reaction products on the surface of the metals being dissolved was also demonstrated for zinc¹⁴) and for alloys of palladium with silver¹⁵). It has a very strong effect in the cyaniding of gold, eliminating one of the possibilities of intensifying the process by vigorous agitation. From this emerged the subsequent direction of investigations into the processes involved in the dissolution of gold:

a) Searches for other oxidizing agents which do not passivate its surface; b) searches for other solvents; c) searches for additives which could weaken the unfavourable effect of the films. Investigations showed that certain oxidizing agents, such as potassium ferricyanide, make it possible to eliminate the passivation of the surface of the gold completely¹⁶). Gold dissolves actively in aqueous solutions of halogens and of chlorine in particular¹⁷). Although films of intermediate product (halides of monovalent gold) are also formed in this case, they are readily soluble in an excess of the halide ions, and the dissolution of the metal occurs under diffusion control even with very strong agitation and has a higher rate than during cyaniding. Replacement of the cyanide by acetone cyanohydrin (ACH) makes it possible to lessen the passivating action of oxygen appreciably¹⁸) on account of the fact that the decomposition product of ACH, i.e., acetone, has some depassivating action. The advantages of ACH in the extraction of gold from stubborn ores were confirmed at the Irkutsk State Scientific-Research Institute of Rare and Nonferrous Metals¹⁹).

Investigation of the dissolving properties of thiourea²⁰) showed that an oxidizing agent such as ferric ions is required for gold and silver in aqueous solutions of this reagent. The passivation of the gold is somewhat weaker in the thiourea process than in the cyanide process; it starts at 300 rpm for gold and at 380-540 rpm for its alloys with silver. The oxidation of thiourea by ferric ions does not lead to its loss, since formamidine disulphide is a fairly active oxidizing agent capable of reacting with gold in the presence of an excess of thiourea. The advantages of thiourea compared with cyanide as a solvent for gold are as follows: The process occurs under kinetic control with more vigorous agitation, it is possible to create a higher concentration of the oxidizing agent (ferric ions), the reagent is less toxic and cheaper than cyanide, and finally thiourea is less sensitive to certain cyanicides. It is, however, less suitable for the dissolution of silver than of gold, since continuous films are formed on the surface. Thermodynamic calculations showed that it is possible to transfer silver into solution without thiourea on account of the oxidizing potential of ferric ions alone²¹). Ferric salts are a little inferior to cyanide in the dissolution rate of silver, and at 25°C the rate constants are equal to $5.9 \cdot 10^{-7}$ for sodium cyanide and $4.6 \cdot 10^{-7}$ litre/cm²·sec^{1/2}·rev^{1/2} for ferric salts, but the dissolution rate can be

increased further through the concentration of ferric ions. A particularly favourable subject for the application of this process is stubborn manganese-silver ores, which require complex and expensive treatment. During extraction of silver from such ores by the complex McKlusky method (preliminary leaching of manganese with sulphur dioxide, washing the cake, neutralisation and subsequent cyaniding) 92-93% of the silver was extracted from one ore, while 94% was extracted by the proposed method.

During investigation of another solvent for metallic silver, i.e., an aqueous solution of ammonia in the presence of oxygen as oxidizing agent, it was suggested that the low rate of this process is due to kinetic complications arising during the reduction of oxygen²²). The addition of copper ions to the solution greatly increased the process rate on account of its catalytic effect. The $\text{Cu}(\text{NH}_3)_4^{2+}$ ion accepts electrons from silver fairly readily, and the $\text{Cu}(\text{NH}_3)_2^+$ ion which forms is oxidized by oxygen readily and without kinetic complications, thereby promoting assimilation of the electrons of the silver by the $\text{Cu}(\text{NH}_3)_2^+$ ions. Since this process occurs without special kinetic complications, the experiments confirmed the thermodynamic calculation. For the reaction $\text{Cu}(\text{NH}_3)_4^{2+} + e = \text{Cu}(\text{NH}_3)_2^+ + 2\text{NH}_3, \text{soln } \Delta G^\circ = 0.83 \text{ kcal}$, and this energy balance is characteristic of a catalyst.

With the thiosulphate ion gold and silver give fairly stable complexes ($K_d = 4.2 \cdot 10^{-30}$ and $2.3 \cdot 10^{-14}$). Thermodynamic calculations indicate a fairly high probability that these metals will dissolve in aqueous solutions of thiosulphate with an oxygen depolariser, but kinetic complications are quite possible. Experiments showed²³) that this is so; gold does not dissolve even at 200°C. The addition of copper sulphate to the optimum thiosulphate-copper ratio of 12.5 increases the dissolution rate of both metals by 18-20 times. The dissolution rate increases almost linearly with increase in the concentration of this "effective solvent", ammonia, and ammonium sulphate. Increase in the oxygen pressure accelerates the dissolution of silver but not of gold, the rate of which is approximately ten times lower than that of silver. The described process occurs fairly vigorously in the ammonia leaching of copper sulphide concentrates in an autoclave, since the oxidation of the sulphides occurs through the formation of thiosulphate, which forms complexes with the noble metals.

Gold possesses a very high affinity for sulphur (for Au_2S , $L_0 = 10^{-76}$), and this sulphide readily gives the AuS^- complex. Experiments carried out in an autoclave at higher temperatures²⁴) with solutions of sulphur in an aqueous solution of ammonia or sodium hydroxide confirmed the possibility of the reaction $2\text{Au} + \text{S}_2^{2-} = 2\text{AuS}^-$. The dissolution rate is higher in ammonia solutions. The process may be of interest for the extraction of gold from certain forms of particularly stubborn concentrates.

At high temperature (90-130°C) and in an alkaline medium cyanide can be replaced by ferrocyanide, which reacts with gold in the presence of oxygen (pressure 1-2 atm). The rate of the process increases greatly with temperature ($\Delta E = 21 \text{ kcal/mole}$) and is proportional to the ferrocyanide concentra-

tion. This is also an autoclave process.

A third way of improving the dissolution of gold is to study the effect of the composition of the solution on the rate of the process. It was necessary to find conditions where the dissolved components would prevent the formation of too compact passivating films on the surface of the gold.

Investigation of the effect of thallium (I) ions on the dissolution of gold in cyanide solutions²⁶⁾ showed that in their presence the boundary for the transition to the kinetic region is shifted from 150 to 410 rpm, i.e., the passivation of the surface of the gold is reduced appreciably. The passivation is also lessened in the kinetic region and, particularly, with vigorous agitation (the maximum dissolution rate in the presence of thallium ions is 3.4-3.9 times higher than without them) and also when oxygen is blown through the solutions, i.e., under the conditions of the most active passivation, where the rate increases by three times to $2.4 \cdot 10^{-6}$ g-atom/cm²·sec. The favourable effect of thallium salts depends little on the amount, and the addition of 4-5 g to 1 t of ore is sufficient. At the concentrations in which the reacting components are present gold is more noble than thallium and its cementation cannot occur. Consequently, the mechanism of the depassivating action can be explained by the adsorption of thallium ions on the surface of the gold (like organic depassivators) or by oxidation of thallium (I) to thallium (III) on the surface of the gold with the formation of $Tl(OH)_3$ (when air is blown through the solution $\Delta G^\circ = -17$ kcal/mole) and by disintegration of the gold oxide film. Our experiments confirmed the passivating action of copper in cyanide solutions²⁶⁾ with low concentrations of cyanide, but if the cyanide concentration exceeds the copper concentration by approximately 25 times, the transition of the process from diffusion to kinetic control is shifted from 150 to 620 rpm. The passivation of the surface of the gold in the region of low copper-cyanide ratios is due to the formation of films of $CuCN$, and its depassivating action with an increased cyanide-copper ratio is accompanied by blockage of the active centres and by destruction of the monolithic oxide film on the surface of the gold.

During the cyaniding of amalgamation tailings tetracyanomercurate can be found in the solutions. In cyanide solutions mercury is more noble than gold, and according to our determinations²⁶⁾ their standard potentials at 25°C are -0.3725 and -0.543V. Consequently, mercury will be deposited on the surface of the gold, and this was confirmed by the experiments. During investigation²⁷⁾ it was found that the concentration of the mercury in the solution plays a major role; in the region of low concentrations (10^{-5} - 10^{-6} g-ion/litre) an appreciable depassivating action is observed, and at high concentrations full amalgamation of the surface and a very strong reduction in the gold dissolution rate are observed. However, the most important consequence of depassivation is the shift of the boundary for the transition from diffusion to kinetic control from 150 to 900 rpm, and this makes it possible to obtain high gold dissolution rates. The mechanism of depassivation by mercury involves blockage of the active centres of the gold by the deposited mercury and the creation of sections for unobstructed approach of the reagents and

removal of the reaction products, the formation of defects in the oxide layer, and the action of local cells.

Our investigations²⁸⁾ showed that increased concentrations of sulphide ion reduce the gold dissolution rate very strongly, and very low concentrations (10^{-7} - 10^{-8} g-ion/litre) depassivate the surface of the gold and keep the process in the diffusion region up to 480 rpm. The mechanism of the depassivation by sulphide ion and by plumbite is the same as with the other investigated compounds. The effect of xanthates on the cyaniding of gold has been investigated in two versions: a) Xanthate treatment of the disc, washing, and dissolution; b) dissolution of the disc in a cyanide solution with the addition of xanthate²⁹⁾. During dissolution of previously xanthate-treated discs in dilute solutions of cyanide the negative effect of the xanthate films showed up clearly, but with increase in the concentration of cyanide the maximum dissolution rates were higher than for the clean discs. Xanthate in solution had a different effect; with low concentrations of cyanide the intensity of agitation did not have an appreciable effect; with high concentrations the rate increases but considerably less than in version (a) and becomes lower the higher the concentration in the solution. With preliminary xanthate treatment of the disc or with the presence of only very low concentrations of xanthate in the solution (in the order of 10^{-5} g-ion/litre) the process occurs under diffusion control even at 1000 rpm. Consequently, under favourable conditions xanthate can be an active depassivator, keeping the process in the diffusion region, and can even alter the stoichiometric equation for the gold dissolution reaction, which in its presence occurs with full reduction of oxygen, i.e., according to the second stage of the Bodlaender equation.

Dialkyl dithiophosphates as depassivators of gold are considerably more effective than xanthates - the negative effect of their excess concentration in the solution and of increased intensity of agitation is less appreciable³⁰⁾. Elongation of the hydrocarbon chain from two to five CH_2 groups has little effect on their depassivating action, which is also not affected by additions of alcohol frothing agents with chain lengths between 3 and 10 CH_2 groups and of pine oil. Thus, the investigations have shown that the investigated reagents (except thallium salts) can passivate or depassivate gold. Their depassivating characteristics are determined by the ratio of the cyanide and reagent concentrations, and the mechanism involves blockage of the active centres and destruction of the monolithic oxide films on the surface of the gold.

Some alloys of noble metals and their chemical compounds were investigated; Alloys of gold with silver and copper³¹⁾; palladium with silver^{1b)}; silver and copper³¹⁾; palladium with silver^{1b)}; silver and gold amalgams¹⁴⁻³²⁾; gold and silver tellurides³³⁾; silver and copper sulphides³⁴⁾.

The presence of silver in the alloy with gold assisted the dissolution of gold both in the prelimiting and in the translimiting region under diffusion control even at 1100 rpm. Investigation of gold-copper alloys gave interesting results. During the dissolution of hardened alloys, in which there are no chemical

compounds, the action of copper additions was similar to the action of silver (highly depassivating). During the dissolution of annealed alloys, in which according to other methods of investigation intermetallic compounds AuCu and AuCu₃ must be formed, the kinetic method of investigation confirmed the presence of these compounds (a great reduction in the dissolution rate with 25 and 50 atm.% of gold).

The positive effect of silver on the dissolution rate was also observed during dissolution of silver-palladium alloys in cyanide solutions with the observance in particular, of the Tamman law ($v/8$).

Of great theoretical interest was an investigation into the cyaniding of silver and gold amalgama and their composition, supplemented by investigation of the dissolution rate of mercury in cyanide solutions²⁶). The effect of variable factors (the intensity of agitation, the concentration of cyanide and oxygen, the alkalinity of the solution, the temperature, and the composition of the amalgam, i.e., β and γ phases and liquid amalgams) on the rate of passage of silver into the solution was investigated. The most interesting was the variation in the composition of the solid phases - silver passed into solution considerably more rapidly than mercury, and the amalgam was gradually depleted in silver. The investigation confirmed the Murphy diagram, but the homogeneity limits of the chemical compounds and the conditions for their synthesis were determined in addition.

Gold amalgams were studied by similar methods (the effect of variable factors on their dissolution rate and the phase diagram of the amalgams, including one which had been kept for 8 years). On the basis of X-ray analysis it was shown that the composition of the amalgams is considerably more complex than indicated in the literature.

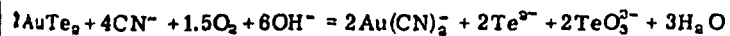
The amalgamation of the surface of the gold greatly reduces its dissolution rate in cyanide solutions. On its surface liquid amalgams are formed similar in their kinetic characteristics to concretions of gold with rock, wetted by mercury which has not reacted chemically with the gold. Dissolution of the liquid amalgams in a special kinetic region and their mercury-like character give few possibilities for intensifying the extraction of gold from them by cyanide treatment, since the rate of passage of gold into solution does not increase with increase in the intensity of agitation or with increase in the cyanide and oxygen concentration and temperature. Solid and, particularly, stale amalgams dissolve considerably more readily than liquid amalgams but more slowly than metallic gold in the kinetic region.

We studied silver sulphide and telluride. Thermodynamic calculation indicates little probability of the dissolution of silver sulphide in cyanide solutions without oxygen ($K = 2 \cdot 10^{-9}$). In its presence the process occurs in the existing kinetic region: $v = k \cdot S \cdot C \cdot P_{O_2}^{1/2}$; $k_{298} = 1.9 \cdot 10^{-10}$ litre/cm² · atm^{1/2} · sec. $\Delta E = 6.4$ kcal/mole. Oxidation of the sulphide sulphur occurs on the reaction surface (the dependence of the rate on $P_{O_2}^{1/2}$). The obtained relationships make it possible to conclude that argentite is a more stubborn mineral in metallur-

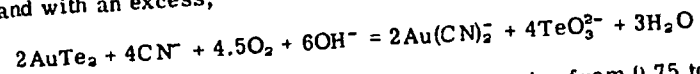
gical respects than metallic silver; the rate constant is lower, and agitation does not affect the dissolution rate.

The investigation of silver telluride (hessite) demonstrated its extreme complexity. The dissolution rate depends on the concentration of cyanide only in the prelimiting region, but its limiting concentrations are too high and the intensity of agitation only affects the rate in the translimiting region. In the prelimiting region the dissolution rate decreases with increase in temperature, and in the translimiting region it increases. In the translimiting region the maximum dissolution rates are proportional to the pressure of oxygen above the solution to the first power, and in the prelimiting region the power index is smaller (approximately 2/3). Reduction in the alkalinity reduces the rate only in the prelimiting region. The reason for all these contradictions lies in two characteristics of the dissolution of silver telluride, i.e., the formation and the properties of oxidized films on its surface and the variation in the composition of the solid phase. The oxidation of the surface of the solid phase increases with increase in temperature in the prelimiting region, i.e., with a deficiency of cyanide the film becomes thicker and thicker, reducing the dissolution rate. In the translimiting region with an excess of cyanide, increase in temperature gives the opposite effect; the dissolution rate of the film becomes higher than its formation rate, its retarding effect is greatly reduced, and the process changes from "pseudo-kinetic" to diffusion control. By electron diffraction and X-ray diffraction analyses of the solid phase it was established that dissolution occurs incongruently and the composition of the solid phase varies according to the following scheme: $Ag_2Te \rightarrow Ag_5Te_3 \rightarrow AgTe$. Analysis of the solutions for silver and tellurium and their mathematical treatment made it possible to establish that the third stage, i.e., dissolution of AgTe, is the slowest.

Gold telluride is encountered in ores in the form of the mineral calaverite, and it belongs to particularly stubborn minerals. The dissolution of this compound in cyanide solutions is very complex, and the effect of individual factors on its rate is not characteristic either of purely diffusion or of purely kinetic control; the dissolution rate in the prelimiting region depends both on the concentration of cyanide and on the pressure of oxygen; the limiting concentration of cyanide is very high, and the rate is independent of the intensity of agitation in the prelimiting region and dependent in the translimiting region; the dissolution rate depends on the pressure of oxygen and on the number of revolutions of the disc raised to a power of less than 0.5; the activation energies in the prelimiting and translimiting regions are fairly large and practically identical; the alkalinity of the solution has a unique effect (an increase in the dissolution rate with low cyanide concentrations). All this demonstrates the complex and stepwise character of the process, and this was confirmed by special tests. The reason for these complications lies in the fact that the stoichiometry of the reaction depends on the concentration of oxygen in the solution. With a deficiency:



and with an excess,

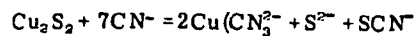


The oxygen required for 1 g-atom of gold varies from 0.75 to 2.25 moles, depending on the composition of the solution, on its temperature, and on the intensity of agitation. The "interchangeability" of cyanide and alkali is most interesting: Comparable dissolution rates can be obtained with low alkalinity and a high concentration of cyanide or with a high concentration of alkali and low cyanide. However, the dissolution rates of gold from the telluride at pH 11 and at 25°C with air blown through the solution are 400 times lower than the dissolution rate of metallic gold in the kinetic region. Ways of intensifying the process have been given in the literature⁷⁾

The possibility of the use of another reagent, elemental chlorine, was investigated in connection with the low rates of the cyaniding of gold telluride³⁶⁾. Under acceptable conditions for practical purposes the rate of extraction of gold by hydrochlorination was approximately 15 times lower than during cyaniding.

Silver chloride is most often contained in the calcines from the chloride roasting of particularly stubborn ores and concentrates and various intermediate products from metallurgical processes, wastes, etc. Silver can be extracted from such types of raw material by cyaniding, but cyanide is expensive in short supply, and toxic and reacts vigorously with many compounds which accompany silver. Other solvents for silver chloride were therefore investigated: Thiosulphate, an aqueous solution of ammonia, thiourea, sodium chloride³⁷⁾. We only give the final results from these investigations, i.e., the rate constants of the reactions at 25°C (they all occur under diffusion control), $k \cdot 10^6$ litre/cm² · sec^{1/2} · rev^{1/2}: Sodium cyanide 0.68; sodium thiosulphate 0.53; aqueous solution of ammonia 0.12; thiourea 0.60; sodium chloride 1.06. From these data it follows that cyanide can be replaced by a different reagent, the choice of which depends on the character of the raw material. The hydrochlorination of metallic silver, which is of interest for the dissolution of silver-bearing gold, was also investigated.

The behaviour of chalcocite and covellite in cyanide solutions was investigated. Chalcocite dissolves in cyanide solutions under diffusion control. In the absence of oxygen in the solution the copper and sulphur pass into solution in the stoichiometric ratio (2:1); in the presence of oxygen with low concentrations of cyanide only half the copper passes into solution, and a new covellite phase is formed. (The rate of passage of copper into solution decreases with time as the film of covellite is formed). The behaviour of covellite is similar to that of chalcocite; in an oxygen-free solution of cyanide it dissolves congruently, and in the presence of oxygen the sulphur remains undissolved and a retarding film is formed on the surface. The difference from chalcocite lies in the fact that the dissolution of covellite occurs under kinetic control. By special tests the stoichiometric equation of the reaction, which explains the structure of covellite, was established:



(The formula $\text{Cu}_2\text{S} \cdot \text{Cu}_2\text{S}_3$ does not change the stoichiometry of the reaction).

The investigation showed that some impurities in the solid phase accelerate the dissolution of gold and palladium (silver, copper), and others retard the dissolution of gold and silver (mercury, tellurium, sulphur). It is very important to choose the correct solvent and oxidizing agent in relation to the composition of the solid phase and other conditions (concentration of reagents, alkalinity of solution, temperature, intensity of agitation etc). Of the many methods for isolation of noble metals from solutions two were investigated, i.e., cementation with zinc³⁸⁾ and precipitation of the platinum metals by organic sulphhydryl reagents³⁹⁾. In spite of the very high stability of cyanide complexes of gold and silver ($K_d = 1.1 \cdot 10^{-41}$ and $1.6 \cdot 10^{-21}$), the cementation process occurs in the diffusion region according to the equation

$$\lg C = \lg C_0 - (k \cdot S \cdot n^{1/2} / 2.303 \cdot V)$$

(direct discharge of the anion without dissociation into its component ions). The effect of the concentration of free cyanide, oxygen, and alkali was investigated. The experimental rate was 93% of the theoretical for gold and 87% for silver. In addition the joint precipitation of gold, silver, and copper from cyanide solutions and their joint effect on the characteristics of the process were investigated, and the diffusion coefficients of potassium cyanide and of the complex cyanides of gold and silver were determined⁴⁰⁾. A cycle of investigations was undertaken into the oxidizability of sulphide minerals in alkaline solutions⁴⁰⁾. Here the complex step-like character of these reactions, which occur with considerable kinetic complications, was determined. A relationship was obtained between the oxidation rate and the pH of the solution, the temperature, and the concentration of oxygen (proportionality to P_2O_5), a mechanism of oxidation was proposed, and the nonapplicability of thermodynamics for calculations of such reactions was demonstrated⁴¹⁾.

Since amalgamation is an effective method for the extraction of gold from ores and concentrates in a number of cases, a series of investigations was carried out into this process⁴²⁾. They made it possible to establish clearly the advantages of kinetic methods of investigation compared with the measurement of wetting angles. Such researches were carried out for the first time and required the creation of the necessary measurement apparatus, making it possible to put forward a series of new theoretical ideas.

In order to establish the theoretical principles of the hydrometallurgy of noble metals the activity products of a series of their poorly soluble compounds, the dissociation constants of the complexes, etc. were determined⁴³⁾ ⁴⁴⁾ ⁴⁵⁾.

A review of investigations carried out by the rotating disc method showed its advantages in the investigation of a series of theoretical problems in hydrometallurgy and the contribution which Soviet scientists have made to this department of science.

References

- 1) P Bagration: Bull. Acad. Sci. (classe phys. mat.), St. Pet., 1843, 2, (9-10), 136.
- 2) J S Maclaurin: J. Chem. Soc., 1893, 63, 724.
- 3) G Bodlaender: Z. Angew. Chem., 1896, 9, 583.
- 4) S B Christy: Trans. AIME 1900, 30, 864; Elektrochem. Zeitsc., 1901, 8, 181, 198, 221.
- 5) I I Andreev: Izv. S P Politekhn. In-ta 1908, 9, 447; Z Elektrochem, 1913, 19, (17), 667.
- 6) A N Frumkin et alia: Kinetics of electrode processes. Izd. MGU 1952.
- 7) I A Kakovskii and Yu M Potashnikov: Kinetics of dissolution processes. Metallurgiya, Moscow.
- 8) I A Kakovskii and Yu B Kholmanskikh: Izv. Akad. Nauk SSSR, OTN, Metallurgiya i Toplivo 1959, (5), 97; 1960, (5), 207.
- 9) I A Kakovsky: Revue de l'Industr. miner., Compt Rend. Sci., Avri 1964, numero Spec. A, 157-180.
- 10) A N Lebedev and I A Kakovskii: Élektrokimiya 1966, 2, (9), 1079.
- 11) I A Kakovskii et alia: Izv. Vuz. Tsvetnaya Metallurgiya 1973, (2), 107; (4), 51.
- 12) I A Kakovskii and G F Cherkasov: Izv. Vuz. Tsvetnaya Metallurgiya 1974, (4), 87.
- 13) A N Lebedev et alia: Tsvetnaya Metallurgiya 1976, (1), 64.
- 14) Trudy In-ta. Uralkhannobr., (13), Sverdlovsk 1967.
- 15) I A Kakovskii and V A Svetlov: Izv. Vuz. Tsvetnaya Metallurgiya 1967, (2), 68 and (3), 36.
- 16) I A Kakovskii and A N Lebedev: Izv. Vuz. Tsvetnaya Metallurgiya 1970, (1), 56.
- 17) V V Gubailovskii et alia: Izv. Akad. Nauk SSSR Metally 1973, (6), 106; 1978, (1), 57.
- 18) A N Lebedev and I A Kakovskii: Tsvetnye Metally 1965, (7), 17.
- 19) Irgiredmet: Nauchnye Trudy (20), 144.
- 20) V I Dodeishchikov et alia: Izv. Vuz. Tsvetnaya Metallurgiya 1975, (2), 77; Izv. Akad. Nauk SSSR Metally 1975, (6), 32.
- 21) I A Kakovskii et alia: Dokl. Akad. Nauk SSSR 1974, 216, (3), 611.
- 22) I A Kakovskii and NG Tyurin: Dokl. Akad. Nauk SSSR 1960, 130, (4), 812.
- 23) NG Tyurin and I A Kakovskii: Application of autoclave processes in the metallurgy of nonferrous and precious metals, 173, Izd. TsIIN Tsvetmet and GNIK, Moscow 1960; Izv. Vuz. Tsvetnaya Metallurgiya 1962, (2), 104.
- 24) I A Kakovskii and L D Sheveleva: Élektrokimiya 1975, 2, (9), 1437.
- 25) L D Sheveleva and I A Kakovskii: Tsvetnye Metally 1976, (1), 77.
- 26) I A Kakovskii: Zh. Fiz. Khim., 1955, 29, (12), 2268.
- 27) L D Sheveleva et alia: Zh. Prikl. Khim., 1979, (4).
- 28) L D Sheveleva et alia: Izv. Vuz. Tsvetnaya Metallurgiya 1979, (2).
- 29) L D Sheveleva et alia: Trudy TsNIGRI, Moscow 1975, 121, 66.
- 30) L D Sheveleva et alia: Tsvetnye Metally 1977, (2), 82.
- 31) Yu B Kholmanskikh et alia: Izv. Akad. Nauk SSSR Metally 1975, (3), 69.
- 32) I A Kakovskii et alia: Izv. Vuz. Tsvetnaya Metallurgiya 1972, (2), 52; 1971, (6), 65; 1972, (1), 57.
- 33) I A Kakovskii and NI Sorokina: Izv. Vuz. Tsvetnaya Metallurgiya 1972, (3), 96; Dokl. Akad. Nauk SSSR Ser. Khim., 1971, 199, (4), 844; 1972, 206, (2), 387.
- 34) I A Kakovskii and Yu M Potashnikov: Izv. Akad. Nauk SSSR OTN Metallurgiya i Toplivo 1962, (3), 41; (5), 81; Izv. Vuz Tsvetnaya Metallurgiya 1962, (6), 62; Dokl. Akad. Nauk SSSR 1962, 145, (6), 1311; 1964, 158, (3), 714.
- 35) I A Kakovskii and S A Kuligin: Dokl. Akad. Nauk SSSR 1966, 169, (5), 1126.
- 36) I A Kakovskii et alia: Tsvetnye Metally 1974, (2), 36.
- 37) I A Kakovskii and V V Gubailovskii: Dokl. Akad. Nauk SSSR 1969, 184, (5), 1157; Tsvetnye Metally 1972, (5), 32; Izv. Vuz. Tsvetnaya Metallurgiya 1975, (1), 139; 1977, (2), 79.
- 38) I A Kakovskii and O K Shcherbakov: Izv. Akad. Nauk SSSR Metally 1967, (1), 76; Tsvetnye Metally 1967, (2), 10.
- 39) I A Kakovskii and K A Karasev: Tsvetnye Metally 1958, (3), 47; 1959, (4), 16.
- 40) I A Kakovskii et alia: Obogashchenie Rud 1973, (4), 39; 1974, (1), 23; (4), 34; 1975, (3), 18; 1978, (4), 19.
- 41) I A Kakovskii: Izv. Vuz. Tsvetnaya Metallurgiya 1977, (6), 3.
- 42) V I Vasev and I A Kakovskii: Izv. Akad. Nauk SSSR Metally 1974, (5), 94; Physical chemistry of the boundaries of contacting phases. Naukova Dumka, Kiev 1976, p.107; Physicochemical investigations of metallurgical processes. Izd. UPI Sverdlovsk 1977, 56, 5; Adhesion of metals and alloys. Naukova Dumka, Kiev 1977, 20.
- 43) I A Kakovskii: Proceedings of third scientific-technical session of the Mekhanobr Institute. Metallurgizdat 1955, 237. Zh. Neorgan. Khim., 1977, 22, (11), 3067.
- 44) B I Peshchevitskii et alia: Izv. Sb. Otd. Akad. Nauk SSSR Ser Khim., 1970, (4), (9), 75.

UDC 622.765

Some aspects of the mechanism of the action of combinations of various reagents in froth flotation

V I Melik-Galkazyan (Kursk Polytechnical Institute)

From flotation practice it is known that specific combinations of reagents intensify the process and make it possible to obtain better characteristics in the separation of minerals than is possible with the use of reagents of one class. In this connection a large number of investigations have been devoted at various times to the problem of determining the mechanism of the reaction of reagent combinations. Since the action of reagents with ions or molecules having heteropolar nature depends significantly on their orientation in the adsorbed layer and it is not possible to establish the character of this orientation by a direct method on the surface of a solid, investigators have resorted to indirect methods, among which flotation itself has played a significant part. Here we started from data from every day practice, according to which

UNIVERSITY OF UTAH
RESEARCH INSTITUTE
EARTH SCIENCE LAB.

Technology for In Situ Uranium Leaching

Ray V. Huff, Donald H. Davidson, David Baughman, and Steven Axen

Introduction

In situ leaching (ISL) is an alternative method of mining uranium from deposits that are low-grade, deep-lying, and water-saturated. ISL recovers uranium by transporting fluids through rock rather than by moving rock, a concept the Chinese developed over 2000 years ago for water production. This technique eventually evolved into production systems for oil, gas, sulfur, and salt. More recently, in situ methods have been developed to produce shale oil, gasified coal, geothermal energy, uranium, and copper.

ISL uranium operations began in the early 1960s with Sabine Production Co. in south Texas. About the same time, Utah Construction and Mining Co. (Anderson and Richie, 1968) started similar operations in Wyoming's Shirley Basin. During the

1970s, six commercial operations were started in south Texas, (USBM, 1978) and a number of pilot operations were in various stages of development in Colorado, Wyoming, and New Mexico.

This paper reviews some of the technical and economic aspects of the ISL process and briefly discusses key subsurface engineering functions associated with well pattern design and operation.

While flow characteristics of a deposit are of prime importance, the following information is also needed: Depth, ore grade, total contained metal, ore thickness, flow conductivity (permeability), void space in rock (porosity), mineral type and distribution, natural groundwater flow, and structural features.

Solvent selection, which is important to the economic success of the operation, takes these factors

into account: Composition, rate of metal solubilization, interaction with gangue minerals, impact on rock permeability, impact on materials of construction, trace metal solubilization, cost, availability, and handling problems.

Overview of ISL

An ISL operation consists of these functions (Fig. 1):

1. Chemicals to dissolve and maintain uranium in solution are prepared at the surface extraction facility.
2. A set of injection wells forces the solvent into rock pores or fractures using pressure in excess of the deposit's hydrostatic pressure.
3. Solvent travels through the rock and reacts with uranium minerals to dissolve them. The solvent usually consists of an oxidant and a complexing agent in an acidic or alkaline medium.

4. A set of production wells creates a low-pressure sump where metal-enriched solution is collected for transport to the surface.

5. The enriched solution is processed to recover uranium and to separate the leaching solution for recycling through the system.

The economic performance of an in situ operation may be estimated by integrating these related factors: (1) the flow rate of solution processed through the system, (2) rates of fluid injection and production from wells, (3) the rate of mineral solubilization in the liquid phase, and (4) the volume of rock swept by the fluid.

As these factors reveal, ISL involves the technical disciplines of petroleum engineering, ore deposit geology, and hydrometallurgical processing.

Wellfield Design

Just as mineral engineers use drillhole information to plan a conventional mine, in situ engineers use similar information to design a well field. A thorough knowledge of deposit geology and reservoir properties is required. Early application of pressure transient testing, such as

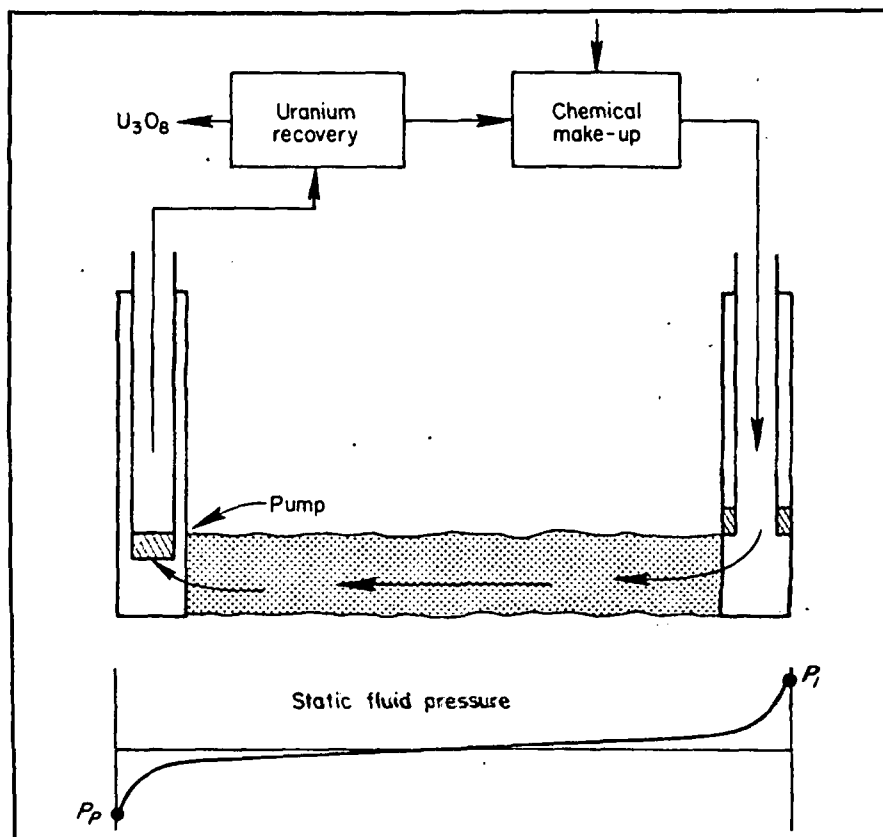


Fig. 1—Overview of in situ leaching.

drawdown and injection tests, (Davidson, et al, 1978) will determine native reservoir properties before they are altered by subsequent tests. Also useful are chemical tracer tests to study subsurface flow.

Boundary wells are necessary to monitor changes in the external wellfield environment and sometimes to contain wellfield leach solutions.

The central issue in wellfield design is the time profile of the produced uranium concentrations (Fig. 2). A time t_1 is required to overcome groundwater dilution of the enriched uranium contained in the pores of the well field. At some later time t_2 , uranium depletion in the flow path between injection and production wells causes a decline in both produced uranium concentrations and total wellfield uranium production. At time t_3 , addition of more wells within unused portions of the ore body are required to maintain efficient overall production.

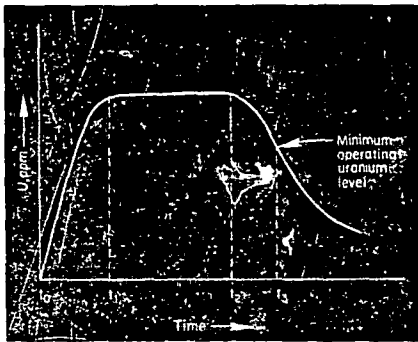


Fig. 2—Time profile of uranium concentration.

Drilling and Completion

Drilling

Drilling usually is done with conventional rotary drills, except in the case of very competent rock where percussion drills are employed. Directional drilling may be desirable. Drilling information such as penetration rate, lost circulation zones, etc., should be recorded, as it will later prove useful during well test analysis. Openhole geophysical logging subsequent to drilling may also provide useful information.

Casing

Soon after the hole has been completed, it should be cased. The engineer must select a casing that will accommodate the production equipment, resist corrosion, and withstand the stresses imposed during setting and cementing, as well as those stresses caused by the rock formation (such as squeezing clay zones and sand movement). Most uranium deposits are within 457 m of the surface. For those relatively shallow depths, firms often specify polyvinyl chloride

(PVC) casing (ASTM). This material presents some difficulty because its low specific gravity allows it to float in heavy drilling mud or cement. This characteristic requires unusual setting and cementing practices. Another problem is that mechanical data and design information for PVC pipe and PVC connections are scanty.

At greater depths where PVC strength is inadequate, the engineer can turn to fiberglass reinforced pipe (FRP). Much more information is available for this type of casing (API), which has been installed in wells deeper than 1524 m. Combination casing strings also can be designed using carbon steel with either stainless steel or fiberglass. The carbon steel must, of course, be isolated from the lixiviant and pregnant solution by using corrosion-resistant tubing and packers.

Cementing

Cementing follows soon after the installation of casing. Design information on Portland cement (ASTM, 1970), API cements (Smith, 1976), and additives are readily available. For applications in acid solutions with pH of 2 or less, epoxy cement can be used. A good cement job is as necessary as good casing and will prevent casing failures due to lack of support. Neither the casing nor the cement can be changed after installation, and repairs are time consuming, difficult, and costly.

Sand Control

Maintaining wellbore integrity is an important operational consideration. Sand movement can cause well collapse or severe permeability impairment. Design systems relating to many different geologic and operating conditions have been developed for oil and gas production and have been discussed in detail by Suman (1975, a, b). These problems are also common in groundwater production.

Injection System

The engineer engaged in an in situ mining activity is faced with design,

installation, and operation of a system to dissolve and transport metallic ions. Fluids capable of dissolving uranium minerals are also often capable of corroding conventional wellfield hardware. Suitable materials for in situ mining operations must be specified, and until service and equipment companies have adjusted to this new requirement, the designer must be concerned with all details. It is the engineer's responsibility to specify construction materials, not only for the fluid ends of high-pressure components but also for valve seats and stems, and even for O-rings in packers, bourdon springs in gauges, and welding procedures.

The engineer may need to develop systems to inject two-phase fluids (gas dispersed in liquid). If a multiphase fluid is employed, the most difficult problem is maintaining a homogeneous dispersion of the two phases through the injection interval. This problem has been addressed in patent literature, and effective procedures have been demonstrated (Hsueh, et al, 1978; Huff and Moynihan, 1978).

Chemical Interactions With Wellfield Design

Chemical requirements for leaching uranium are twofold: (1) use of an oxidizing agent, unless minerals are all oxidized and no reductants are present, and (2) complexing the solubilized uranium with sulfate or carbonate to maintain it in solution.

For uranium minerals in the +4 valence state, uranium solubilization requires oxidation and maintenance in the +6 state. Current in situ leaching operations use hydrogen peroxide or oxygen as an oxidant. Both behave in a chemically similar fashion—peroxide, on contact with minerals in the rock, decomposes to oxygen and water. If insufficient pressure exists in the reservoir to maintain oxygen in solution, free gas forms.

Peroxide is more convenient to inject, but it is about 10 times more expensive than oxygen (per pound of uranium produced). Approximately

Table 1—Oxidant Types

Type	Advantages	Disadvantages
Oxygen (O ₂)	Least expensive (\$0.16 per pound), based on ore-reducing capacity in Texas	Handle gas and liquid in well from surface to formation; may have free gas in formation that can vent vertically or reduce leaching rate
Hydrogen peroxide (H ₂ O ₂)	Do not have to handle gas and liquid in wellbore	More expensive than oxygen (about \$2 per pound); decomposes to oxygen on contact with rock, thus behaves like oxygen in formation
Chlorate (ClO ₂)	Do not have to handle gas and liquid in wellbore; no free gas exists in formation	More expensive than oxygen (about \$2 per pound); end product of oxidation is Cl ⁻ , which may interfere with surface extraction plant and is corrosive to stainless steel; sodium form may lead to clay swelling and permeability reduction; potassium form may be more expensive

Table 2—Solvent Types

Type	Advantages	Disadvantages
Sulfuric acid (H ₂ SO ₄)	Probably least damaging to environment; probably increases injection permeability; less likely to mobilize molybdenum, which interferes with uranium recovery; low rates of radium mobilization	Reacts with rock to increase pH of solution between wells; may liberate selenium and arsenic; may plug production wells with gypsum
Alkaline carbonate system	Maintains pH control with minimal rock interaction; may mobilize less selenium and arsenic	NH ₄ ⁺ form leads to environmental concern; Na ⁺ form may swell clays and damage permeability; may plug production wells with calcite or generation of carbon dioxide gas; molybdenum in solution can interfere with uranium extraction on surface

\$2 per pound operating cost is associated with present peroxide use. Liquid-soluble oxidants such as sodium chlorate can also be used. Table 1 summarizes pros and cons for various oxidants. Solubilized uranium is maintained in solution by forming an anion complex with carbonate (CO₃) or sulfate (SO₄). The former corresponds to an alkaline solvent, the latter to an acidic solvent.

Choice of a solvent is related to the ability of the fluid to maintain pH as it travels between wells. For rock formations that contain acid-consuming gangue such as calcite, the tendency is to use an alkaline solution. Other considerations are related to solubilization of trace elements and their environmental or process consequences. Table 2 summarizes some pros and cons of each solvent type. Laboratory screening tests can determine potential trace element composition of produced fluid.

Chemical Reactivity of Uranium Minerals

The rate of solubilization of uranium is likely to be affected by combinations of oxygen concentration, pH, and anion concentration. The chemical activity of the oxygen dissolved in the liquid usually controls rates of mineral dissolution. When combinations of ore-reducing capacity and formation pressure cause free oxygen gas to form in rock, chemical reactivity is controlled by oxygen solubility—not total oxygen concentration—with the possibility of free gas blinding some mineral surfaces and reducing net rates of uranium solubilization. With respect to the anion, it is likely that higher sulfate and CO₃ concentrations will increase reactivity, but they also will increase the tendency to precipitate gypsum (CaSO₄) and calcite (CaCO₃). Reactivity effects must be balanced against potential permeability damage due to mineral precipitation.

Effect of Oxidant Concentration on Injection

As the oxygen concentration is increased to achieve higher metal concentrations, some level is reached at

which free oxygen gas forms. This free gas increases the resistance of liquid flow in the rock (by reducing permeability). The productivity of the well unit (the product of flow rate and concentration, expressed in pounds per day of metal) will continue to increase, although at a lower rate than with a soluble oxidant, until a point is reached at which free gas inhibition of flow rate exceeds the added oxidizing power. Beyond this point, additional wells must be used to achieve higher metal concentrations.

Effect of Oxidant Concentration on Well Spacing When Free Oxygen Exists

When free oxygen gas exists in the formation, uneven flows of oxygen and solvent will occur in both the vertical and horizontal directions. Well separations and injected oxygen concentrations have to be balanced when free gas is present in the deposit to insure that an oxidizing condition can be reached within the well pattern.

Free gas can segregate vertically in an unproductive manner in the leach zone (Fig. 3). The vertically migrating oxygen is not available to oxidize minerals in the bulk of the rock between wells. Two actions can be taken to compensate for vertical migration:

1. Increase the level of oxygen injection. This will reduce injection permeability and increase chemical and operating costs. Too much excess free gas could lead to mineral blinding, reducing the rate of leaching.
2. Reduce well spacing. This will increase the number of wells and their total cost and may not provide sufficient time for oxygen to react with the uranium.

Recovery System

Downhole production equipment (pumps, tubing, packers, etc.) operates in corrosive environments, as does the equipment in an injection system. Packers and tubing used in the injection wells usually meet production well requirements, but the chief concern is downhole pumps. Few choices are available. At least two manufacturers provide all stainless steel electric submersible pumps that can handle in situ flow rates. A conventional oilfield electric submersible has been built from corrosion-resistant materials and tested in a leaching operation. This pump was installed at 914 m and produced 2 L/s of corrosive fluid for approximately three months with no apparent problems.

Suitable corrosion-resistant sucker

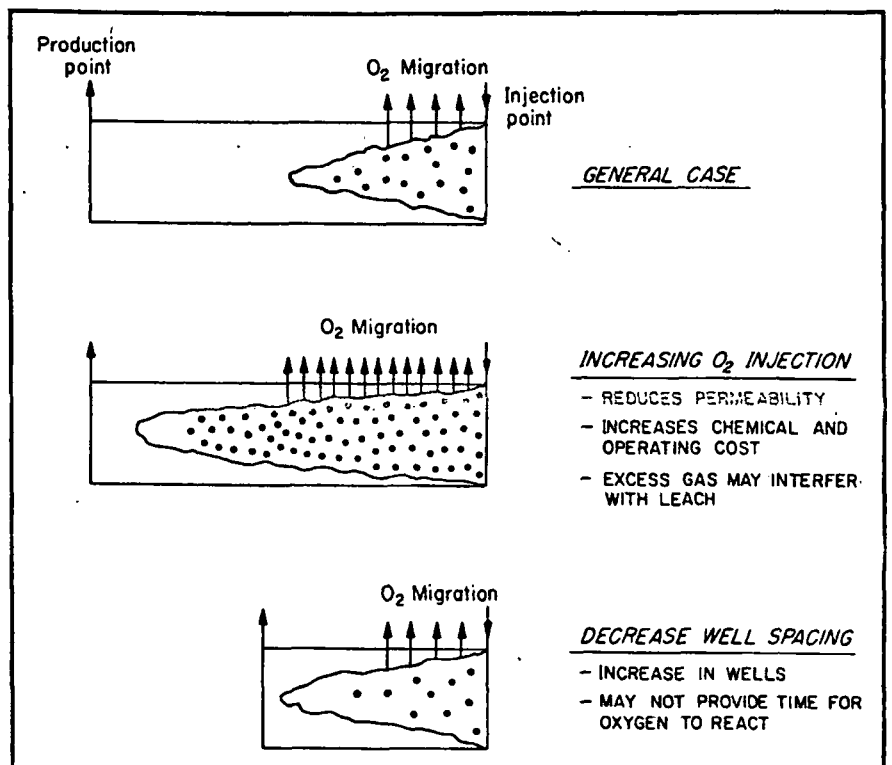


Fig. 3—Compensating for vertical gas migration.

Some problems in the determination of the comparative effectiveness of capital investments in non-ferrous metallurgy
S R Alimkhodzhaev (Tashkent Polytechnical Institute - Department of Economics and Organisation of the Mining Industry)

SUBJ
MING
TKD

Summary

In non-ferrous metallurgy the production efficiency is closely related to the rational utilisation of minerals during their recovery and subsequent processing, since the losses of useful minerals are still high. At the present time the losses of individual non-ferrous metals in all departments, including losses in mineral extraction, vary in the range of 20-25%. In order to improve the utilisation of mineral resources it is necessary to take account of the level of losses of useful minerals when making technical

decisions.

A method for determination of the economic effectiveness of new techniques and new technology in non-ferrous metallurgy is examined. Various technological schemes for the treatment of an ore containing various amounts of extractable components are discussed with the aim of improving the rational utilisation of raw material and increasing the extraction of the useful components.

**UNIVERSITY OF UTAH
RESEARCH INSTITUTE
EARTH SCIENCE LAB.**

800. Non-Ferrous Metals Research
v 6 N 6 1978

UDC 669.5:0534.094(088.8)

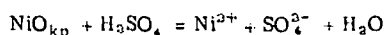
Thermodynamics and kinetics of the dissolution of nickel oxide in sulphuric acid solution

yes

E M Sergievskaya and I A Vorob'eva (Moscow Institute of Steel and Alloys - Department of the Metallurgy of Heavy Non-Ferrous Metals)

Nickel oxide is one of the possible forms in which nickel is contained in roasted zinc concentrate. The present article, therefore, gives data on an investigation into the thermodynamics and kinetics of the dissolution of nickel oxide in sulphuric acid solutions at elevated temperatures and concentrations of sulphuric acid in the solution.

In order to determine the possibility of the realisation of reactions between nickel oxide and sulphuric acid solutions we calculated the Gibbs energies at 25°C. The data for the calculation of the thermodynamic functions were taken from the reference literature. For the change in the Gibbs energy of the reaction



we obtained a value $\Delta G_{298}^0 = -19.7\text{kcal}$, which shows that the dissolution of NiO in sulphuric acid solution is possible.

The calculated value for the equilibrium concentration of sulphuric acid is vanishingly small value

$$(\text{H}_2\text{SO}_4)_{eq} = \frac{[\text{NiSO}_4][\text{H}_2\text{O}]}{K_c} = \frac{0.07 \cdot 0.93}{1.14 \cdot 10^{10}} = 0.5 \cdot 10^{-14}$$

where: $N_{\text{NiSO}_4} = 0.07$ and $N_{\text{H}_2\text{O}} = 0.93$ are the mole fractions of NiSO_4 and H_2O in the solution.

A dynamic method was used for investigation of the dissolution rate of nickel oxide. From nickel oxide of analytical grade we prepared briquettes, which were sintered at 500°C. The briquettes were covered with an acid-resistant varnish, leaving a working surface 5.66cm^2 in area. The dissolution rate in a given time interval, related to unit surface area ($\text{mg}/\text{cm}^2 \cdot \text{min}$), was determined by measurement of the concentration of the cation of the dissolving oxide in the solution.

During the experiment the sulphuric acid concentration in the solution remained practically constant, and the variation of the dissolution rate could therefore occur either on account of diffusion of the reagent or the reaction products or on account of the rate of the chemical reaction itself at the interface.

In all the experiments the rate of movement of the solution amounted to $40\text{cm}^3/\text{min}$, and the length of the experiments was 2h. The nickel in the solution was determined by polarography. The effect of temperature and of the concentration of sulphuric acid in the solution on the dissolution rate of nickel oxide in sulphuric acid was investi-

gated. The experiments were carried out at 60, 70, 80 and 90°C with a sulphuric acid concentration of 0.72 mole/l in the solution.

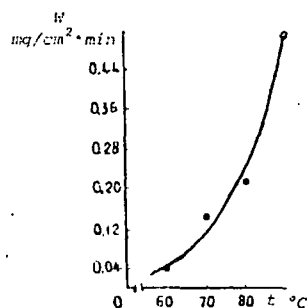


Fig. 1 The dependence of the dissolution rate of nickel oxide on temperature. $C_{\text{H}_2\text{SO}_4} = 0.72\text{mole/l}$.

The results from the experiments are shown in fig. 1. The dissolution rate of nickel oxide depends to a large degree on temperature and varies according to a curve which increases with increase in temperature particularly from 80 to 90°C.

The dissolution rate constants of nickel at various temperatures were calculated with allowance for the activity coefficients of the acid given in the table. The dissolution rate constant of nickel oxide also depends on temperature. From the data in the table we calculated the coefficients A and B of the Arrhenius equation $k = AT^{-1}B$ and determined the activation energy (E) for the dissolution of nickel oxide. As a result we obtained A, B and E values of 11 656, 34.0, and 23.3kcal/mole respectively. The temperature coefficient of the dissolution rate of nickel oxide in the range of 60-90°C is 2.6.

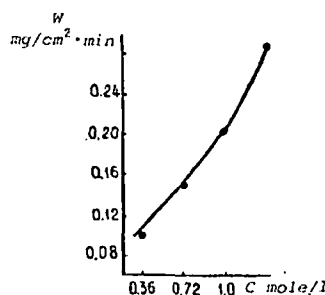


Fig. 2 The dependence of the dissolution rate of nickel oxide on the sulphuric acid concentration in the solution. Temperature 70°C.

The dependence of the rate constant for the dissolution of nickel oxide in sulphuric acid on temperature

°C	γ	ω mg/cm ²	K
60	0.101	0.041	20563
70	0.094	0.143	113
80	0.084	0.209	39459
90	0.078	0.526	376

The values of the activation energy for the dissolution of nickel oxide and the high value of the temperature coefficient show that the kinetics of the dissolution process in sul-

phuric acid are controlled by the rate of the true chemical reaction at the interface. The dependence of the dissolution rate of nickel oxide on the sulphuric acid concentration in the solution was studied at 70°C with sulphuric acid concentrations varying between 0.36 and 1.5 mole/l. The results are shown in fig. 2. The variation of the dissolution rate of nickel oxide with the sulphuric acid concentration is curvilinear, and an increase in the dissolution rate is observed with increase in the sulphuric acid concentration in the solution. It is clear that the factor which controls the dissolution of nickel oxide in this case is the rate of the heterogeneous chemical reaction at the interface.

The investigations into the dissolution of nickel oxide in sulphuric acid show that there are considerable kinetic hindrances to this process.

UDC 669.536

Effect of lead compounds on the behaviour of indium in zinc sulphate solutions *yes*

M V Kravets and E V Margulis (North-Caucasian Mining-Metallurgical Institute - Department of General, Physical and Analytical Chemistry)

The existing technology for the extraction of indium from zinc raw material involves the leaching of Waelz oxides with sulphuric acid solutions. Here up to 30% of the indium contained in the Waelz oxides remains in the leaching residue (the lead cake)¹. It has been noted that during the leaching of indium-containing intermediate products with sulphuric acid increase in the lead content of the materials reduces the extraction of indium in the solution².

In this connection, in the present work we studied the effect of lead compounds on the behaviour of indium. During a check on the suggestion about adsorption capture of indium by lead compounds the authors started from the fact that under production conditions adsorption occurs on the already formed surfaces of the lead compounds: PbO; 4PbO · PbSO₄; 3PbO · PbSO₄; PbSO₄. The synthesis of the known lead oxosulphates was realised in accordance with published recommendations³. A series of solutions containing 100g/l Zn₂nsO₄ and 50g/l of In with pH values of 0.0, 0.3, 0.7, 1.0 and 1.3 were thermostated at 20, 50 and 90°C. On the attainment of the given temperature in the solutions a sample of lead oxosulphate from the above-mentioned series was added in the quantity required for the creation of a solid-liquid ratio of 1:5. After holding at the given temperature for 20 min with vigorous stirring the solutions were filtered, and their indium contents were determined. In none of the in-

vestigated cases was capture of the indium by the precipitate observed.

During the leaching of two industrial intermediate products (Waelz oxides and zinc cakes) containing 10.3% Pb and 0.019% In and 3.2% Pb and 0.006% In respectively at 92-95°C with an initial sulphuric acid concentration of 160-180g/l and a solid-liquid ratio of 1:10, the extraction of indium into solution amounted to 90.1 and 88.4%. Consequently, the presence of lead compounds is not the reason for the losses of indium with the lead cakes.

References

- 1) K A Bolshakov (Ed.): Chemistry and technology of rare and trace elements: Vysshaya shkola, Moscow 1976, p. 304.
- 2) A T Drobchecko et alia: Tr. In-ta Unipromed' Sverdlovsk Metallurgizdat 1958, (3), 154.
- 3) V G Khlopov: Selected works: Izd. Akad. Nauk SSSR, Moscow-Leningrad 1957, 1.
- 4) B A Nikitin: Selected works: Izd. Akad. Nauk SSSR, Moscow-Leningrad 1956.
- 5) E V Margulis: Investigation of basic lead sulphates: Izv Akad. Nauk SSSR, Neorganicheskie Materialy 1972, 8, (2), 393.

UDC 669.714.2

Refining of aluminium alloys of the Al-Si-Cu system from iron

V M Grigorenko, V A Popov, and A A Ofengenden (All-Union Scientific-Research Institute of Secondary Non-Ferrous Metals Production)

An increased content of deleterious metal impurities and of iron, in particular, is observed in alloys obtained from secondary raw material (GOST 1583-73). A characteristic feature of alloys of the AK5M2 and AK5M7 types of the Al-Si-Cu system without modifying additions is their satisfactory casting characteristics. The phase composition of alloys of the AK5M2 type¹ in the casting state is as follows: Si + Mg₂Si + CuAl₂ + AlSiMnFe + α -solid solution. The W(Al_xMg₈Si₄Cu₄) phase may form on cooling. Alloys of the AK5M7 type are distinguished by their increased copper content.

The present article gives the results from laboratory investigations into the refining of cast aluminium alloys of the AK5M2 and AK5M7 type from iron by filtration through a volume filter² consisting of a layer of granulated salt NaCl and heat-treated aluminium filings.

During the experiments the aim was to determine the effect of the following factors on the degree of purification of the alloys from iron (the final content of iron in the alloy C) and on the yield of the filtrate (ϕ): filtration temperature of the alloy t; the initial iron content of the alloy C₀; the ratio of the amount of manganese to iron ψ ; the height of the filter layer H; the metallostatic pressure over the filter h; the weight of filtered metal m. The experimental procedure and the treatment of results have been described before³.

Approximating functions for the final iron content of the alloy C and the yield of usable filtrate ϕ were given in the literature³. A comparison of the data calculated by means of the published formulae³ and the experimental data is given in the table.

SER
MNG
TLQC

JOURNAL OF COMPUTATIONAL PHYSICS 12, 187-201 (1973)

UNIVERSITY OF UTAH
RESEARCH INSTITUTE
EARTH SCIENCE LAB.

The Linear Q and the Calculation of Decaying Spherical Shocks in Solids*

J. A. VIECELLI

Lawrence Livermore Laboratory, University of California, Livermore, California 94550

Received March 7, 1972

The effect of the linear Q on the decay of a spherical shock wave in a solid, as calculated by Lagrangian finite difference techniques, is determined by a study of the partial differential equations approximated by the difference equations. It is shown that the computed solutions approach an asymptotic form determined by the linear Q terms, and the decay law imposed by the linear Q is given. Finally, it is suggested that the physics of the weak decaying shock problem indicate that the numerical linear Q needs to be replaced by terms modeling a true physical damping mechanism.

INTRODUCTION

A computational physics problem in explosion technology is the accurate calculation of a decaying spherical shock wave in a solid. A particular example currently under investigation is the accurate calculation of surface spallation resulting from the detonation of a contained nuclear explosion. The velocity of the spall is twice the particle velocity of the incident shock wave, hence the determination of spall velocity depends on accurate calculation of particle velocity. In addition to military applications, accurate calculation of decaying shocks in solids is necessary for such technologies as the nuclear explosion stimulation of gas and oil wells.

A characteristic of an explosion contained by a solid, almost always the earth, is that the pressure and particle velocity decays rapidly with increased distance from the detonation point. Thus, not far from the explosion, the material response of the medium is nearly linear in the sense that the convective terms in the Eulerian description of momentum conservation are small compared with the pressure terms. Blast waves that satisfy this condition are called weak decaying shocks in the remainder of the paper.

Computer programs, based on finite difference approximations to the differential equations of motion, have been used to calculate shock waves in solids [1-4]. These

* This work was performed under the auspices of the U. S. Atomic Energy Commission.

programs integrate the following Lagrangian equations of motion in two spatial dimensions with axial symmetry:

$$\frac{\partial u}{\partial t} = -\frac{1}{\rho} \frac{\partial P}{\partial R} + \frac{1}{\rho} \frac{\partial \tau_{RZ}}{\partial Z} + \frac{1}{\rho} \frac{\partial \tau_R}{\partial R} + \frac{2\tau_R + \tau_Z}{\rho R} + G_R \quad (1)$$

$$\frac{\partial v}{\partial t} = -\frac{1}{\rho} \frac{\partial P}{\partial Z} + \frac{1}{\rho} \frac{\partial \tau_{RZ}}{\partial R} + \frac{1}{\rho} \frac{\partial \tau_Z}{\partial Z} + \frac{\tau_{RZ}}{\rho R} + G_Z \quad (2)$$

$$\frac{\partial \tau_R}{\partial t} = \frac{2\mu}{3} \left(2 \frac{\partial u}{\partial R} - \frac{\partial v}{\partial Z} - \frac{u}{R} \right) \quad (3)$$

$$\frac{\partial \tau_Z}{\partial t} = \frac{2\mu}{3} \left(2 \frac{\partial v}{\partial Z} - \frac{\partial u}{\partial R} - \frac{u}{R} \right) \quad (4)$$

$$\frac{\partial \tau_{RZ}}{\partial t} = \mu \left(\frac{\partial u}{\partial Z} + \frac{\partial v}{\partial R} \right) \quad (5)$$

$$\frac{\partial R}{\partial t} = u \quad (6)$$

$$\frac{\partial Z}{\partial t} = v. \quad (7)$$

Here R is the radial coordinate, Z is the axial coordinate, u is the radial component of velocity, v is the axial component of velocity, t is the time, ρ is the density, P is the pressure, G_R and G_Z are the components of gravitational acceleration, τ_R , τ_Z and τ_{RZ} are the deviatoric stresses, and μ is the shear modulus. The equation of state is usually in the form:

$$P = f(\Theta), \quad \Theta = \frac{\rho}{\rho_0} - 1. \quad (8)$$

The density of a zone in the finite-difference approximation is determined by dividing the mass of the Lagrangian zone (which remains constant throughout the calculations) by the volume of the zone, which in turn, is calculated from the coordinates of the mesh points defining the zone at the current time. Yield and failure are incorporated by altering the stresses τ_R , τ_Z , τ_{RZ} at each time step of the integration according to a prescription based on the current state of stress. In the case of elastic behavior, the stresses are left unaltered and the pressure is computed from

$$P = k\Theta, \quad (9)$$

where k is the bulk modulus.

The computer programs for solving these equations, such as the TENSOR program [1, 2] and the HEMP program [3, 4], rely on different finite-difference

approximations to the al feature common to all el of $P + Q$ for P where (see Richtmyer [5]). The energy can be converted motion in one spatial dir waves and has the form

where ρ is the density, C_0 spatial difference interval

As noted earlier, the s rapidly with distance. As or second order, terms t difference equations of m or first order terms to th of Q but a fairly typical

$$Q = \begin{cases} C_0 \rho \\ -C \end{cases}$$

where C_1 is a constant, α width. As the wave deca other terms in the equati converting the kinetic ene internal energy.

In fact, the inclusion of basic differential equation and takes the limit Δt -difference equations app model of a viscoelastic so of C_1 such that η is large effects arising from the di ential equations. For th equations approach very equations with dissipation

approximations to the above partial differential equations. However, they have one feature common to all elastic-plastic Lagrangian difference codes: the substitution of $P + Q$ for P where Q is the "pseudo-viscosity" introduced by Von Neumann (see Richtmyer [5]). The purpose of Q is to provide a mechanism by which kinetic energy can be converted to internal energy as the material is shocked. In the case of motion in one spatial dimension, the quadratic Q is intended for very strong shock waves and has the form

$$Q = \begin{cases} C_0 \rho (\Delta x)^2 \left(\frac{\partial u}{\partial x}\right)^2 \frac{\partial u}{\partial x} < 0 \\ 0 & \frac{\partial u}{\partial x} > 0, \end{cases} \quad (10)$$

where ρ is the density, C_0 is a constant of the order of one, and Δx is the size of the spatial difference interval.

As noted earlier, the spherical shock wave from an explosion in a solid decays rapidly with distance. As a result, one quickly reaches a range at which quadratic, or second order, terms become small compared with the first order terms in the difference equations of motion. To counteract this, investigators have added linear or first order terms to the expression for Q . There have been many formulations of Q but a fairly typical example in one spatial dimension is

$$Q = \begin{cases} C_0 \rho (\Delta x)^2 \left(\frac{\partial u}{\partial x}\right)^2 - C_1 \rho \alpha \Delta x \left(\frac{\partial u}{\partial x}\right) \frac{\partial u}{\partial x} < 0 \\ -C_1 \rho \alpha \Delta x \left(\frac{\partial u}{\partial x}\right) & \frac{\partial u}{\partial x} > 0, \end{cases} \quad (11)$$

where C_1 is a constant, α is the compressional sound velocity, and Δx is the mesh width. As the wave decays, the linear terms in this Q remain comparable to the other terms in the equations of motion and continue to perform the function of converting the kinetic energy of oscillation between neighboring mesh points into internal energy.

In fact, the inclusion of linear Q terms amounts to adding dissipation terms to the basic differential equations. If one defines the viscosity coefficient $\eta \equiv C_1 \rho \alpha \Delta x$ and takes the limit $\Delta t \rightarrow 0$, $\Delta R \rightarrow 0$, $\Delta Z \rightarrow 0$ while holding η constant, the difference equations approach the differential equations for the Voigt-Kelvin model of a viscoelastic solid. In practice, one almost always operates with a value of C_1 such that η is large enough that the Q terms dominate any of the truncation effects arising from the difference approximation to the other terms in the differential equations. For this reason, the solutions obtained from the difference equations approach very closely the solutions one obtains for the differential equations with dissipation terms added.

The intent of this paper is to provide a quantitative understanding of the effect of the linear Q upon the attenuation of a weak spherical shock. Because the phenomena is so nearly linear, except in the immediate neighborhood of the explosion, it is easier to attack the problem at the level of the partial differential equations rather than that of the difference equations. The specific Q investigated is used in a version of the TENSOR program [1, 2]. The critical role Q plays in determining the pulse shape and particle velocity in a weak spherical shock will be demonstrated, and it will be shown that the presence of a linear Q implies an inverse three-halves power decay law.

ASYMPTOTIC SOLUTION FOR THE SPHERICAL SHOCK WITH LINEAR Q

With the tensor version of the linear Q used in the program, the differential equations are

$$\frac{\partial u}{\partial t} = -\frac{1}{\rho} \frac{\partial(P + Q - \tau_R - Q_R)}{\partial R} + \frac{1}{\rho} \frac{\partial(\tau_{RZ} + Q_{RZ})}{\partial Z} + \frac{2\tau_R + \tau_Z + 2Q_R + Q_Z}{\rho R} \quad (12)$$

and

$$\frac{\partial v}{\partial t} = -\frac{1}{\rho} \frac{\partial(P + Q - \tau_Z - Q_Z)}{\partial Z} + \frac{1}{\rho} \frac{\partial(\tau_{RZ} + Q_{RZ})}{\partial R} + \frac{\tau_{RZ} + Q_{RZ}}{\rho R}, \quad (13)$$

where τ_R , τ_Z , and τ_{RZ} are the deviatoric stresses and the Q , Q_R , Q_Z , and Q_{RZ} are given by

$$Q_R = \frac{2\eta}{3} \left(2 \frac{\partial u}{\partial R} - \frac{\partial v}{\partial Z} - \frac{u}{R} \right), \quad (14)$$

$$Q_Z = \frac{2\eta}{3} \left(2 \frac{\partial v}{\partial Z} - \frac{\partial u}{\partial R} - \frac{v}{R} \right), \quad (15)$$

$$Q_{RZ} = \eta \left(\frac{\partial u}{\partial Z} + \frac{\partial v}{\partial R} \right), \quad (16)$$

$$Q = -\lambda \left(\frac{\partial v}{\partial Z} + \frac{1}{R} \frac{\partial u R}{\partial R} \right); \quad (17)$$

$$\eta = C_1 \rho \alpha \langle \Delta x \rangle, \quad (18)$$

$$\lambda = C_1 \rho \alpha \langle \Delta x \rangle. \quad (19)$$

Here $\langle \Delta x \rangle$ is the characteristic mesh length and C_1 is an input constant. In a two-dimensional calculation $\langle \Delta x \rangle$ is determined from a weighted average of the

distances between quantities, the model of a vi

The deviat assumption o Lagrangian c Eulerian coor and, in turn, results in a p placements Δ displacement vector potenti one need only

$$\frac{\partial^2 \phi}{\partial t^2} = \left(\right.$$

The radial dis

The velocity p

so that the par

In deriving th problem with t while, in fact, t the mesh width that is effective the linear Q is program used b expansion regio strictly satisfied.

distances between the mesh points defining a zone. In one-dimensional calculations $\langle \Delta x \rangle$ is just the width of a zone. Although η and λ are numerical and not physical quantities, the notation denoting shear viscosity and bulk viscosity has been used to emphasize the equivalence of the linear Q formulation to the Voigt-Kelvin model of a viscoelastic solid.

The deviatoric stresses are determined by the original Eqs. (3-5). With the assumption of small displacements, the spatial differentials with respect to the Lagrangian coordinates may be replaced by spatial differentials with respect to Eulerian coordinates. Substitution of Eqs. (6 and 7) into Eqs. (3-5, 14-16, and 17) and, in turn, substitution of these equations and Eq. (9) into Eqs. (12 and 13) results in a pair of linear partial differential equations for the Lagrangian displacements ΔR and ΔZ . In the theory of elasticity it is shown that the elastic displacement equations can be further simplified by the introduction of scalar and vector potentials. In the case of spherical symmetry the vector potential is zero and one need only solve for the scalar displacement potential given by

$$\frac{\partial^2 \phi}{\partial t^2} = \left(\frac{k + \frac{4\mu}{3}}{\rho} \right) \frac{1}{r^2} \frac{\partial}{\partial r} \left(r^2 \frac{\partial \phi}{\partial r} \right) + \left(\frac{\lambda + \frac{4\eta}{3}}{\rho} \right) \frac{1}{r^2} \frac{\partial}{\partial r} \left(r^2 \frac{\partial^2 \phi}{\partial r \partial t} \right). \quad (20)$$

The radial displacement is then given by

$$\Delta R = - \frac{\partial \phi}{\partial r}. \quad (21)$$

The velocity potential is given by

$$\Phi = \frac{\partial \phi}{\partial t}, \quad (22)$$

so that the particle velocity is given by

$$u = - \frac{\partial^2 \phi}{\partial r \partial t}. \quad (23)$$

In deriving the basic differential equation corresponding to the spherical shock problem with the linear Q , I have taken the coefficients η and λ to be constants while, in fact, they usually have some spatial variation as a result of variations in the mesh width, density, and sound speed. Furthermore, I have used a linear Q that is effective in both compression and expansion regions; in many formulations the linear Q is set to zero in expansion regions. The version of the TENSOR program used has constant input values for η and λ and leaves the linear Q on in expansion regions so that all of the requirements for the analytic solution are strictly satisfied.

The driving mechanism that approximates the explosion closely at early times is that of a small cavity expanding at constant velocity. This boundary condition is satisfied if the solution approaches the form

$$\phi = \frac{\phi_0 t}{r} \quad (24)$$

in the neighborhood of the origin. To solve for the asymptotic form of the decaying spherical shock with linear Q , put $\phi = A/r$ and substitute into Eq. (18) to get

$$\frac{\partial^2 A}{\partial t^2} = \alpha^2 \frac{\partial^2 A}{\partial r^2} + \nu \frac{\partial^3 A}{\partial r^2 \partial t}, \quad (25)$$

where

$$\alpha^2 = \frac{k + \frac{4}{3}\mu}{\rho} \quad (26)$$

and

$$\nu = \frac{\lambda + \frac{4}{3}\eta}{\rho}. \quad (27)$$

Taking the Laplace transform H of A with respect to time gives

$$s^2 H - sA(0) - A(0) = \alpha^2 \frac{\partial^2 H}{\partial r^2} + \nu \frac{\partial^2}{\partial r^2} \{sH - A(0)\}. \quad (28)$$

Since the material is initially at rest, A and \dot{A} are identically zero, thus

$$\frac{d^2 H}{dr^2} - \left(\frac{s^2}{\alpha^2 + \nu s} \right) H = 0. \quad (29)$$

The solution, which decays to zero as $r \rightarrow \infty$, is

$$H(r, s) = A(s) \exp\{-rs(\alpha^2 + \nu s)^{-1/2}\}. \quad (30)$$

The Laplace transform of the boundary condition at $r = 0$ is

$$L\{\phi_0 t\} = \phi_0 s^{-2}. \quad (31)$$

Therefore, the transform of the solution is

$$H(r, s) = \phi_0 s^{-2} \exp\{-rs(\alpha^2 + \nu s)^{-1/2}\}. \quad (32)$$

Taking the time derivative and the Laplace transform of the solution

$$F(r, t)$$

The inversion may be performed

corresponding to the asymptotic form

$$\Phi(r, t)$$

where

and

Therefore the solution for $t > 0$

$$u = \frac{\phi_0}{2r^2} \left\{ 1 + \dots \right\}$$

The analytic solution for u is plotted as small circles in Figure 1. The values of $\phi_0 = 1.6 \times 10^8 \text{ cm}^3 \text{ sec}^{-1}$, $t = 0.35 \text{ sec}$. Figure 1 also shows the results of the same problem. These are plotted as small circles. The analytic solution only by using the boundary condition at $r = 0$ are two additional variables and Poisson's ratio, which choice is arbitrary, since only the shear modulus are determined.

Taking the time derivative of the solution corresponds to multiplying the transform of the solution by s , since $A(+0) = 0$, therefore the transform of \dot{A} is

$$F(r, s) = \phi_0 s^{-1} \exp\{-rs(\alpha^2 + \nu s)^{-1/2}\}. \quad (33)$$

The inversion may be performed easily when

$$\frac{r\alpha}{2\nu} \gg 1,$$

corresponding to the asymptotic limit to give the velocity potential

$$\Phi(r, t) = A/r = \frac{\phi_0}{2r} [1 + \operatorname{erf}(\tau \sqrt{\sigma})], \quad (34)$$

where

$$\tau = \frac{\alpha t}{r} - 1 \quad (35)$$

and

$$\sigma = \frac{r\alpha}{2\nu}. \quad (36)$$

Therefore the solution for the particle velocity is

$$u = \frac{\phi_0}{2r^2} \left\{ 1 + \operatorname{erf}(\tau \sqrt{\sigma}) + (2 + \tau) \left(\frac{\sigma}{\pi}\right)^{1/2} \exp(-\sigma\tau^2) \right\}. \quad (37)$$

DISCUSSION OF RESULTS

The analytic solution has been evaluated for a particular case and the results are plotted as small circles in Fig. 1. The parameters for this case are $\phi_0 = 1.6 \times 10^8 \text{ cm}^3 \text{ sec}^{-1}$, $\nu = 7.5 \times 10^7 \text{ cm}^2 \text{ sec}^{-1}$, $\alpha = 2.3 \text{ km sec}^{-1}$, and $t = 0.35 \text{ sec}$. Figure 1 also includes the results for a TENSOR calculation of the same problem. These are plotted as small crosses. The elastic constants enter into the analytic solution only by way of the compressional sound velocity, thus there are two additional variables in the finite-difference problem. These are the density and Poisson's ratio, which I chose to be 2.0 g cm^{-3} and $1/3$, respectively. The choice is arbitrary, since once these two variables are fixed, the bulk modulus and shear modulus are determined by the sound velocity.

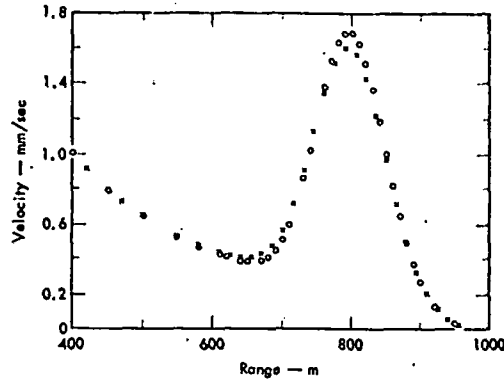


FIG. 1. Shock particle velocity plotted as a function of range. The small circles are points evaluated from the analytic solution. The crosses are points obtained from a finite-difference solution. The time is 0.35 sec.

Spherical symmetry was simulated in the numerical problem by choosing a wedge-shaped mesh with one edge along the z axis of axial symmetry and the other edge at an angle of 10 deg from the z axis. The wedge began at an inner radius of 20 m and extended out to 1150 m. The analytic result is the asymptotic solution for a cavity expanding at constant velocity. Thus it is necessary to start the numerical calculation with a cavity small enough to ensure that the asymptotic state is reached before comparing results. Furthermore, the cavity must not be driven with too large a velocity, else the linearity assumption would be violated. These precautions must be taken to guarantee that the source function in the numerical problem is well defined in terms of the source in the analytical solution.

It should be emphasized that the asymptotic state is eventually reached whether or not the linearity assumption is violated in the neighborhood of the cavity. For a nonlinear source, there is always some particular amplitude for the linear source that produces the same asymptotic state as the original nonlinear source. The precautions mentioned ensure that the numerical problem starts with the equivalent linear source amplitude known beforehand. The cavity velocity corresponding to the value of ϕ_0 in the analytical solution is 40.0 cm sec⁻¹. That value satisfies the analytical boundary condition given by Eq. (24) for an initial cavity radius of 20.0 m.

The numerical calculation was done on a mesh containing 140 radial zones. The zoning was not uniform so as to permit relatively fine zoning next to the cavity. This is necessary to get a good approximation to the analytical source at zero radius. The slight amplitude discrepancy observed in Fig. 1 is the result of this approximation. This was confirmed by making several runs, each with a smaller driving cavity and finer zoning. The amplitude of the numerical solution was

observed to converge as the zone size increased. The zone size increased gradually and the zone size remained constant.

By referring to Eqs. (1) and (2), the value of ϕ_0 which is the value of the parameter n in the computer solution code supports the contention that the asymptotic state dominates truncation error. In this case, the free surface velocity and the calculation code for the pulse approaches zero as the time in Fig. 2, but the close agreement is maintained.

Normalized velocity

FIG. 2. Normalized shock particle velocity versus range. The crosses are points evaluated from the finite-difference solution. The time is 0.35 sec.

An indication of how the asymptotic form imposed by the source in Fig. 2. The TENSOR code and the asymptotic solution simulated the explosion of a spherical cavity source was a spherical cavity rock at a pressure of 1.7 GPa. The radius of the cavity out to a

observed to converge to the analytical result as the resolution in the cavity region increased. The zone size at the cavity for the run in Fig. 1 was 2.0 m. The zone size increased gradually to 15.0 m at a radius of 550.0 m. Beyond this radius the zone size remained constant at 15.0 m.

By referring to Eqs. (18), (19), and (27) one can see that beyond 550 m the zone size and the parameters ν and α are equivalent to a linear Q coefficient of 0.1, which is the value normally used in TENSOR calculations. The fact that the computer solution continues to agree with the analytical solution beyond 550 m supports the contention that the linear Q , as actually used in practical calculations, dominates truncation effects arising from other terms in the equations. To check this, the free surface was moved out to 2000 m (with the same 15.0 m zone size) and the calculation continued until the pulse reached 1500 m. At the greater range, the pulse approaches a symmetrical Gaussian form, similar to the example shown in Fig. 2, but the close agreement between computer and analytical solutions is maintained.

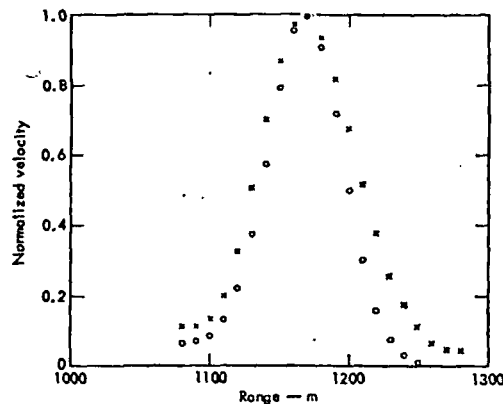


FIG. 2. Normalized shock particle velocity plotted as a function of range. The small circles are points evaluated from the analytic solution. The crosses are points obtained from the finite-difference solution. The time is 0.375 sec.

An indication of how closely an actual explosion calculation approaches the asymptotic form imposed by the linear Q is given by the particle velocity plot in Fig. 2. The TENSOR finite-difference results are indicated by the small crosses and the asymptotic solution by the small circles. The numerical calculation simulated the explosion of a 25.0 kton explosion in the earth at a depth of 1280 m. The source was a spherical cavity, initially with a radius of 5.0 m, containing vaporized rock at a pressure of 1.74 mbar. The gas expanded adiabatically, forcing the walls of the cavity out to a radius of approximately 30 m. The containing rock was

programmed to have a shear strength of only a few kilobars, hence severe plastic flow occurred. In addition, the numerical simulation included overburden and several different layers of earth and rock materials, so that the portion of the shock propagating vertically passed through a density and strain energy gradient. It is not necessary to go further into the details of the numerical run except to note that the average values of \bar{a} and \bar{v} were 3.12×10^6 cm sec⁻¹ and 1.85×10^7 cm² sec⁻¹, respectively. These values were used in evaluating the analytical solution. The plot shown in Fig. 2 was taken along a radius, which extended vertically to the surface, located at 1280 m. The failure of the numerical solution to go to zero on the leading side of the pulse is explained by the fact that the shock is just beginning to strike the surface. Despite all of the nonlinearities, and inelastic behavior in the source region the resulting blast wave is in close agreement with the predictions of the asymptotic linear theory.

The development and discussion has been based on a formulation of the linear Q which is active in both compression and expansion zones, however many investigators simply turn the linear Q off in expansion regions maintaining that there should not be a dissipative mechanism there. An analytical solution for this type of linear Q might be derivable by perturbation methods, but I was not able to do it. To examine this case, the first problem (the run shown in Fig. 1) was rerun with the Q terms set to zero in expansion regions. Figure 3 is a duplicate of Fig. 1 with the addition of the run with the Q turned off in expansion. It can be seen that this run is the same as the first except in the expansion region where the removal of the linear Q has introduced an oscillatory perturbation. The decay rate for the run with the Q turned off in expansion was observed to follow an inverse 1.5 power law.

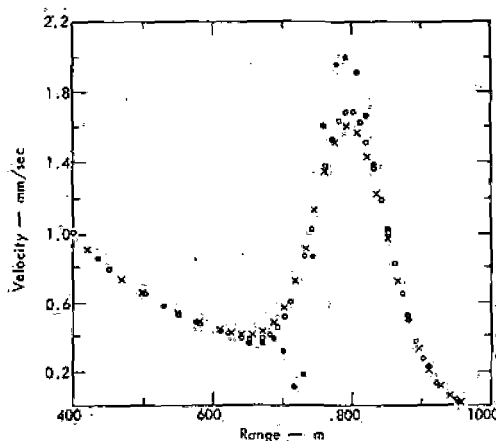


FIG. 3. Duplicate of Fig. 1 with the addition of a run with the linear Q set to zero in expansion regions. Data points from this run are indicated by the solid dots. The time is 0.35 sec.

The intent of this Q and its effect on a intended it to be a discontinuities in \bar{v} assumed inviscid flow at a shock. One of the is the fact that unless of weak decaying wave short wavelength near shock front has peculiar applications to gases.

The underlying physics different from that of viscous effects can be. In the former case, an attenuation mechanism decay rate. A comparison Lighthill [6]. The shock, just a smooth materials this point is shock fronts from later partially fused volcanic the time the front has stage that numerical linear damping mechanism.

In practice the solid because the calculation. In the case of decaying a type of Voigt solid, the parameters. The fact physical model of decay made more rational. The physical model of decay and whether or not the is to make the linear equation in both compression Eqs. (14-17) input viscous.

It is evident from the pulse are strongly influenced. It is, therefore, decaying shock problem.

The intent of this work has been to gain a theoretical understanding of the linear Q and its effect on a weak blast pulse in a solid. The originators of the quadratic Q intended it to be a convenient computational device for including strong shock discontinuities in invicid gas dynamic calculations. Since the physical model assumed invicid flow it was natural to suppress viscosity effects everywhere except at a shock. One of the main reasons for the subsequent development of the linear Q is the fact that unless some kind of linear damping is included in the calculation of weak decaying waves the solutions quickly become obscured in a hashwork of short wavelength noise. The idea that viscosity must be suppressed except at the shock front has persisted through the development of the linear Q , first in applications to gases and then finally to solids.

The underlying physics of weak decaying shocks in solids, and gases also, is different from that of high-pressure, high-speed gas dynamics. In the latter case viscous effects can usually be ignored except in shocks or thin boundary layers. In the former case, at some point in the decay of the shock pulse, the physical attenuation mechanisms come to have a dominant effect on the pulse form and decay rate. A comprehensive discussion of the shock decay process is given by Lighthill [6]. The shock transition region thickens until there is no recognizable shock, just a smoothly varying attenuated sound pulse. In solids and earth materials this point may be very near the site of the explosion. For example, the shock fronts from large nuclear explosions in Nevada Tuffs (a kind of compacted partially fused volcanic ash) are spread over as much as several hundred meters by the time the front has traveled a kilometer. It is at this finite-amplitude sound wave stage that numerical noise becomes a problem unless suppressed by some kind of linear damping mechanism.

In practice the solid mechanics programs cannot compute purely elastic response because the calculations must always be made with a finite number of zones. In the case of decaying explosion waves what they do calculate is the response for a type of Voigt solid, but with viscosity coefficients that depend on purely numerical parameters. The fact that some type of viscosity is required for an adequate physical model of decaying shocks suggests that the use of the linear Q could be made more rational. This could be done by making it correspond exactly to some physical model of damping, rather than have it depend on zone size and shape, and whether or not the zone is in expansion or compression. The easiest thing to do is to make the linear Q correspond exactly to the Voigt model by keeping the Q on in both compression and expansion and by making the coefficients η and λ in Eqs. (14-17) input viscosities.

It is evident from the preceding results that the amplitude and shape of the blast pulse are strongly influenced by a linear Q , so that the spall velocity is also strongly affected. It is, therefore, useless to attempt to calculate spall velocities in weak decaying shock problems without first replacing the linear Q by some physical

hence severe plastic
led overburden and
portion of the shock
nergy gradient. It is
a except to note that
 $1.85 \times 10^7 \text{ cm}^2 \text{ sec}^{-1}$,
al solution. The plot
ically to the surface,
go to zero on the
ock is just beginning
lastic behavior in the
ith the predictions of

lation of the linear Q
however many investi-
aintaining that there
solution for this type
was not able to do it.
ig. 1) was rerun with
uplicate of Fig. 1 with
can be seen that this
re the removal of the
decay rate for the run
inverse 1.5 power law.

Q set to zero in expansion
ie time is 0.35 sec.

model of damping such as the Voigt model. While the Voigt model may not be the best physical model, it is at least free from arbitrary numerical parameters such as zone size and shape. Furthermore, with the Voigt model one can show that a fundamental quantity, the integrated momentum per unit surface area of the pulse, is independent of the viscosity coefficients. Integrating Eq. (37) in the limit of large radius

$$M \sim \frac{\phi_0}{r} \int_{-\infty}^{\infty} \sqrt{\frac{\sigma}{\pi}} e^{-\sigma\tau^2} d\tau = \frac{\rho\phi_0}{r} \quad (38)$$

This is an important quantity because it can be measured experimentally and because it is the impulse that can be delivered by the blast pulse if it is absorbed inelastically. In the case of an underground explosion, the surface spall acts as the absorber, carrying most of the momentum of the blast pulse with it as it flies up from the surface. The significance of the result in Eq. (38) is that one can expect to calculate the impulse delivered by the blast wave correctly independent of the viscosity coefficients. Although it may not be possible to calculate the spall velocity correctly because realistic viscosity coefficients are not known or because they must be made abnormally large for numerical smoothing, it should still be possible to correctly calculate the impulse delivered by the blast wave.

Knowledge of the decay law imposed by the damping mechanism is also useful. The decay law for the Voigt model obtained from Eq. (37) is

$$u \sim C_1^{-1/2} r^{-3/2} \quad (39)$$

This result can be used to infer the decay rate for other types of physical damping mechanisms that may be added to the model. For example, the adiabat and Hugoniot are usually represented by the single curve, Eq. (8), in calculations because physically they are practically identical for many solids not shocked above the melting point. However, some earth materials exhibit porosity, so that after shocking, the material follows a different adiabat lying below the adiabat for the unshocked material. As a result the shock pulse undergoes an additional attenuation in traversing the material, and the decay law follows a higher inverse power than 1.5. The difference can then be ascribed to the porosity.

The results presented in this paper may appear paradoxical. It has been shown that the traditional linear Q is essentially a Voigt viscosity but with nonphysical viscosity coefficients proportional to the spatial difference interval. It has also been demonstrated that the presence of these terms ensures that the late time pulse amplitude follows a viscous decay law. If this is so, then how can the numerical solutions obtained from the traditional linear Q finite difference programs ever converge to the asymptotic solutions for purely elastic response? Obviously, by making the difference interval smaller one reduces the artificial viscosity coefficients

proportionately, but independent of the one makes the difference

This paradox can be resolved by using a different dimension the plane Green's function for source at the origin. Green's function is

where A_0 is a constant used instead of r since the response for any convolution with the

$\psi(x,$

where

To make the example width $2a$. Then the solution

$$\psi(x, t) = \frac{A_0}{\sqrt{v}}$$

Then, at the center of

For large β corresponds

$$\psi_c(x) = A_2$$

and for small β corresponds

$\psi_c(x)$

proportionately, but this will not affect the asymptotic decay rate since it is independent of the magnitude of the viscosity coefficients. No matter how small one makes the difference interval there is still a finite viscosity term in the equations.

This paradox can be resolved by considering a simple example. In one spatial dimension the planar response of a Voigt solid is governed by Eq. (25). The Green's function for a source at the origin is obtained by solving Eq. (25) with a source at the origin having a delta function time dependence. The solution for the Green's function is

$$G(x, t; 0, t') = \frac{A_0}{\sqrt{\nu x}} \exp \left[\frac{-\alpha^3}{2\nu x} (\tau - \tau')^2 \right] \quad (40)$$

where A_0 is a constant and τ is the retarded time. The spatial variable x has been used instead of r since planar rather than spherical geometry is being considered. The response for any kind of time dependence of the source $\psi_0(\tau')$ is then given by convolution with the Green's function

$$\psi(x, t) = \frac{A_0}{\sqrt{\nu x}} \int_{-\infty}^{\infty} \psi_0(\tau') \exp[-\beta(\tau - \tau')^2] d\tau', \quad (41)$$

where

$$\beta = \alpha^3 / (2\nu x).$$

To make the example as simple as possible consider a rectangular time pulse of width $2a$. Then the solution is

$$\psi(x, t) = \frac{A_0}{\sqrt{\nu x}} \int_{\tau-a}^{\tau+a} \exp(-\beta\xi^2) d\xi = \frac{A_0}{\sqrt{\nu r\beta}} \int_{(\tau-a)\sqrt{\beta}}^{(\tau+a)\sqrt{\beta}} \exp(-y^2) dy. \quad (42)$$

Then, at the center of the pulse, the amplitude is

$$\psi_0 = A_1 \int_{-a\sqrt{\beta}}^{a\sqrt{\beta}} \exp(-y^2) dy. \quad (43)$$

For large β corresponding to small x this reduces to

$$\psi_c(x) = A_2 \left[1 - \frac{1}{a} \sqrt{\frac{2\nu}{\pi\alpha^3}} \exp\left(-\frac{\alpha^2\alpha^3}{2\nu x}\right) \left(\sqrt{x} - \frac{\nu x^{3/2}}{a^2\alpha^3} + \dots\right) \right], \quad (44)$$

and for small β corresponding to large x

$$\psi_c(x) = A_3 \left[a \sqrt{\frac{\alpha^3}{2\nu x}} - \frac{a^3}{3} \left(\frac{\alpha^3}{2\nu x}\right)^{3/2} + \dots \right]. \quad (45)$$

If the material response were purely elastic the rectangular pulse would simply maintain its shape and amplitude. In the visco-elastic case the pulse maintains its shape and amplitude during the initial stages of travel, except for a very slight rounding at the edges. Then there is a transition stage in which the pulse changes shape and its amplitude begins to decay. Finally, the asymptotic state is reached; the pulse shape assumes Gaussian form and the amplitude becomes inversely proportional to the square root of the range. How these different stages arise is easily understood by referring to the convolution integral Eq. (41). For short ranges the width of the Gaussian Green's function Eq. (40) is very narrow in comparison with the width of the rectangular pulse. Convolution with the rectangular pulse simply reproduces the rectangular pulse. When the range is sufficiently great the width of the Green's function becomes comparable to the width of the initial rectangular source pulse. Convolution then strongly alters the shape and amplitude of the initial pulse. Finally, at very great range the Gaussian Green's function becomes much wider than the initial rectangular pulse. Convolution of the two functions then simply reproduces the Green's function except for change of amplitude scale.

The viscosity ν appears in the solution Eq. (40) as a scale factor multiplying the range x . Thus, the effect of reducing the viscosity is to delay the onset of the asymptotic stage. By making the viscosity vanishingly small, the range at which the asymptotic stage begins can be made to approach infinity. This behavior explains why solutions obtained from numerical calculations with the traditional linear Q will converge to elastic solutions in the limit of vanishingly small difference interval. Unfortunately, practical computer calculations must be made with a finite mesh interval, usually large, perhaps no smaller than about 5% the width of the purely elastic disturbance. In decaying wave calculations, the transition to the asymptotic stage occurs well within the ranges of interest for practical choices of zoning.

Finally, it should be noted that the linear Q will affect the calculation of other types of decaying waves specific to solids. In particular, solids can support Rayleigh waves that propagate along a free surface rather than through the bulk of the solid. In the case of purely elastic behavior and a finite size source, these waves have an amplitude proportional to the inverse square root of the range; however, the traditional linear Q programs calculate amplitudes that are observed to be proportional to the inverse first power of the range. The results that have been obtained for surface waves will be published in a separate paper or made available in the form of a laboratory report.

ACKNOWLEDGMENTS

This work was supported by the U.S. Atomic Energy Commission and the Advanced Projects Research Agency. I would like to thank W. J. Hannon for allowing me to modify a copy of the

TENSOR program to the
and Barbara K. Crowley,
which encouraged me to go

1. G. MAENCHEN AND S. S. SACK, pp. 181-210, Academic Press, 1968.
2. J. T. CHERRY, S. SACK, "Adiabatic Flow," *Lawrence Livermore Report UCRL-7322*, Rev. I (1968).
3. M. L. WILKINS, *Calculations of the Effects of Nuclear War*, Vol. 3, pp. 211-263, Academic Press, 1969.
4. M. WILKINS, "Calculations of the Effects of Nuclear War," *Lawrence Livermore Report UCRL-7322*, Rev. I (1968).
5. R. D. RICHTMYER AND K. W. MONTGOMERY, 2nd ed., pp. 311-338, McGraw-Hill, 1961.
6. M. J. LIGHTHILL, *Viscosity and Turbulence*, G. K. Batchelor and Cambridge, England, 1963.

TENSOR program to the form suggested in this work. Also, I would like to thank John W. White and Barbara K. Crowley for their enthusiastic response to the original version of this paper which encouraged me to get on with the present revision.

REFERENCES

1. G. MAENCHEN AND S. SACK, The tensor code, in "Methods in Computational Physics," Vol. 3, pp. 181-210, Academic Press, New York, 1964.
2. J. T. CHERRY, S. SACK, G. MAENCHEN, AND V. KRANSKY, "Two-Dimensional Stress-Induced Adiabatic Flow," Lawrence Livermore Laboratory Report UCRL-50987 (1970).
3. M. L. WILKINS, Calculation of elastic-plastic flow, in "Methods in Computational Physics," Vol. 3, pp. 211-263, Academic Press, New York, 1964.
4. M. WILKINS, "Calculation of Elastic-Plastic Flow," Lawrence Livermore Laboratory Report UCRL-7322, Rev. I (1969).
5. R. D. RICHTMYER AND K. W. MORTON, "Difference Methods for Initial-Value Problems," 2nd ed., pp. 311-338, Interscience, New York, 1967.
6. M. J. LIGHTHILL, Viscosity effects in sound waves of finite amplitude, in "Surveys in Mechanics" (G. K. Batchelor and R. M. Davies, Eds.), pp. 250-351, Cambridge University Press, Cambridge, England, 1956.

else would simply
pulse maintains its
for a very slight
the pulse changes
c state is reached;
becomes inversely
ent stages arise is
p. (41). For short
is very narrow in
olution with the
hen the range is
comparable to the
strongly alters the
ange the Gaussian
ilar pulse. Convo-
unction except for

or multiplying the
the onset of the
range at which the
behavior explains
additional linear Q
difference interval.
with a finite mesh
width of the purely
to the asymptotic
ces of zoning.
alculation of other
support Rayleigh
e bulk of the solid.
ese waves have an
nge; however, the
e observed to be
lts that have been
or made available

the Advanced Projects
modify a copy of the

SUBJ
MNG
TMSO

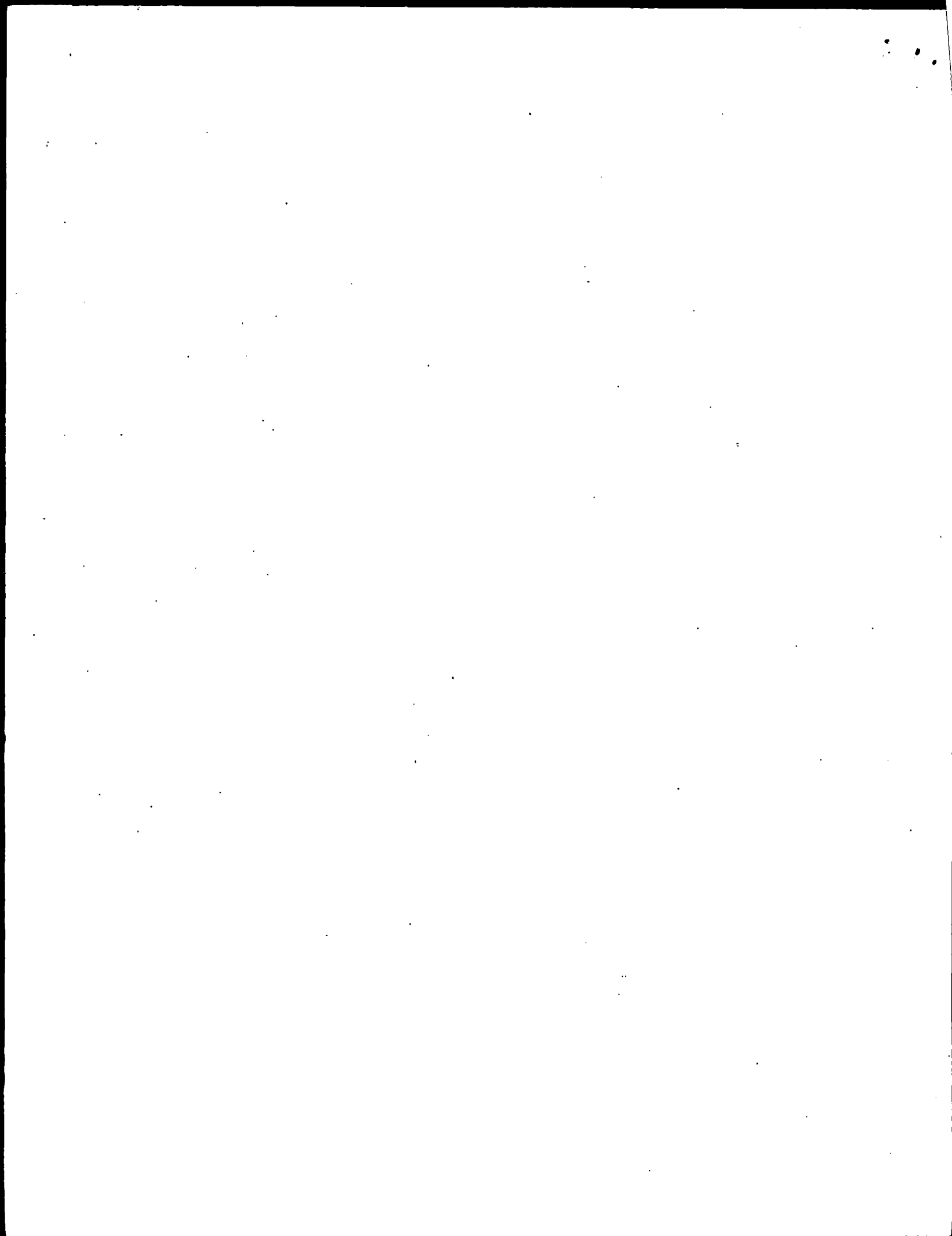
UNIVERSITY OF UTAH
RESEARCH INSTITUTE
EARTH SCIENCE LAB.

TREATMENT OF
MANGANIFEROUS SILVER ORES
FOR RECOVERY OF SILVER
IN VIEW OF
CHANGED PRECIOUS METAL ECONOMICS

By

Clement K. Chase
Senior Metallurgical Engineer
Mountain States Research & Development
Tucson, Arizona

For Presentation at the
1981 AIME Annual Meeting
February 22-26, 1981
Chicago, Illinois



TREATMENT OF
MANGANIFEROUS SILVER ORES
FOR RECOVERY OF SILVER
IN VIEW OF
CHANGED PRECIOUS METAL ECONOMICS

By

Clement K. Chase
Senior Metallurgical Engineer
Mountain States Research & Development
Tucson, Arizona

ABSTRACT

Since the dawn of cyanidation leaching techniques for precious metals, certain manganese-bearing silver ores have been a problem due to low silver extractions. Since simultaneous occurrence of silver and manganese is common in nature, this situation has made many otherwise attractive silver deposits uneconomic in the past.

Several older techniques have been useful but at \$1.29 per ounce of silver, the economics were unfavorable. With the new look in silver prices and some improvements in processing technology, neglected silver districts offer new promise.

INTRODUCTION

Probably the first metal known to man was gold for reasons everyone will appreciate: the attractive color, the luster, malleability, durability, and its occurrence in the metallic state in nature. Gold has been cherished by man from antiquity. Silver and copper were next, since they occasionally occurred in native form. Later their reduction from oxidized ores was discovered, accidentally perhaps.

Processes for recovery of silver have an ancient lineage, dating back into antiquity. Amalgamation, retorting, chloride roasting followed by amalgamation, hyposulfite leaching, and the Patio Process were used from the 15th century until the beginning of the 20th century when an important revolution occurred: the almost universal advent of the cyanidation process.

Not all ores, however, were amenable to these earlier processes or even to the cyanide process. A common denominator for many of these refractory ores is the presence of manganese associated with the silver. The non-amenability of manganiferous silver ores to common cyanide extraction techniques is well known, although the exact mineralogical reason for this is elusive. However, it is known that dissolution of the manganese frees the silver for treatment and recovery by usual methods; salt roasting also does this. This paper attempts a survey of this potentially rewarding subject.

Another cause of poor recovery is silica encapsulation of the silver. This requires an extremely fine grind for silver liberation. Such fine grinding has been uneconomic in the past.

HISTORICAL PERSPECTIVE

In the past, many otherwise interesting silver deposits have lain untouched in the ground due to processing difficulties and resulting low extractions. Although several types of silver deposits are in this category, one of the most common (and most refractory) is the type where the silver is mineralogically tied up in compounds with manganese. These deposits frequently occur both in oxidized and sulfide form. This paper will deal with schemes for leaching the oxidized deposits since the sulfide deposits are often amenable to flotation concentration with subsequent smelting for product recovery. A discussion of the types of ores suitable for sulfide flotation is included.

The economics of special ore treatment methods were limited for many years by a silver price fixed by governmental fiat at \$1.293 per troy ounce (\$0.038 U.S. per gram). Since the advent of escalating oil prices due to the short-sighted actions of the OPEC cartel, with its resulting world depression, and the flight of investment money to the precious metals, the price of silver has risen to heights that make attractive more complex processing methods, even in the face of general world cost inflation. This justifies a new look at old methods. Ores

with a value of \$100 per ton are worth considerable processing effort.

SOME GENERAL TYPES OF SILVER ORES WITH SOME POSSIBLE EXTRACTION METHODS

1. Silver sulfide ores (amenable to flotation-smelting recovery techniques).
2. Oxidized, clean silver ores (amenable to cyanidation recovery).
3. Oxidized silver ores resistant to cyanidation recovery. Frequently these ores contain manganese.
4. Complex silver sulfide ores such as tennantite, tetrahedrite, and other combinations of silver with arsenic and antimony. (Suitable for flotation).
5. Argentiferous galena ores. (Flotation).
6. Argento-jarosite ores. (Difficult at best).
7. Silver ores with sulfide manganese. (Suitable for flotation).

POSSIBLE EXTRACTION METHODS

There are several approaches to the problem of silver recovery from manganiferous ores. These are listed with the knowledge that particular ores may be economically amenable to some unmentioned processes and that not all attempted processes are known to the author.

1. SO₂ leach, followed by thorough washing, liming to a suitable pH, and standard cyanidation. [18]
2. Chloride oxidation roasting followed by cyanidation or amalgamation. [68]
3. The venerable Patio Process - a combination of treatment with copper sulfate plus sodium chloride, followed by amalgamation for recovery of the silver.
4. The Washoe pan amalgamation process. (All processes using mercury today are environmentally difficult).
5. The Kerley thiosulfate leach process. This process is said to be effective for problem ores containing high percentages of manganese, copper, arsenic, tellurium, etc., or combinations of the above. The process is being offered by ThioTech of Sahuarita, Arizona. [51]
6. Direct smelter recovery of high grade ore or concentrates.
7. A chloridizing reduction roast (Segregation Process) followed by flotation. This could be particularly useful in a copper-silver-manganese ore such as that from the Berenguela Mine of the Lampa Mining Co.

near Puno, Peru. It could also be used on a combination of a refractory Ag ore mixed with an oxide copper ore. [78]

- 8. Flotation where suitable (sulfides).
- 9. Brine leach (as the tetrachloro-complex).

OPERATING PILOT AND PRODUCTION PLANTS

Two plants have operated in the past employing variations of roasting to render silver recoverable from manganiferous ores.

Salt Roasting Process at Kildún

At Cia. Minera Kildún y Anexas at Matehuala, S.L.P., Mexico, American Smelting and Refining Company (now ASARCO, Inc.) operated a commercial 400 MTPD salt roasting-cyanidation plant for eight years on ore averaging 2 grams gold per metric ton (0.06 oz. gold per short ton) and 500 grams silver per metric ton (14 oz. silver per short ton) in a gangue assaying 4 to 5% manganese. The New York silver price during this operating period was under 45¢ U.S. per ounce. The results of this operation were reported by R.J. Mellen in 1963. The thoughtful article by Mellen discusses problems frankly: corrosion due to high chloride liquors and roaster vapors, clinkers, the effect of grind on roasting success, and the operation of the calcine cooler.

In initial testing, straight cyanidation of this ore gave only about 20% silver recovery, although gold recovery was 86%. Salt roasting tests indicated that gold recovery could be improved somewhat and silver recovery raised to 87%, a worthwhile accomplishment, particularly in the present international precious metal price situation:

<u>Time Period</u>	<u>Au Value/MT Ore</u>	<u>Ag Value/MT Ore</u>
1937-1944	\$ 2.00	\$ 6.43
1980	34.00	286.00

The costs of roasting do not appear as heavy as they did 40 years ago.

In the described operating plant, the ore was roasted with 5% NaCl in two direct-fired rotary kilns with retention time of 30 minutes at a temperature over 800°C. The calcines were quenched, ground in mill solution, the pregnant liquor was separated by CCD, and the values precipitated by zinc dust. Operational problems were many but were overcome by a determined staff.

Techniques developed in the late 1940's and early 1950's for the salt roasting of vanadium ores should be of ready applicability to salt roasting of silver ores. Use of cast stainless steel rabble arms in a skinner-type hearth roaster, continuous quench of calcine directly from the roaster, and various corrosion-proofing techniques come to mind. Use of modern techniques, machinery, and plastics, coupled with current precious metal prices, should make

an ore deposit such as the one at Matehuala very attractive today.

The Segregation Process

The Segregation Process was originally a method for treatment of oxide copper ores but was proved by tests to be suitable for silver-copper ores, also. The process roasts an ore at 700-800°C with, usually, sodium chloride and a reducing agent such as coke, charcoal, or recently, petroleum coke. The copper (and silver, if present) are volatilized, migrate, and are reduced on the carbon particles as metallic copper/silver alloy, whence they can be floated or leached. The flotation concentrate is commonly sent to a smelter as a high-grade concentrate.

The process was originally accidentally discovered in 1923 in experimental work on the oxide copper ores from the Sagasca deposit in Chile. These ores contain a natural level of sodium chloride and it was found that in attempting to reduce the copper with coal, the copper was reduced and then migrated to the coal surfaces where it was deposited as metallic copper.

The process was further developed in the period between 1923 and 1931. A series of patents were secured by the original Minerals Separation Company. Commercial development of the process was considered in 1931 in several locations but gathering world depression was not propitious for such efforts. However, several large scale pilot plants were operated. The following is a very brief history of pilot operations.

Segregation Process at Berenguela Mine

The second plant to be operated successfully using a roasting process was in reality conceived as a pilot plant but it was a large one and was skillfully operated by a knowledgeable staff. It used the Segregation Process for an unusual copper-silver manganiferous ore near Puno, Peru from the Berenguela Mine which was once operated by the Lampa Mining Co. (British).

Mineral Separation Company in Southern Rhodesia, Africa

A 50 ton per day pilot plant was operated in Southern Rhodesia by the Minerals Separation Company using a hearth roaster in a two-stage process. The plant operated for four months in 1931, treating a 5% oxide copper ore with a recovery of 87% by flotation in a concentrate assaying 68% copper.

Union Minière de Haut Katanga Present-Day Zaïre in Africa

This plant had a capacity of 350 TPD. It operated for several months in 1931 using two direct-fired rotary kilns in a two-stage process.

Akjoujt Mine in
Mauritania, West Africa

A small pilot plant of 50-75 TPD capacity was operated in Mauritania in 1959 on a problem oxide copper ore at 3% copper and 3 grams of gold per ton. The recovered concentrate assayed 60-70% copper and 2 ounces gold per ton. A commercial plant was planned and built, but failed because of operating problems.

Lake Shore Mill
Transarizona Resources Corp., Arizona

A commercial operation of the Segregation Process was attempted south of Casa Grande, Arizona for several years beginning in 1960. Original operation was in an indirectly heated rotary kiln. Later, the plant was converted to a direct-fired operation. Recovery was near 85% with a concentrate running 50% copper. Operations were not sufficiently economic for a continued run, partly due to dust losses.

N'Changa, Anglo-American Corporation
Southern Rhodesia

The process used here was named TORCO - Treatment of Refractory Copper Ores. It used a fluid solids roaster. A 10 TPD pilot plant was successful but a larger plant at 500-1000 TPD suffered from operational difficulties and did not run for long. A two-stage process was used; however, problems developed in transferring hot material from one stage to the next.

This experience with various copper operations using the Segregation Process is cited for reference value in small and large operations. Considerable operational experience has been gathered over the years on this intriguing metallurgical process.

It now appears that there are four effective methods for recovering silver from manganiferous ores: the sulfur dioxide leach, the oxidizing salt roast, the segregation process, and Thio Tech's thiosulfate leach. The segregation process has been demonstrated as being suitable for manganiferous silver ores by R.D. Groves and by operations on the Berenguela ore.

Fresnillo, Mexico SO₂ Leaching Process

This was a commercial application of the McClusky process using the sulfur dioxide preparatory leach for treatment of manganiferous silver ores. It was used on a portion of the silver ores treated and the SO₂-leached pulp was limed and joined with the other ground ores for cyanidation.

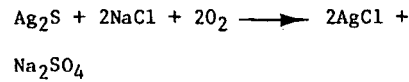
Candelaria - Modern Heap Leaching for Silver

A modern heap leach is in operation at the Candelaria Mine near Hawthorne, Nevada. The operating general partner is Occidental Minerals Corporation. Tonnage treated is 8000 per day. The ore is generally believed to be manganiferous. The mining operation is on such a scale that substantial silver production is

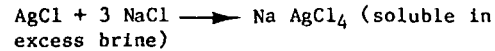
assured.

APPLICABLE CHEMISTRY OF SILVER EXTRACTION

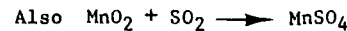
Chloride Roasting Followed by Cyanidation:



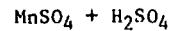
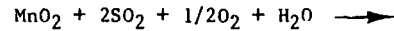
Chloridizing Leach:



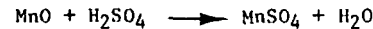
Chemistry of Manganese Removal From Tie-Up With Silver:



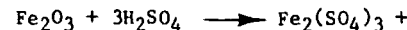
(somewhat pH dependent)



(The generated H₂SO₄ helps to dissolve divalent Mn).



(also soluble in H₂SO₄ is the iron portion of jarosite).



PRODUCT RECOVERY METHODS

In all the above methods where cyanidation is used, product recovery is frequently accomplished by zinc dust precipitation with subsequent fire refining. In cases of gold-bearing ores, concentration of values from low-grade cyanide solutions by adsorption on activated charcoal with subsequent electrowinning of a doré bullion is a useful method but in the case of silver ores running several or more ounces per ton, the sheer bulk of the necessary carbon points to the direct zinc dust precipitation method as preferable. An alternate precipitation method involves the use of NaHS or Na₂S as suggested by Reno USBM to precipitate a silver sulfide product. Use of this method has been held back by poor settling and filtration rates for the silver sulfide precipitate and the insidious toxicity of possible hydrogen sulfide gas, to say nothing of hydrogen cyanide.

The recovery methods employing sulfur dioxide to dissolve the manganese offer the possibility of a manganese recovery step. This may be economic in those ores containing

substantial manganese values. Parenthetically, it is felt that even very low values of manganese may be sufficient to render the silver difficult to dissolve with cyanide if the manganese and silver are syngenetic.

BIBLIOGRAPHY

Considerable effort has been given to collection of an adequate bibliography since it is felt that this may be the major contribution.

The author wishes to acknowledge the fine cooperation of the following individuals in the task of getting these references together: Norman E. Dausinger, Tucson, AZ; Judith A. Eisele, Reno, NV; James B. Fletcher, Miami, AZ; Douglas N. Halbe, Denver, CO; Thomas Henderson, Jr., Tucson, AZ; William C. Larson, Twin Cities, MN; Edward Martinez, S. Plainfield, NJ; George M. Potter, Tucson, AZ; Barry N. Watson, Tucson, AZ, and Norman L. Weiss, Tucson, AZ.

The bibliography is quite complete in regard to the Segregation Process (reducing chloride roast) since these references are difficult to find in print. The process combines a roast for liberation of metal values with the efficient flotation process for recovery of the values and is of demonstrated effectiveness in recovery of silver from manganiferous ores.

Paul Eimon's paper has a rather complete and excellent geologically-oriented bibliography appended.

BIBLIOGRAPHY

- [1] Adamson, R. J., "Gold Metallurgy in South Africa" Cape and Transvaal Printers Ltd., Cape Town, South Africa, 1972, 452 pp.
- [2] Addison, R., "Gold and Silver Extraction from Sulfide Ores", The Mining Congress Journal, October 1980.
- [3] Agey, W. W., J. V. Batty, H. W. Wilson, and W. J. Wilson, "Beneficiation of Calico District, California, Silver-Barite Ores", U.S. Bureau of Mines RI 7730, 1973.
- [4] Anon., "Metallurgical Progress", Mining Magazine, 36, 1927, p. 131.
- [5] Anon., "Segregation Process for Copper Ores", Mining Magazine, 42, Jan. 1930, p. 59.
- [6] Anon., "Concentrating Copper Ores - A New Process", Mining Jnl. (London), 168, Jan. 11, 1930, p. 33.
- [7] Anon., Editorial, Mining Magazine, 42, 1930, p. 331.
- [8] Anon., "U.S.B.M. Charts Segregation Process", Eng. & Min. Jnl., 160, Nov. 1959, pp. 98-99.
- [9] Anon., "Segregation Process to be Used at New Copper Project (Transarizona)", Mining World, 21, Dec., 1959, p. 19.
- [10] Anon., "Arizona Copper Silicates Respond to Segregation", Eng. & Min. Jnl., 161, Nov. 1960, pp. 86-87.
- [11] Anon., "Flowsheet on the Segregation Process", Deco Trefoil, Bull. No. M7-F94, Jan.-Feb., 1965, pp. 17-18.
- [12] Anon., "Bureau of Mines Copper Recovery Process to Get Large-Scale Trial", News Release by U.S. Dept. of Interior, Feb. 20, 1965.
- [13] Apell, G. A., S. W. Hazen and E. G. Howe, "Lake Valley Manganese Deposits, Sierra County, N. Mex.", U. S. Bureau of Mines RI 4099, 1947.
- [14] Anderson, James A., Reading Notes on: "The Geochemistry of Manganese Oxides - Guide to Sulfide Ore Deposits", Harvard University, PhD Thesis, 1964.
- [15] Back, A. E., S. F. Ravitz and K. E. Tame, "Formation of Dithionate and Sulfate in the Oxidation of Sulfur Dioxide by Manganese Dioxide and Air", U. S. Bureau of Mines RI 4931, 1952.
- [16] Bechaud, L. J., Jr., "Minerals Beneficiation", Review, Min. Cong. Jnl., 47, Feb. 1961, p. 63.

- [17] Belladen - Noli et Sommariva Gaz. Chim. - Ital. 58 (1928) 443-9.
- [18] Bender, F. N. and Carl Rampacek, "Percolation Leaching of Manganese Ores With Sulfur Dioxide", U. S. Bureau of Mines RI 5323, 1957.
- [19] Berezowsky, R.M.G.S. and V. B. Sefton, "Recovery of Gold and Silver from Oxidation Leach Residues by Ammoniacal Thio-sulfate Leaching", AIME Annual Meeting, Feb. 18-22, 1979, New Orleans, La.
- [20] Blessing, Lee R., "Experimental Work on Manganese Silver Ores", University of Arizona, MS Thesis, 1936.
- [21] Bodart, J., Contribution a l'etude des equilibres heterogenes Hydrolyse des chlorures metalliques par la vapeur surchauffee. These Bruxelles, probablement 1928.
- [22] Bouton, C. M., W. C. Riddell and L. H. Duschak, "Silver in Chloride Volatilization", TP 317, U. S. Bureau of Mines (1924).
- [23] Bradford, R. H. and C. M. Mac Farlane, "A Consideration of Some of the Problems of the Chloride Volatilization Process", TP No. 3, Mining and Metallurgical Investigations, Utah Engineering Exp. Station (1928).
- [24] Brewer, L., "The Fusion and Vaporisation Data of the Halides", In L.L. Quill, The Chemistry and Metallurgy of Miscellaneous Materials, Thermodynamics, McGraw Hill (1950).
- [25] Brewer, L. and N. L. Lofgren, "The Thermodynamics of Gaseous Cuprous Chloride", Monomer and Trimer, J. Am. Chem. Soc. 72 (1950) 3038.
- [26] Carpenter, J. A., R. R. Elliott and B. F. W. Sawyer, "The History of Fifty Years of Mining at Tonopah, 1900-1950", Univ. of Nev. Bull., Vol 45, No. 3, 1953, 153 pp.
- [27] Clevenger, G. H. and M. H. Caron, "The Treatment of Manganese-Silver Ores", U.S. Bureau of Mines Bulletin 226, 1925, 110 p.
- [28] Coffin, L.D., Treatment of Roasted Chalcopyrite in the Anglo American Corporation Mini-Segregation Plant in the Recovery of Metallic Copper, AMAX Report, Project No. 912 (753), Report No. 74-2, June 4, 1974.
- [29] Crawford, W.E., AIME Transactions #112, 1934. (McClusky Process, Operated at Fresnillo, Mexico).
- [30] Diaz, C. M., "Mechanism for the Segregation Process and Its Potential Application to Nickel Ores", M.S. Thesis, Dept. of Mineral Engineering, Columbia Univ., 1958, pp. 1-59.
- [31] Dorr, J.V.N., "Cyanidation and Concentration of Gold and Silver Ores", McGraw-Hill Book Co., New York, 1936, 1st Edit.
- [32] Dorr, J.V.N. and F.L. Bosqui, Cyanidation and Concentration of Gold and Silver Ores, McGraw-Hill Book Co., New York, 1950, 511 pp.
- [33] Egleston, T., The Metallurgy of Silver, Gold, and Mercury in the United States, Vol. I, Silver, John Wiley & Sons, New York, N.Y., 1887.
- [34] Eimon, P.I., "Bulk Silver Deposits in Volcanics, North American Cordillera - The Evolving Geologic Model, Publications, Predictions".
- [35] Fichte, R., Die Thermodynamischen Eigenschaffen du Metallchloride, VEB. Verlag Technik Berlin (1953).
- [36] Freeman, G. A., C. Rampacek and L. G. Evans: "Copper Segregation at the Lake Shore Mine", Jnl. of Metals, 13, May, 1961, pp. 370-372; Mining Eng., 13, Oct., 1961, pp. 1153-1155.
- [37] Giudice, Phil, "Silver Considerations on Exploration", (paper) November 4, 1977.
- [38] Glassner, A., "The Thermochemical Properties of the Oxides, Fluorides and Chlorides, to 2500°K", U.S. Atomic Energy Commission, Report ANL.5750, The Supt. of Documents, Washington, U.S.A. (1959).
- [39] Gonser, B. W. and E. E. Slowter, "The Coating of Metals With Tin From the Vapour Phase (Stannizing)". Research at Battelle Memorial Institute, Int. Tin Research Council, Series A No. 76 (1938).
- [40] Groves, R. D., "The Segregation Process Applied to a Manganese-Silver Ore", U. S. Bureau of Mines Internal Memorandum, Personal communication.
- [41] Guilissen, "Theorie du Procede de Segregation", Courte Note Pour l'Union Miniere du Haut Katanga, March 23 (1928).
- [42] Hamilton, E.M., "Manual of Cyanidation", McGraw-Hill Book Company, New York, N.Y., 1920.
- [43] Harder, Edmund Cecil, "Manganese Deposits of the United States", USGS Bulletin 427, 1910.
- [44] Havens, R., S. J. Hussey, J. A. McAllister and K. C. Dean, "Beneficiation of Oxide Manganese and Manganese-Silver Ores from Southern Arizona", U. S. Bureau of Mines RI 2024, Feb. 1954.
- [45] Heinen, H. J., D. G. Peterson and R. E. Lindstrom, "Silver Extraction from Marginal Resources", Oral Presentation, The 104th TMS-AIME Annual Meeting, New York, N.Y., Feb. 16-20, 1975.

- [46] Hedley, N. and H. Tabachnick, "Chemistry of Cyanidation", American Cyanamid Bulletin 23, June 1958.
- [47] Henley, K.J., "Gold-Ore Mineralogy and Its Relation to Metallurgical Treatment", Minerals Sci. Engng., Vol. 7, No. 4, 1975, pp. 289-312.
- [48] Hewett, D.F., "Manganese is a Clue to Deep Base and Precious Metals", Mining World, July 1963.
- [49] Hewett, D. F., "Silver in Veins of Hypogene Manganese Oxides", Geological Survey Circular 553, 1968.
- [50] Iwasaki, I., J. Takahashi and H. Kahata, "Extraction of Nickel from Iron Laterites and Oxidized Nickel Ores by a Segregation Process", AIME, New York, March 1966.
- [51] Kerley Chemical Company, Sahuarita, Arizona 85629, Personal communication.
- [52] Kroll, W. J., "Chlorine Metallurgy", Metal Industry, Sept. 26, Oct. 3, 10, 17, 24, 31, Nov. 7 (1952).
- [53] Kubaschewski, O. and E. Li Evans, "Metallurgical Thermochemistry", Pergamon, 3rd Ed. (1958).
- [54] Kudryk, V., "Silver from Low-Grade Refractory Ore", AIME Annual Meeting, Feb. 15-19, 1970, Denver, Colorado.
- [55] Layng, H. R., "Chloridizing Volatilization", Engineering and Mining Journal Press, Nov. 12, 1921, T. P. Holt, Engineering and Mining Journal 117 (1924) 922.
- [56] Leaver, E. S. and J. A. Wolf, "Re-Treatment of Mother Lode (California) Carbonaceous Slime Tailings", Bu Mine TP 481, 1930, 20 pp.
- [57] Letcher, O., "Minerals Separation Devices Process for Mixed Copper Ores," Eng. & Min. Jnl., 128, Nov. 16, 1929, p. 786.
- [58] Liddell, D. M., Handbook of Nonferrous Metallurgy, McGraw-Hill Book Co., New York, N.Y. 1945, "Brine Leaching of Silver Ores", pp. 530-534.
- [59] Liddell, D. M., Ibid, "Manganese-Silver Ores", pp. 535-536.
- [60] Lloyd, P. J. D., "Maximizing the Recovery of Gold From Witwatersrand Ores", Minerals Sci. Engng., Vol. 10, No. 3, 1978, pp. 208-221.
- [61] Mackay, K.E. and N. Gibson, "Development of the TORCO Plant at Rhokana Corporation, Limited, Zambia", Transactions of the Institute of Mining and Metallurgy, Volume 77, pp. C19-31, 1968.
- [62] Marcuson, S.W., "Application of the Segregation Process to Roasted Copper Concentrates", Mineral Science Engineering, Vol. 12, No. 1, January 1980.
- [63] Martinez, E., "The Copper Segregation Process - Review of the Literature", ASARCO internal memo, 1965.
- [64] Martinez, E., "Thermoanalysis of Copper Segregation", Mining Engineering, August 1966, pp. 70-73.
- [65] Martinez, E., "The Copper Segregation Process Studied by Thermoanalysis", Transactions SME/AIME, Vol. 238, June 1967, pp. 172-179.
- [66] McKinney, W.A. and L.G. Evans, "Segregation of Copper Ores by Direct-Firing Methods", U.S. Bureau of Mines, RI 6215 (1962).
- [67] McKinney, W.A. and P.T. Waddleton, "Use of Various Salts as Copper-Volatilizing Agents in the Segregation Process", U.S. Bureau of Mines, RI 6044 (1962).
- [68] Mellen, R.J., "How Silver-Gold Ores Respond to Salt Roasting-Cyanidation", Engr. Mng. Jnl., Vol. 164, No. 4, pp. 76, 77, 83, April 1963.
- [69] Mellen, R. J., "Crushing Changes Necessitated by Roasting Conditions at Compañía Minera Kildún y Anexas", Mining Technology, March 1945.
- [70] Mellen, R. J., "Compañía Minera Kildún y Anexas - 300 Ton Salt Roasting and Cyanidation Mill", American Smelting & Refining Co. memo.
- [71] Meunier, J., "Gazéification et Oxydation des Combustibles", Masson, Paris (1958).
- [72] Moulden, J.C. and B. Taplin, Metals Production, Limited, British Patent 250,991, 1924.
- [73] Nolan, T.B., "The Underground Geology of the Western Part of the Tonopah Mining District, Nevada", Univ. of Nev. Bull., Vol. 24, No. 4, 1930.
- [74] Opie, W.R., L.D. Coffin, and D.C. Cusanelli, "A Minimum Pollution Low-Energy Pyrometallurgical Process for Treating Chalcopyrite Concentrates", The Extractive Metallurgy of Copper, American Institute of Mining, Metallurgical, and Petroleum Engineers, Volume 1, Chapter 20, pp. 416-426, 1976.
- [75] Opie, W.R., "Pilot-Scale Test to Evaluate the TORCO Segregation Unit for Treating Chalcopyrite Calcine", AMAX Interoffice Memorandum to J. Towers, December 6, 1974.

- [76] Opie, W.R., L.D. Coffin, D.L. Armant, and Otto F. Cimler, "Selective Recovery of Copper from Copper-Nickel Sulfide Concentrates by Applying the Segregation Technology", Metallurgical Transactions B, Volume 10B, pp. 27-32, March 1979.
- [77] Pinkney, E.T. and N. Plint, "Treatment of Refractory Copper Ores by the Segregation Process", Transactions of the Institute of Mining and Metallurgy, Volume 76, pp. C114-132, 1967.
- [78] Pollandt, F. and M. E. Pease, "Extraction of Copper and Silver by the Segregation Process in Peru", Bulletin of the Institution of Mining and Metallurgy No. 646, September 1960. Discussion - Bull. 649 (Dec. 1960) 652 (March 1961).
- [79] Potter, G. M., and Roshan B. Bhappu, "The Chemistry of Gold and Silver Recovery from Natural Resources", Mountain States Research and Development paper presented at the American Chemical Society Annual Meeting, Anaheim, Calif., 1978.
- [80] Potter, G. M., "Some Trends in Gold and Silver Metallurgy" - Original: "Algunas Tendencias en la Hidrometalurgia del Oro y Plata", Memoria de la Asociación de Ingenieros de Mina, Metalurgistas y Geólogos de Mexico, Guanajuato, GTO, Mexico, Nov. 1978.
- [81] Potter, G. M., "Merrill-Crowe Precipitation of Precious Metals by Zinc Dust", presented at Hydrometallurgy Division, Spring Meeting, Arizona Conference, SME-AIME, May 10, 1980.
- [82] Ralston, O. C., "Segregation Process for Oxidized Copper and Other Ores", Unpublished review, 1957.
- [83] Rampacek, Carl, H. C. Fuller and J. B. Clemmer, "Operation of a Dithionate-Process Pilot Plant for Leaching Manganese Ore From Maggie Canyon Deposit, Artillery Mountains Region, Mohave County, Arizona", U.S. Bureau of Mines RI 5508, 1959.
- [84] Rampacek, C. and W. A. McKinney, "The Copper Segregation Process", Paper presented at AIME meeting in New York, Feb. 1960 (Preprint No. 60B61).
- [85] Rampacek, C., W. A. McKinney and P. T. Waddleton, "Treating Oxidized and Mixed Oxide-Sulfide Copper Ores by the Segregation Process", U. S. Bureau of Mines, RI 5501 (1959).
- [86] Rey, M., "Le Procédé de Segregation des Minerais de Cuivre Oxydes Pauvres", Congrès International des Mines, de la Metallurgie et de la Geologie Appliquée, Paris, October 1935, Egalement: Revue de Metallurgie 33 (1936), 293.
- [87] Rey, M., "The Segregation Process for Low-Grade Copper Oxide Ores", 7th Int. Cong. Min. Met. & Appl. Geol., Met. Ses., Vol. II-3, Paris, Oct. 20-26, 1935, pp. 55-62; Rev. Met., 33, 1936, pp. 295-302.
- [88] Rey, M., "The Enrichment of the Copper Minerals of the Akjoujt Mine in Mauritania", Rev. Ind. Min., 41, Aug., 1959, pp. 667-669.
- [89] Rey, M., "Mines de Cuivre de Mauritanie-Copper Segregation Process Testing", 1954-1962, (January 1967), Report for Anglo American.
- [90] Rey, M.R.W., "Early Development of the Copper Segregation Process", Transactions of the Institute of Mining and Metallurgy, Volume 76, pp. C101-107, 1967.
- [91] Rey, M., "Memoirs of Milling and Process Metallurgy #4 - Segregation Processing", IMM Transactions C, Vol. 89, September 1980, pp. 101-107.
- [92] Romslo, T. M. and S. F. Ravitz, "Arizona Manganese-Silver Ores", U. S. Bureau of Mines RI 4097 July 1947.
- [93] Sano, K., "On the Reduction Equilibria of Cobaltous Chloride and Nickelous Chloride by Hydrogen", The Science Reports of the Tohoku University, Series I, Vol. XXXVII No. 1 (1953).
- [94] Schafer, H. and K. Etzel, "Über die Wanderung von Kupfer (I) Oxyd und von Kupfer in Temperaturgefalle, Z. Anorg. Allg. Chem. 291 (1957) 294.
- [95] Scheiner, B. J., D. L. Pool and R. E. Lindstrom, "Recovery of Silver and Mercury from Mill Tailings by Electrooxidation", U. S. Bureau of Mines RI 7660.
- [96] Scheiner, B. J., D. L. Pool, J. J. Sjöberg and R. E. Lindstrom, "Extraction of Silver from Refractory Ores", U.S. Bureau of Mines RI 7736, 1973.
- [97] Stanczyk, M. H. and P. A. Bloom, "Copper Recovery from Segregation Flotation Concentrates by Ammoniacal-Ammonium Carbonate Leaching", U. S. Bureau of Mines RI 5826, 1961.
- [98] Stetefeldt, C. A., "Russell's Improved Process for the Lixiviation of Silver Ores", Transactions AIME, Vol. 13, 1885.
- [99] Sutulov, A., "Beneficiation of Chilean Oxidized Copper Ores by Segregation Process", World Mining, 15, No. 8, 1962, p. 28.
- [100] Sutulov, A., "Proceso de Segregation en Beneficio de Cobres Chilenos", Universidad de Concepción (1962) 66 pp.

- [101] Sutulov, A., "Evaluating Copper Segregation Results by Screen Sizing Analysis", AIME Trans., 226, March, 1963, pp. 17-20.
- [102] Trans. AIME, Vol. 17, p. 767, 1889 - The Goodale Process.
- [103] Watson, B. N., "Large Low Grade Silver Deposits in N. America", World Mining, March 1977.
- [104] Watson, B. N., "Bulk Tonnage, Low-Grade Silver Deposits - Update 1980", Precious Metals Symposium, Northern Nevada Section, SME/AIME with the Nevada Bureau of Mines and Geology and the Nevada Division of Mineral Resources, Sparks, Nevada, Nov. 17-19, 1980.
- [105] Varley, T., E. P. Barrett, C. C. Stevenson and R. H. Bradford, "The Chloride Volatilization Process of Ore Treatment", Bull. 211, U.S. Bureau of Mines (1923).
- [106] Wyman, W. F. and S. F. Ravits, "Sulfur Dioxide Leaching Tests on Various Western Manganese Ores", U.S. Bureau of Mines RI 4077, 1947.
- PATENTS, SEGREGATION PROCESS
- [1] U.S. Patent 1,234,426, July 24, 1917, Vermaes Process.
- [2] U.S. Patent 1,232,216, Aug. 3, 1917, Caron Process.
- [3] Brit. Pat. No. 250,991, J. C. Moulden and B. Taplin, Oct. 29, 1924. Oxidized copper ore heated to a temperature below the melting point of copper, 500 to 700°C, with a reducing agent in the presence of a halogen or compound such as NaCl or CaCl₂ to effect reduction of copper oxide to metallic copper. Copper may be leached out after cooling or recovered by gravity concentration.
- [4] Brit. Pat. No. 255,961, J. C. Moulden and B. Taplin, May 2, 1925. Heat treatment as in (1). Copper separated from treatment by froth flotation after grinding and screening, if required.
- [5] Brit. Pat. No. 264,584, E. Edser and B. Taplin, Oct. 21, 1925. Oxidized ores containing lead, silver, antimony or bismuth can be similarly treated. If CaCO₃ is present in ore, pyrites and chlorides, such as those of Mn, Fe or Cu, may be added.
- [6] Brit. Pat. No. 300,701, T. J. Taplin and B. Taplin, July 19, 1927. The procedure described in (1) is modified. Ore is partly reduced by reducing agent with halogen present and then treated to an oxidizing step for a short time, after which the reduction-halogenation is resumed. If native copper or copper sulfide is present in ore, the treatment may commence with an oxidizing step.
- [7] Brit. Pat. No. 318,314, T. J. Taplin and B. Taplin, June 5, 1928. Gases evolved during segregation treatment can be recovered by scrubbing with water and returned to process. Gases can be scrubbed and treated with CaCO₃ or other material to form halides of Ca, Cu, Mg, Mn, Fe, etc.
- [8] U.S. Pat. 1,679,337, J. C. Moulden and B. Taplin, July 31, 1928. Similar to (1). Temperature for segregation lower than melting point of copper, but sufficiently high to cause reaction (suitably 500° to 700°C). Mix ore with 2 - 2.5% of reducing agent and up to 0.5% NaCl or other halide like CaCl₂, MgCl₂, CaF₂, etc. Ore can be heated first in oxidizing atmosphere to oxidize any sulfides present. Recommends that soluble alkaline salts be removed prior to treatment or neutralized with H₂SO₄ or HCl. Chlorine or HCl gas can be used after ore-coal mixture is at operating temperature.

RELATED PATENTS

- [9] Brit. Pat. No. 321,213, H. Lavers and B. Taplin, August 2, 1928. Adaptation of (2) in which a mixed sulfide-oxide ore is treated to segregation and then both metallic copper and residual sulfide froth floated together. Screening of coarse carbon with copper is also advocated.
- [10] Brit. Pat. No. 348,024, T. J. Taplin, January 1, 1930. Ore subjected to sulfating roast or other material containing CuSO_4 can be treated by segregation process.
- [11] U.S. Pat. No. 1,865,153, T. J. Taplin, June 28, 1932. Similar to (8). Found that segregated copper from copper sulfate is sulfided to a considerable extent, especially on its surface. This effect is believed to be due to the sulfur-bearing gases evolved. Mixed oxide-sulfide ores can be treated by first applying a sulfating roast.
- [12] Brit. Pat. 387,713, T. J. Taplin, February 13, 1933. Ore is passed downward through a multiple hearth heating furnace wherein it is roasted and preheated to $>650^\circ\text{C}$. The discharge falls into a heat insulated pit to which is fed continuously a mixture of NaCl and coal or coke, whereby Cu, Ag, Pb, Bi, and Sb reduced by segregation to charge.
- [13] Brit. Pat. 389,865, F. B. Jones, March 27, 1933. Crushed ore mixed with carbonaceous material and NaCl is heated to $450^\circ - 800^\circ\text{C}$ in rotating tubular furnace from which air is excluded. Product is crushed and subjected to froth flotation to recover gold and copper.
- [14] U.S. Pat. No. 3,148,974, C. Rampacek, September 15, 1964. A two-stage process is described consisting of an indirect-fired stainless steel preheat kiln and a direct-fired reactor to which the hot ore, reducing agent, and salt are added. The direct-firing of the reactor controls the temperature of the reactor furnace while simultaneously controlling the furnace atmosphere so that it is neither too highly oxidizing nor reducing. If copper sulfide or other sulfide minerals are present, these are oxidized in the preheat kiln. The air-natural gas ratio used is from about 1.2 to 1 times the ratio required to give complete combustion of the gas.
- [15] U.S. Pat. No. 3,834,89, Eisel, J.A., and H. J. Heinen, Recovery of Gold - A variation of the segregation process using gaseous chlorine and a volatile compound of iron, aluminum or gallium, together with activated carbon. Recovery is by flotation.
- [16] L. J. Bechaud and H. Hartjens. Segregation in the form of a sulphide (lead-copper) using pyrrhotite as reagent. U.S. Patent Application. Serial No. 781.442. December 19, 1958.
- [17] H. Mino. Use of ammonium chloride. Jap. Patent Showa 39.30021, December 1964.

SUBJ
MNG
TOBF

UNIVERSITY OF UTAH
RESEARCH INSTITUTE
EARTH SCIENCE LAB.



2

Proposal for Research

1 December 1977

SRI No. ERU 77-350

TARGET ORE BODIES FOR SOLUTION MINING

Mr. Richie Coryell, Program Manager
Nonrenewable Resources
National Science Foundation
Washington, D.C. 20550

Dear Mr. Coryell:

During the summary sessions of the recent RANN-Stanford University sponsored "Workshop on Solution Mining," it was strongly recommended that a survey of "Target Ore Bodies for Solution Mining" be given first priority. Such a study would provide direction to much of the corollary research outlined in the "Workshop on Solution Mining," and summary findings could be available to the mining industry in a few month's time. SRI International proposes to undertake this survey as a short-term project and supplement our staff where necessary with pertinent assistance from recognized mining exploration consultants.

I PROJECT BACKGROUND AND GUIDELINES

The parameters of ore deposits worth careful consideration were outlined in the workshop sessions as:

"Those metalliferous deposits of gross \$100 million value, both above and below the water table, and to a depth of 5,000 feet, and ore value not less than \$5/ton."

A number of the ore bodies in the above category that will be included in our proposed survey have long been classified as "technological" or "metallurgical" reserves in resource studies such as the Paley Report and various defense metal inventories. These deposits generally are not economically practical to mine at the present time. There are, however, a number of these "teaser" deposits, having considerable total metal content, that have been the object of detailed studies and test plant setups. Considerable information about all of these low grade and marginal deposits in general has been accumulated by the geological staffs of oil and mining exploration companies since World War II.

SRI International

333 Ravenswood Ave. • Menlo Park, California 94025 • (415) 326-6200 • Cable: STANRES, Menlo Park • TWX: 910-373-1246

Although exploration companies do not customarily reveal information regarding their claims and reserves, these problem deposits, when under claim, are usually classified as being "without present value." Therefore, the necessary data for an industry-wide and all-metal survey designed for improving the picture should, with government sponsorship, be more readily available.

II OBJECTIVES

The proposed survey will focus on those ore deposits that qualify on the basis of the defined parameters outlined in the aforementioned Workshop statement. That is, those deposits of \$100 million value (at \$5/ton) to a depth of 5,000 feet. For each deposit in this class, pertinent and available data will be accumulated, organized, and supplied to NSF on the following topics:

- Size and shape of the deposit
- Depth
- Grade and penalty items
- Ore minerals and gangue
- Structure
- Permeability
- Porosity
- Fluid saturation
- Ownership data.

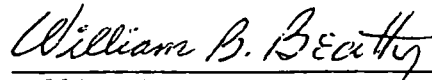
The area to be covered by the proposed study includes the continental United States, Alaska, and Canada.

III METHOD OF APPROACH AND STATEMENT OF WORK

SRI has conducted resource surveys for exploration departments of many of the larger oil and mining companies. To supplement information acquired during these surveys, qualified mining exploration consultants have been contacted and selected based on their extensive background in metal exploration and their associations with oil and mining companies and other related companies. Four of these consultants are presently available and will provide significant input: Neil Campbell (Pacific Northwest and Canada), W. C. Peters and Kenyon Richard (Tucson), and Charles Park (Stanford University). In addition, data bank inventories will be reviewed in the Bureau of Mines and the Geological Survey in Washington, D.C.; exploration companies in Salt Lake City, Denver, and Tucson will be interviewed. Travel to visit the consultants and companies will be necessary, as well as payment of consultants' fees and expenses.

The estimated cost for this proposed survey, based on a cost plus fixed fee contract, will be \$31,035. A cost estimate and contractual provisions are enclosed with this letter proposal. Biographies of senior personnel anticipated to participate in this program are also attached. A final report supplying the data outlined in this proposal will be issued three months after the date of contract acceptance. If there are any questions, please call me at 415 326-6200, ext. 2734.

Sincerely,



William B. Beatty
William B. Beatty
Senior Geologist
Radio Physics Laboratory

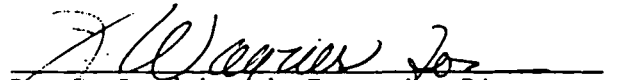
WBB/lmh

Enclosures

Approved:



David A. Johnson, Director
Radio Physics Laboratory



Ray L. Leadabrand, Executive Director
Electronics and Radio Sciences Division

LAMBERT T. DOLPHIN, JR.

Program Manager
Radio Physics Laboratory
Electronics and Radio Sciences Division

SPECIALIZED PROFESSIONAL COMPETENCE

Underground electromagnetic probing and sensing; ionospheric propagation and clutter; short pulse radar techniques; exploratory phenomenology and radar physics; acoustic radars and radio-acoustic radars; remote sensing and archaeology, mining, and geophysics

REPRESENTATIVE RESEARCH ASSIGNMENTS AT SRI (since 1956)

Developed radars for clutter measurements in California and in Alaska
Investigated auroral and meteor clutter effects at VHF and UHF
Investigated radar reflection from the moon at VHF
Studied radar clutter and radio propagation effects of nuclear explosions
Led extensive measurement program to study rocket launch and re-entry trails
Developed novel series of HF multimegawatt radars
Investigated spark gap switching techniques
Studied usefulness of over-the-horizon radar methods
Led development and testing of a family of underground electromagnetic sounders

ACADEMIC BACKGROUND

A.B. in physics (1954), California State University (San Diego);
two years of graduate study in physics, Stanford University

PROFESSIONAL ASSOCIATIONS

Acoustical Society of America; American Association for the Advancement of Science; American Geophysical Union; American Research Center in Egypt; American Scientific Affiliation; Egypt Exploration Society; Institute of Electrical and Electronics Engineers

December 1976

WILLIAM B. BLATTY, SENIOR GEOLOGIST
RADIO PHYSICS LABORATORY
ELECTRONICS AND RADIO SCIENCES DIVISION

Specialized professional competence

- Geophysical exploration and geological research; mining engineering and development; general resource appraisals and worldwide economic studies for metals, industrial minerals, and hydrocarbons

Representative research assignments at SRI (since 1949)

- Worldwide mining development reviews for company diversification needs
- Continuing reviews of coal, tar sands, oil shales, and related technology
- Extensive mining survey for government of India and protectorates
- Arctic construction and mining methodology; long-range resource studies
- Mineral resources and mining industries of Japan and Taiwan
- Geology of desert regions and their mineral potentials; solar salt
- Deep crustal studies of seismic and transmissive properties to 30,000 feet, including drilling costs and feasibilities
- Appraisals of structure and geology of archaeological sites in desert regions, alluvial fans and valleys, and submarine shelves
- Hazard potentials of earthquake and landslide areas and hydrology thereof

Other professional and business experience

- Company agent for Honolulu Oil Corporation: oil and seismic exploration in California, Texas, and Canada
- Kaiser Engineers (Oakland, California): iron ore, coal, and limestone reserve studies: appraisals, open pit mine design, and general economic geology
- Professional consulting work in mining appraisals and engineering for American Smelting & Refining and Southern California Edison Co.

Academic background

- B.S. in mining engineering and geology (1937), University of Washington

Representative publications

- "Hellbent for Bentonite," given at Eleventh Forum of Industrial Minerals, Kalispell, Montana (June 1975)
- "Japanese Steel Industry Dominates Outlook for Western Coals," *Coal Age* (November 1972)
- "ABCs of Industrial Minerals," *Mining Congress J.* (February 1972)
- "Geothermal Gradients in the Western Cordillera," University of Nevada
- "Nature and Environment of Deep Mines of the World," SRI
- "Mineral Resource Data in the Western States" and "Heat Flow and Thermal Gradients in the Earth's Crust," Stanford University

Professional associations and honors

- American Association of Petroleum Geologists; Association of Professional Geological Scientists; Society of Economic Geologists; Society of Exploration Geophysicists; Society of Mining Engineers; Tau Beta Pi (fellow)

March 1976

ROGER S. VICKERS

Senior Physicist
Radio Physics Laboratory
Electronics and Radio Sciences Division

SPECIALIZED PROFESSIONAL COMPETENCE

Subsurface remote sensing; laser spectroscopic studies; optical techniques in geochemistry; atmospheric radiation transfer; infrared emission spectra of geologic materials; design of planetary satellite experiments; management plans for earth resources programs

REPRESENTATIVE RESEARCH ASSIGNMENTS AT SRI (since 1974)

Subsurface sensing for archaeology
Use of DF lasers in the detection of methane and ethane
Short pulse radars to measure ice thickness and snow depth
Study of transient responses of loaded dipole antennas

OTHER PROFESSIONAL EXPERIENCE

Associate professor, Colorado State University: microwave remote sensing; laser spectroscopic studies; short pulse radar design
Vice President, Environmental Resources Associates: remote sensing and geophysics; mission planning and data analysis
Research physicist, Colorado State University: air-sea interface measurements; atmospheric radiation transfer
Research physicist, Stanford University: infrared emission spectroscopy
Research physicist and project manager, IIT Research Institute: solar system physics; stimulated fluorescence spectroscopy; earth resource mission studies

ACADEMIC BACKGROUND

B.Sc. (with honors, 1959) and Ph.D. (1963) in physics, University of Southampton (United Kingdom); intensive short course in advanced infrared technology (1967), University of Michigan

PUBLICATIONS

Many journal and symposium papers, project and technical reports

PROFESSIONAL ASSOCIATIONS AND HONORS

European Society of Exploration Geophysicists; Institute of Physics (London); Institute of Glaciology (Cambridge)
I-R 100 award recipient, 1976

May 1977

Proposal for Research No. ERU 77-350

TARGET ORE BODIES FOR SOLUTION MINING

Contractual Provisions

I ESTIMATED TIME AND CHARGES

The estimated time required to complete this research effort and report on its results is 3 months. SRI International could begin work on receipt of a fully executed contract.

A cost estimate follows Section IV.

II CONTRACT FORM

It is requested that any contract resulting from this proposal be written on a cost-plus-fixed-fee basis.

III ACCEPTANCE PERIOD

This proposal will remain in effect until 31 January 1978; however, SRI will be pleased to consider an extension if required.

IV NEGOTIATED OVERHEAD RATES

SRI's indirect rates are retroactively determined by negotiation with the DoD Tri-Service Overhead Negotiations Committee. We therefore request that FPR 1-7.403-9, Negotiated Overhead Rates, be incorporated in the General Provisions of any contract resulting from this proposal.

1 December 1977

COST ESTIMATE

Personnel Costs

Project Supervision, 20 man-hours at \$15.30/hr	\$ 306
Senior Geologist, 505 man-hours at \$12.81/hr	6,469
Research Analyst, 160 man-hours at \$8.10/hr	1,296
Secretary, 40 man-hours at \$4.59/hr	<u>184</u>
Total Direct Labor (Schedule A)	\$8,255
Payroll Burden at 31.5% (Schedule B)	2,600
Total Salaries and Wages	\$10,855
Overhead at 90% of Salaries and Wages (Schedule B)	9,770
G&A at 21% of Salaries and Wages (Schedule B)	2,280
Total Personnel Costs	<u>\$22,905</u>

Direct Costs

Travel (Schedule C)	\$1,841
Communications (Schedule E)	300
Consultants (Schedule F)	3,000
Report Production (Schedule D)	<u>776</u>
Subtotal	\$5,917
Support Cost at 3.6% of Direct Costs (Schedule B)	<u>213</u>
Total Direct Costs	\$ 6,130
Total Estimated Cost	\$29,035
Fixed Fee	<u>2,000</u>
TOTAL ESTIMATED COST PLUS FIXED FEE	\$31,035

SCHEDULE A--DIRECT LABOR

Direct labor charges are based on the actual salaries for the staff members contemplated for the project work plus a factor of 2.5% of base salary for merit increases during the contract period of performance. The precise factor applied is dependent on the estimated period of performance. Frequency of salary reviews and level of merit increases are in accordance with the SRI's Salary and Wage Payment Policy as published in Topic No. 505 of the SRI Administration Manual and as approved by the Defense Contract Administration Services Region.

SCHEDULE B--INDIRECT RATES

The indirect rates (research overhead, payroll burden, support cost burden etc.) reflect a revision in our methods of allocating indirect expenses, effective 2 January 1977, as required by Cost Accounting Standard 410. We request that these rates not be specifically included in the contract, but rather that the contract provide for reimbursement at billing rates acceptable to the Contracting Officer, subject to retroactive adjustment to fixed rates negotiated on the basis of historical cost data. Included in payroll burden are such costs as vacation, holiday and sick leave pay, social security taxes, and contributions to employee benefit plans.

SCHEDULE C--TRAVEL

1 trip to Vancouver/Spokane at \$243	\$ 243
1 trip to Salt Lake City/Denver at \$233	233
1 trip to Tucson, Arizona at \$172	172
1 trip to Washington, D. C. at \$424	424
Subsistence, 2 days at Vancouver at \$58/day	\$ 116
3 days at Spokane at \$30/day	90
3 days at Salt Lake City at \$30/day	90
2 days at Denver at \$30/day	60
2 days at Tucson at \$30/day	60
3 days at Washington, D.C. at \$42.50/day	128
Car rental, 15 days at \$15/day	<u>225</u>
Total	\$1,841

Air fares are based on prices established in the Official Airline Guide dated November 1977.

Domestic subsistence rates and travel by private auto are established standards based on cost data submitted to the Defense Contract Audit Agency and are considered acceptable by them for bidding purposes.

SCHEDULE D--REPORT COSTS

These rates have been submitted to DCASMA-SF for review and acceptance.

Report costs are estimated on the basis of the number of pages of text and illustrations and the number of copies of reports required in accordance with the following rates per page.

Editing	\$ 4.12
Composition	3.83
Coordination	1.12
Proofreading	1.68
Illustration	20.92
Press and Bindery	0.022 per impression

Following is a cost breakdown of the estimated cost of report production:

Text preparation, 58 pages at \$10.75 per page (including editing, composition, report coordination, and proofreading)	\$624
Illustration, 6 pages at \$20.92 per illustration	\$126
Press, bindery, and photography for 1160 printed pages at \$0.022 per printed page	<u>\$ 26</u>
Total	\$776

SCHEDULE E--OTHER DIRECT COSTS

Communications

This is an engineering estimate of the toll charges for telephone calls during the period of performance. It is estimated at \$300.

SCHEDULE F--CONSULTANTS

It is estimated that the following consultants will be required for three days each at the anticipated rate of \$250/day.

Mr. Neil Campbell, 3 days at \$250	\$750
Mr. W. C. Peters, 3 days at \$250	750
Mr. Kenyon Richard, 3 days at \$250	750
Mr. Charles Park, 3 days at \$250	<u>750</u>
Total	\$3,000

THE TREVIÑO PROJECT:

UNIVERSITY OF UTAH
RESEARCH INSTITUTE
EARTH SCIENCE LAB.

CONOCO'S SECOND SOUTH TEXAS IN SITU LEACH PLANT WILL PRODUCE 450,000 LB/YR OF YELLOW CAKE

Michael P. Sassos, Associate editor

Despite a depressed uranium market, in which spot prices for U_3O_8 have dropped to about \$25/lb, the Treviño project, Conoco's second *in situ* leaching plant, and one of five currently under development in south Texas, is scheduled for initial production by late-1981 at a rate of 450,000 lb/yr of yellow cake. The 100% Conoco-owned plant is located about 90 mi east of Laredo, in Duval County, and has estimated uranium reserves for a plant life of 7-10 years. Total cost of the project will run about \$8 million.

In addition to the five plants under development, 14 *in situ* solution projects and one pilot plant are fully operational in south Texas, with an annual recovery rate of about 3 million lb of yellow cake.

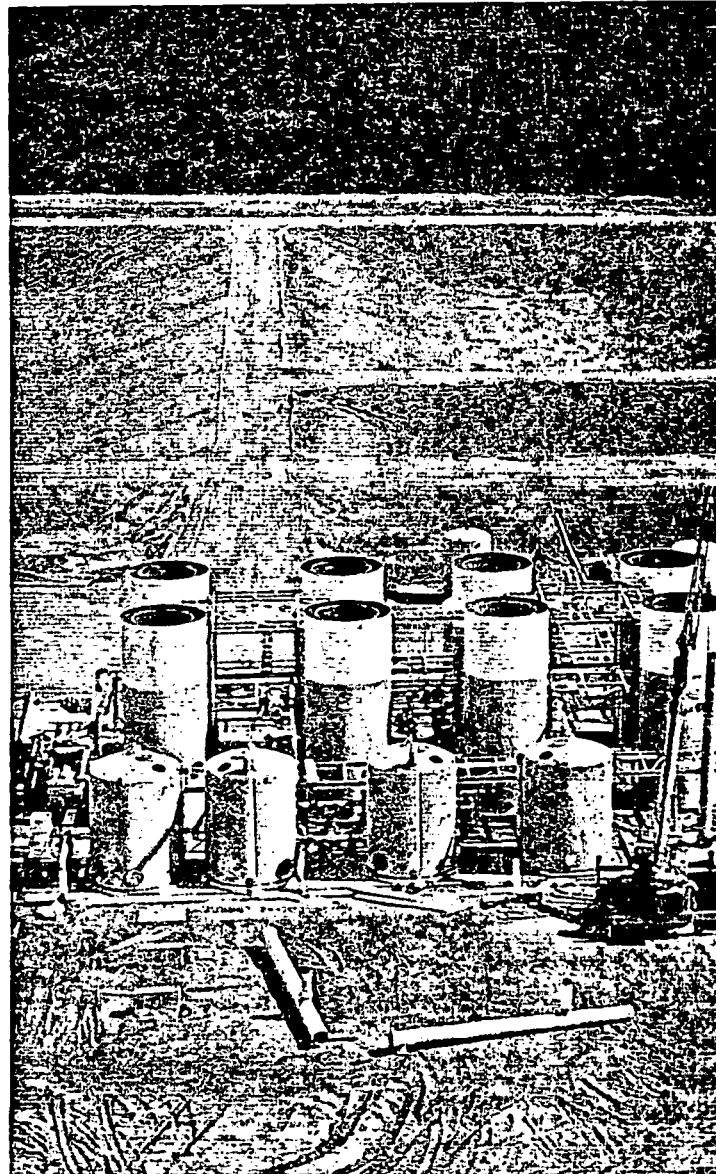
Conoco's solution mining method utilizes the fact that the roll-front uranium mineralization in the south Texas uranium deposits occurs in multiple permeable sandstone units separated by impermeable clay layers. Leach solutions are pumped into the uranium-bearing formations through injection wells and later recovered from adjacent production wells. The intermediate impermeable zones prevent the downward migration of the leachate.

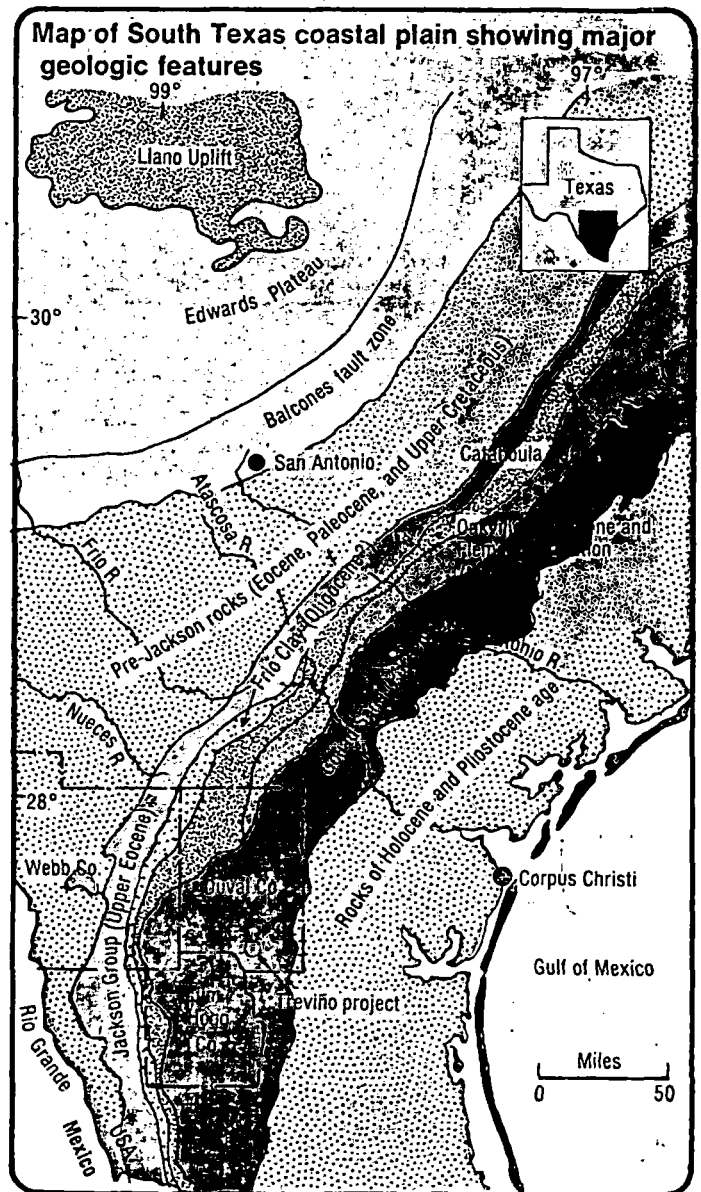
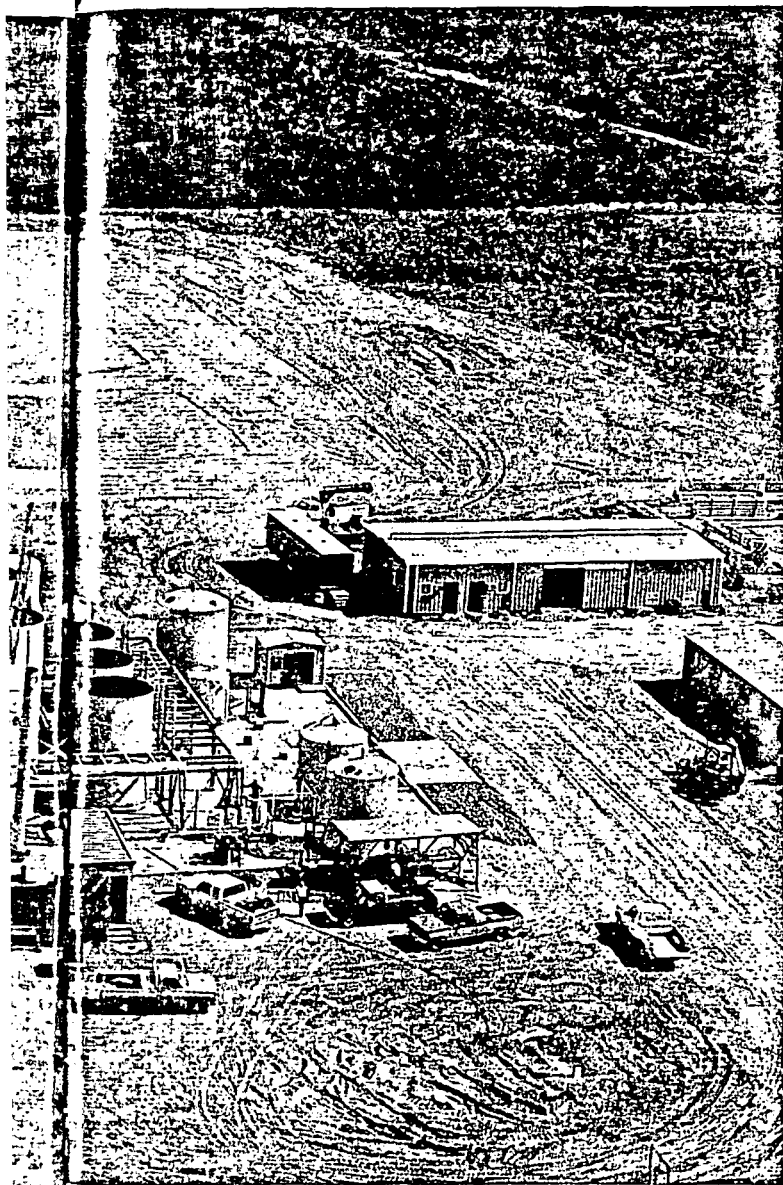
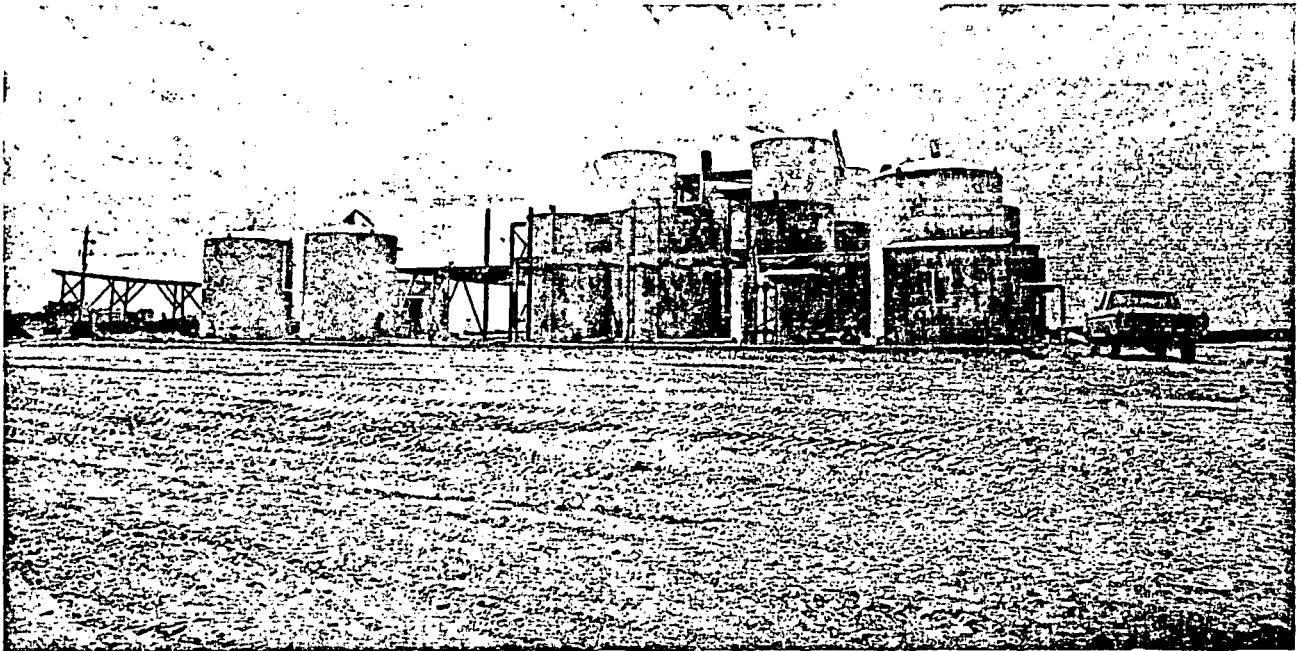
Delineation of the Treviño orebody began in 1977 and lasted for 2½ years on a property that totals 6,000 acres. The study disclosed that a number of roll-fronts exist at depths ranging from 150 to 320 ft. Additional test wells were drilled to provide information on reservoir permeability, porosity, and natural groundwater flow.

Drilling of the injection and production wells commenced in March 1981 at a spacing between wells of 85-100 ft, depending on sub-surface permeability. The result is the well-known "five-spot" pattern, where four injection wells are spaced around a single production well.

Conoco's other *in situ* leaching project, the 25% owned Benavides project, is also located in Duval County and began production in February 1980. A total of 46,000 lb of U_3O_8 were produced during its first year of operation.

Conoco's Treviño uranium recovery plant consists of a complex of tanks holding various chemicals, pipes, and valves (foreground), office facilities (right), and surface holding ponds (top).







Production area (left) and plant (right) occupy an area of about 30 acres. Surface vegetation is typical of the semi-arid south Texas location.

URANIUM MINERALIZATION

Roll-front uranium mineralization occurs in the sandstone member of the Miocene Oakville formation, which consists of interbedded calcareous sands, silts, and carbonaceous bentonitic clays. The rock formations strike northeast-southwest and dip about 1° to the southeast. Predominantly northeast-striking faults typical of the Atlantic coastal plain are present and form a series of horsts and grabens.

The principal source of uranium is believed to be the

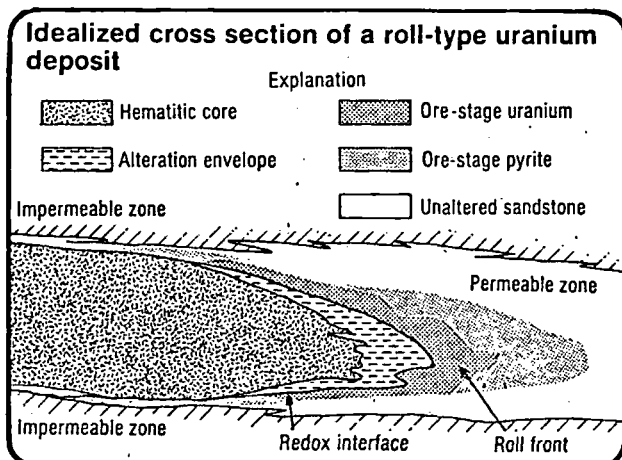
Catahoula tuffs¹. Oxygenated alkaline groundwaters probably leached uranium from the tuffs and transported it down-dip to chemically reducing environments that favor uranium precipitation. Possible reducing agents for uranium deposition are hydrogen sulphide gas seeping through faults and fractures from underlying petroleum reservoirs (allogenic) and/or carbonaceous material found within the sedimentary rocks (authigenic).

WELL-FIELD PREPARATION

A total of 130 4-in.-dia injection and production wells were drilled using conventional rotary drills. To resist corrosion and withstand the stresses imposed by the rock formations, each well is cased with fiberglass. Since not all of the stratigraphic formations contain uranium mineralization, the casings are selectively perforated.

Twenty monitor wells are used for periodic sampling and testing of the groundwater for variations in pH, conductivity, amount of sulphate, and escaping leaching solutions. If the monitor wells detect leaching solutions escaping from the production area, the leachate can be pulled back by either increasing the rate of production or decreasing the rate of injection.

For the leaching process, Conoco uses an oxidizer consisting of gaseous oxygen and water. The leachate is pumped into the formations at a rate of 40-50 gal/min per well and at pressures of 20-40 lb/in², depending on the depth of the well and permeability. Sodium bicarbonate is added to maintain the uranium in solution; it combines with the uranium and



Source: Granger and Warren, 1974.



Conoco's well-field design is the well-known "five-spot" pattern (four injection wells around a single production well).

forms stable uranium tricarbonate. The pregnant leach solution is then pumped to the surface for uranium recovery in the plant.

THE TREVINO PLANT

At the plant, pregnant lixiviant first passes through three ion exchange columns loaded with resin beads, which selectively retain the uranium by adsorption. The barren solution is then pumped to a recharging tank for chemical treatment, after which it is filtered for its contained sand and returned to the well site for reinjection. When sufficient uranium has been adsorbed by the resin, it is pumped to elution.

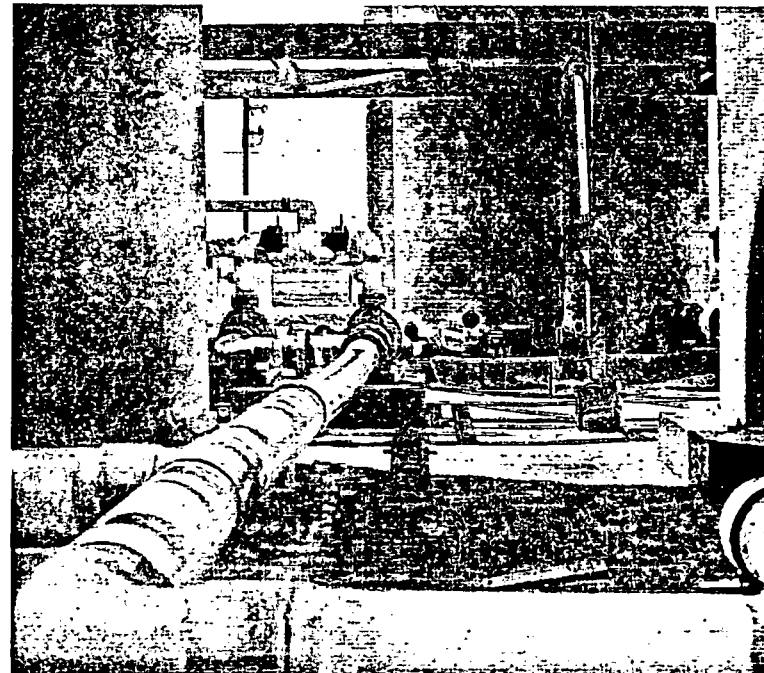
At the elution stage, barren eluant consisting of NaCl and NaOH is pumped through the beads, freeing the uranium and forming a pregnant eluant that is ready for precipitation with chemical agents. The eluant is pumped to a precipitation unit, where the carbonate is decomposed, and the uranium is precipitated as uranium peroxide. Subsequent thickening forms a slurry that is about 70% solids and contains 30% U_3O_8 . The slurry will be trucked to Kerr McGee's enrichment plant in Oklahoma for processing. ■

REFERENCES

- 1) Eargle, D.H., K.A. Dickinson, and B.O. Davis, "South Texas Uranium Deposits," AMERICAN ASSOCIATION OF PETROLEUM GEOLOGISTS BULLETIN, vol. 59, No. 5 (1975), pp 766-779.
- 2) Eargle, D.H., G.W. Hinds, and A.M.D. Weeks, "Uranium Geology and Mines, South Texas," Texas University (Austin), BUREAU OF ECONOMIC

GEOLOGY GUIDEBOOK, No. 12 (1971), 61 p.

- 3) Granger, H.C., and C.G. Warren, "Zoning in the Altered Tongue Associated with Roll-Type Uranium Deposits, in Formation of Uranium Ore Deposits," Vienna, International Atomic Energy Agency (1974), pp 185-200.



Connecting pipes feed solutions to tanks in the processing plant.

THE PUSH-PULL TEST
A METHOD OF EVALUATING FORMATION ADSORPTION PARAMETERS
FOR PREDICTING THE ENVIRONMENTAL EFFECTS ON
IN-SITU COAL GASIFICATION AND URANIUM RECOVERY

J. I. Drever and C. R. McKee
In-Situ Consulting, Inc. and The University of Wyoming
Departments of Geology and Petroleum Engineering
Laramie, Wyoming 82071

ABSTRACT

The push-pull test, which is a simple injection and pumping sequence of groundwater spiked with solutes of interest, is presented as a method of determining the adsorption characteristics of a formation. Adsorption properties are necessary to predict restoration from both in-situ coal gasification and in-situ uranium extraction.

The major problems in applying laboratory measurements to the field concern scaling the effect of particle size and obtaining representative samples. Laboratory measurements are conducted on gram to kilogram scale samples, whereas the push-pull test evaluates a sample weighing approximately 130 to 1,000 metric tons, depending on volume injected and porosity. The problems in translating laboratory results to the field appear to be less severe for sedimentary uranium bodies than for coal. Laboratory measurements are useful in delineating ranges in adsorption properties and in planning the field experiment.

The adsorption behavior of a formation can often be described by a linear Langmuir-type isotherm in which the significant parameters are the cation exchange capacity (C) and an exchange constant which can be derived from the distribution coefficient measured at

low concentration (k_d). Laboratory procedures for their measurement on coal and uranium are presented.

Two field push-pull tests were conducted on uranium formations in Wyoming. Adsorption properties estimated from these tests on the basis of a simple cell model were compared to the laboratory values. In the first case, excellent agreement was observed between the values estimated from the field test and the values measured in the laboratory. In the second case, the value for k_d determined in the laboratory was five times higher than the field value.

It is recommended that push-pull tests be conducted on coal formations being considered for in-situ gasification in view of the great uncertainty in extrapolating laboratory adsorption properties in the field.

1.0 INTRODUCTION

The largest single issue confronting in-situ processes at present is restoration of groundwater. Two restoration modes are possible - induced and natural restoration. Induced restoration is brought about by using engineering knowledge together with various combinations of pumping, injecting, and surface processing with or without chemical additives. Natural restoration relies upon the slower but sure processes of nature such as groundwater flow, dispersion, and sorption phenomena to reduce post mining concentrations to acceptable levels. Furthermore, natural restoration may also be used in conjunction with induced restoration.

To predict the outcome of either method, it is essential to have a knowledge of the adsorption and absorption properties of the medium. Adsorption of ions from solution can usually be regarded as an ion exchange process involving exchange of surface ions with ions in solution. Absorption involves an exchange of fluid between main permeability paths and regions of lower permeability. In coal,

respect, oxidation and particle size effects are particularly pronounced in coal (Dalton and Campbell, 1978; Drever, Murphy, and McKee, 1980).

Does Knowledge of the properties of a small sample on the order of grams allow extrapolation to large-scale behavior? Dalton and Campbell were able to obtain satisfactory agreement regarding postburn behavior from laboratory data. In their work, they were presumably concerned with small particle sizes both in the laboratory and field situations. However, contaminants will leach from the burn zone into the larger-scale fractures. Laboratory tests do not tell us how much of the surface area will be exposed. Will adsorption behavior in-situ be different from the laboratory? Do freshly broken surfaces resulting from handling and crushing behave differently from the naturally occurring surfaces exposed in fractures? Scaling from small laboratory-sized particles on the order of millimeters to larger blocks delineated by fractures on the scale of meters is not straightforward (Drever, Murphy, and McKee, 1980).

These considerations have led us to the use of the push-pull test to evaluate formation adsorption properties and to confirm predictions based on laboratory studies. The push-pull test is a relatively simple concept. Figure 1 shows a vertical cross section of test arrangement. An easily erected pool or bladder is prepared on site. Water from the well is filtered and pumped into the bladder. Appropriate amounts of the species to be studied are mixed into the bladder together with formation water. The solution

absorption would result from fluid migrating from the main fracture system into the smaller fractures within the matrix. Absorption occurs in uranium sands due to fluid exchanging with lower permeability sands and clays through advection.

Adsorption at present appears to be the dominant mechanism affecting solute transport. The field results we will present from in-situ uranium can be explained entirely on the basis of adsorption. In addition, limited field tests in coal reported by Dalton and Campbell (1978) were satisfactorily explained on the basis of adsorption theory.

Absorption cannot be ruled out as an important mechanism in large-scale fluid migration. However, owing to a lack of data in support of absorption at present, we will address only the evaluation of formation adsorption properties.

To evaluate the adsorption characteristics of a formation, two approaches are possible - laboratory and field. Considerable discussion has been raised in the past concerning the merits of the two approaches. It is our contention that laboratory measurements when properly conducted are useful to identify the range of possible values. However, some uncertainties will always remain. Among these are selection of a representative sample. In the laboratory approach, samples are extracted from their natural environment. Sample removal may generate new surface area which would otherwise be unavailable to the fluid. Existing surfaces can be altered from handling and crushing or exposure to the atmosphere. In this

**PLAN VIEW OF PUSH-PULL TEST
ISOTROPIC PERMEABILITY**

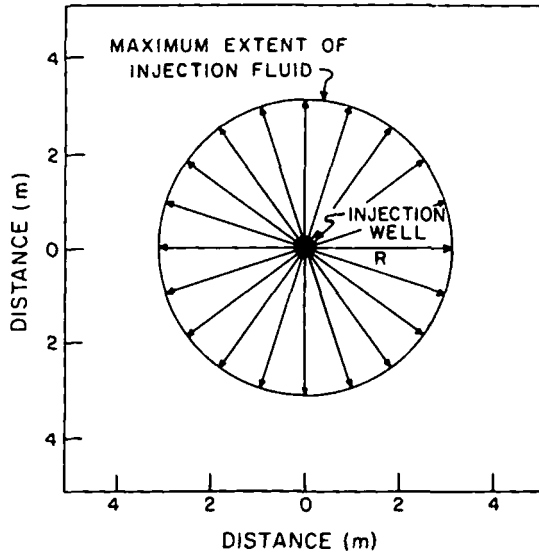


Fig. 2. Plan view of the push-pull test, assuming isotropic permeability.

of a few percent, approximately 1,000 metric tons of coal would be exposed to solution. The test also possesses an additional advantage in that it is relatively easy to obtain the necessary permits.

From the recovered solution concentration as a function of volume pumped, adsorption parameters can be obtained. This information, together with dispersion coefficients, can be used to predict the fate of a plume migrating downstream. Furthermore, the time and pore volumes required to restore a uranium ore body after mining can be estimated. The theory for determining the adsorption

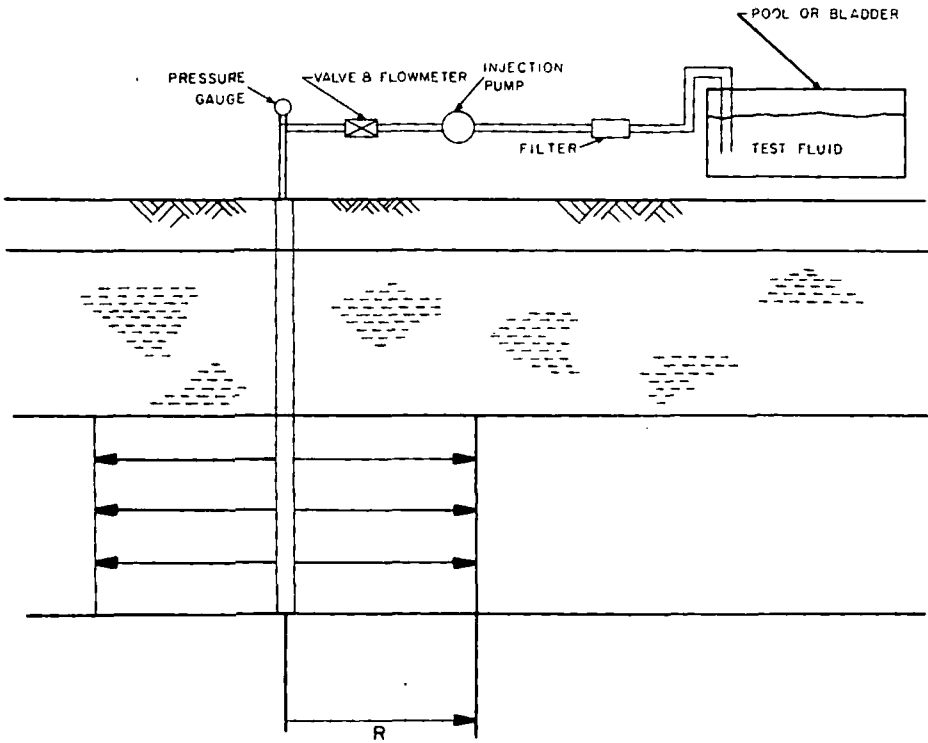


Fig. 1. Layout of push-pull test.

is then injected into the formation and allowed to reside for a few days. Figure 2 shows the affected area in plan view. The next step is to lower a pump into the well to recover the solution and measure its resulting concentration as a function of volume produced. Typically, 15,000 to 20,000 liters of solution are injected, with approximately 10 times this amount being recovered on pumping.

If we are testing a sedimentary ore body with a porosity of 28%, the push-pull method would test approximately 130 metric tons of ore. In the case of coal with a fracture porosity on the order

The concentration of the adsorbed species, Y , is given by

$$Y_1 = CX_1 \quad Y_2 = CX_2, \quad Y_1 + Y_2 = C \quad (2.3)$$

where C is the cation exchange capacity of the solid in meq/kg.

For the same reason, the sum of M_1 and M_2 must be a constant

$$M_1 + M_2 = G \quad (2.4)$$

where G is the total concentration of cations in solution. Using equations (2.3) and (2.4), the mole fraction and concentration of species 2 can be eliminated from equation (2.2) to obtain

$$\frac{Y_1}{C-Y_1} = K'_{ex} \frac{M_1}{G-M_1} \quad (2.5)$$

Although laboratory measured values of K'_{ex} can be found in the literature for various pairs of ions on various minerals (for example, Gilbert and Van Bladel, 1970), we do not believe these values are of much use in predicting the behavior of a real-world aquifer. The minerals in the aquifer (and, hence, their K'_{ex} values) are likely to be different from those on which measurements were made. Furthermore, it is difficult to extrapolate from simple two-ion systems to the complicated chemistry of a groundwater system in which several ions are competing for exchange sites. Our approach has been to measure, in the laboratory, the exchange properties of each aquifer-groundwater system in which we were interested and to predict the results of the push-pull test on the basis of these results. If the laboratory prediction ¹⁴and field data do not agree, exchange parameters can be estimated from the field data. The procedure will be discussed in a subsequent sec-

parameters which are required for predicting restoration behavior is given in the following section.

2.0 ION EXCHANGE THEORY

Ion exchange involving two monovalent cations can be described by a mass-action equation (Garrels and Christ, 1965; Hill, et al, 1978)

$$\left(\frac{a_1}{a_2}\right)_{\text{solid}} = K_{\text{ex}} \left(\frac{a_1}{a_2}\right)_{\text{liquid}} \quad (2.1)$$

where a represents an activity and K_{ex} is the thermodynamic exchange constant and 1 and 2 refer to the two ions. Since activity coefficients of ions on a solid exchanger are not well known, it is common to rewrite equation (2.1). This is accomplished by substituting mole fractions for activities in the solid phase and concentrations for activities in solution. Equation (2.1) then becomes

$$\frac{X_1}{X_2} = K'_{\text{ex}} \frac{M_1}{M_2} \quad (2.2)$$

where X represents the mole fractions on the solid and M the concentrations in solution in equivalents/kg. K'_{ex} , the exchange constant, now includes all activity corrections for both solid phase and solution. It will no longer be a true constant, but will vary with X_1 and X_2 . However, the variation appears to be within the error of our experimental measurements of K'_{ex} . Since electro-neutrality must be satisfied for exchange sites, we have

$$X_1 + X_2 = 1.$$

k_d is equal to the limiting slope of the exchange curve at low concentrations (the dashed line on Figure 3). Although k_d is used rather than K'_{ex} in subsequent discussions as an adsorption parameter, it should be emphasized that the model is applicable over the whole concentration range described by the Langmuir-type adsorption isotherm (equation 2.5).

Rewriting equation (2.5) in terms of k_d and C , we obtain

$$\frac{Y_1}{1-Y_1/C} = k_d \frac{M_1}{1-M_1/G} \quad (2.7)$$

In this equation, the cation exchange capacity, C , and the distribution coefficient for dilute concentrations are the unknowns. G in equation (2.7) represents the total concentration (in meq/gm) of cations in the groundwater which is a known quantity. Our approach is equivalent to treating the sum of all cations which are not of species 1 as a single monovalent cation M^+ . This approach cannot be rigorously justified on theoretical grounds, but can be regarded as a convenient approximation. In theory, when the principal ion competing with a monovalent ion such as NH_4^+ is divalent, for example Ca^{++} , equation (2.5) should have the form

$$\frac{Y_{NH_4}^2}{C-Y_{NH_4}} = K'_{ex} \frac{[NH_4]^2}{G-[NH_4^+]}, \quad (2.8)$$

where square brackets denote concentration. We have measured adsorption curves such as Figure 3 using groundwater in which the molar Na/Ca ratio varied from 2.5 to 26. In all cases, a simple linear equation (equation 2.5 or 2.7) fitted the data as well as,

tion. A typical example showing the adsorption characteristics of ammonium ion from a sedimentary uranium property is given in Figure 3. We will use the ammonium ion as an example in our present work since it is a problem cation in in-situ uranium processes as well as an unavoidable by-product of coal gasification (Hill, et al, 1978 and Campbell, Pellizzari, Santor, 1978).

The adsorption curve in Figure 3 is characterized by two numbers - the cation exchange capacity, C, and the exchange constant, K'_{ex} . The exchange constant is related to the distribution coefficient at low concentration, k_d , by the equation

$$k_d = K'_{ex} \frac{C}{G}; \quad (2.6)$$

ADSORPTION ISOTHERM FOR NH_4^+ BETWEEN FORMATION AND SOLUTION

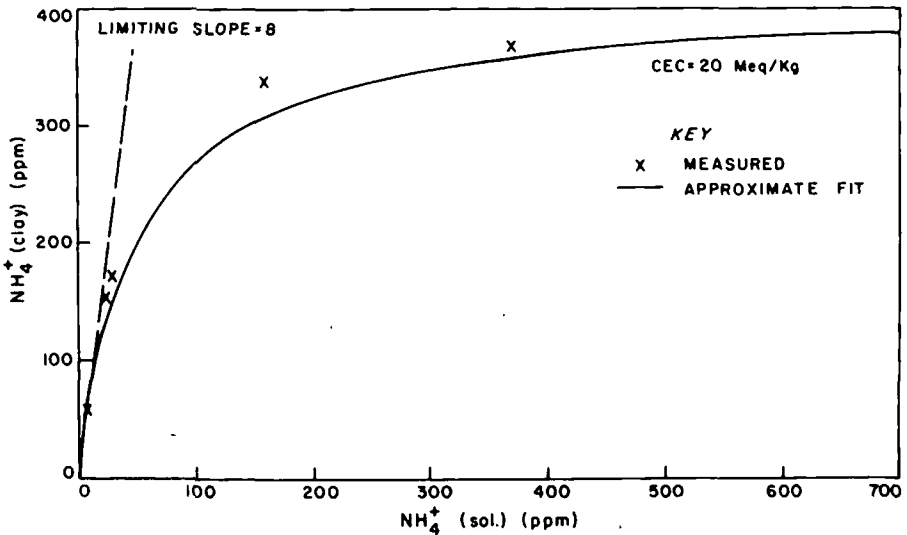


Fig. 3. Typical adsorption curve showing relationship between ammonium adsorbed on sediment and ammonium in solution. Solution was an artificial groundwater, Na^+ = 173 ppm, Ca^{2+} = 122 ppm, K^+ = 10 ppm, Mg^{2+} = 14 ppm.

cite, it may be necessary to dissolve them out prior to saturation with NH_4^+ , since they can interfere with the exchange measurements. The cation exchange capacity (CEC) is then measured on one split of the sample by modification of the method of Busenberg and Clemency (1973). For measurement of K'_{ex} and k_d , approximately six splits of ammonium-saturated sample are equilibrated with different volumes of groundwater, and then the ammonium concentration in solution and on the sediment is measured. The graph of NH_4^+ adsorbed on the sediment versus NH_4^+ in solution (Figure 3) is generally linear at low NH_4^+ concentrations, and k_d is calculated from the slope of the linear portion. We have observed limiting slopes or distribution coefficients in the range of 2 to 10. Cation exchange capacities have ranged from 0.2 - 7 meq/100 g. In general, fairly good agreement has been obtained between laboratory data and push-pull tests. Two examples were permitted to be released in this article. One (Figure 4) showed excellent agreement between laboratory and field results, the other (Figure 6) poor agreement, hence, demonstrating the necessity of comparing field results to laboratory projections.

3.2 Coal Samples

Our laboratory experiments with coal have been limited to examining the distribution of low concentrations of lead, cadmium, mercury, and selenium (Drever, Murphy, McKee, 1980). These were in the nitrate form with the exception of selenium which was copper selenate. All elements were in the +2 valence state with the exception of selenium which was +6. For these elements, we are

or better than, an equation with squared terms (equation 2.8) or and equation with an exponent between 1 and 2.

As we remarked in the introduction, there are two approaches in determining the necessary constants C and k_d . They are laboratory and field tests, the simplest field test being the push-pull test. Before discussing the theory of the push-pull test, we will first present the laboratory measurement techniques we have employed.

3.0 LABORATORY MEASUREMENTS OF ADSORPTION PARAMETERS

Adsorption measurements on granular sediments associated with uranium ore bodies are slightly different from those for coal. We, therefore, discuss them under separate headings.

3.1 Uranium Core Samples

As previously mentioned, we will use the ammonium ion to illustrate the procedure.

Measurements are made on core material from the aquifer. Samples are taken from permeable lithologies which will be in contact with lixiviant during mining. It is important to exclude impermeable shale units, as these will not be in effective contact with the lixiviant. The core samples are lightly ground where necessary to disaggregate the sample. Next, the material is saturated with NH_4^+ by treatment with 1M NH_4CO_3 solution and then cleaned of excess ammonium salts by repeating washing with distilled water, using centrifugation followed by membrane filtration to retain solid phases. If the samples contain much gypsum or cal-

Some difficulties were encountered with insoluble carbonates of lead and cadmium forming. Considerable scatter was also observed. Nevertheless, certain trends were noted for sub-millimeter scale particles. Lead and cadmium were strongly adsorbed ($k_d \sim 100$). Mercury exhibited a k_d of about 40, while selenium was not adsorbed. The dependence of k_d decreases approximately linearly with increasing particle size (Drever, Murphy, and McKee, 1980). This was in agreement with our expectations for k_d to be proportional to the specific surface area which has the dimensions of 1/length. Time dependent problems were noted.

In view of these problems and the uncertainty of projecting the coal results to the field, we are advocating the use of the push-pull test. This will, hopefully, provide a guide and scale-up procedure in translating laboratory results in the field.

4.0 INTERPRETING THE PUSH-PULL TEST

The results of a push-pull test can be satisfactorily explained on the basis of a simple ion exchange model that assumes no mixing or dispersion (plug flow). The volume injected from the surface holding pool is termed a pore volume. In the examples given below, the pore volume was divided into 10 cells (the number is arbitrary, depending on the amount of resolution required; results based on 20 cells are almost indistinguishable from those based on 10 cells). As each increment of solution to fill a cell volume is injected (or extracted in the "pull" part of the test), the solution in each cell is displaced into the next cell. Within

always working in the low concentration range where the distribution coefficient is approximately constant. This is the limiting slope region in Figure 3.

Cores from granular sediments in the previous case readily disaggregate to a definite size distribution. Beyond this point, considerable effort is required to reduce the grain size further. Coal, on the other hand, is characterized by fractures on various scales. The choice of particle size is somewhat arbitrary and limited by convenience and available equipment. Currently, the approach has been to begin with sub-millimeter particles and progress to the centimeter size scale in order to study the effects of various particle sizes.

Adsorption characteristics were studied by preparing an 8% weight suspension of a limited range of particle sizes in a groundwater sample. The groundwater sample was prepared in the laboratory from its previously determined composition. Aliquots of a standard solution of a given trace element were added to the suspension. After equilibration, an aliquot of solution is removed from the suspension and analyzed for the element of interest. The suspensions were continuously stirred throughout the experiment. As a control, 100 ml of groundwater was treated and analyzed in exactly the same manner as the coal suspension. The concentration of adsorbed metal can be calculated from the difference between the concentration in the control and coal experiments. This concentration can be used to calculate a distribution coefficient for each element between coal and groundwater.

containing 650 ppm ammonia as ammonium carbonate-bicarbonate were injected into a single well. This is the "push" part of the test. Next, 52,500 gallons (200,000 liters) were "pulled" or pumped from the well. The ammonium ion concentration was periodically measured. The same wells employed in the push-pull test were also used to obtain the core and groundwater samples. As mentioned in a previous section, a composite sample was gathered from the permeable core sections. This was done to duplicate the material injected fluid would most likely contact.

4.1 Push-Pull Test #1

Laboratory values for the cation exchange capacity and distribution coefficient or limiting slope were 4 meq/100 g and 3, respectively. Using these values in the model, we obtained the comparison between field data and calculations based on laboratory data shown in Figure 4. A best fit in this instance resulted without the necessity of history matching by adjusting parameters. The fit in Figure 4 was obtained in two stages. In the first pore volume produced, the ion concentration of the stronger ammonium solution was included in the groundwater concentration G of equation (4.1). Thereafter, only the concentration of cations in the natural groundwater was used.

Another interesting feature of the push-pull tests is that the bulk of the ammonia does not attain the full extent shown in Figure 2. The radius (R) given in Figure 2 refers to the distance from the well that non-adsorbed species would propagate. The true situation is shown in Figure 5. In this figure, we note that the

each cell, concentrations are assumed to be uniform. Equilibrium is assumed to be reversible and rapid compared to the rate of water movement.

The distribution of NH_4^+ between solid and solution in the i th cell after the n th increment of solution has been injected is given by

$$\frac{Y_{i,n}}{C - Y_{i,n}} = K'_{\text{ex}} \frac{M_{i,n}}{G_{i,n} - M_{i,n}} \quad (4.1)$$

where the symbols are the same as in equation (2.5) with the subscripts changed to correspond to the cell model. The material balance equation for NH_4^+ is

$$Y_{i,n} - Y_{i,(n-1)} = \frac{\phi}{(1-\phi)\rho} (M_{(i-1),(n-1)} - M_{i,n}) \quad (4.2)$$

(ϕ is the porosity and ρ the grain density of the sediment) and for the total cations is

$$G_{i,n} = G_{(i-1),(n-1)} \quad (4.3)$$

Equations (4.1), (4.2), and (4.3) are solved simultaneously for each cell for each increment of solution pumped into or out of the well. The predicted concentration of ammonium in water pumped from the well as a function of volume pumped is then compared with field data. Since "plug flow" is assumed, the result does not depend on the assumed geometry (one-dimensional, cylindrical, spherical) of the pore volume underground.

As an example of the procedure, we will discuss two specific push-pull tests conducted on in-situ uranium properties in Wyoming. In both cases, 4,000 gallons (15,000 liters) of water

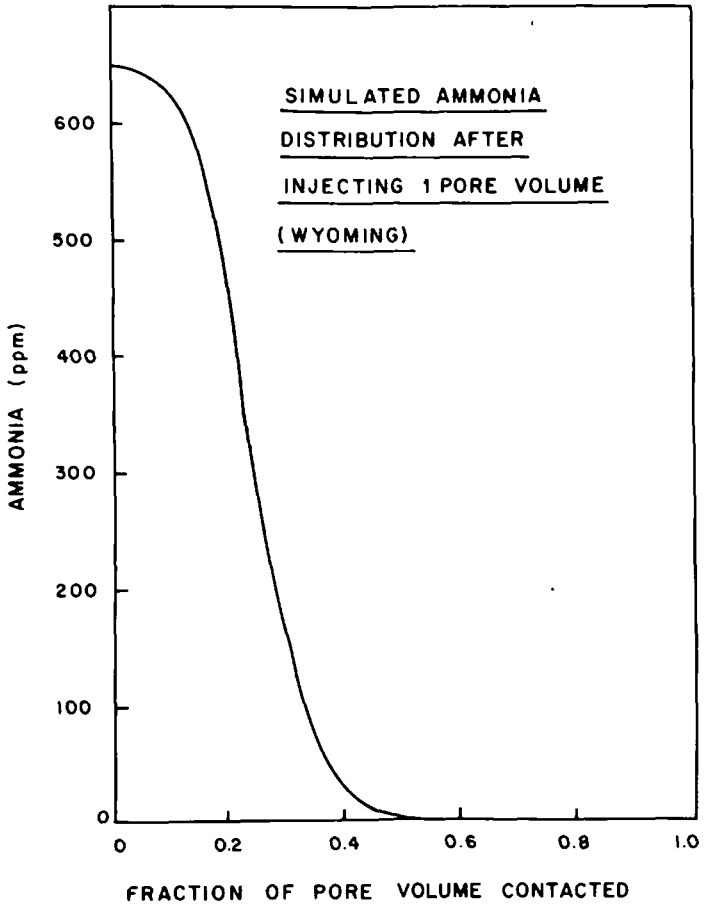


Fig. 5. Calculated distribution of dissolved ammonia after injection of 1 pore volume. Parameters are in Fig. 4.

From Figure 4, a concentration of 10 ppm is attained when 30,000 gallons have been pumped. Superficially, it would appear as if $30,000/4,000$ or 7.5 pore volumes are required to lower the concentration to 10 ppm. However, restoration is occurring by sweeping the smaller volume. The number of pore volumes passing through the small volume is, therefore, enhanced by the ratio

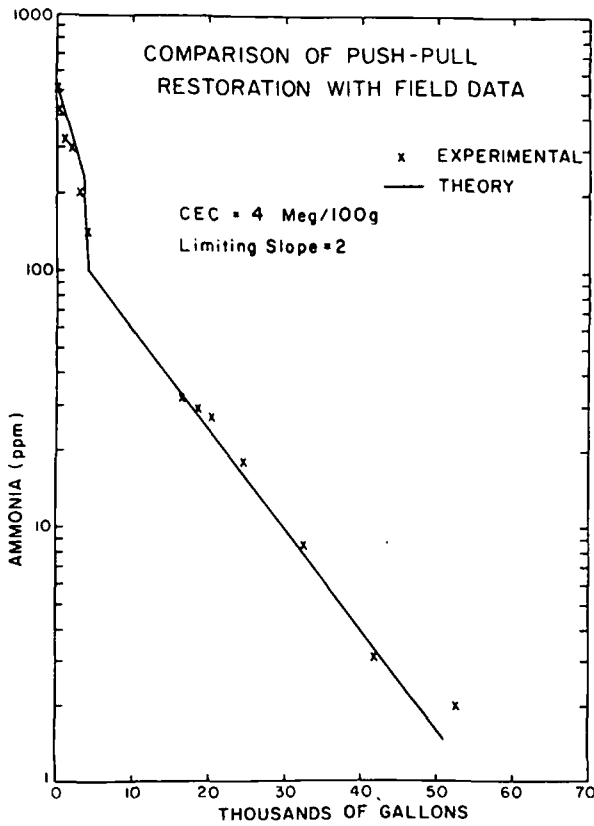


Fig. 4. Push-pull restoration: comparison of field data (crosses) with prediction based on laboratory measurements (CEC = 4 meq/100 g, $k_d = 3$). Concentration of ammonia injected = 650 ppm.

bulk of the ammonium ion lies within .25 pore volume of the subsurface material contacted and corresponds to a distance of .5R. This is the major reason the push-pull test has been misinterpreted in many recent tests. As an illustration, consider the number of pore volumes required to restore the groundwater to 10 ppm of ammonia.

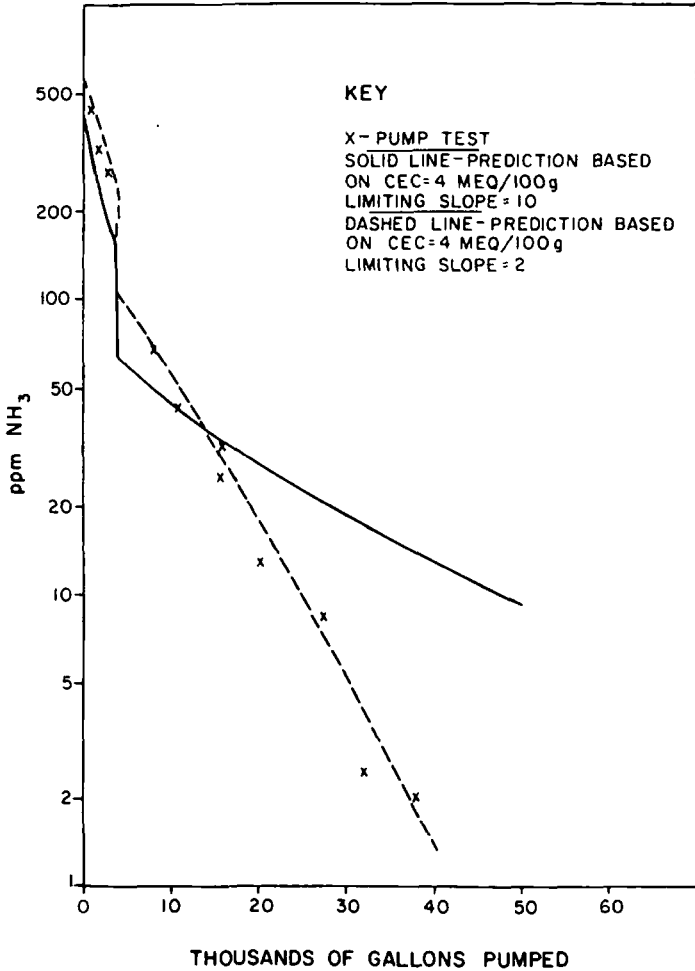


Fig. 6. Push-pull restoration: comparison of field data (crosses) with prediction based on laboratory data (CEC = 4 meq/100 g, $k_d = 10$; solid line) and "best fit" values (CEC = 4 meq/100 g, $k_d = 2$; dashed line). Concentration of ammonia injected = 650 ppm.

$1/.25 = 4$. The actual number of pore volumes required to restore 10 ppm is then 4×7.5 or 30 pore volumes. In an actual well field, the number of pattern pore volumes would be greater owing to the different lengths and arrival times of various flow paths. The path with lower response times would restore sooner than longer flow paths. The longer paths would, therefore, be rate controlling and result in the number of pattern pore volumes larger than 30.

4.2 Push-Pull Test #2

For this case, the cation exchange capacity determined in the laboratory was 4 meq/100 g. The limiting slope was found to be 10. Results calculated from laboratory data as shown in Figure 6 did not compare well with field data, particularly in the low concentration range. To obtain a better match, a series of type curves were prepared by varying the parameters as shown in Figure 7. The best fit was obtained with $C = 4$ meq/100 g and $k_d = 2$.

It is apparent from the type curves in Figure 7 that k_d can be determined fairly precisely, but, under the conditions of these particular tests, the CEC cannot be determined with any confidence. This is a consequence of the ammonia distribution underground shown in Figure 4. If the CEC is large, the injected ammonia will all be close to the injection site, and one "pore volume" will correspond to many pore volumes of the volume that is actually saturated. If the CEC is small, the injected ammonia will spread out farther, and one "pore volume" will correspond to fewer pore volumes of the volume that is saturated. This pore volume effect almost exactly cancels out the effect of CEC changes on the push-

pull recovery curve. In order to determine CEC from the push-pull test, it is necessary to use a high enough concentration of ammonium ion in the injected solution to saturate (or almost saturate) all the sediment contacted by the injected solution. The pore volume effect discussed above no longer operates, and the recovery curve is sensitive to changes in CEC (Figure 8). For problems of trace element migration, as in in-situ coal gasification, it is often not necessary to know the CEC. The important adsorption parameter is k_d .

From these examples, several lessons are apparent. First, they stress the necessity of confirming laboratory predictions in the field. Secondly, they demonstrate that reliable values can only be obtained if the pull or pumping portion of the test is run for approximately 10 pore volumes. If pumping had continued for only two or three pore volumes, we might have concluded that this agreement in Figure 6 was close enough. Thirdly, if it is necessary to measure the in-situ CEC, a high concentration of the adsorbing species must be present in the injected solution. The appropriate concentration is best estimated on the basis of laboratory CEC determination.

5.0 SUMMARY AND CONCLUSIONS

We have addressed the problem of verifying laboratory measurements using the simplest possible field experiment, namely, the push-pull test. A number of reasons were listed as to necessity of field verification. It was concluded that coal adsorption

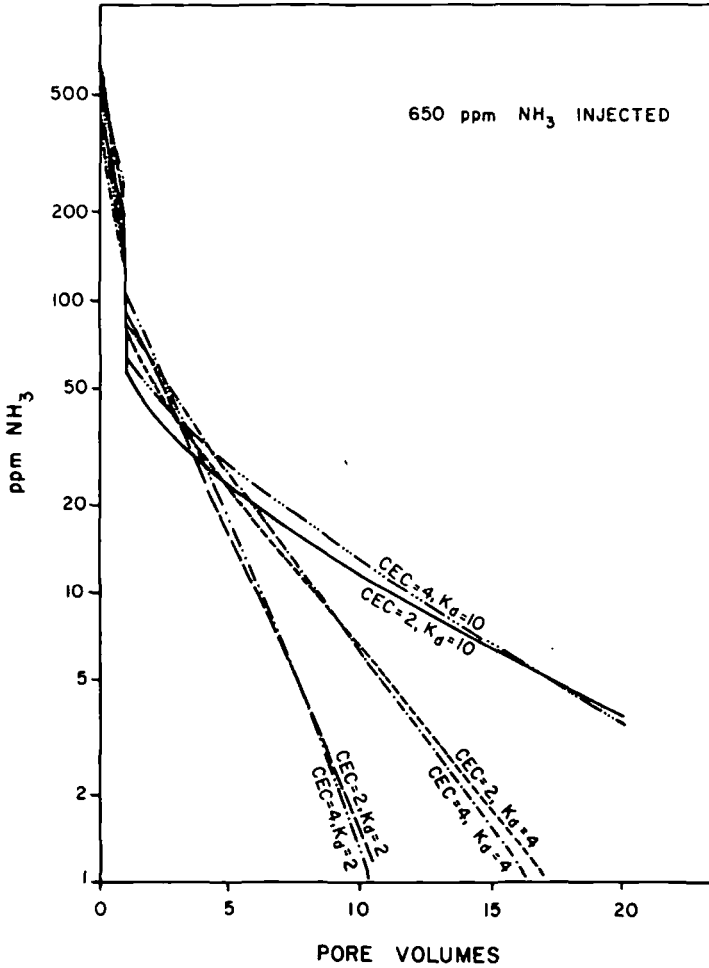


Fig. 7. Predicted recovery curves for push-pull test. Concentration of ammonia injected = 650 ppm, porosity = 0.30, grain density = 2.6 g/cm³. The discontinuity at 1 pore volume is caused by the change in total ion concentration from the value in the spiked solution to the groundwater value. CEC values are in meq/100 g.

measurements presented the greatest uncertainty owing to a lack of knowledge concerning the actual in-situ area exposed to fluids.

The laboratory measurement techniques used by us were briefly described for both uranium and coal. Central to our approach is the determination of the adsorption isotherm. This method is superior to column testing where the study is performed with one given inlet concentration thereby obtaining only one point on the entire adsorption curve. We noted that disaggregation of the uranium aquifer sample produced a fairly definite particle size. The good agreement with laboratory and field measured adsorption properties indicated that no significantly additional surface area was exposed in the disaggregation process. However, the distribution coefficient in the dilute region did not always agree with the field result.

In coal, a trend in the behavior of k_d with particle size was observed. An inverse dependence of adsorption properties upon particle size was established. However, it was not clear whether the results could be extrapolated to blocks on the scale of a meter or so. Even then, it would be quite difficult to establish the surface area contacted without adequate field testing. Furthermore, it was uncertain whether the surface behavior of broken pieces was similar to the naturally exposed surface area adjacent to high permeability paths in-situ. For these reasons, we were led to the push-pull test to verify results and to aid in scaling laboratory to field results.

Concerning the push-pull test, we listed two examples from

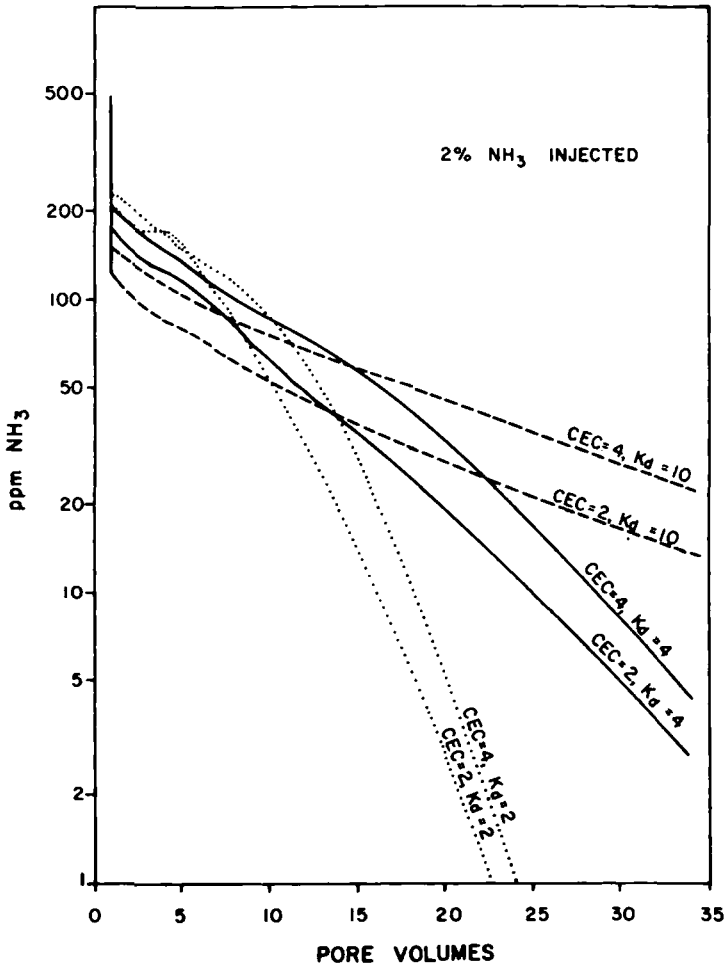


Fig. 8. Predicted recovery curves for push-pull test. Concentration of ammonia injected = 2%, grain density = 2.6 g/cm³, porosity = 0.30. Concentrations in first pore volume are off scale. CEC values are in meq/100 g.

REFERENCES

- Busenberg, E., Clemency, C. V., Determination of the Cation Exchange Capacity of Clays and Soils using an Ammonia Electrode, *Clays and Clay Minerals*, v. 21, pp. 213-217 (1973).
- Campbell, J. H., Pellizzari, E., Santor, S., Results of a Groundwater Quality Study Near an Underground Coal Gasification Experiment (Hoe Creek 1), Lawrence Livermore Laboratory Rept. No. UCRL-52405 (1978).
- Dalton, V. A., Campbell, Laboratory Measurements of Groundwater Leaching and Transport of Pollutants Produced during Underground Coal Gasification, *In-Situ*, 2(4), 295-328 (1978).
- Drever, J. I., Murphy, J., McKee, C. R., Adsorption of Lead, Cadmium, Mercury, Selenium and Phenol by Coal. To be published (1980).
- Garrels, R. M., Christ, C. L., Solutions Minerals and Equilibria, Freeman, Cooper & Co., San Francisco, CA (1965).
- Gilbert, M., Van Bladel, Thermodynamics and Thermochemistry of the Exchange Reaction between NH_4^+ and Mn^{2+} in a Montmorillonite Clay, *J. Soil Sci.*, 21, pp. 38-49 (1970).
- Hill, A. D., Walsh, M. P., Breland, W. M., Silverberg, I. H., Humenick, M. J., Schechter, R. S., Restoration of Uranium In-situ Leaching Site, *Soc. Pet. Eng. Paper No. 7534* (1978).

our work on in-situ uranium properties. No examples were available from coal properties. The two cases listed were from Wyoming. In the first case, excellent agreement was obtained between field and laboratory values. The agreement in the second case was rather poor with the distribution coefficient, k_d , displaying a large discrepancy. We noted that improper interpretation of the push-pull test would lead to a severe underestimate of the number of pore volumes required to restore the formation. This was due to the bulk of a strongly adsorbed solute remaining close to the well in a volume V_a which is significantly less than volume injected V_1 . The number of pore volumes transmitted through V_a is larger by ratio

$$(V/V_1)V_a$$

where V is the volume of fluid pumped to reduce the concentration to the level of interest.

We conclude that the push-pull test is a viable technique for comparing laboratory to field adsorption values. Furthermore, the type curve method can be used in the absence of laboratory values to obtain in-situ formation values.

ACKNOWLEDGEMENT

This work was supported by the Laramie Energy Technology Center of the Department of Energy and the Departments of Mineral Engineering and Geology of the University of Wyoming. The field push-pull tests were carried out by Geoffrey Hunkin.

ECONOMIC GEOLOGY

AND THE
BULLETIN OF THE SOCIETY OF
ECONOMIC GEOLOGISTS

Vol. 57

MARCH-APRIL, 1962

No. 2

TRANSPORTATION AND PRECIPITATION OF URANIUM AND
VANADIUM AT LOW TEMPERATURES, WITH SPECIAL
REFERENCE TO SANDSTONE-TYPE URANIUM
DEPOSITS¹

P. B. HOSTETLER AND R. M. GARRELS

CONTENTS

	PAGE
Abstract	137
Introduction	138
U-O ₂ -H ₂ O system	139
U-O ₂ -H ₂ O-CO ₂ system	142
Open system	143
Closed system	144
V-O ₂ -H ₂ O system	147
U-V-K-O ₂ -H ₂ O-CO ₂ system	149
Discussion, with reference to the ores of the Colorado Plateau	552
Correlation with natural ground waters	152
Environment of ore deposition	155
Formation of coffinite and vanadium silicates	158
Summary	160
Acknowledgments	161
Appendix	162
References	166

ABSTRACT

Uranium and vanadium in sandstone-type deposits of the western United States apparently have been transported to their present environment from external sources by low-temperature aqueous solutions. In this paper an attempt is made to interpret the characteristics of aqueous solutions capable of transporting significant quantities of uranium and vanadium through continental sedimentary rocks, and the changes in these

¹ Publication authorized by the Director, U. S. Geological Survey.

characteristics that might result in precipitation of uraninite and other ore minerals in concentrations of ore grade. On the basis of present knowledge, the transportation environment is shown to be that of weakly alkaline, moderately reducing ground water, with an average or larger than average concentration of dissolved carbonate species ($\text{H}_2\text{CO}_3 + \text{HCO}_3^- + \text{CO}_3^{--}$). Precipitation is induced by reduction, probably by carbonaceous material or hydrogen sulfide, or both. Uranium is transported mainly in the form of the highly stable uranyl dicarbonate and tricarbonate complexes. Precipitation results from reduction of hexavalent aqueous uranium species to form uraninite, reduction of tetravalent vanadium to form montroseite, and fixation of uranyl ions by combination with potassium ions and quinivalent vanadium to form the mineral carnotite.

INTRODUCTION

STUDIES over the past several years have shown that the complex mineralogy of the sandstone-type uranium ores is the result of the oxidation of an originally simple mineral suite (18, 37). Apparently, the minerals of this primary suite were precipitated simultaneously from aqueous solution long after deposition of the enclosing sediments (27, 30, 34, 35). In any given deposit the primary minerals are few, the common ones being uraninite, UO_{2+x} , coffinite, $\text{UO}_2(\text{SiO}_4)_{1-x}(\text{OH})_{4x}$, montroseite, $\text{VO}(\text{OH})$, vanadium silicates, pyrite, chalcopryrite, bornite, chalcocite, calcite, quartz, and gypsum.

It is noteworthy that in these minerals the elements are in the lowest valence states characteristic of natural occurrences. Indeed, it has been demonstrated that the conditions under which the primary minerals can co-exist at equilibrium in an aqueous medium at low temperatures and pressures are near the most strongly reducing environments attainable (18). This relation has led to the postulation that the presence of ore is the result of precipitation largely induced by reduction processes; a view bolstered by the widespread occurrence of woody materials replaced by ore minerals, and by the important ore occurrences reasonably ascribed to the reducing effects of hydrogen sulfide (26).

Coleman (11), in a summary of criteria suitable for the estimation of the environment of precipitation of the ore minerals, arrived at a temperature of the order of 100°C , and a pressure of the order of a few hundred atmospheres. This temperature estimate has been substantiated by the recent work of Breger and Chandler (7), who investigated the temperature dependence of extraction of humic constituents from coalified wood in mineralized horizons. Thus deductions based on low temperature and pressure chemistry are relevant to the actual process of ore formation.

Whatever the source of uranium and vanadium, all workers are in agreement that in numerous instances these elements had to be carried long distances (a mile or more) through the pores of the host sediments before deposition occurred (18, 27, 36). These sediments are characteristically lenticular continental sandstones and mudstones. Quartz, mica, and feldspar are common minerals of these rocks and there is a variety of clay minerals, including chlorite, montmorillonite, mixed layer mica-montmorillonite, and kaolinite.

The problems of ore-element transportation and deposition can be stated in the following questions:

1. In what aqueous environments, within the range of natural conditions, can all the ore-elements be transported simultaneously at some reasonable concentration?
2. If such environments exist, are they compatible with conditions expected during transportation of waters through the pores of the host rocks?
3. What changes in environment, induced by local variations in the nature of the host rocks, can be expected to lead to precipitation of the ore mineral suite?

Our attempts to answer these questions must be looked upon as a preliminary study. In our present state of knowledge we can hope only to delineate sets of conditions that are favorable for the transportation and deposition of ore elements, and then to test these conditions against actual occurrences. We emphasize the degree of solubility of uranium and vanadium in the presence of other ions common in subsurface waters in order to elucidate possible modes of ore-element transport. This simplifies the treatment of stability relationships among the insoluble ore minerals, which are of widespread occurrence, by eliminating the need for consideration of soluble, locally distributed minerals. Our approach is to begin with a discussion of uranium solubility in pure water, and then to assess the effects of addition of other constituents.

U-O₂-H₂O SYSTEM

Relations among uranium, oxygen, and water have been summarized by Garrels (19) and by Deltombe, de Zoubov, and Pourbaix (13). The only solid phases expected to occur stably in the presence of water and variable concentrations of oxygen are uraninite, UO_{2+x}, and schoepite, UO₂(OH)₂·H₂O, which spontaneously dehydrates when exposed to the atmosphere (10). Natural uraninites apparently maintain the cubic UO₂ structure for x values up to 0.6 (8). U₃O₈, easily prepared in the laboratory, has not been found in nature (16) and is probably metastable. Thermochemical data are available only for stoichiometric UO₂. Figure 1 shows schematically the composition relations among UO₂, UO₂(OH)₂·H₂O, O₂, and H₂O, and shows that the composition of uraninite in the presence of hydrogen and water is UO₂, but that for conditions sufficiently oxidizing to permit the coexistence of UO₂(OH)₂·H₂O, its composition is UO_{2.6}.

Stability ranges of UO₂(OH)₂·H₂O and stoichiometric UO₂ are shown as functions of oxidation potential (Eh) and hydrogen-ion activity (pH) in Figure 2. However, a good deal more information than is shown in Figure 2 can be gleaned from Eh-pH diagrams that portray thermochemical consideration of the solubility of uraninite and schoepite. This involves the calculation of the activities of all the ions in the system, in equilibrium with whichever solid phase is stable under specified Eh and pH conditions. For the details of such calculations the reader is referred to the papers of Garrels (19) and Deltombe et al. (13). Deltombe et al. and Garrels considered only three

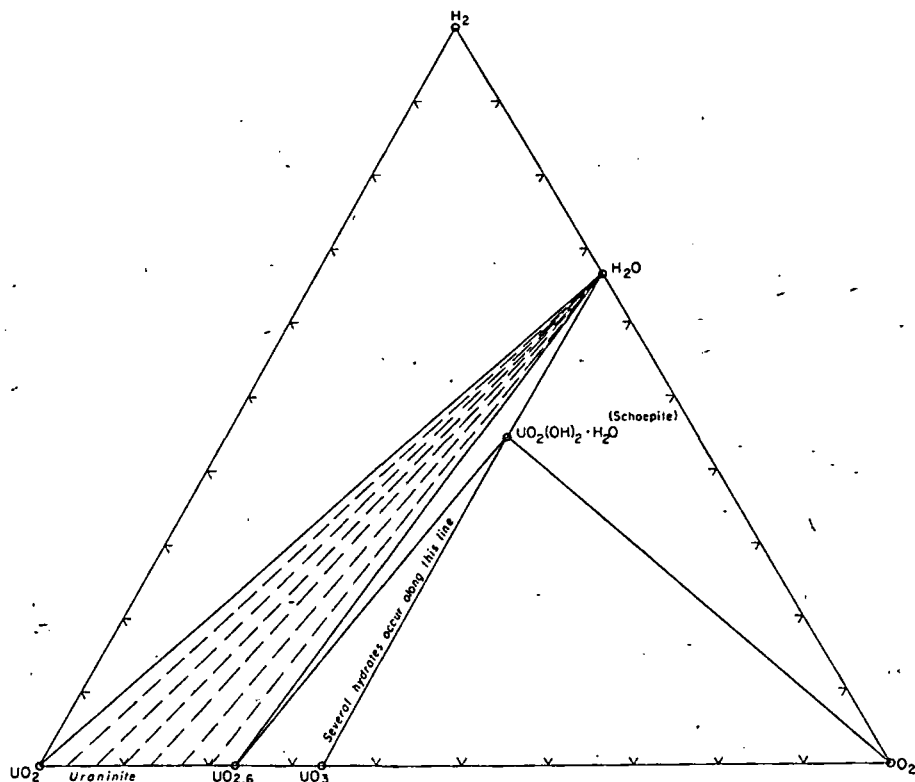


FIG. 1. Composition diagram showing probable relations among uraninite, schoepite, water, oxygen, and hydrogen at 25° C and 1 atmosphere total pressure. Percentages are molecular. Hydrates of composition lying between UO_3 and $\text{UO}_2(\text{OH})_2 \cdot \text{H}_2\text{O}$ are not considered.

ions, UO_2^{+2} , U^{+4} and $\text{U}(\text{OH})^{+3}$. Uranium is present in the hexavalent state in UO_2^{+2} and in the tetravalent state in U^{+4} and $\text{U}(\text{OH})^{+3}$. Figure 3 shows the relationship of these ions to schoepite and uraninite and to the additional hexavalent uranium species, HUO_4^- and $\text{UO}_2(\text{OH})^+$. Thermodynamic data for HUO_4^- and $\text{UO}_2(\text{OH})^+$ were derived from Gayer and Leider (24) and Bjerrum et al. (4) respectively.

It should be pointed out that for Figure 3 and for ensuing diagrams it is not, in general, possible to reach any selected Eh-pH value within the framework of the simple system under discussion. The addition of one or more components is necessary to reach selected Eh-pH values. The assumption is that the additional components will not disturb the diagrammed equilibrium relationships, and in simple, dilute systems such is usually the case. We return to a more critical discussion of this point in the section on correlation with natural ground waters.

In Figure 3 unbroken lines drawn between the stable solid phases and the fields of the ions indicate that total ionic activity of dissolved uranium

species in equilibrium with either solid phase is 10^{-6} . In other words, in the presence of uraninite or schoepite (whichever is stable), total ionic activity is fixed at 10^{-6} for the Eh and pH conditions shown by the solid lines. Along these lines the solid phase is no longer stable if total ionic activity is less than 10^{-6} ; all uranium is in solution. In the fields shown for the solid phases total ionic activity in equilibrium with that solid phase is less than 10^{-6} , while in the areas diagrammed for the ions total ionic activity must rise to a value greater than 10^{-6} before either uraninite or schoepite can be precipitated as a stable phase (Fig. 2 shows the stable solid phase). A dashed line representing a total ionic activity of 10^{-4} in equilibrium with the stable solid phase is included in Figure 3 to give the reader an idea of the activity gradient involved. A family of contours, parallel to the 10^{-6} and 10^{-4} contours, could be drawn to represent other values of total ionic activity in equilibrium with the solid phase. There are discrete Eh-pH conditions for which most of the uranium in solution is tied up in one ion; therefore, lines drawn between ions show conditions for which the activities of the two ions are identical.

The foregoing discussion is based on the conventions of Eh-pH diagram-

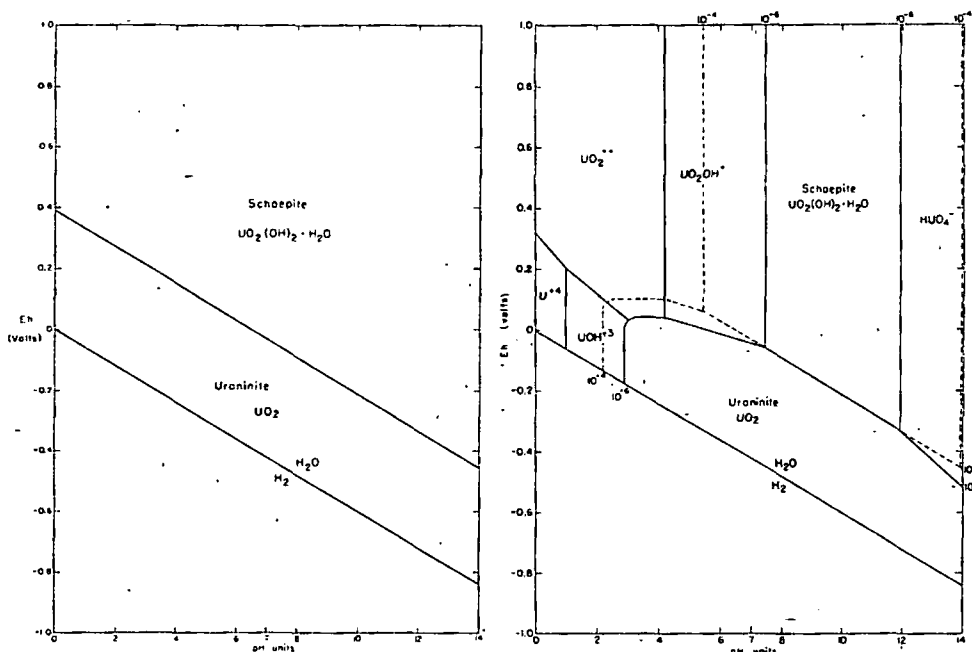
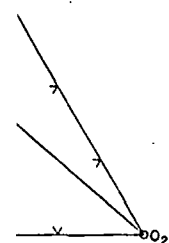


FIG. 2. (Left) Equilibrium diagram of the U-O₂-H₂O system at 25° C and 1 atm. Stability ranges of solid phases are plotted as a function of hydrogen-ion concentration and oxidation potential.

FIG. 3 (Right) Aqueous equilibrium diagram of the U-O₂-H₂O system at 25° C and 1 atm. Fields of solid phases and dissolved species are plotted as a function of hydrogen-ion concentration and oxidation potential. Boundaries of solid phases at total activity of uranium-bearing ions = 10^{-6} in unbroken lines, and at total activity = 10^{-4} in dashed lines.



ong uraninite,
total pressure.
een UO₂ and

avalent state
ure 3 shows
the additional
dynamic data
der (24) and

diagrams it is
in the frame-
one or more
e assumption
d equilibrium
ie case. We
on correlation

l phases and
ved uranium

ming developed by Pourbaix (31). It must be clearly recognized that the solubility areas, labeled with the ion that is their chief contributor, do not represent stoichiometric solubilities, but rather are areas in which the solubility is at least the value shown for thermodynamic equilibrium between solid phases and ionic activities. True solubility exceeds that calculated by a factor that depends on total concentration of all ions (ionic strength) and the degree of completeness of our knowledge of the ions which must be considered. In this system not all aqueous species have been considered, for a number of polyuranate complexes have been reported (4). Thermodynamic data or equilibrium constants reported for these species are in poor internal agreement. Nevertheless, it is clear that the polyuranate complexes are not sufficiently stable to alter significantly the relationships shown in Figure 3; their total effect is to increase slightly the solubility of schoepite over that portrayed in Figure 3.

Figure 3 shows that in the $U-O_2-H_2O$ system uranium is soluble only in acid or distinctly alkaline solutions and that the chief contributing ions in acid solution are the UO_2^{+2} and $UO_2(OH)^+$ species, with small fields of the U^{+4} and $U(OH)^{+3}$ ions also present. HUO_4^- is the main contributor to uranium solubility in alkaline solutions.

No species are shown below the water breakdown line, that is, for Eh-pH values at which the partial pressure of hydrogen exceeds one atmosphere. The assumption is that any reducing agent sufficiently powerful to reduce water and produce hydrogen at pressures of one atmosphere or greater (such as the U^{+3} ion) reacts with an excess of water to produce a more highly oxidized species.

The field shown in Figure 2 as " UO_2 " should be, as shown in Figure 1, a field of a solid changing in composition from UO_2 at the water-hydrogen boundary to $UO_{2.6}$ at the uraninite-schoepite boundary. In the absence of thermochemical data for UO_{2+x} we have assumed that only UO_2 is present. This places the uraninite-schoepite boundary at its lowest possible position on the Eh scale; the boundary between $UO_{2.6}$ and schoepite may be as much as a tenth of a volt higher, but parallel to the boundary shown. Our procedure gives uraninite its minimum stability, and somewhat overemphasizes the strength of the reducing agents necessary for its precipitation.

At any rate, we can conclude that nearly pure water is a poor transporting agent for uranium, except at pH values of about 5 or less. As will be seen later, such pH values are incompatible with the geologic occurrences of the ores.

$U-O_2-H_2O-CO_2$ SYSTEM

Essentially pure water is not to be expected in subsurface waters that are in intimate contact with rock minerals. Examination of analyses of ground waters reveals that dissolved CO_2 , in one form or another, is an important and ubiquitous constituent. The range of CO_2 content is large, but values of 100-300 ppm are common, whereas values of less than 10 and more than 10,000 ppm are uncommon.

Carbon dioxide markedly increases the solubility of the solid uranium

phases previously discussed. Bullwinkel (9) has studied its effects theoretically and experimentally, and concludes that the solid phases involved in the $U-O_2-H_2O-CO_2$ system are uraninite, schoepite, and rutherfordine, UO_2CO_3 . The dissolved species, in addition to those already considered, are $[UO_2(CO_3)_2 \cdot 2H_2O]^{-2}$ and $[UO_2(CO_3)_3]^{-4}$. These complexes are hereafter referred to as UDC (uranyl dicarbonate complex) and UTC (uranyl tricarbonate complex) respectively. We have computed the free-energy of formation values of rutherfordine, UDC, and UTC using the data of Bullwinkel (9) and the recent ΔF°_f of schoepite given by Deltombe et al. (13). The equilibrium constant for the dissociation of UTC to UDC plus carbonate, reported by Blake and others (5), is in good agreement with that reported by Bullwinkel (9).

The $U-O_2-H_2O-CO_2$ system may be considered from two standpoints, either open to an externally controlled P_{CO_2} , or closed, with a fixed amount of CO_2 in the system. An Eh-pH plot with P_{CO_2} equal to the partial pressure of CO_2 in the atmosphere is useful for portraying surface weathering conditions. However, atmospheric CO_2 has limited access to percolating ground waters, so it is more realistic to consider such waters as constituting a closed system in which a fixed addition, or periodic additions, of CO_2 proportionate among various CO_2 -bearing species according to an Eh-pH characterized environment. In such a closed system P_{CO_2} is variable, a function of pH. The total of the activities of all CO_2 -bearing species is constant for any addition of CO_2 reaching equilibrium. This constant is referred to as ΣCO_2 .

Details of the calculations required in constructing the diagrams presented here are given in the Appendix.

Open System.—Relations among uranium-bearing solid and dissolved species as functions of Eh, pH, and a P_{CO_2} value of $10^{-3.4}$ atm. (the partial pressure of CO_2 in the atmosphere) are shown in Figure 4. The general Eh-pH- P_{CO_2} diagram is shown in Figure 5 (Fig. 4 is a cross-section of Fig. 5 at $P_{CO_2} = 10^{-3.4}$ atm.) As in Figure 3, unbroken contours between ions and solid phases represent a total activity of dissolved uranium species of 10^{-6} , while dashed contours represent a total activity of 10^{-4} . For clarity, 10^{-4} total ionic activity contours are omitted in Figure 5. In Figure 4 and thereafter, formulas designating fields for solid phases are underscored.

Comparing Figures 4 and 5 with Figure 3 shows the marked effect of CO_2 , even at low partial pressures. Whereas Figure 3 is composed largely of areas indicating fields of solid phases, Figures 4 and 5 are dominated by areas of dissolved species. Uranyl carbonate complexing causes a wide field of solubility to exist under oxidizing conditions at essentially all pH values. The field of schoepite, $UO_2(OH)_2 \cdot H_2O$, as an insoluble compound is almost entirely eliminated, and although rutherfordine, UO_2CO_3 , does appear as a new phase, it occupies a minor part of the diagrams. For a given temperature, the schoepite-rutherfordine transition depends only on activity of water and P_{CO_2} . Assuming that $a_{H_2O} = 1$, Garrels (20) has shown that the equilibrium P_{CO_2} between these two phases is very close to the partial pressure of CO_2 in the atmosphere.

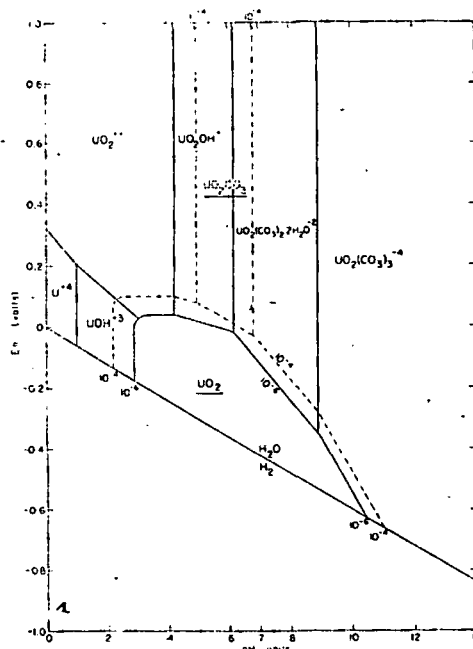


FIG. 4. Aqueous equilibrium diagram of the $\text{U-O}_2\text{-H}_2\text{O-CO}_2$ system at 25°C and 1 atm., and with P_{CO_2} constant at $10^{-8.4}$ atm. Boundaries of solid phases are drawn for total ionic activity of 10^{-6} (unbroken lines) and 10^{-4} (dashed lines). Formulas designating fields for solid phases are underlined.

Note that in Figure 4 a field for rutherfordine is only defined for a total activity of uranium bearing ions of 10^{-4} ; there is no field for this mineral when total ionic activity drops to 10^{-6} . Thus, in a weathering environment the concentration of uranium in solution must be around 10^{-5} moles/liter or greater before rutherfordine can be precipitated under the most favorable pH conditions (around pH 6.0).

In acid, oxidizing solutions uranium is transported as UO_2^{+2} and $\text{UO}_2(\text{OH})^+$, in neutral solutions as UDC, and in alkaline solutions as UTC. Not only does addition of CO_2 tend to eliminate schoepite, it causes the field of uraninite to diminish. As P_{CO_2} increases in the system stronger and stronger reducing agents are required to remove uranium from solution as uraninite.

Closed System.—The complexing effect of CO_2 on uranium is also vigorous for those conditions where the total amount of CO_2 (ΣCO_2) in the system may be regarded as fixed. In Figure 6 ΣCO_2 is taken as 10^{-3} (that is, the sum of the activities of all ions that contain CO_2 , including UDC and UTC, is 10^{-3}). This corresponds to a modest 44 ppm CO_2 in solution. Uranium, as UDC and UTC, is soluble in a wide range of environments. The small field of rutherfordine (again defined only for total uranium ion activity of 10^{-4}) indicates the restricted conditions under which this mineral forms.

Schoepite is soluble under all but very alkaline conditions when uranium ion activity is 10^{-4} . It has no field of stability when aqueous uranium drops to 10^{-6} . The expansion of the UTC field, at the expense of the UDC field, under mildly reducing conditions is interesting. Recalling that the total amount of carbonate is fixed, it is obvious that the activity of carbonate and bicarbonate must increase as the uranyl carbonate complexes begin to break

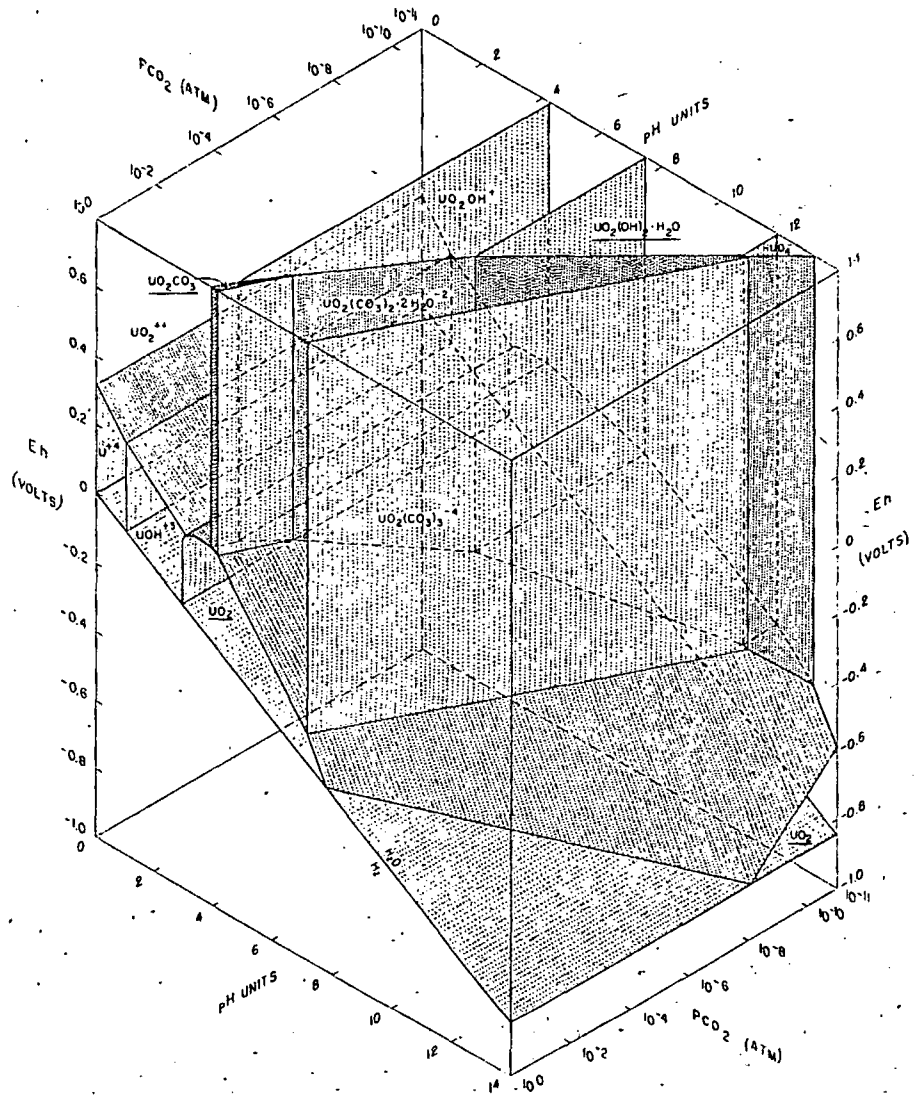


FIG. 5: Aqueous equilibrium diagram of the U-O₂-H₂O-CO₂ system at 25° C and 1 atm. PCO₂ is the third coordinate. Boundaries between solid phases and dissolved species are drawn for total ionic activity of 10⁻⁶.

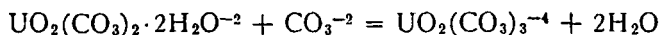
em at 25° C
solid phases
ashed lines).

for a total
his mineral
nvironment
moles/liter
st favorable

UO₂⁺² and
is as UTC.
es the field
onger and
solution as

also vigor-
the system
that is, the
and UTC,
Uranium,
The small
activity of
eral forms.

down under reducing conditions. The increased activity of CO_3^{2-} and HCO_3^- is reflected by an increase in the UTC/UDC ratio, as can be seen from the following reaction:



The uranyl carbonate complexes are stable enough to tie up considerable concentrations of uranium under slightly reducing conditions.

ΣCO_2 is raised to 10^{-2} in Figure 7, thus enlarging the dominant areas of UDC and UTC. Increasing ΣCO_2 extends the area of UTC relative to

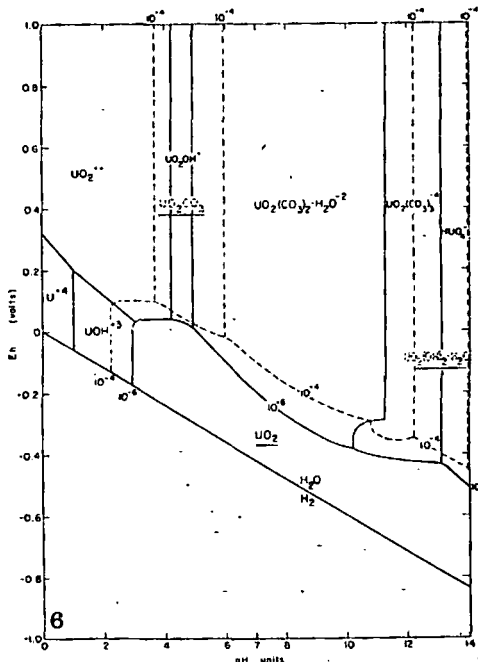


FIG. 6. Aqueous equilibrium diagram of the U-O₂-H₂O-CO₂ system at 25° C and 1 atm., and with $\Sigma\text{CO}_2 = 10^{-3}$. Boundaries of solid phases are drawn for total ionic activity of 10^{-6} (solid lines) and 10^{-4} (dashed lines).

UDC because UTC contains more carbonate. Conversely, the field of UTC disappears entirely when ΣCO_2 falls to $10^{-3.8}$. The upper boundary of the uraninite field in equilibrium with the uranyl carbonates is noticeably lower in Figure 7 than in Figure 6.

The trends discussed for Figure 7 are continued for Figure 8 where ΣCO_2 is 10^{-1} .

Equilibrium between carbonate species, water, and graphite is ignored in Figures 7 and 8 because it is generally irreversible. The effects of organic matter, hydrocarbons, and other reducing agents on the solubility of uranium is considered in a subsequent section. It is curious to note that in spite of

merization states of the ions, but these differences are of very little importance in this study.

U-V-K-O₂-H₂O-CO₂ SYSTEM

The addition of vanadium and potassium to the U-O₂-H₂O-CO₂ system can now be discussed. No new ionic complexes are introduced. Carnotite, K₂(UO₂)₂V₂O₈·1-3H₂O, is the only new and well-defined solid phase that is insoluble, although a number of soluble solid phases are known. Mention will be made below of the rather widespread, but poorly defined, mineral, rauvite. No measured value of ΔF°, of carnotite is available, however, we were able to compute a value from experimental solubility determinations conducted by Marvin and Magin (Marvin, R. F., and Magin, G. B., written communication). Data resulting from these experiments are not sufficiently accurate to permit a rigorous free-energy calculation, nor is such a calculation essential for the purpose of this paper. Instead, the lowest possible free-energy value

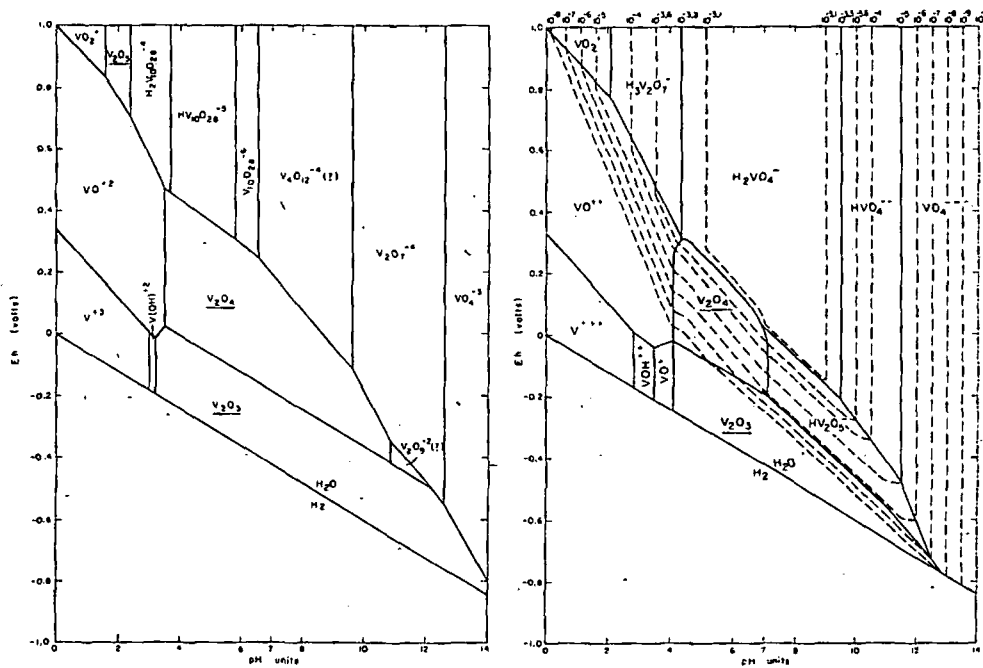


FIG. 10. (Left) Aqueous equilibrium diagram of the V-O₂-H₂O system at 25° C and 1 atm.; after Evans and Garrels (14). Boundaries between solid phases and dissolved species are drawn for total ionic activity of 10⁻². The formulas designating fields of solid phases are underlined.

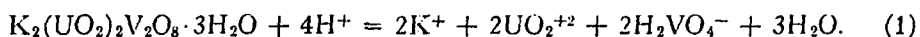
FIG. 11. (Right) Aqueous equilibrium diagram of the V-O₂-H₂O system at 25° C and 1 atm. Ionic nomenclature is from Deltombe et al. (12). Boundaries between solid phases and ions in solution are drawn for total ionic activity of 10⁻³ (unbroken lines). Dashed lines represent ionic activity contours of the H₂VO₄⁻ ion.

at 25° C
at ionic

marked
V₂O₅
of ionic
Deltombe
and poly-

was chosen consistent with Marvin and Magin's determinations. Thus, the field of carnotite shown in ensuing diagrams is the largest possible.

Briefly, calculations were made in the following manner. In pure water (devoid of CO_2) at a pH of 7.0 carnotite has a solubility of 3×10^{-7} moles/liter at 25° C. Assuming that ²:



The concentration of each of the ionic species is $2 \times 3 \times 10^{-7} = 10^{-6.22}$ moles/liter. As the solubility of carnotite in pure water is very low, concentration can be equated with activity. The activity gradient of UO_2^{+2} in equilibrium with schoepite is two orders of magnitude change per unit change in pH. At a pH of 7, and in the absence of CO_2 , the activity of UO_2^{+2} in equilibrium with schoepite is $10^{-8.4}$. At this pH, however, most of the soluble uranium is present as $\text{UO}_2(\text{OH})^+$. The activity of this ion in equilibrium with schoepite should be $10^{-5.55}$. Marvin and Magin's data, though, indicate that in pure water, carnotite slowly hydrolyzes to a colloidal hydrated uranium oxide, which suggests either schoepite is somewhat more stable, or $\text{UO}_2(\text{OH})^+$ less stable, than previously considered. The latter seems more probable.

The equilibrium constant for the reaction given by (1) is:

$$K_a = \frac{(\text{K}^+)^2 (\text{UO}_2^{+2})^2 (\text{H}_2\text{VO}_4^-)^2}{(\text{H}^+)^4}. \quad (2)$$

Substituting ionic activities and assuming that if $a_{\text{UO}_2^{+2}}$ rises above $10^{-8.4}$ carnotite, rather than schoepite, will be stable (to give a minimum $\Delta F^\circ_{f \text{ carnotite}}$):

$$K_a = 10^{-13.7}. \quad (3)$$

Since

$$\Delta F^\circ_{\text{reaction}} = RT \ln K_a = -1.364 \log K_a \quad (4)$$

$$\Delta F^\circ_{\text{reaction}} = 18.6 \text{ Kcal}. \quad (5)$$

The free-energies of all products and reactants are known except for carnotite.

$$\Delta F^\circ_{\text{reaction}} = \Delta F^\circ_{\text{products}} - \Delta F^\circ_{\text{reactants}} \quad (6)$$

$$\Delta F^\circ_{f \text{ carnotite}} = -1,294 (+0 \text{ to } +5) \text{ Kcal}. \quad (7)$$

A rough check on this value was provided from data given by Barton (3). Barton assumes $\text{V}_4\text{O}_{12}^{-4}$ is the vanadium ion causing precipitation of carnotite. Barton's experiments consisted, in part, of a determination of the time required to precipitate carnotite from a concentrated solution containing K_2SO_4 ,

² Calculations on this and the following pages concerning carnotite stability are made on the basis of the H_2VO_4^- ion of Deltombe et al. (12) rather than the $\text{V}_4\text{O}_{12}^{-4}$ ion of Evans and Garrels (14) because this choice enormously simplifies such calculations. While this procedure may be criticized for seeming to perpetuate a less probable interpretation of vanadium chemistry, careful comparison of the two interpretations shows that for neutral, alkaline or reducing conditions it makes no difference which interpretation is used in deriving carnotite stability. The scheme of Deltombe et al. (12) does give carnotite a slightly greater range of stability in acid environments than does that of Evans and Garrels (14).

$\text{Na}_4(\text{UO}_2)(\text{CO}_3)_3$ and NaVO_3 , at various pH values. We obtained the approximate pH value of such a solution just saturated with carnotite by extrapolating precipitation time to infinity. Concentrations were modified by estimated activity coefficients. As the extrapolation was only an approximation, we derived a free-energy value for carnotite which lies in the range between -1288 and -1293 Kcal.

The question of carnotite stability relative to that of other solid phases in the system is resolved by a comparison of the activity of the common ion, either UO_2^{+2} or H_2VO_4^- , in equilibrium with each solid phase at a specified Eh and pH. The activity of the common ion is not only a function of Eh and pH, but also depends on the activities of the other two ions involved in the precipitation of carnotite. In this study carnotite stability is shown on the framework of the $\text{U}-\text{O}_2-\text{H}_2\text{O}-\Sigma\text{CO}_2$ system and potassium and vanadium are added to this system in such a way that $K^+ = 10^{-3}$ and total activity of all vanadium-bearing ions (ΣV) = 10^{-3} . In ground waters, an activity of 10^{-3} for K^+ is quite reasonable. The ΣV value given is high, but it may have been achieved locally during the time of ore deposition on the Colorado Plateau and has certainly been achieved in subsequent leaching and oxidation. ΣCO_2 is varied between 10^{-3} and 10^{-1} . Contours representing the activity of H_2VO_4^- in equilibrium with the various oxides of the $\text{V}-\text{O}_2-\text{H}_2\text{O}$ system are shown in Figure 11. These contours are drawn on the basis that the sum of the activities of all vanadium ions is 10^{-3} .

Assume, for purposes of illustration, a pH of 4.0, an Eh above +0.38 volts, and a ΣCO_2 value of 10^{-3} , so that either carnotite or rutherfordine, UO_2CO_3 , (Fig. 6) is the stable solid. The activity of $K^+ = 10^{-3}$ and the activity of $\text{H}_2\text{VO}_4^- = 10^{-3.4}$ (Fig. 11). From equations (2) and (3):

$$(\text{UO}_2^{+2})^2 = \frac{(10^{-13.7})(10^{-4})^4}{(10^{-3.0})^2(10^{-3.4})^2} \quad (8)$$

$$\text{UO}_2^{+2} = (10^{-16.9})^{\frac{1}{2}} = 10^{-8.45} \quad (9)$$

Comparing this activity of UO_2^{+2} with that of UO_2^{+2} in equilibrium with rutherfordine under the above conditions, from Figure 6 ($a_{\text{UO}_2^{+2}} = 10^{-4.7}$), indicates that carnotite is the stable phase. Based on similar calculations (see Appendix), Figure 12 was drawn for $\Sigma\text{CO}_2 = 10^{-3}$. Solid phases are numbered, with carnotite occupying the lion's share of the diagram. "Montroseite" (Fig. 12) represents synthetic, crystalline V_2O_5 , for which thermodynamic data are available. A free-energy value for true montroseite (VOOH or $\text{V}_2\text{O}_5 \cdot \text{H}_2\text{O}$) would enlarge the diagrammed field of "montroseite" slightly. Areas indicating a certain degree of solubility, shown stippled on Figures 12, 13, and 14, are based on total activities of 10^{-4} for uranium-bearing ions ($\Sigma\text{U} = 10^{-4}$), 10^{-3} for vanadium-bearing ions, and 10^{-3} for K^+ , indicating that 40 ppm of potassium, 51 ppm of vanadium, and 24 ppm of uranium are carried in solution. The weight percent ratio of vanadium to uranium in solution is 2/1, a value approximating the general ratio of these elements in many parts of the Colorado Plateau.

Note that in Figure 12 the only solubility indicated is under quite acid conditions. ΣCO_2 is increased to 10^{-2} in Figure 13 where a further area of solubility is shown to occur for a mildly reducing, neutral to alkaline environment. Increased solubility under these conditions is due to the increased activity of the uranyl carbonate complexes in equilibrium with carnotite and uraninite. Vanadium in this environment is transported in the tetravalent state (Fig. 10). A hypothetical solution carrying the amounts of potassium, uranium, and vanadium given above would thus precipitate carnotite if subjected to oxidizing conditions. Uraninite and one of the tetravalent vanadium minerals, haggite or doloresite, would form if the solution were acidified. Paramontroseite is presumably metastable and forms by oxidation of montroseite (14). Uraninite and montroseite would be precipitated if the solution had access to a distinctly reducing environment containing either carbonaceous material or H_2S .

A ΣCO_2 value of 10^{-2} is reasonable for natural ground waters. For example, a series of spring and well water samples taken across the southern part of the Powder River Basin in Wyoming (W. N. Sharp, written communication) show total alkali values, as HCO_3^- , varying from 175 to 320 ppm. These values approach the $\Sigma\text{CO}_2 = 10^{-2}$ value of 440 ppm. The pH of these waters is around 8.0, varying from 7.6 to 8.4. Should these waters be subjected to slightly reducing conditions, they would be capable of carrying considerable vanadium and uranium in solution.

The carnotite "curtain" continues to rise, and the UO_2 field to shrink in Figure 14, where $\Sigma\text{CO}_2 = 10^{-1}$. The ionic strength of solutions containing this much CO_2 precludes the equality of activity and molarity, hence the amounts of uranium, potassium and vanadium actually carried in solution are somewhat greater than given above.

DISCUSSION WITH REFERENCE TO THE ORES OF THE COLORADO PLATEAU

The portions of Figures 12, 13 and 14 which indicate the Eh-pH conditions necessary for aqueous transport of uranium and vanadium should be critically examined from two standpoints:

- 1) correlation with natural ground waters.
- 2) the environment of ore precipitation from such waters.

Correlation with Natural Ground Waters.—Considering the distance of migration of ore solutions on the Plateau, and the absence of intensive wall-rock alteration there, it is very unlikely that the ore solutions were sufficiently acid (pH 3 or less) to satisfy the acid requirements for aqueous solubility shown in Figures 12, 13, and 14.

Solutions characterized by those areas of Figures 13 and 14 which show solubility as a function of UDC and UTC have already been mentioned as having characteristics in common with some natural ground waters (neutral to alkaline, mildly reducing, moderately large amounts of CO_2). None of these characteristics is at variance with the commonly assumed aqueous environment of ore deposition on the Plateau. The effects of other ionic

r quite acid
ther area of
ine environ-
ne-increased
arnotite and
e tetravalent
of potassium,
otite if sub-
nt vanadium
ified. Para-
montroseite
solution had
carbonaceous

rs. For ex-
the southern
tten commu-
to 320 ppm.
pH of these
eters be sub-
of carrying

to shrink in
s containing
, hence the
in solution

PLATEAU

h-pH condi-
n should be

distance of
tensive wall-
e sufficiently
us solubility

which show
1 mentioned
waters (neu-
O₂). None
ned aqueous
other ionic

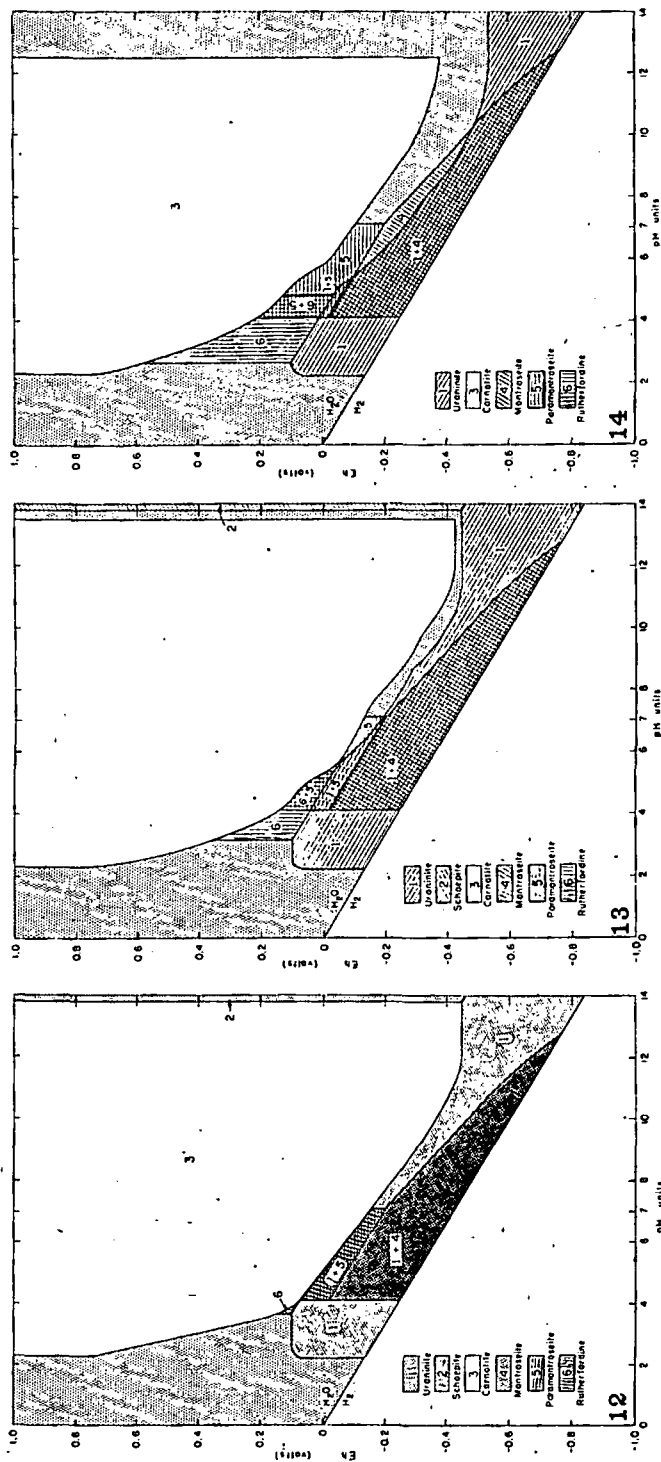


FIG. 12. Aqueous equilibrium diagram of the U-V-K-O-H₂O-CO₂ system at 25° C and 1 atm. Stability fields of solid phases are numbered and areas indicating soluble conditions, are stippled. The boundary between solid phases and solution (see text) is fixed for $\Sigma U = 10^{-4}$, $\Sigma V = 10^{-8}$, $\Sigma K = 10^{-8}$, and $\Sigma CO_2 = 10^{-8}$.

FIG. 13. Aqueous equilibrium diagram of the U-V-K-O-H₂O-CO₂ system at 25° C and 1 atm. Other conditions as in Fig. 12 except that ΣCO_2 is fixed at 10^{-2} .

FIG. 14. Aqueous equilibrium diagram of the U-V-K-O-H₂O-CO₂ system at 25° C and 1 atm. Other conditions as in Fig. 12 except that ΣCO_2 is fixed at 10^{-1} .

species commonly found in subsurface waters and the associated problem of electrostatically balancing a large excess of HCO_3^- and CO_3^{--} ions remain to be discussed.

Significant additions of new ionic species into solutions of the U-V-K-O₂-H₂O-CO₂ system requires evaluation of three possible phenomena. First, such introduction may cause a reaction with existing ionic species to precipitate new insoluble solid phases (we are not concerned here with the soluble ones). Secondly, new ionic complexes, characteristic of definite Eh and pH conditions, may be formed, thus causing an increase in solubility. Lastly, even if the first two effects do not occur, any addition of new species increases the ionic strength of the solution. This effect is not shown on our diagrams, inasmuch as they are drawn for thermodynamic solubility (activities). Increasing the ionic strength causes solubility, in moles/liter, to exceed calculated thermodynamic solubility. Most subsurface waters are sufficiently dilute (concentration of major species less than 0.1 molal) so that true and calculated solubilities are approximately equal.

Specifically, subsurface waters containing notable uranium, vanadium, potassium and CO₂ will certainly also contain significant amounts of at least several of the following: sulfate, chloride, sodium, calcium and magnesium. No insoluble phases are formed as a result of addition of SO_4^{-2} and Cl^- , but these ions will form complexes with the uranyl and uranous ions. The uranyl sulfate complexes, $\text{UO}_2(\text{SO}_4)_2^{-2}$ and $\text{UO}_2(\text{SO}_4)_3^{-4}$, are stable only for pH values less than 3.5, while the uranous sulfate complexes, $\text{U}(\text{SO}_4)_3^{-2}$ and $\text{U}(\text{SO}_4)_4^{-4}$, form under even more acid conditions (29), hence the importance of such complexes in most natural waters is negligible. From the work of Ahrlund and his associates (1, 2) it is clear that uranyl and uranous chloride complexes have stability ranges very similar to their sulfate analogues.

The cations, Na^+ , Mg^{+2} , and Ca^{+2} , must be appealed to for electrostatic balance in natural solutions. Ca^{+2} can be quantitatively considered with the following limitations. For calcite:



From the thermochemical data of Latimer (28):

$$K_a = (\text{Ca}^{+2})(\text{CO}_3^{-2}) = 10^{-8.35} \quad (11)$$

If $\Sigma\text{CO}_2 = 10^{-2}$ or 10^{-1} , maximum $a_{\text{Ca}^{+2}}$ values in solution can be calculated with the aid of $a_{\text{CO}_3^{-2}}$ determined for the construction of Figures 7 and 8 (see Appendix). If $\Sigma\text{CO}_2 = 10^{-2}$, calcium ions can electrostatically balance all HCO_3^- and CO_3^{-2} ions in solution if the pH is no higher than about 7.5; if $\Sigma\text{CO}_2 = 10^{-1}$, the highest pH is only about 6.0. Similarly, dolomite or magnesite would control the amount of magnesium ions that could be carried in solution.

Although no solubility data are available for tyuyamunite, $\text{Ca}(\text{UO}_2)_2\text{V}_2\text{O}_8 \cdot 5\text{H}_2\text{O}$, we suppose that it is one or two orders of magnitude more soluble than carnotite. If such is the case, Ca^{+2} activities of 10^{-2} to 10^{-1} would suffice

to give a stability field for tyuyamunite similar to that of carnotite in Figures 12-14.

Rauvite, $x\text{UO}_3 \cdot y\text{V}_2\text{O}_5 \cdot z\text{H}_2\text{O}$, is fairly widespread on the Colorado Plateau. Apparently y is somewhat greater than x (14). Two analyses reported by Frondel (16) show about 2.7 percent CaO each, but it is not known whether calcium is an essential constituent of rauvite. Low pH and moderately large concentrations of pentavalent vanadium should theoretically favor the formation of rauvite rather than carnotite or tyuyamunite. Indeed, Barton (3) has found that rauvite, rather than carnotite, is precipitated from acid solutions of pH 1.5-2.0 and 0.01 molar in uranium and vanadium. The association of rauvite with navahoite, $\text{V}_2\text{O}_5 \cdot 3\text{H}_2\text{O}$, at Monument Valley (38) suggests that where aqueous pentavalent vanadium is sufficiently concentrated in an acid environment for the formation of navahoite, then rauvite is stable relative to carnotite or tyuyamunite. As the formation of rauvite appears to be restricted to acid, oxidizing environments it is unnecessary to consider further the stability of this mineral within the framework of a mildly reducing, neutral-alkaline ground water.

Na^+ is the most likely choice to balance a large excess of anions. The addition of Na^+ to the systems discussed above produces no insoluble minerals, hence Na^+ can balance the solutions electrostatically over the entire Eh-pH range of interest.

The net effect of the addition of those ionic species common in natural ground waters to the neutral-alkaline solutions of the type indicated in Figures 13 and 14 is that the boundaries between solid phases and solution remain valid as drawn (no significant complexing with SO_4^{-2} or Cl^- for these pH conditions) and that sufficient quantities of the cations, Ca^{+2} , Mg^{+2} , and especially Na^+ , can be carried in solution to electrostatically balance all the anions present. Accordingly, part of the area of solubility shown in Figure 13 is particularly compatible with subsurface waters because of its pH values and reasonable CO_2 content (440 ppm). The narrow Eh range of the solubilities shown definitely suggests that ore deposition is characterized by certain redox potentials and indicates the desirability of evaluating activity gradients for this area of solubility. This evaluation is shown in Figure 15 where the increment of decreasing total ionic activity is an order of magnitude and $\Sigma\text{CO}_2 = 10^{-2}$. Shaded lines in Figure 15 thus represent solid phase-solution contours for a total activity of uranium-bearing ions equal to 10^{-5} , and total activities of 10^{-4} for K^+ and vanadium-bearing ions. Five ppm vanadium, 4 ppm potassium and 2.4 ppm uranium can be carried in solution under conditions indicated by the shaded lines. The conditions for solubility indicated on Figure 13 are shown here with dashed lines. For an Eh-pH characterized environment varying from the shaded to the dashed lines, vanadium solubility may increase from 5 to 50 ppm, potassium from 4 to 40 ppm, and uranium from 2.4 to 24 ppm.

Environment of Ore Deposition.—In Figure 15 ionic activity contours for ions in equilibrium with carnotite are more widely spaced than contours for ions in equilibrium with uraninite and montroseite, indicating that the

(10)

(11)

$\text{UO}_2)_2\text{V}_2\text{O}_5$
more soluble
would suffice

stability of carnotite is much more sensitive to decreasing amounts of uranium and vanadium in solution than is the stability of uraninite or montroseite. Indeed, if the activity of potassium, uranium and vanadium ions should each drop to $10^{-6.3}$ carnotite would completely disappear from Figures 13 and 15, whereas uraninite has a sizeable field of stability under such conditions (Fig. 7). Such values, reasonable for uranium and vanadium, are distinctly low for potassium, but even if K^+ is raised to 10^{-3} , the field of carnotite stability is very small.

Consider a potential ore solution migrating slowly through pore spaces in the host rock under thousands of feet of sediments. Such a solution would almost certainly be devoid of significant oxygen. Redox potential would be

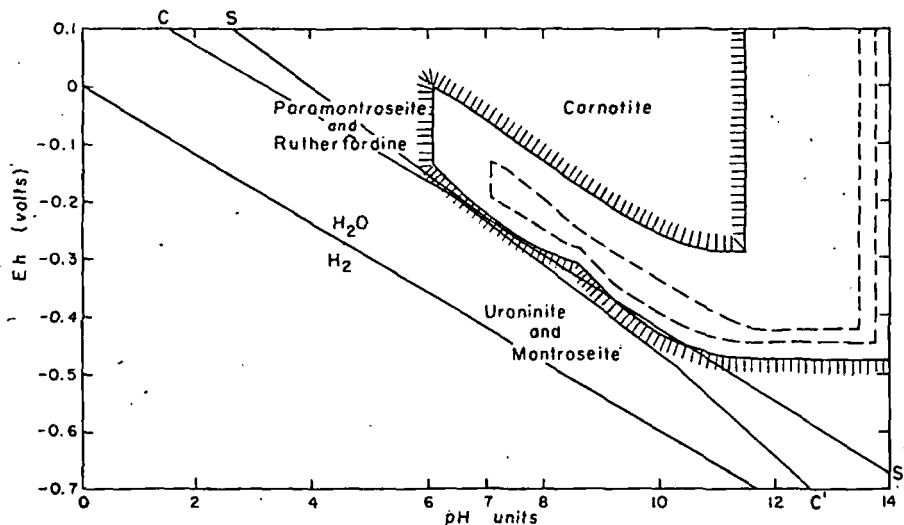


FIG. 15. Aqueous equilibrium diagram of the U-V-K-O₂-H₂O-CO₂ system at 25° C and 1 atm., and with ΣCO_2 fixed at 10^{-2} . Boundaries between solid phases and solution are fixed for $\Sigma\text{U} = 10^{-5}$, $\Sigma\text{V} = 10^{-4}$, and $\Sigma\text{K} = 10^{-4}$ (shaded lines), whereas dashed lines represent solid phase-solution boundaries for $\Sigma\text{V} = 10^{-3}$, $\Sigma\text{K} = 10^{-3}$ and $\Sigma\text{U} = 10^{-4}$.

poorly buffered. Since carnotite is stable over a wide range of Eh and pH conditions its formation would be most critically controlled by the amounts of uranium, vanadium and CO₂ in solution.

Migration through pockets of carbonaceous material or areas of entrapped H₂S would, of course, make the solution Eh more reducing. Two likely redox potentials are shown in Figure 15 by lines c-c' and s-s'. Line c-c' represents a calculated equilibrium potential between graphite and aqueous carbonate species which is analogous to an equilibrium potential between carbonaceous material and carbonate species. Line c-c' was calculated for $\Sigma\text{CO}_2 = 10^{-2}$, but the change in potential is only 15 mv. when ΣCO_2 is altered by a factor of 10. Line s-s' shows the redox potential of equal con-

centrations of SO_4^{-2} and sulfide ions as calculated by Garrels and Naeser (22). Migrating solutions at 25°C containing SO_4^{-2} and encountering gaseous H_2S would reach a potential very close to this line independently of the amount of sulfur species in each phase because of the very steep activity gradient involved for each aqueous sulfur species away from line s-s'.

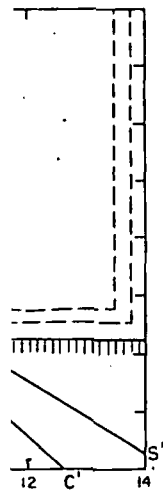
Between pH 6 and pH 10 both potentials are very close to the bottom of the area designating solubility in Figure 15. At 25°C and 1 atmosphere pressure the reducing environment indicated by these potentials is sufficient to precipitate uraninite and montroseite if solution concentration is about 0.5 ppm or higher for uranium and 2 ppm or higher for vanadium. Natural uraninite precipitated in such an environment, however, is probably closer to $\text{UO}_{2.6}$ than to UO_2 , indicating that the saturation concentration of uranium is somewhat less than 0.5 ppm because $\text{UO}_{2.6}$ is more stable and therefore less soluble than UO_2 . An environment of rising temperature should not significantly reduce the effectiveness of H_2S and woody material as precipitation agents for uraninite and montroseite from natural solutions. Rafalsky (32) heated uranyl sulfate solutions with aluminum sulfide in closed silica ampules and found that at 150°C the concentration of soluble uranium in the presence of uraninite is 1.6 ppm. At 125°C Miller (29) noted about 1.2 ppm uranium in solution after precipitation of uraninite by H_2S . It thus seems likely that the Plateau uraninite was deposited from solutions that contained a minimum of about 0.5 ppm uranium.

It is noteworthy that the uranyl carbonate complexes become increasingly unstable above 120°C . Rafalsky's data (32) indicate that uranium solubility in carbonate solutions diminishes by a factor of about 100x between 100 and 200°C and that the decrease in solubility is slight between 100 and 120°C but becomes much greater above 120°C . A similar temperature range ($120\text{--}215^\circ\text{C}$) was used in Miller's experiments (29) and the resulting decrease in uranium solubility was found to be one order of magnitude. Neither author offers any data for uranium solubility in carbonate solutions between 25 and 100°C , but Rafalsky's work between 100 and 120°C suggests that solubility is either fairly constant in the 25– 100°C interval or may even rise to a maximum somewhat under 100°C . Increased H_2S pressure (up to 9,000 lbs/sq inch) also decreases uranium solubility, according to Miller (29), but its total effect is small.

The foregoing considerations lead to a consistent pattern of aqueous transport and deposition of ore elements on the Colorado Plateau. The ubiquitous spatial and temporal relationship of uranium and vanadium ore minerals points to a common origin and transportation medium for these elements. Although this common origin cannot be pinpointed, it seems likely that in late Cretaceous or early Tertiary time, perhaps even earlier, a heavy load of overlying sediments forced uranium- and vanadium-bearing solutions out of sediments rich in volcanic ash, such as the Chinle Formation of Late Triassic age and the Brushy Basin Member of the Morrison Formation of Late Jurassic age (36). These solutions, comparable to the type discussed in the previous two sections of this study, migrated through pore spaces and

s of uranium
montroseite.
should each
s-13 and 15,
ditions (Fig.
distinctly low
otite stability

pore spaces
olution would
tial would be



CO_2 system at
n solid phases
shaded lines),
or $\Sigma V = 10^{-3}$,

f Eh and pH
the amounts

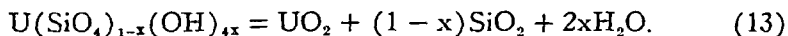
of entrapped
Two likely
s'. Line c-c'
and aqueous
ntial between
calculated for
hen ΣCO_2 is
of equal con-

permeable channels in the Shinarump Member of the Chinle Formation or the Salt Wash Member of the Morrison Formation, where they undoubtedly encountered reducing environments with concomitant ore precipitation (see Jensen (26), p. 611-615, for a more complete discussion of this point). These environments may have been pockets of carbonaceous material and/or H_2S , or even H_2 which may have been locally produced by the reaction of H_2S with Fe_2O_3 . Gaseous hydrogen will precipitate uraninite and montroseite from very dilute solutions.

By the end of Cretaceous time the thickness of the stratigraphic column atop the Salt Wash Member in the Uravan district was nearly the same as that above the Shinarump Member in northeastern Arizona, a thickness of about 6,000 feet (L. C. Craig, oral communication). Normal geothermal gradients across this thickness during the time of ore-solution migration would mean temperatures around $75^\circ C$. This is well below the temperature ($120^\circ C$) at which the uranyl carbonate complexes begin to break down. Of course, a deeper depth of burial, or higher geothermal gradients, might have produced temperatures in excess of $120^\circ C$ in the vicinity of the migrating solutions, in which case uraninite should precipitate as a result of decomposition of UDC and UTC. Because this control of ore formation, unlike those given earlier, is selective towards uranium, there is no reason for uraninite so formed to be found in association with trivalent vanadium minerals, sulfides or carbonaceous material. Lack of such ore on the Plateau supports the hypothesis that temperatures in the environment of ore deposition were not above 100 to $120^\circ C$.

Formation of Coffinite and Vanadium Silicates.—Ore deposition has many ramifications that are not discussed here, such as comparison of precipitation conditions for locally abundant copper, molybdenum and selenium minerals of the Plateau with those precipitation conditions given here for uranium and vanadium minerals. Such a comparison would make an excellent future study (many of the pertinent thermochemical data are known for $25^\circ C$). Some remarks about the stability of coffinite, $U(SiO_4)_{1-x}(OH)_{4x}$, and the vanadium silicates are appropriate because of their widespread occurrence as primary minerals on the Plateau. No thermochemical data are available for these minerals.

Coffinite and uraninite are the only known minerals from the Colorado Plateau in which the dominant uranium is in the +4 oxidation state, and their intimate association indicates mutual low solubility under reducing conditions (21). The uraninite-coffinite equilibrium may be written:



At a given temperature and total pressure, equilibrium between the solid phases is a function of the activity of water and aqueous silica. In high-temperature hydrothermal veins and in pegmatites reaction (13) goes to the right. The environment of ore deposition on the Plateau must have been such that reaction (13) went either way, depending on small a_{H_2O} and a_{SiO_2} fluctuations. Descriptions of corroded quartz grains in impregnated sand-

stone and nearby secondary quartz overgrowths (33, 39) indicate a liquid phase that hovered around quartz saturation values.

As coffinite is rapidly altered under oxidizing conditions (21), it seems probable that in the presence of excess quartz coffinite occupies much the same position as uraninite in the Eh-pH diagrams previously shown.

The vanadium silicates of the Plateau ore deposits are the vanadium mica (roscoelite, $K(Al,V)_2(Al,Si_3)O_{10}(OH,F)_2$), and vanadium-bearing clays (chlorites and mixed layer montmorillonite-micas and montmorillonite-chlorites). Several workers (15, 23, 39), emphasizing the pronounced chemical and mineralogical similarity between mineralized and nearby barren clays, have concluded that most of vanadium clays originated by replacement of octahedrally coordinated aluminum by vanadium in preexisting clay minerals. Roscoelite and some of the vanadium clays probably precipitated directly from solution (15).

The presence of montroseite at those localities on the Plateau where roscoelite is abundant (6) suggests that, at low temperatures and moderate concentrations of K^+ , Al and +3 vanadium, roscoelite has a field of stability similar to montroseite on Figures 12-15. Apparently, a decreasing V/U ratio is accompanied by a relative decrease of roscoelite and increase of montroseite in primary vanadium ore (39). Abundant clay minerals in both types of ore (high roscoelite or high montroseite) indicate that soluble K, Al, and Si do not change noticeably as the V/U ratio fluctuates and that the formation of roscoelite is probably more sensitive to decreasing concentrations of +3 vanadium than is montroseite.

Most of the vanadium in the mineralized clays is tetravalent, even in oxidized ore (15, 23). This observation has led to the suggestion (Garrels et al., (23)) that the vanadium was transported in the tetravalent state in the ore solutions. Reasoning based on available thermochemical data (Figs. 13-15) supports the notion that vanadium was tetravalent during transport. However, if this reasoning is correct, an equally fundamental question remains; namely, why should only those clay minerals in ore deposits contain +4 vanadium? Barren clay minerals a few inches from mineralized clays contain only one tenth as much vanadium as the mineralized clays (15). This selective substitution of octahedral Al by +4 vanadium is especially puzzling as the ore solutions probably migrated considerable distances (27, 36). We conclude this paper by speculating a bit on this question.

First, +3 vanadium may replace octahedrally coordinated aluminum more readily than does +4 vanadium. If this is true then most of the vanadium was originally emplaced in the clay minerals in the trivalent state. The Eh values of the sulfide-sulfate and carbon-carbonate redox potentials which we believe control primary mineralization (lines s-s' and c-c' of Fig. 15) require most, but not all, of the aqueous vanadium at these potentials to be trivalent. The association of vanadium clay minerals with montroseite, as in the Uravan district (33, 39) and with roscoelite and montroseite, as at Placerville and Rifle (6), also implies trivalent aqueous vanadium at the site of clay mineralization. The intimate association of roscoelite with the vanadium clays is

(13)

particularly suggestive of original +3 vanadium in the clays, for Hathaway (25) has shown that completely transitional mixed layering occurs between pure roscoelite and randomly interstratified roscoelite-montmorillonite clays.

From her study of the present oxidation states of vanadium in selected, mixed-layer roscoelite-montmorillonite clays in partially oxidized ore, Foster (15) concludes that the vanadium was originally emplaced in the +4 state. Foster (15) argues that assuming that all vanadium was originally trivalent leads to abnormally large negative charges for the sum of the tetrahedral and octahedral layers of the clay minerals. Foster assumes, though, that none of the vanadium is lost in the theoretical oxidation of vanadium in these clays to the +4 state. The increase in stability of aqueous ionic species bearing +4 vanadium compared to those containing +3 vanadium (cf. Fig. 2 in Evans and Garrels (14)) suggests that oxidation of vanadium from the +3 to +4 state in clays would be accompanied by a modest loss of vanadium to solution. If the clays described by Foster were to lose only ten percent of their vanadium during theoretical oxidation the total negative charge of the tetrahedral and octahedral layers would be reasonable for mixed layer roscoelite-montmorillonites (about -0.90).

Clearly, analyses are needed of the oxidation state of vanadium in vanadium clays closely associated with unoxidized assemblages.

A second hypothesis, put forward by Roach and Thompson (33) to explain the presence of vanadium clay in otherwise unmineralized sandstone at the Peanut Mine, states that these clays originated from tetravalent vanadium made available during oxidation of primary vanadium minerals.

A third, but less plausible, method for selectively replacing Al^{+3} by V^{+4} within the clay minerals of the ore deposit appeals to relatively impermeable boundaries, such as festoon surfaces, to detain migrating ore solutions for a sufficient length of time for replacement to occur. Replacement by tetravalent vanadium presumably occurred away from local "hot spots" of carbonaceous material. The released aluminum might eventually react with aqueous potassium, silica, and trivalent vanadium (available nearer carbonaceous material) to form roscoelite.

SUMMARY

1. Eh-pH diagrams at 25° C were constructed with the aid of published thermodynamic data for the $U-O_2-H_2O$ and $U-O_2-H_2O-CO_2$ systems. Uraninite, UO_{2+x} , and schoepite, $UO_2(OH)_2 \cdot H_2O$, are the only solid phases expected to be stable in the presence of water and variable concentrations of oxygen in the system $U-O_2-H_2O$. The addition of CO_2 to this system causes formation of stable uranyl carbonate complexes and a significant increase in the solubility of uraninite and schoepite.

2. Following a rough calculation of the free-energy of carnotite, Eh-pH diagrams of the $U-V-K-O_2-H_2O-CO_2$ system were drawn for various values of total carbonate (ΣCO_2). These diagrams show stability fields for carnotite and other uranium and vanadium solid phases, and indicate the conditions

necessary for vanadium and uranium solubility. One set of conditions was found to indicate solubility in a mildly reducing, neutral to alkaline environment containing fairly abundant CO_2 , and thus is comparable with some natural ground waters.

3. Analysis of solubility controls indicates that increasing CO_2 increases solubility. Oxidizing conditions cause carnotite to precipitate from solution while more reducing conditions cause montroseite and uraninite to form.

4. The possible effects of other ionic species commonly found in natural ground waters were investigated within the Eh-pH framework of aqueous transport in the U-V-K-O₂-H₂O-CO₂ system. No significant changes in such transport were found. Sodium and, to a lesser degree, calcium and magnesium can balance electrostatically the concentrations of HCO_3^- , CO_3^{2-} , and other anions in solution. Activity gradients showing varying transportation conditions were presented.

5. In the presence of excess quartz the field of coffinite stability is probably very similar to that of uraninite. With favorable conditions (moderate concentration of its constituent elements) the field of formation of roscoelite should approximate that of montroseite.

6. Carnotite stability is very sensitive to changes in ionic activity rather than changes in Eh and pH (except for distinctly reducing conditions); its precipitation is critically controlled by the amounts of uranium, vanadium and CO_2 in solution. The reducing environment provided by ore-solution migration into carbonaceous and/or H_2S rich areas was shown to be sufficient to precipitate uraninite and montroseite from dilute solutions at 25° C. Temperatures above 120° C might be sufficient to precipitate uraninite from the postulated ore-bearing solutions because of the breakdown of the uranyl carbonate complexes. Sulfides, carbonaceous material and trivalent vanadium minerals would not be expected to occur with uraninite formed in this way. The lack of such ore is interpreted as supporting evidence for a depositional temperature of 120° C or less.

ACKNOWLEDGMENTS

We are grateful to our colleagues of the U. S. Geological Survey, Alice D. Weeks, Paul B. Barton, Richard P. Fischer, and especially Charles L. Christ, for stimulating criticism and helpful suggestions concerning much of the material of this study. Theodore Botinelly, Lawrence C. Craig, John C. Hathaway, and J. J. Hemley of the U. S. Geological Survey, and Clifford Frondel of Harvard University, also contributed many ideas during discussions of the problems presented here, and to them we extend our thanks.

U. S. GEOLOGICAL SURVEY,
DENVER, COLORADO
AND
LABORATORY OF MINING GEOLOGY,
HARVARD UNIVERSITY,
CAMBRIDGE, MASSACHUSETTS

APPENDIX

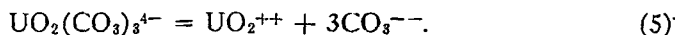
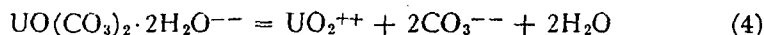
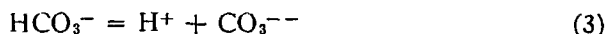
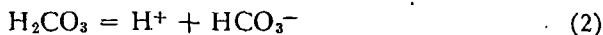
This Appendix was prepared for those readers who desire the details of construction of the Eh-pH diagrams here presented. An introduction to the methods of Eh-pH diagramming, based on the use of free-energy data to calculate equilibrium constants, is given by Pourbaix (31). All free-energy values used in our calculations have been taken from Latimer (28) except as noted below. The values for uraninite and schoepite are from Deltombe et al. (13), while those for rutherfordine and the uranyl carbonate complexes are from Bullwinkel's data (9) corrected for the recent ΔF°_f of schoepite given by Deltombe et al. A value for H_2VO_4^- was calculated from the published equilibrium constants of Gayer and Leider (24). Bjerrum et al. (4) tabulate six fairly consistent constants for the dissociation of $\text{UO}_2(\text{OH})^+$ at 25° C. We averaged these and so obtained a ΔF°_f of $\text{UO}_2(\text{OH})^+$ at 25° C. The value for carnotite was derived in the text. Free-energy values for the vanadium oxides are taken from Evans and Garrels (14), while that of H_2VO_4^- is from Deltombe et al. (12). All free-energy values pertinent to the construction of the diagrams presented in this paper are listed in Table 1.

TABLE 1
FREE-ENERGY VALUES FROM THE ELEMENTS, AT 25° C AND 1
ATMOSPHERE TOTAL PRESSURE

Aqueous species	ΔF°_f (Kcal)	Solid phases	ΔF°_f (Kcal)
H_2O	- 56.69	UO_2	- 246.6
H^+	0.0	$\text{UO}_2(\text{OH})_2 \cdot \text{H}_2\text{O}$	- 398.8
OH^-	- 37.6	UO_2CO_3	- 385.0
$\text{H}_2\text{CO}_3^\circ$	-149.00	V_2O_3	- 271.0
HCO_3^-	-140.31	V_2O_4	- 381.0
CO_3^{--}	-126.22	V_2O_5	- 344.0
K^+	- 67.46	$\text{K}_2(\text{UO}_2)_2\text{V}_2\text{O}_8 \cdot 3\text{H}_2\text{O}$	-1,294.0
H_2VO_4^-	-248.8		
UO_2^{++}	-236.4		
U^{+4}	-138.4		
$\text{U}(\text{OH})^{+3}$	-193.5		
$\text{UO}_2(\text{OH})^+$	-287.4		
H_2VO_4^-	-317.6		
$\text{UO}_2(\text{CO}_3)_2 \cdot 2\text{H}_2\text{O}^{--}$	-630.0		
$\text{UO}_2(\text{CO}_3)_3^{4-}$	-648.0		

U-O₂-H₂O-PCO₂ DIAGRAMS

The following equations are pertinent:



The thermodynamic equilibrium constants for reactions (1)–(5) are as follows:

$$\frac{H_2CO_3}{P_{CO_2}} = 10^{-1.47} \quad (6)$$

$$\frac{(HCO_3^-)(H^+)}{H_2CO_3} = 10^{-6.38} \quad (7)$$

$$\frac{(CO_3^{--})(H^+)}{HCO_3^-} = 10^{-10.31} \quad (8)$$

$$\frac{(UO_2^{++})(CO_3^{--})^2}{UO_2(CO_3)_2 \cdot 2H_2O^{--}} = 10^{-20.4} \quad (9)$$

$$\frac{(UO_2^{++})(CO_3^{--})^3}{UO_2(CO_3)_3^{4-}} = 10^{-24.2} \quad (10)$$

For a fixed P_{CO_2} , H_2CO_3 is calculated from (6). For a given pH value CO_3^{--} can be calculated from equations (7) and (8). Next, all ions containing uranium are considered to be in equilibrium with schoepite.



or,

$$K_a = \frac{UO_2^{++}}{(H^+)^2} \quad (12)$$

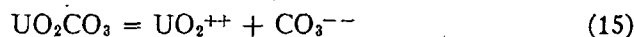
Hence, UO_2^{++} can be calculated from stipulated pH values by (12). Lastly, activities for the uranyl carbonate complexes can be derived from equations (9) and (10) with the aid of CO_3^{--} and UO_2^{++} values calculated above.

If P_{CO_2} is high enough, rutherfordine (UO_2CO_3) is the stable hexavalent uranium solid phase rather than schoepite.



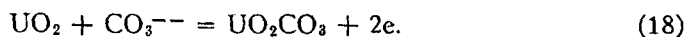
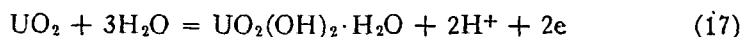
$$K_a = \frac{1}{P_{CO_2}} \quad (14)$$

When P_{CO_2} is $10^{-3.8}$ the two solid phases rutherfordine and schoepite are in equilibrium. For P_{CO_2} values higher than this, UO_2^{++} must be determined from CO_3^{--} values (above) as follows:



$$(UO_2^{++})(CO_3^{--}) = 10^{-16.4} \quad (16)$$

For reducing conditions uraninite becomes the stable solid phase.



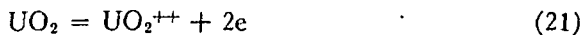
details of
production to
energy data to
free-energy
except as
Deltombe
complexes
schoepite given
published
(4) tabu-
(OH)⁺ at
25° C.
for the
that of
ment to
Table 1.

Employing the Nernst equation for equations (17) and (18):

$$E_h = E^\circ + \frac{0.06}{2} \log (H^+)^2 \quad (19)$$

$$E_h = E^\circ + \frac{0.06}{2} \log \frac{1}{(CO_3^{--})} \quad (20)$$

E° for each reaction is evaluated from free-energy data. Depending on the P_{CO_2} value under consideration, either (19) or (20) is chosen. If P_{CO_2} is less than $10^{-3.8}$ the Eh-pH boundary between uraninite and schoepite is found by substituting pH values in (19). For P_{CO_2} greater than $10^{-3.8}$ the rutherfordine-uraninite boundary is established by substituting the CO_3^{--} values derived from equations (7) and (8) in equation (20). In each case the solid-solid boundary has a linear slope of 60 mv/pH unit. In the UO_2 field then:



$$E_h = E^\circ + \frac{0.06}{2} \log (UO_2^{++}). \quad (22)$$

UO_2^{++} is calculated from (22) for arbitrary Eh values (UO_2^{++} is not pH dependent in the UO_2 field as expressed in (21)). UCD and UTC activities are then calculated as before; these ion activities are now both Eh and pH dependent.

U-O₂-H₂O-Σ CO₂ DIAGRAMS

Equation (1) is no longer applicable since P_{CO_2} is variable. Equations (2)-(5) and, hence, (7)-(10) are used, but note that now, after selecting arbitrary pH values, CO_3^{--} cannot be solved from equations (7) and (8) because there are three unknowns. Since Σ CO₂ is fixed, the following expression is used.

$$\Sigma CO_2 = H_2CO_3 + HCO_3^- + CO_3^{--} + 2UO_2(CO_3)_2 \cdot 2H_2O^{--} + 3UO_2(CO_3)_3^{4-} \quad (23)$$

Rewrite equations (7)-(10) so that ionic activity sought is a function of UO_2^{++} and CO_3^{--} :

$$HCO_3^- = \frac{(CO_3^{--})(H^+)}{10^{-10.31}} \quad (24)$$

$$H_2CO_3 = \frac{(HCO_3^-)(H^+)}{10^{-6.38}} = \frac{(CO_3^{--})(H^+)^2}{10^{-16.69}} \quad (25)$$

$$UO_2(CO_3)_2 \cdot 2H_2O^{--} = \frac{(UO_2^{++})(CO_3^{--})^2}{10^{-20.4}} \quad (26)$$

$$UO_2(CO_3)_3^{4-} = \frac{(UO_2^{++})(CO_3^{--})^3}{10^{-24.2}} \quad (27)$$

If $\text{UO}_2(\text{OH})_2 \cdot \text{H}_2\text{O}$ is the stable solid phase, UO_2^{++} is fixed for arbitrary pH values. Equations (24)–(27) are substituted in equation (23) which is solved for CO_3^{--} using the desired ΣCO_2 value. Equation (23) is best solved by approximation as it is a third-order equation. Remaining ion activities are then determined using (24)–(27).

Equation (16) is used to determine the $\text{UO}_2\text{CO}_3 - \text{UO}_2(\text{OH})_2 \cdot \text{H}_2\text{O}$ boundary.

$$\text{UO}_2^{++} = \frac{10^{-16.4}}{\text{CO}_3^{--}} \quad (16)$$

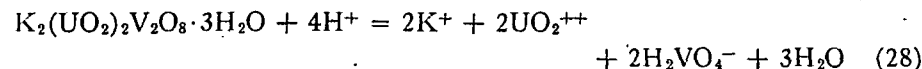
Substitute this expression for UO_2^{++} in equations (26) and (27). As above, substitute (24)–(27) in equation (23) and solve for CO_3^{--} . Finally, use this CO_3^{--} value to determine UO_2^{++} in equilibrium with rutherfordine from (16). If this value for UO_2^{++} is less than UO_2^{++} in equilibrium with schoepite for a given pH then UO_2CO_3 is the stable solid. The boundary between the two phases (UO_2^{++} values in equilibrium with each are identical) is dependent on both ΣCO_2 and pH, but not on Eh.

The rutherfordine-uraninite and uraninite-schoepite bounding equations have been given ((17)–(20)). The uraninite-schoepite boundary is not dependent on CO_2 . Use the CO_3^{--} values obtained from (23) and (16) for establishing the uraninite-rutherfordine boundary.

Ionic activities in equilibrium with UO_2 are cumbersome to determine when ΣCO_2 is fixed. UO_2^{++} values for (26) and (27) are derived from (22) for arbitrary Eh values. Substituting (26) and (27) in (23) indicates that CO_3^{--} is both pH and Eh dependent. Activities for each ion must be calculated on a point-by-point basis in the field of stability of uraninite.

U-V-K-O₂-H₂O-CO₂ DIAGRAMS

Carnotite stability must be considered in relation to both uranium and vanadium solid phases.

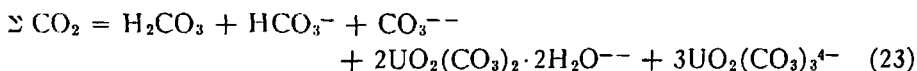


$$\frac{(\text{K}^+)^2(\text{UO}_2^{++})^2(\text{H}_2\text{VO}_4^-)^2}{(\text{H}^+)^4} = 10^{-13.7} \quad (29)$$

For any Eh-pH value, the activity of H_2VO_4^- is taken from Figure 11 (see text). $\text{K}^+ = 10^{-3}$, and UO_2^{++} values are taken from the results of calculations for the U-O₂-H₂O- ΣCO_2 diagrams. When these values, for the particular Eh and pH in question, are inserted in the left-hand side of equation (29), carnotite is the stable solid if the value of the left-hand side of the equation exceeds $10^{-13.7}$. Carnotite is not stable relative to the other uranium and vanadium solids if the left-hand side of (29) is less than $10^{-13.7}$. Equation (29) is thus used as a criterion for determining at specified Eh and pH conditions, whether carnotite is or is not stable relative to the combination of the stable uranium oxide (or carbonate) plus the stable vanadium

oxide plus potassium hydroxide. The solid-solid boundaries for Figures 12-14 are drawn for those Eh-pH conditions where the left-hand side of (29) is equal to $10^{-13.7}$.

Keeping ΣCO_2 constant, equations (23)-(27) remain applicable:



$$\text{HCO}_3^- = \frac{(\text{CO}_3^{--})(\text{H}^+)}{10^{-10.31}} \quad (24)$$

$$\text{H}_2\text{CO}_3 = \frac{(\text{CO}_3^{--})(\text{H}^+)^2}{10^{-16.69}} \quad (25)$$

$$\text{UO}_2(\text{CO}_3)_2 \cdot 2\text{H}_2\text{O}^{--} = \frac{(\text{UO}_2^{++})(\text{CO}_3^{--})^2}{10^{-20.4}} \quad (26)$$

$$\text{UO}_2(\text{CO}_3)_3^{4-} = \frac{(\text{UO}_2^{++})(\text{CO}_3^{--})^3}{10^{-24.2}} \quad (27)$$

Rearranging equation (29):

$$\text{UO}_2^{++} = \left[\frac{(10^{-13.7})(\text{H}^+)^4}{(\text{K}^+)^2(\text{H}_2\text{VO}_4^-)^2} \right]^{1/3} \quad (30)$$

UO_2^{++} values from equation (30) are substituted in (26) and (27), and ion activities in equilibrium with carnotite are determined in the manner described above.

REFERENCES

1. Ahrland, S., 1951, The complex chemistry of the uranyl ion. VI. The complexity of uranyl chloride, bromide, and nitrate: *Acta Chem. Scand.*, v. 5, p. 1271-1282.
2. —, and Larssen, R., 1954, The complexity of uranium (IV) chloride, bromide, and thiocyanate: *Acta Chem. Scand.*, v. 8, p. 137-150.
3. Barton, P. B., Jr., 1958, Synthesis and properties of carnotite and its alkali analogues: *Am. Mineralogist*, v. 43, p. 799-817.
4. Bjerrum, J., Schwarzenbach, G., and Sillén, L. G., 1958, Stability constants, Part II: *Inorganic Ligands: Spec. Pub. No. 7, The Chemical Society, London.*
5. Blake, C. A., Coleman, C. F., Brown, K. B., Hill, D. G., Lowrie, R. S., and Schmitt, J. M., 1956, Studies in the carbonate-uranium system: *Jour. Am. Chem. Soc.*, v. 78, p. 5978-5983.
6. Botinelly, T., and Fischer, R. P., 1959, Mineralogy and geology of the Rifle and Garfield Mines, Garfield County, Colorado: *U. S. Geol. Survey Prof. Paper 320, Pt. 19, p. 213-218.*
7. Breger, I. A., and Chandler, J. C., 1960, Extractability of humic acid from coalified logs as a guide to temperatures in Colorado Plateau sediments: *ECON. GEOL.*, v. 55, p. 1039-1047.
8. Brooker, E. J., and Nuffield, E. W., 1952, Studies of radioactive compounds: IV, pitchblende from Lake Athabaska, Canada: *Am. Mineralogist*, v. 37, p. 363-385.
9. Bullwinkel, E. P., 1954, The chemistry of uranium in carbonate solutions: Topical Report RMO-2614, The Merrill Co., San Francisco.
10. Christ, C. L., and Clark, J. R., 1960, Crystal chemical studies of some uranyl oxide hydrates: *Am. Mineralogist*, v. 45, p. 1026-1061.
11. Coleman, R. G., 1957, Mineralogical evidence on the temperature of formation of the Colorado Plateau uranium deposits: *ECON. GEOL.*, v. 52, p. 1-4.
12. Deltombe, E., de Zoubov, N., and Pourbaix, M., 1956, Comportement électrochimique du vanadium: Rapport Technique No. 29, Centre Belge d'Etude de la Corrosion.

boundaries for Figures
left-hand side of (29)

is applicable:

$3\text{UO}_2(\text{CO}_3)_3^{4-}$ (23)

(24)

(25)

$\text{---})^2$ (26)

(27)

(30)

(5) and (27), and ioned
in the manner

The complexity of uranyl
71-1282.

chloride, bromide, and thio-
and its alkali analogues:

stability constants, Part II:
London.

Latimer, W. M., and Schmitt, J. M.,
Chem. Soc., v. 78, p.

of the Rifle and Garfield
Paper 320, Pt. 19, p.

acid from coalified logs
ECON. GEOL., v. 55, p

compounds: IV, pitch-
p. 363-385.

solutions: Topical Report

of some uranyl oxide

rate of formation of the
4.

Comportement électrochimique du
la Corrosion.

13. —, 1956, Comportement électrochimique de l'uranium: Rapport Technique No. 31, Centre Belge d'Étude de la Corrosion.
14. Evans, H. T., Jr., and Garrels, R. M., 1958, Thermodynamic equilibria of vanadium in aqueous systems as applied to the interpretation of the Colorado Plateau ore deposits: *Geochim. et Cosmochim. Acta*, v. 15, p. 131-149.
15. Foster, M. D., 1959, Chemical study of the mineralized clays: U. S. Geol. Survey Prof. Paper 320, Pt. 10, p. 121-132.
16. Frondel, C., 1958, Systematic mineralogy of uranium and thorium: U. S. Geol. Survey Bull. 1064.
17. Garrels, R. M., 1953, Some thermodynamic relations among the vanadium oxides and their relation to the oxidation state of the vanadium ores of the Colorado Plateaus: *Am. Mineralogist*, v. 38, p. 1251-1265.
18. Garrels, R. M., 1955, Geochemistry of oxidation of the uranium deposits of the Colorado Plateau: preprint 250, Nuclear Engineering and Science Congress, published by Am. Inst. Chem. Engineers, New York.
19. —, 1955, Some thermodynamic relations among the uranium oxides and their relation to the oxidation states of the uranium ores of the Colorado Plateaus: *Am. Mineralogist*, v. 40, p. 1004-1021.
20. —, 1957, Some free-energy values from geologic relations: *Am. Mineralogist*, v. 42, p. 780-791.
21. —, and Christ, C. L., 1954, Behavior of Colorado Plateau uranium minerals during oxidation: U. S. Geol. Survey Prof. Paper 320, Pt. 6, p. 81-89.
22. —, and Naeser, C. R., 1958, Equilibrium distribution of dissolved sulfur species in water at 25° C and 1 atm. total pressure: *Geochim. et Cosmochim. Acta*, v. 15, p. 113-130.
23. —, Larsen, E. S., 3rd, Pommer, A. M., and Coleman, R. G., 1959, Detailed chemical and mineralogical relations in two vanadium-uranium ores: U. S. Geol. Survey Prof. Paper 320, Pt. 15, p. 165-184.
24. Gayer, K. H., and Leider, H., 1955, The solubility of uranium trioxide, $\text{UO}_3 \cdot \text{H}_2\text{O}$, in solutions of sodium hydroxide and perchloric acid at 25° C: *Jour. Am. Chem. Soc.*, v. 77, p. 1448-1450.
25. Hathaway, J. C., 1959, Mixed-layered structures in vanadium clays: U. S. Geol. Survey Prof. Paper 320, Pt. 11, p. 133-138.
26. Jensen, M. L., 1958, Sulfur isotopes and the origin of the sandstone-type uranium deposits: *ECON. GEOL.*, v. 53, p. 598-616.
27. Kerr, P. F., 1958, Criteria of hydrothermal emplacement in Plateau uranium strata: *Proc. of the Second U. N. Int. Conf. on the Peaceful Uses of Atomic Energy*, v. 2, p. 330-334.
28. Latimer, W. M., 1952, Oxidation potentials: 2nd edit., Prentice-Hall Inc., New York.
29. Miller, L. J., 1958, The chemical environment of pitchblende: *ECON. GEOL.*, v. 53, p. 521-545.
30. Miller, S. D., and Kulp, J. L., 1958, Isotopic study of some Colorado Plateau ores: *ECON. GEOL.*, v. 53, p. 937-948.
31. Pourbaix, M., 1949, Thermodynamics of dilute aqueous solutions: Edward Arnold and Co., London.
32. Rafalsky, R. P., 1958, The experimental investigation of the conditions of uranium transport and deposition by hydrothermal solutions: *Proc. of the Second U. N. Int. Conf. on the Peaceful Uses of Atomic Energy*, v. 2, p. 432-444.
33. Roach, C. H., and Thompson, M. E., 1959, Sedimentary structures and localization and oxidation of ore at the Peanut Mine, Montrose County, Colorado: U. S. Geol. Survey Prof. Paper 320, Pt. 17, p. 197-202.
34. Stieff, L. R., Stern, T. W., and Milkey, R. G., 1953, A preliminary determination of the age of some uranium ores of the Colorado Plateau by the lead-uranium method: U. S. Geol. Survey Circ. 271.
35. Stieff, L. R., and Stern, T. W., 1959, Isotopic study of some Colorado Plateau ores: *ECON. GEOL.*, v. 54, p. 752.
36. Waters, A. C., and Granger, H. C., 1953, Volcanic debris in uraniumiferous sandstones and its possible bearing on the origin and precipitation of uranium: U. S. Geol. Survey Circ. 224.
37. Weeks, A. D., 1955, Mineralogy and oxidation of the Colorado Plateau uranium ores: U. S. Geol. Survey Prof. Paper 300, p. 187-193.
38. —, and Thompson, M. E., 1954, Identification and occurrence of uranium and vanadium minerals from the Colorado Plateaus: U. S. Geol. Survey Bull. 1009-B, p. 13-62.
39. —, Coleman, R. G., and Thompson, M. E., 1959, Geochemistry and mineralogy of the Colorado Plateau uranium ores; summary of the ore mineralogy: U. S. Geol. Survey Prof. Paper 320, Pt. 5, p. 65-79.

TWO-STAGE COUNTERFLOW LEACHING OF COPPER-NICKEL BESSEMER MATTE

UDC 669.243:541.135.6

L. A. Sinev and V. F. Borbat

Separation of copper and nickel is becoming more urgent because of expanding metal production based upon copper-nickel sulfide ore processing. This work gives research results on selective leaching of Ni from Bessemer matte at atmospheric pressure in sulfate-chloride solutions.

Leaching was conducted of Bessemer matte samples containing (%): 47.37 Ni, 34.04 Cu, 0.82 Co, 2.96 Fe, and 21.89 S. For subsequent processing the copper should be kept entirely in the residue from leaching, but the Ni and Co should pass into the solution. Direct current application in the leaching process (electroleaching) was tested for this purpose, the optimum process characteristics being $t = 90^{\circ}\text{C}$, liq:sol ratio (3.5-4.0):1, $\tau = 80$ min, $\varphi_a = +0.5$ V, $[\text{H}_2\text{SO}_4]_{\text{in}} = 190$ g/lit, and $[\text{HCl}]_{\text{in}} = 80$ g/lit. Graphite impregnated with naphthalene was used as the insoluble anode; the cathode material can be titanium, stainless steel, or copper. Fig. 1 shows the kinetics of the electroleaching process.

The copper sulfide concentrate contains 72% Cu and 0.5% Ni. Calculation of the rational composition and x-ray structural analysis showed copper present as chalcocite and covellite. Ni and Co extraction into solution in this operation is 98-99%; the solution Cu content does not exceed 0.2-0.3 g/lit. The solution contains (g/lit): 50-60 Ni, 2.2-2.6 Co, and 6-8 Fe. Part of the sulfur which is combined with nickel in the initial Bessemer matte passes into the residue as part of the redeposited covellite, the remainder being eliminated as hydrogen sulfide. The platinum group metals are almost entirely in the sulfide residue.

Electroleaching yields high-grade copper concentrate. However, solutions from this operation contain up to 2.3 g-eq/lit of free acid and are not suitable for subsequent processing. To obtain the minimum free acid in these solutions, research was conducted to develop a schedule for leaching fresh Bessemer matte with acid nickelferous solution. The process of leaching nickel sulfide with a solution containing (g/lit): 50 Ni^{2+} , 70 Cl^- , and 98 SO_4^{2-} with a high rate of mixing and blowing the pulp with air is characterized by very rapid consumption of free acid. After 1.5 hours of leaching, the final solution acidity is 0.15 g-eq/lit and the copper content doesn't exceed 30 mg/lit; the nickel concentration is 100-120 g/lit.

A two-stage counterflow leaching scheme for Bessemer matte (Fig. 2) was proposed on the basis of the research. The end products are a high-grade copper sulfide concentrate in which the platinum group metals are concentrated and a slightly acid nickel-cobalt solution containing 6-8 g/lit Fe and no more than 0.02-0.03 g/lit Cu. Both leaching operations are conducted at 90°C and at atmospheric pressure. There are no platinum metals in the solution, because the solution is saturated with hydrogen sulfide in both operations. According to preliminary data, leaching time in each of the two operations is assessed at 1.5 hr.

Technical and economic evaluation of the scheme in the version with nickel solution evaporation, nickel sulfate calcining to the lower oxide, and reduction of the oxide to nickel powder by the State Nickel Industry Research and Design Institute showed that expenditure on production of a ton of commercial nickel was 400 rubles less than in the existing technology.

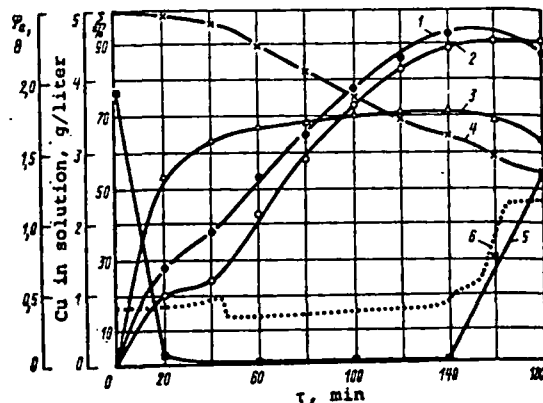


Fig. 1. Electroleaching kinetics of Bessemer matte in sulfate-chloride solutions:

1-3 - extraction (ϵ) of Ni, Co, and Fe into solutions, respectively; 4 - residual acidity K; 5 - solution Cu content; 6 - φ_a .

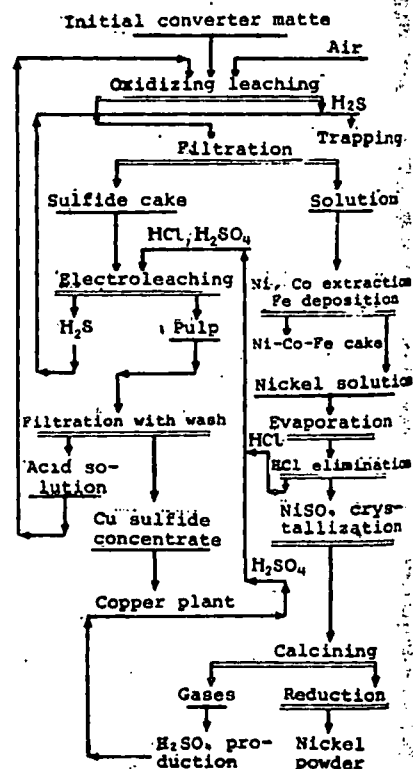


Fig. 2. Proposed flowsheet for Bessemer matte processing.

TESTING A SOLVENT-EXTRACTION METHOD FOR PRODUCING COPPER AND NICKEL SULFATES

UDC 669.334.9:66.061.5

Kh. I. Baikenov, A. V. Stryapkov, S. E. Dyusembaeva, L. S. Borodina,
and E. A. Simkin

Copper and nickel were separated by solvent extraction from copper production solutions with naphthenic acids in an installation containing two two-stage counterflow extractors of mixer-settler type in the copper (nickel) extraction stage, one two-stage extractor of the same type in the metals re-extraction stage, a system of tanks, a crystallizer, a Nutsch filter, rotameters, and pumps. The technology was perfected with sulfate production solutions containing, g/liter: 50 - 60 Cu, 30 - 40 Ni, 10 - 15 As, 0.5 - 1.0 Fe, and up to 80 - 100 H₂SO₄. To improve subsequent filtration, the solutions were diluted prior to solvent extraction to a basic constituents content of ~ 20 g/liter and neutralized with dry soda to pH 4.0 - 4.2. The arsenic-iron cake was removed and the filtrate was treated as initial solution and used for extraction of metals.

It was established in the course of the tests that the best results were achieved by using a counterflow process.

A 1M solution of distilled naphthenic acids in kerosene was used as the extractant. The filtrate was fed into the first mixing chamber and the extractant into the fourth. The capacity of the apparatus reached 120 liters/hr in terms of total phases, and the O:A ratio was 1.5:1. A 6% solution of soda was fed into each mixing chamber in the extractors in order to maintain pH 4.5 - 4.8 in stages I - II (5 - 25 liters/hr) and pH 4.8 - 5.0 (0 - 5 liters/hr) in stages III - IV. When the process is operated in this way the raffinate contains < 0.01 g/liter Cu. Nickel was extracted in a similar way, the ratio of the phase flows reaching O:A (0.5 - 1):1. Copper and nickel were re-extracted with 7% sulfuric acid solution at an O:A ratio of (10 - 12):1. The copper re-extract, containing 80 - 100 g/liter Cu, was evaporated and allowed to crystallize to produce copper sulfate in accordance with State Standards for products of the highest grades (A). The nickel re-extract, containing 80 - 100 g/liter Ni and < 0.1 g/liter Cu, was treated by cementation with nickel powder, evaporated, and allowed to crystallize to produce nickel sulfate. The organic phase was washed with one volume of water and returned to the extraction process.

All the discharged solutions which had been in contact with the organic were acidified and allowed to settle in a tank, after which they were in accordance with the requirements of maximum permissible concentrations for dissolved organic.

SUBJ
MING
TSEM

In col
of Physi
an autoc
bufferin
Concentr
selectiv
of extra
The pr
powder f
5.6 Fe²⁺
Si⁴⁺ (ea
In the
surface
to reduc
feeding
absorption
over, a
temerat
: 150°
treased
and de-w
0.07 g/
the wall
As a r
however,
average
solid
It was
upper c
10-40 mi
Experi
0.7 Cu
0.75 g/l
the depo
40°C, I
Kineti
eters u
Table 1
precipitate
the bulk
with a r
these pa
surface
to 30 at
Grindi
density
this is
the) tha
Apparent
structur
Data o
separati

Taking
chemical

THE SCIENCE OF BLASTING

UNIVERSITY OF UTAH
RESEARCH INSTITUTE
EARTH SCIENCE LAB.

Reprinted from:

Proceedings of the Fifth Conference on
Explosives and Blasting Technique

Society of Explosives Engineers
Annual Meeting, St. Louis, Missouri
February 7-9, 1979

by

Stephen R. Winzer, Victor I. Montenyohl,
and Andrew Ritter

Martin Marietta Laboratories
1450 South Rolling Road
Baltimore, Maryland 21227

THE SCIENCE OF BLASTING

Reprinted From:

Proceedings of the Fifth Conference on
Explosives and Blasting Technique

Society of Explosives Engineers
Annual Meeting
St. Louis, Missouri

February 7-9, 1979

by

Stephen R. Winzer, Victor I. Montenyohl, and Andrew Ritter

Martin Marietta Laboratories
1450 South Rolling Road
Baltimore, Maryland 21227

A narrated, 27-minute, 16-mm motion picture covering the topics discussed in this paper is available from Martin Marietta Laboratories.

THE SCIENCE OF BLASTING

by

Stephen R. Winzer, Victor I. Montenyohl and Andrew Ritter
of Martin Marietta Laboratories
Baltimore, Maryland

ABSTRACT

Thirty-seven open pit production blasting operations have been monitored using high-speed cameras running between 500 and 7000 frames per second. Analysis of the resulting films reveals irregularities in timing including sequencing errors and crowding (holes firing less than 8 ms apart), confirming results of laboratory testing of ms delay blasting caps (Winzer, 1978). Where blasting parameters are otherwise constant and within recommended guidelines (stemming, spacing, burden, etc.), timing problems dominate the overall performance of the blasting operation. Model tests in layered Homalite 100, designed to simulate joint or bedding planes in rock, indicate the importance of the stress waves generated by the explosive in developing the crack network which is ultimately responsible for the fragmentation seen in the resulting muckpile. These mechanisms are strongly supported by high-speed film studies at Pinesburg, Maryland. Experiments in controlling relief in deep shots (where depth approaches the lateral extent of the bench blasted) using borehole geometry and hybrid initiation systems (electronic timer and pyrotechnic delays) were carried out. The results suggest that the 1 ms/ft. of burden guideline developed by Bergmann *et al.*, 1974 is too short, and that much longer times are necessary to optimize fragmentation and muck digability. Longer times are found to reduce noise, vibration, and flyrock.

INTRODUCTION

Much has been written over the years on blasting problems. These works range from "how to" articles in trade journals, through engineering studies carried out at specific sites to address specific problems, to basic research carried out in the laboratory. The principle difficulty with many of these studies has been the often tenuous relationship between laboratory studies seeking to understand the Illustrations and figures at end of paper.

fundamental mechanism of fragmentation or relationships between burden and spacing or timing, and use of the results of these efforts in field situations. Understanding the different parts of the development of a production blast is severely hampered by the speed at which the event takes place. Because of these difficulties, most attempts to study the operation at production scales rely on qualitative or semi-quantitative evaluation of the resulting muck. Not only are such evaluations difficult to carry out, but they do not allow separation of the components of a blast (timing, pattern, delay sequence, explosive, etc.) in order to identify the principal contributions of each to overall performance.

During the past three years, we have developed a system for high-speed cinematographic monitoring of production blasting operations. Use of high-speed cinematography for recording blasting operations is not new; some work has been done as far back as the early 1950's (Blunt, 1953; Patterson and Forsyth, 1956; Frantti, 1958; Blair, 1960). However, its systematic use as a research tool and as a tool for evaluation of production operations has been restricted. During the past three years, we have monitored thirty-seven production quarry blasting operations, using a variety of patterns, initiators, and explosives, in sedimentary, crystalline igneous, and metamorphic rocks. The analysis of these motion pictures, taken at framing rates of 500-7000 per second, coupled with laboratory studies in flawed transparent polymers and rock carried out by researchers at the University of Maryland as part of a joint NSF sponsored research project, reveal several important factors which affect overall performance of the blasting operation. Of these, the most important are timing, fragmentation mechanisms, relief, and structural control. This paper will discuss the evidence generated by our high-speed cinematographic studies as it bears on the above factors.

TIMING: KEY TO CONTROLLED BLASTING

The importance of delay initiation of borehole detonations in a bench blasting operation has been recognized since the introduction of ms delay initiators in the mid 1940's. In the 1950's, high-speed cinematography had recorded considerable variation in firing times of non-electric relay connectors (Frantti, 1958). Since that time, a number of discussions of optimum timing have appeared in the literature (Cf. Bergmann *et al.*, 1974; Hagan, 1977). Discussions such as Bergmann's stemmed from tests of single rows of small-diameter blastholes drilled in large blocks of stone. Timing was achieved by using measured lengths of detonating cord which gave instantaneous detonation of the borehole column. From this work, Bergmann *et al.*, 1974, concluded that a delay interval equal to or somewhat greater than 1 ms/ft. of burden would provide optimum fragmentation. Approaches such as that of Hagan, 1977, and Andrews, 1975, used data like that developed by Bergmann *et al.*, 1974, and empirical testing of different delay sequences in the field to develop general patterns and approaches to timing of production blasts. There are two problems with these approaches. First, Bergmann's approach neglects mass effects from multiple row shooting (the effective burden tends to increase as the shot progresses rearward from the free face), and it does not deal with the fragmentation mechanisms operating during a production blast (the effects of joints, bedding planes and the like on the development of the crack pattern). Second, empirical approaches such as those of Hagan, 1977, and Andrews, 1975, do not include a method of evaluating the actual times at which the holes in their patterns fire.

One of the first results of our high-speed monitoring of production shooting was the discovery that considerable irregularity existed in the firing times of the boreholes in the various patterns that we monitored. These irregularities manifested themselves as deviations from the nominal firing times up to and including actual reversals in the firing of initiators one or more periods removed

the overall performance of the shot. But on other occasions where this pattern was used, as much as 1/3 of the shot contained oversize pieces and proved hard to dig, due to sequencing and crowding errors in the higher period caps.

Another example of the problems caused by timing errors is given in Fig. 4. This series of photographs, part of a high-speed film running at about 3000 frames/sec, shows the effect of combined cap error and error in a mechanical sequential blasting machine. Fig. 5a-c gives the drill pattern and the delay pattern achieved by using a combination of period 6-14 DuPont caps and a Trojan type C timer set to fire at 10 ms intervals. The pattern, a 6 1/2' x 13' staggered, using 3" holes on a 34' bench, is designed to develop as a flat V. The timing, even for the nominal firing times, is somewhat irregular. The high-speed film sequence clearly shows several holes which fire early and are, thus, unrelieved. The net result of this timing irregularity is flyrock, with concomitant noise and vibration. Noise from shots such as these produces complaints, and the firing of unrelieved holes can be expected to produce increased ground vibrations. In virtually all such cases, the unrelieved holes produce flyrock, some of which can travel for hundreds or even thousands of feet.

In summary, then, accurate timing must be considered imperative in producing consistent blasting results and in reducing noise, vibration, flyrock, backbreak, and poor fragmentation. In the overwhelming majority of cases that we have studied in detail (37 production shots), poor performance can be directly related to timing problems. Timing problems tend to overwhelm other blasting parameters; however, some evidence pertaining to other important factors in designing successful blasting patterns can be derived from the high-speed work.

FRAGMENTATION MECHANISMS AND STRUCTURAL CONTROL

Rock is a heterogeneous medium, a fact often ignored in blasting practice. All rocks contain a variety of visible discontinuities and flaws, including mappable features such as joints, bedding planes, faults, and the like. In addition to these, any other contrast in density will contribute to initiation and propagation of cracks. Such contrasts include boundaries between dissimilar grains (i.e., quartz-feldspar), boundaries between similar or identical minerals with different crystallographic orientations, filled cracks, recemented bedding planes, etc. Early studies of rocks subjected to meteorite impact reveal shock and stress-wave damage associated with all of the above factors (Dence, 1978; Kieffer, 1971, 1975; Ahrens and Rosenberg, 1968; French and Short, 1968).

General discussions of rock fragmentation by explosives have concentrated on the development of a radial borehole crack network, pressurized by gases emanating from the borehole (Cf. Langefors and Kihlstrom, 1963; Ash, 1973; Porter and Fairhurst, 1971; Kutter and Fairhurst, 1971). Reflected stress waves have been considered to be a minor contributor to the overall blasting process. Although the contribution to overall breakage by large-scale discontinuities is acknowledged (Cf. Ash, 1973), most fragmentation models proceed from experiments carried out in homogeneous polymers like Plexiglass or Homalite 100.

It has been shown by Dally *et al.*, 1975, that in homogeneous Homalite 100 and Plexiglass models the cracks are formed radial to the borehole, and that only up to 12 cracks propagate any distance from the borehole. Reasoning from such observations and applying them literally to field practice, one might expect to find generally large pie-shaped fragments in a muckpile following a production blast. As examination of muckpiles from production blasting reveals, such pie-shaped fragments are rare or absent. Ash, 1973, gets around this problem by introducing a theory of flexural beam bending, wherein the rock mass is handled as a beam

anchored at collar and toe. This rock beam bends outward in response to expanding borehole gases and fails along its length in tension.

New work in Homalite models with induced flaws, joints, and bedding planes simulating those found in rock bear on the problem of fundamental fragmentation mechanisms (Dally and Fourney, 1977; Barker and Fourney, 1978; Fourney *et al.*, in prep). Their work indicates that the importance of the stress wave has been severely underestimated. In essence, explosively loaded flawed Homalite models induce crack propagation by interaction of the stress waves with the flaws induced into the model. Initial tests, with small flaws routed in the surface of the Homalite models, resulted in considerable enhancement of fragmentation at the same explosive loading (Dally and Fourney, 1977). Later work indicates that stress waves reflected or refracted from layered media induce cracks to propagate at the layer interface (Fourney *et al.*, in prep).

In both cases, two fundamentally important observations can be made: 1) the cracks are initiated and caused to propagate solely by the interaction of stress waves, specifically in models with small isolated flaws the tensile tail of the P wave and the leading edge of the shear wave; and 2) in flawed, nonlayered homalite, barrier branching of propagating radial cracks caused by interaction of the propagating crack with the reflected stress wave and activation of flaws by the stress waves are the principle fragmentation mechanisms. Near the borehole, radial cracks dominate; remote from the borehole, crack networks from initiated flaws dominate. In layered media, the radial crack network is suppressed, and cracks initiate at the layer boundaries and propagate into the layers. The results of the work in flawed Homalite models have been confirmed in rock (Holloway, personal commun., 1978).

These studies, when coupled with high-speed cinematographic observation of production bench blasting, shed new light on arguments pertaining to fundamental fragmentation mechanisms. Fig. 6 is a schematic diagram of the principle structural features of the Chambersburg limestone at Pinesburg Quarry, Maryland. High-speed filming of production quarry blasting at Pinesburg reveals production of large boulders from the middle and lower portions of the face. These boulders are defined by the joint sets and bedding planes evident in the quarry. To explain their production, it is instructive to look at model blasting tests in layered Homalite 100 (Fig. 7). These models were designed to identify fragmentation mechanisms in layered media, analogous to jointed or bedded rock. In the model shown here, layers of Homalite 100 were cemented together with Eastman 910 adhesive to simulate a tight joint or a cemented bedding plane (Fourney *et al.*, in prep). The three photographs in Fig. 7 show the developing crack network in a layered model test. Note the absence of a radial crack network and the decreasing number of cracks formed in layers further outward from the borehole. What this model illustrates is the development of a crack network, which defines the resulting fragmentation, as a result of stress wave interaction with simulated joints and bedding planes. The fragmentation further from the borehole is coarser due to attenuation of the stress waves from crossing successive planes and from distance.

Fig. 8a is a schematic block diagram developed from high-speed footage of a production blast at Pinesburg, Maryland, that shows how the results obtained from the layered model tests relate to full-scale blasting. The major structural features at Pinesburg are dipping strata, rolling over by 80° from west to east, and two approximately orthogonal vertical joint sets, one nearly perpendicular to the face, and one intersecting it at a very shallow angle (Montenyohl, 1978). Two formations are quarried here, the Chambersburg and the St. Paul.

The originally thin bedding in the Chambersburg has been recemented by low-grade metamorphism, resulting in blocky beds up to 4' thick. The blasting pattern used at Pinesburg in the Chambersburg formation is a single row of holes, 6 1/8" in diameter, drilled on a burden of 17-18' and a spacing of 11'. The bench height is about 40', and most shots are decked. The initiation system used is the Nonel Primadet noiseless trunkline system, using a #3 (75 ms) cap in the bottom and a #4 (100 ms) cap in the upper deck, located directly above the decking. ANFO (Atlas) is the principle explosive, with cartridge ANFO or slurry used in wet toes or in wet holes. In drier holes, where seeping water might be a problem, the ANFO is loaded in plastic sleeves. The delay system initially used relied on 17 ms surface connectors to achieve the overall delay pattern; later shots used 42 ms connectors.

Examination of high-speed films from three production blasts in the Chambersburg formation yielded similar results, regardless of delay sequence (Fig. 8b). The schematic diagram in Fig. 8, drawn from the high-speed footage, presents a graphic picture of the face and an interpretation of what we feel is a logical explanation of what has occurred. The spacing of the primary joint set parallel or subparallel to the face is 6-11'; thus, two to three such sets will be crossed on going from the boreholes to the free face.

Reasoning from the work in layered models done by Fourney *et al.*, in prep, we can expect the P wave and the leading edge of the S wave to initiate and propagate cracks perpendicular to the subparallel joint plane, as well as the other joint plane and the bedding planes. As the stress waves cross these planes (where they are not open), they will be both reflected and attenuated. As the distance from the borehole increases, and the number of planes crossed increases, the number of cracks initiated decreases, and they do not propagate as far. The net result is an increase in block size towards the face, manifesting itself in the production of large boulders defined by the free face, bedding planes, and the vertical joint sets, especially the last set of joints which are subparallel to the face.

We feel that the performance of production blasting at Pinesburg is strong evidence supporting the fragmentation mechanisms revealed by the tests conducted in flawed and layered Homalite models by Dally and Fourney, 1975; Barker and Fourney, 1978; and Fourney *et al.*, in prep.

RELIEF: CONTROL THROUGH TIMING AND BOREHOLE GEOMETRY

Proper relief is probably the single most important parameter in production blasting, and, at present, one of the more difficult to control on a day-to-day basis. Relief is accomplished through two primary factors in the design of a blast, the burden as drilled and the timing of the sequence of detonations of the boreholes. In practice, both approaches are used together, but often without knowledge of the actual relief developed in the shot. One of the best studies of relief through timing was that of Bergmann *et al.*, 1974. They established, through studies of single row blasts in large rock blocks, a relationship of 1 ms/ft of burden for the optimum delay time between individual boreholes and the free face. These delay relationships have been used by many blasting engineers to design delay patterns, especially for use with the sequential blasting machines.

One of the more successful examples of manipulation of relief through borehole geometry is the Swedish wide-space technique developed by Kihlstrom, 1973 and Bhandari, 1974 a, b. This method involves radically altering the S/B ratio of a drilled pattern while keeping the S x B constant. The result is a pattern in which a very shallow burden with an extended spacing is used. S/B ratios range

from 3:1 to 8:1.

We have tested the delay and borehole geometry methods, singly and in combination, and monitored the results using high-speed cinematography. The results of this work bear on attempts to control relief and on the amounts of relief necessary to produce the desired results. One of the principal obstacles to control of relief in present-day production shooting is the irregularity of the initiators discussed in the first section of this report.

The problem of insufficient relief caused by initiator irregularity occurs in shots where only caps are used to achieve the delay sequence, and in shots using a hybrid system such as an electronic timer and electric blasting caps, or surface non-electric delay connectors and downhole delay caps. As discussed in Winzer, 1978, both crowding (adjacent caps firing less than 8 ms apart) and sequencing errors are likely with presently available initiators. When these problems occur in a shot, they disturb the developing pattern and almost always result in less relief for some portion of the shot. Examples of this behavior were given in Figs. 4 and 5 of the production blast in Ferguson, Iowa.

The relief in the Ferguson shot, based on the difference in time between nearest adjacent boreholes, is about 8 ms/ft between rows and 1.5 ms/ft between adjacent holes. The relief measured to the echelon portion of the V is 9.1 ms/ft. Analysis of the high-speed films from this shot reveals variations in this figure from as little as 0.15 ms/ft to 13.3 ms/ft between rows, and 0.4 to 10.8 ms/ft between adjacent holes in a row. Fig. 4 shows the results of these variations. Where timing errors are large, including sequencing errors, the effective burden on the hole in question can change from 6 1/2' to as high as 18 1/2'. The result of this change is that the direction of best relief is to the top of the bench; thus, the hole is relieved by breaking upward. The resulting vertical motion can be supersonic (mainly gases and small rocks, including the stemming), and the immediate result is both noise and flyrock. Over the period of development of the shot, these errors show up in differential motion of the burden. Between-row errors tend to translate throughout the portion of the shot in which they occur because the overall forward motion of the burden is slowed down by the initial error. Even if the remainder of the rows go off near their nominal times, they fire into slow moving or stationary burden.

An example of the problem of differential acceleration of the burden is quite clearly shown in Fig. 9a, b, and c. In this shot, a 3 row pattern is used. Hole diameter is 4 1/2", burden is 10' and spacing is 12' and the bench height is 44'. In this shot, the first row of holes is drilled on an angle to attempt to get the toe burden equivalent to the crest burden, a problem caused by excessive backbreak from previous shooting (Fig. 9a). The actual firing times, derived from the high-speed film, are shown on the right-hand side of the figure. Notice the last three holes in the second row. These holes should have fired at 150, 175, and 200 ms respectively. Because they fired early, the front row, even though lightly burdened, has not had time to move (Fig. 9b), and the second and third rows pile up on this side of the shot. Fig. 9b shows this as swelling (center of photo), and motion which is actually towards the rear of the shot rather than away from the face. Motion at the opposite end is outward (extreme upper right corner), as the timing here is close to the nominal, and thus this portion of the shot is well relieved. Rapidly moving rock at the face is caused by light burden from some of the angled holes along the front row.

Another aspect of the relief problem which we see in the films relates to the amount of time between rows in deep shots (shots with generally more than 4 rows). Fig. 10 represents a wide-space blasting pattern designed after Kihlstrom,

1973, and tested in Kansas on a limestone bench. The pattern consists of 10 rows of 4" diameter holes, 21' deep. The first and last rows are drilled on an 8' burden with a 10' spacing, while the middle 8 rows are drilled on a 5' by 20' burden and spacing with a S/B ratio of 4:1. The shot was delayed in an echelon opening from one end with the delay sequence achieved using a REO sequential blasting machine and DuPont ms delay electric caps in periods 3-8. The timer interval was set for 42 ms. Working on the basis of minimum distance between rows of holes going off nominally 8 ms apart, the result is a flat echelon with a delay of 14 ms/ft measured on the echelon. Examination of the high-speed films of this shot revealed considerable vertical motion developing as the shot progressed backward, culminating in the highest vertical velocities on the rear row of holes. This was recognized as a relief problem, and the counter was to attempt to increase the relief in the shot by increasing the interval.

A second shot was tried. This one differed slightly from the first, as the borehole size was increased to 4 1/2". The new pattern, shown in Fig. 11, is on the same size bench, but the burden and spacing are 11' x 13' (rows 1 and 7) and 6' x 26' for rows 2-6. The S/B ratio works out to 4.33:1 for rows 2-6. The timer interval was increased to 58 ms, which gives an interval of 15.3 ms/ft of burden measured in the same manner as the first shot. This increase in time results from a decrease in the angle between the echelon and the face. Fig. 12 shows two frames taken at about the same time in the shot development for each of the two shots. In the 58 ms shot, it is clear that there is considerably less vertical motion along the rear rows and a decrease in the amount of flyrock produced overall. It is also clear from the photographs that considerably more relief could be tolerated in this shot.

These, and several other films we have analyzed, suggest that the 1 ms/ft burden guideline is too short. Even in single row shots, we have seen fragmentation and muckpile digability improve as we go from 1.5 ms/ft to 3.8 ms/ft (measured between boreholes), and we have shot as high as 15.3 ms/ft in 7 row shots, with need for more relief. We notice that, with the echelon type pattern, we can shoot a three row shot with excellent results using 10 ms/ft between echelons, but when the depth is increased to 7-10 rows, 15 ms/ft is not enough. This discrepancy suggests that another factor must be considered. From our analysis of high-speed films, this factor would appear to be differential burden motion caused by the increase in mass of rock to be accelerated as one goes back into a deeper shot.

The problem can be diminished by increasing the interval between rows when using a sequential blasting machine or by skipping periods between rows, but one rapidly ends up with the situation where the interval between the front rows becomes too long, with its incident increase in noise from lightly burdened holes or cutoffs by differential movement of the burden. What is really needed is an increasing interval as one goes deeper into the shot, and we intend to experiment with this type of machine in the future.

CONCLUSIONS

We have filmed and analyzed 37 production quarry blasts using a variety of 16 mm high-speed motion picture cameras, at framing rates between 500 and 7000 per second. We find that the principal obstacle to consistent, controlled production blasting is the variability of currently available initiators, both electric and non-electric. Timing errors resulting from shifts in the mean firing time from the manufacturers' nominal firing times, and increasing scatter in firing times around the means at the longer delay times, result in flyrock, back-break, tight muckpiles, and production of oversize. Such errors can be expected

to enhance vibration problems and noise through firing of unrelieved holes.

Analysis of high-speed films lends support to fragmentation mechanisms defined in flawed and layered Homalite models by Dally and Fournay, 1977; Barker and Fournay, 1978; and Fournay et al., in prep. The results of our analysis of these films to date suggest that the role of stress waves in fragmentation is of considerably greater importance than previously suspected. Our work also indicates that currently used guidelines for determining relief may not hold for multi-row production blasts, and that much longer between-row delay times may be necessary to optimize fragmentation and muck digability and minimize flyrock and backbreak.

The influence of major structural discontinuities on fragmentation, alluded to by Ash, 1973, and by Larson and Pugliese, 1974, are confirmed, and the manner in which they control the production of oversize developed from combined model tests in layered Homalite and high-speed cinematography of bench blasting in carefully mapped limestone.

Considerable work remains to be done to fully quantify the results reported here and to establish, on a firmer basis, the relationships between shot design, actual delay sequence, and the production of vibration and airblast. Control of these factors will be of increasing importance as more and more operations of which blasting is a part find themselves in close proximity to residential and commercial structures. It becomes increasingly imperative that research be carried out in these areas in a manner which, as fully as possible, quantifies all parameters involved.

ACKNOWLEDGEMENTS

This research was supported in part by NSF Grant #DAR 77-05171 and by Martin Marietta Aggregates. We would like to thank Mr. Ed Laughlin, Martin Marietta Aerospace for the supporting art work, and Mr. M.A. McDaniels, Mr. Al LeBoeuf, Mr. Russ Warren, and Mr. Bill Simmons for their contribution to the high-speed cinematography.

REFERENCES

- Ahrens, T.J. and Rosenberg, J.T. (1968) Shock metamorphism, experiments on quartz and plagioclase, in French, B.M. and Short, N.M. (Eds.) Shock Metamorphism of Natural Materials, Mono Book Corp., Baltimore, pp. 59-81.
- Andrews, A.B. (1975) Air blast and ground vibration in open pit mining. Mining Congr. J. pp. 20-25.
- Ash, R.L. (1973) The influence of geological discontinuities on rock blasting. Ph.D. Dissertation, Univ. of Minnesota, 289 p.
- Barker, D.B. and Fournay, W.L. (1978) Photoelastic investigation of fragmentation mechanisms. Part II - Flaw initiated network. Rept. to N.S.F., Univ. Md. Aug. 1978.
- Bergmann, O.R., Wu, F.C. and Edl, J.W. (1974) Model rock blasting measures effect of delays and hole patterns on rock fragmentation. Eng. Mining J. 175, pp. 124-127.
- Bhandri, S. (1975a) Improved fragmentation by reduced burden and increased spacing in blasting. Mining Mg. 131, pp. 187-195.

- Bhandari, S. (1975b) Burden and spacing relationships in the design of blasting patterns. 16th Symp. Rock Mech, pp. 210-220.
- Blair, B.E. (1960) Use of high-speed camera in blasting studies. U.S. Bu. Mines Rept. of Investigations 5584, 32p.
- Blunt (1953) Use of photography in the underground explosion test program, 1951-1952. Jour. of the SMPTE 60, pp. 405-417.
- Dally, J.W. and Fourney, W.L. (1977) The influence of flaws on fragmentation. Proc. 6th Int. Colloq. on Gasdynamics of Expl. and React. Sys. Stockholm, Sweden.
- Dally, J.W., Fourney, W.L. and Holloway, D.C. (1975) Influence of the containment of the borehole pressures on explosive induced fracture. Int. J. Rock Mech. Mining Sci. and Geomech. Abstr. 12, pp. 5-12.
- Dence, M.R. (1968) Shock zoning at Canadian craters: Petrography and structural implications, in French, B.M. and Short, N.M. (Eds.) Shock Metamorphism of Natural Materials, Mono Book Corp., Baltimore, pp. 169-184.
- Françti, G.E. (1958) High speed photographic observations in taconite and limestone blasting. Proc. U. Min. Symp. Rock Mech. Duluth, pp. 60-69.
- French, B.M. and Short, N.M. (Eds.) (1968) Shock Metamorphism of Natural Materials, Mono Book Corp., Baltimore, 664 p.
- Fourney, W.L., Barker, D.B. and Holloway, D.C. Fragmentation mechanisms in a layered medium, in prep.
- Hagan, T.N. (1977) Good delay timing - prerequisite of efficient bench blasts. Aust. Inst. Mining Metall. Proc. 263, pp. 47-54.
- Kieffer, S.W. (1971) Shock metamorphism of the Coconino sandstone at Meteor Crater, Arizona J. Geophys. Res. 76, pp. 5449-5473.
- Kieffer, S.W. (1975) Droplet Chondrules. Sci. 189, pp. 333.
- Kihlstrom, B. (1973) The Swedish wide-space blasting technique. Natnl. Symp. on Fragmentation, Aust. Geomech. Soc. Adelaide 8-14.
- Kutter, H.K. and Fairhurst, C. (1971) On the fracture process in blasting. Int. Jour. Rock Mech. Mining Sci. 8, pp. 181-202.
- Långefors, U. and Kihlstrom, B. (1963) The Modern Technique of Rock Blasting. John Wiley and Sons, N.Y. 405 p.
- Larson, W.C. and Pugliese, J.M. (1974) Effects of jointing and bedding separation on limestone breakage at a reduced scale. U.S. Bu. Mines Rept. of Investigations 7863, 13 p.
- Montenyohl, V.I. (1978) Defect structures in the Pinesburg Station quarries. Rept. to N.S.F., MML TR 78-22c, June 1978.
- Patterson, E.M. and Forsyth, W. (1956) The photography of moving rock during blasting. Mine and quarry Eng. pp. 234-240.

Porter, D.D. and Fairhurst, C. (1971) A study of crack propagation produced by the sustained borehole pressure in blasting, in Dynamic Rock Mechanics, G.B. Clark, Ed. Proc. 12th Symp. Rock Mech. pp. 497-515.

Winzer, S.R. (1978) The firing times of ms delay blasting caps and their effect on blasting performance. Rept. to NSF Contr. #DAR 77-05171, June 1978.

Winzer S.R. (in press) Initiator firing times and their relationship to blasting performance. Proc. 20th U.S. Symp. Rock Mech., Austin, Tex.

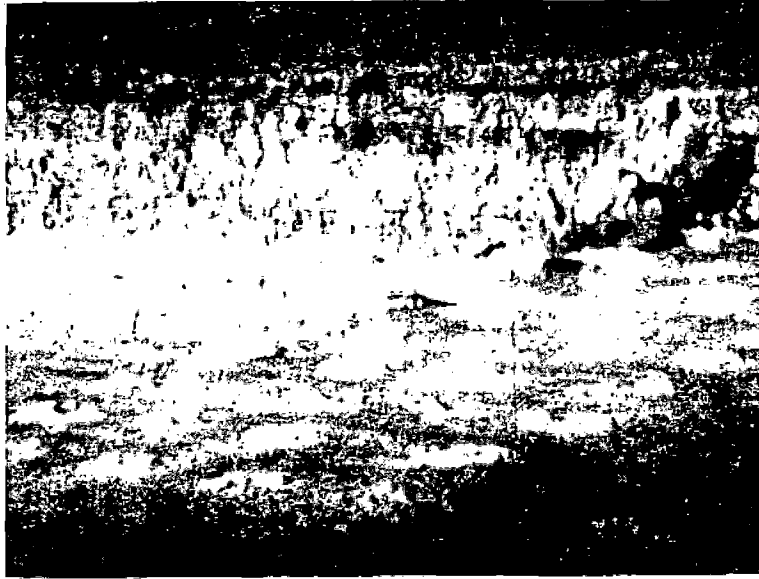


Figure 1a



Figure 1b



Figure 1c

Figure 1. Sequence of high-speed photographs, taken at 2700 frames/second, of a production blast at Moline, Kansas. This shot used electric initiators, periods 3-8, and the REO sequential blasting machine to achieve the desired delay sequence. Period 6, 7, and 8 initiators are in the holes closest to the camera. Firing times of some of these holes are on the film, with the arrow pointing to the hole which has fired. Reversals in the mean firing times of this manufacturer's period 7 and 8 caps and crowding of period 6, 7, and 8 caps are the cause of the reversals and crowding seen here in the field. These errors produce the cratering seen in the left portion of Fig. 1c.

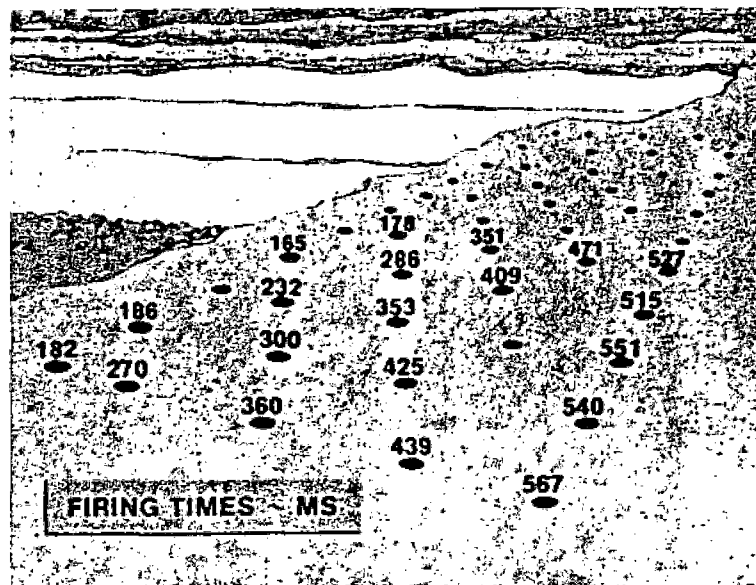


Figure 2. Firing times for some holes in the Moline, Kansas, production shot. The diagram is drawn in perspective as though seen through the camera which took the high-speed film shown in Fig. 1. Note the sequencing errors in rows 1 and 6, and the crowding in row 4. All the initiators in these holes are either period 6, 7, or 8 (150, 175, or 200 ms).



Figure 3. Muckpile and face characteristics of the Moline, Kansas, production shot. A few large pieces can be seen in this portion of the muckpile; their occurrence correlates with the sequencing errors found in this part of the shot. Backbreak was confined to the section (the last 1/3 of the shot) where the period 6-8 initiators were located.



Figure 4a



Figure 4b



Figure 4c

Figure 4. High-speed motion picture footage from Ferguson, Iowa. The film is running at about 3000 frames/second. In this sequence, three holes can be seen to fire early. All three are two or more rows back from the free face, and are, thus, completely unrelieved. Vent velocities seen here are more than 1400 ft/sec and are, thus, supersonic, contributing to noise. The net result of the errors seen here is flyrock and noise.

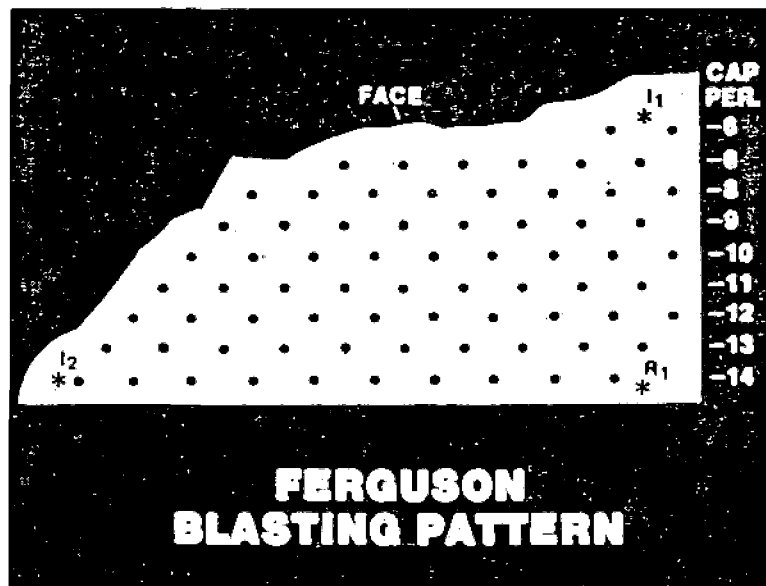


Figure 5a

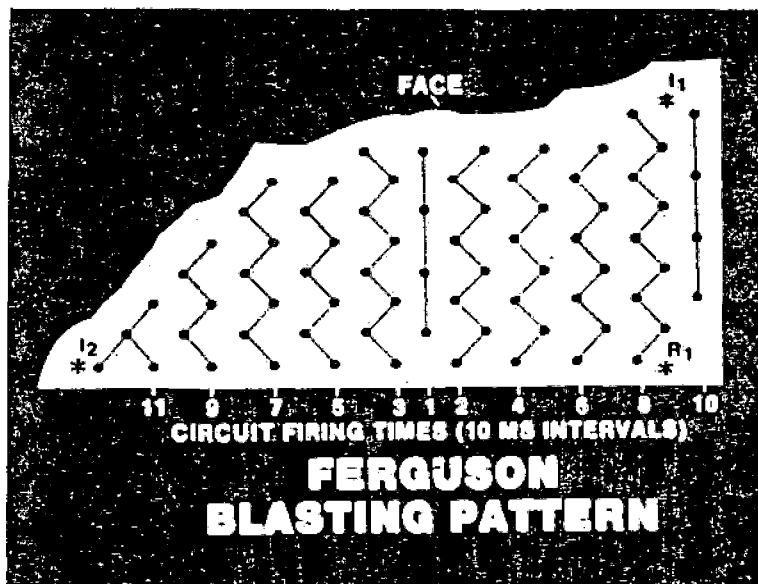


Figure 5b

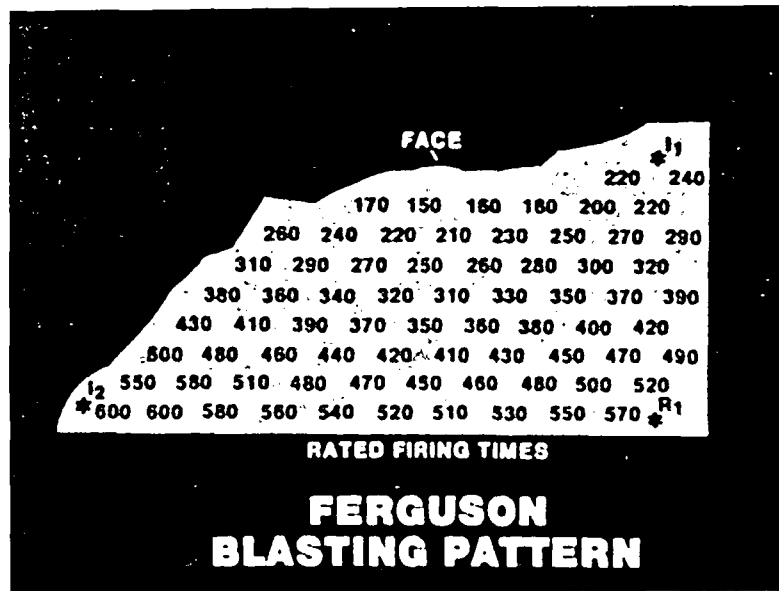


Figure 5c

Figure 5. Drill pattern and delay sequence for production blasting pattern at Ferguson, Iowa. The drill pattern is a 6 1/2 x 13', staggered, using a 3" hole. Bench height is ~34'. Delay sequence is obtained by using a combination of a Trojan type C timer and ms delay electric caps, periods 6-14. Nominal firing times are given in Fig. 5c.

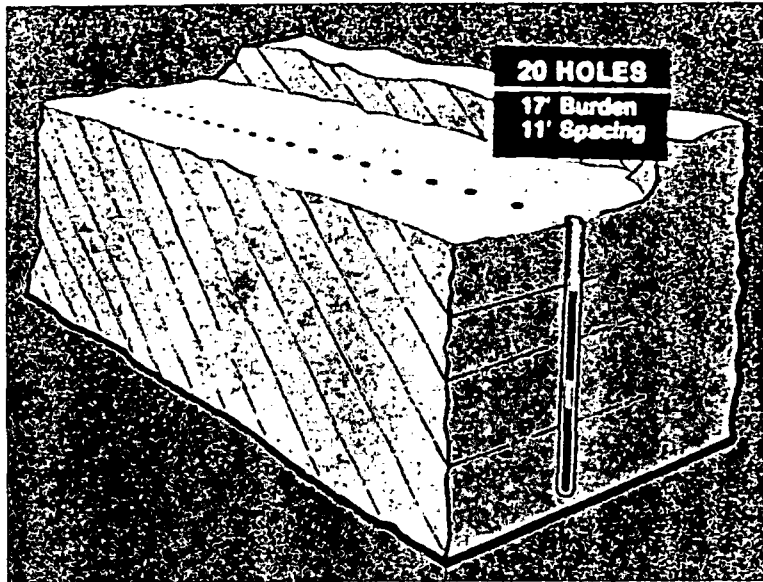


Figure 6a

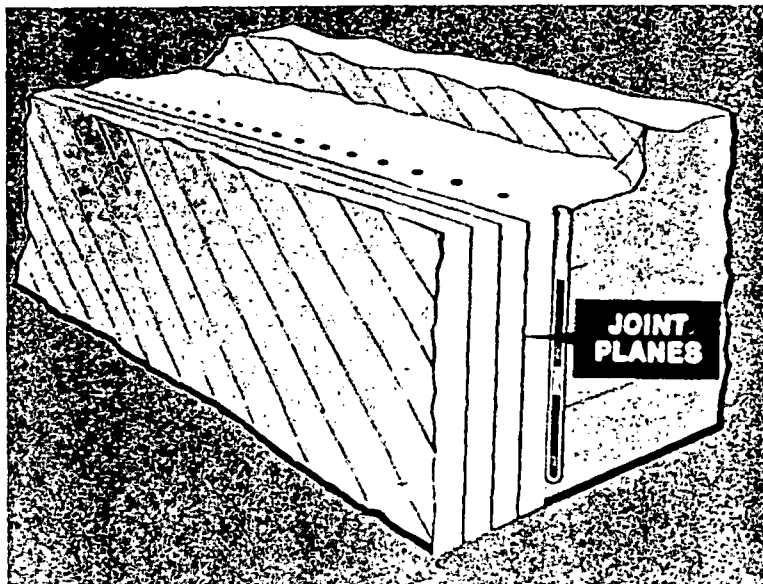


Figure 6b

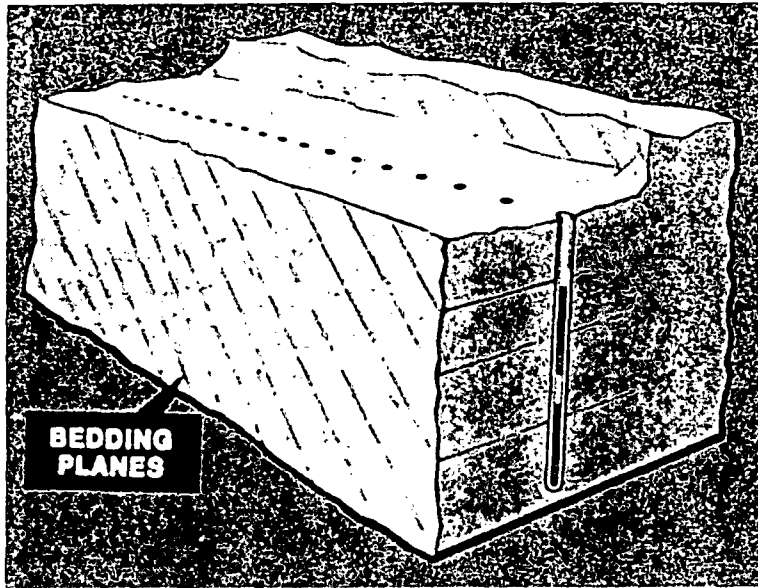


Figure 6c

Figure 6. Structural schematic of Pinesburg Quarry, Chambersburg Limestone. Dip of strata increases to the east. Joint planes shown actually run at a very low angle to the face, with a second set of vertical joints 90° to it (almost perpendicular to the face).

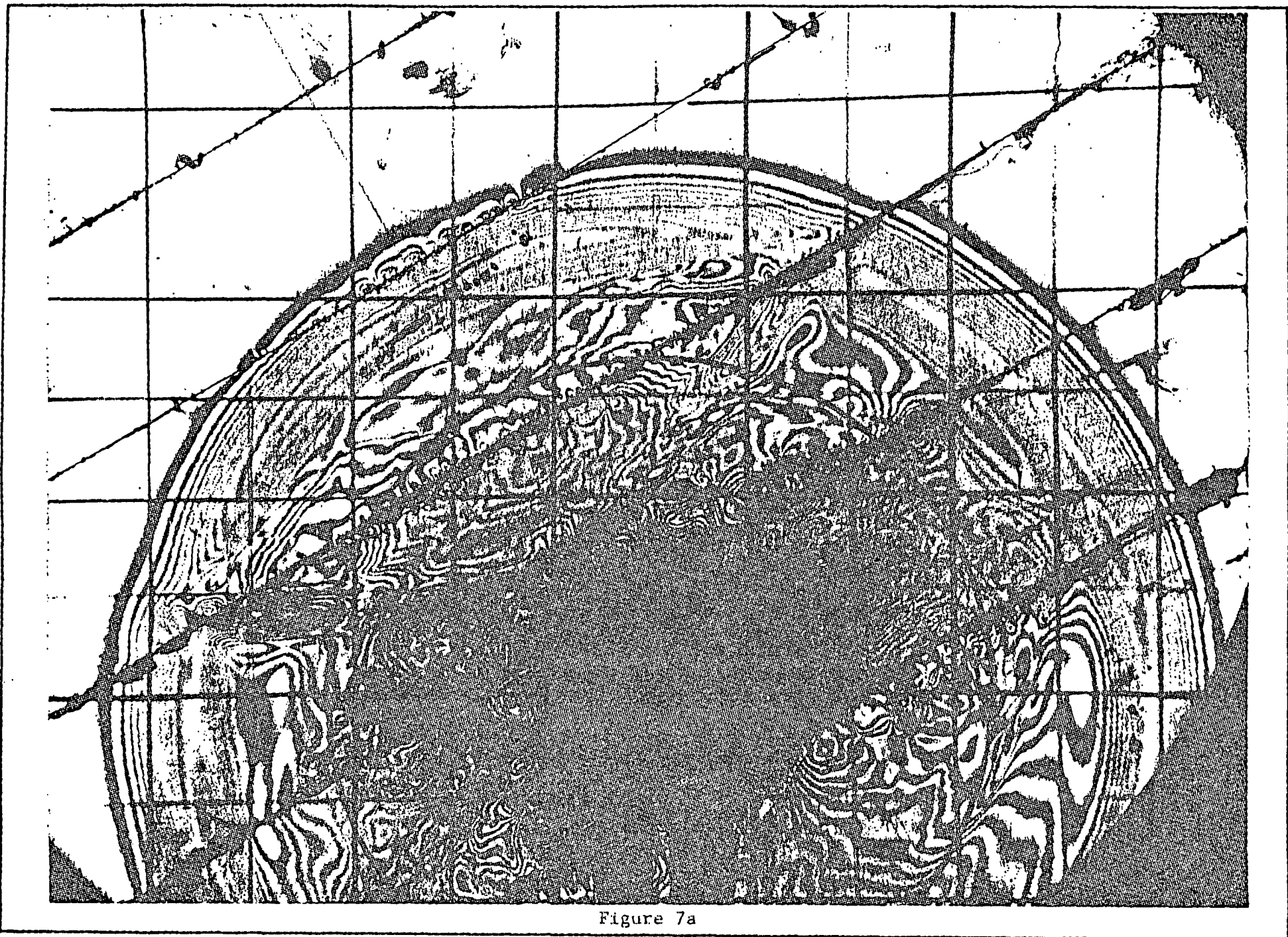
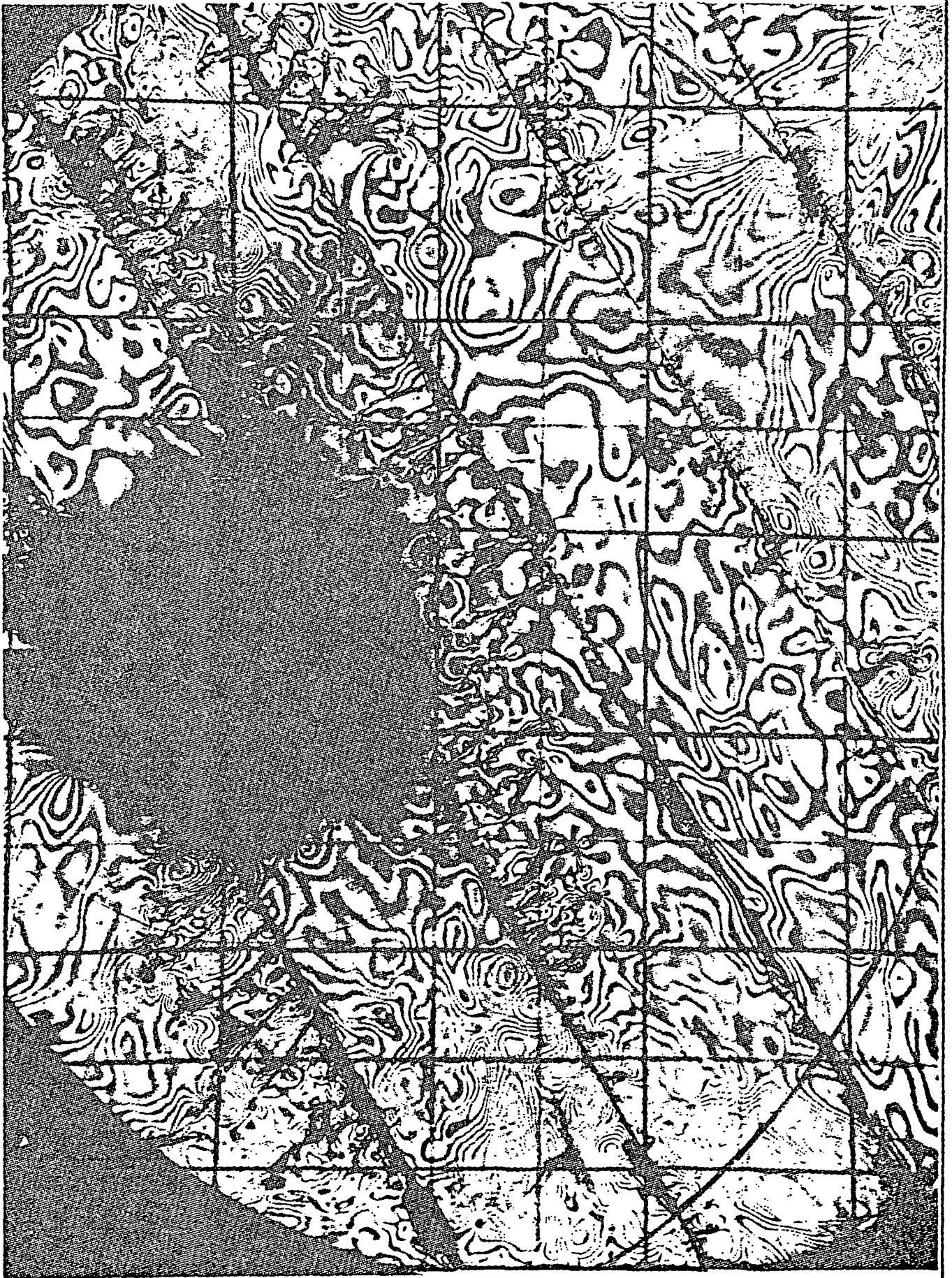


Figure 7a

Figure 7b



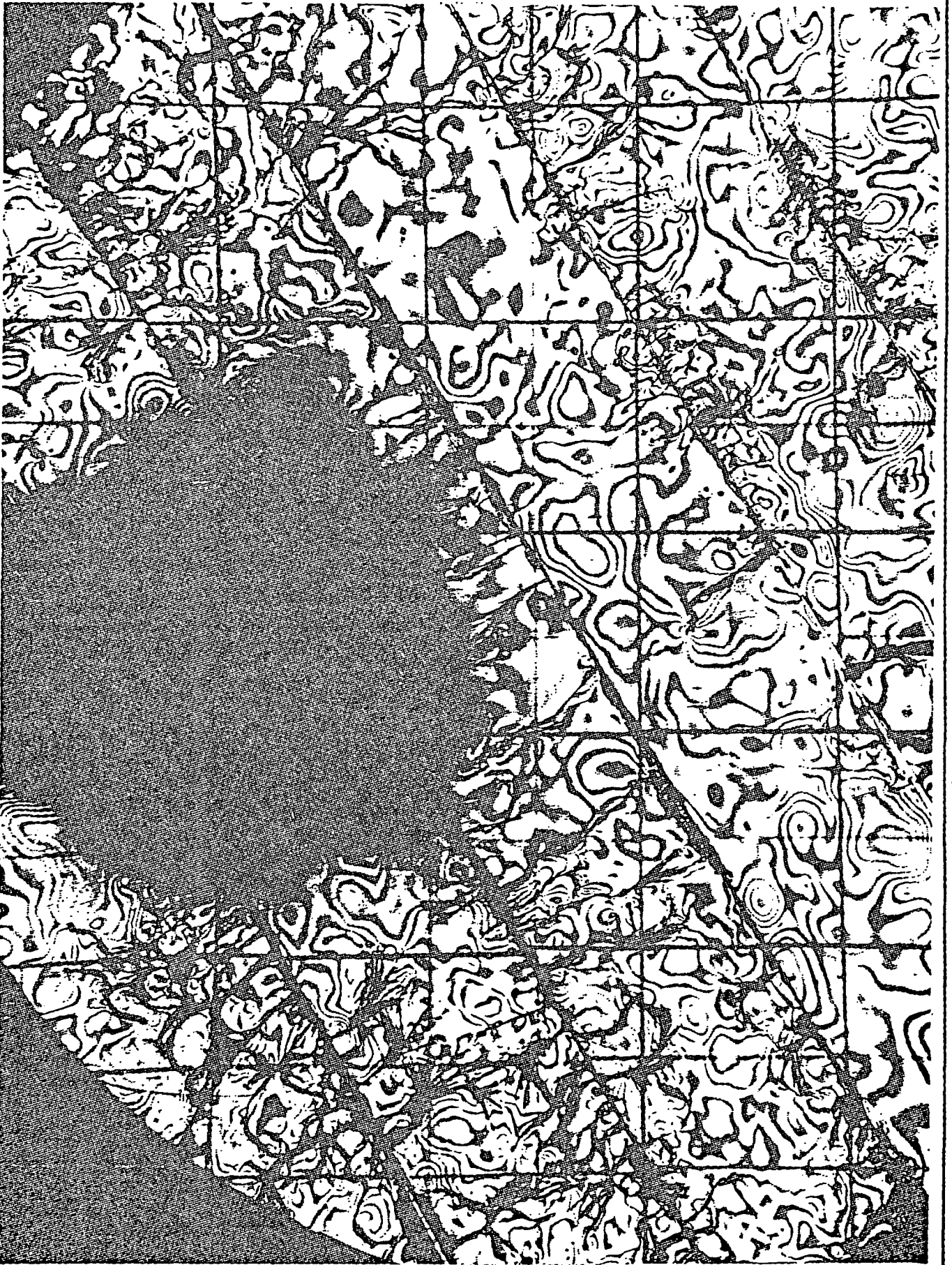


Figure 7c

Figure 7. Blasting tests in layered Homalite 100. This series of three high-speed photographs taken with a Cranz-Shardin multiple spark gap camera shows the development of a crack network by interaction of stress waves with layer-type discontinuities. These discontinuities simulate joints or bedding planes. Note the suppression of the radial borehole crack network and the fact that cracks propagate by the energy contained in the stress waves alone; there is no gas pressurization. The crack density decreases with distance from the borehole and with the number of planar discontinuities crossed.

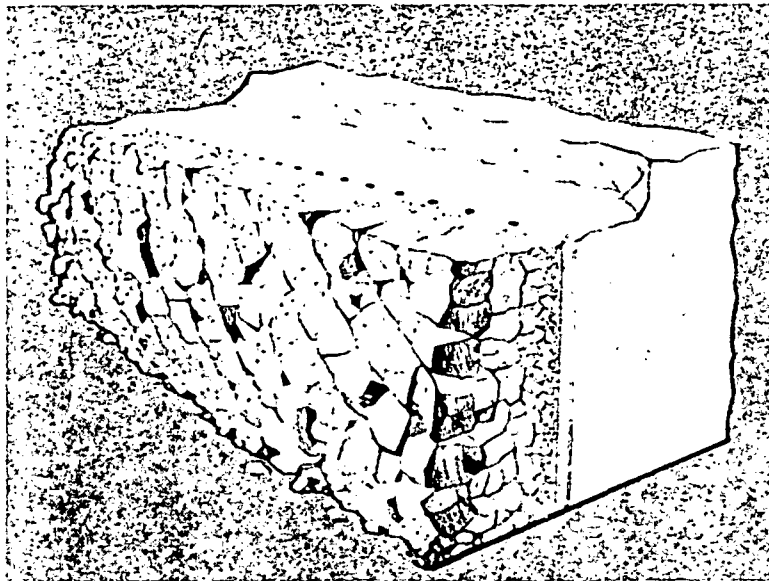


Figure 8a



Figure 8b

Figure 8. Structural schematic of the Chambersburg Limestone Pinesburg Quarry, in the first few hundred milliseconds following initiation of the explosive (Fig. 9a). This schematic is made from high-speed footage of the disintegration of the face (Fig. 9b) and illustrates the contribution of joint and bedding planes to the development of oversize blocks at Pinesburg.

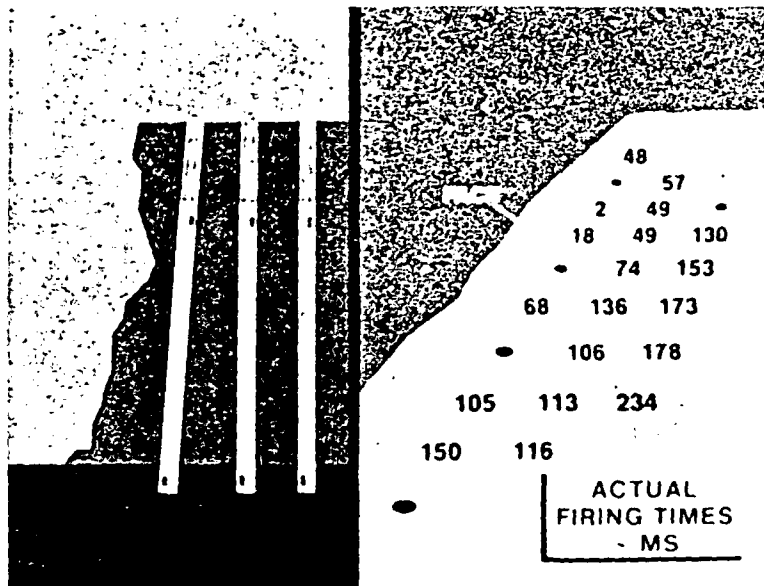


Figure 9a. Cutaway diagram of three row blasting pattern. Left hand side shows the vertical borehole pattern, with the first row angled to improve toe burden. Due to the irregular nature of the face, light burdened holes occur along the first row. Right hand side shows actual firing times as determined from high-speed films of the shot.



Figure 9b. Frame from one of the high-speed films taken of the shot shown in Fig. 9a. This frame, from the 500 frame/second camera, is taken about 300 ms into the shot, some 60 ms after the last hole has fired. See text for details.

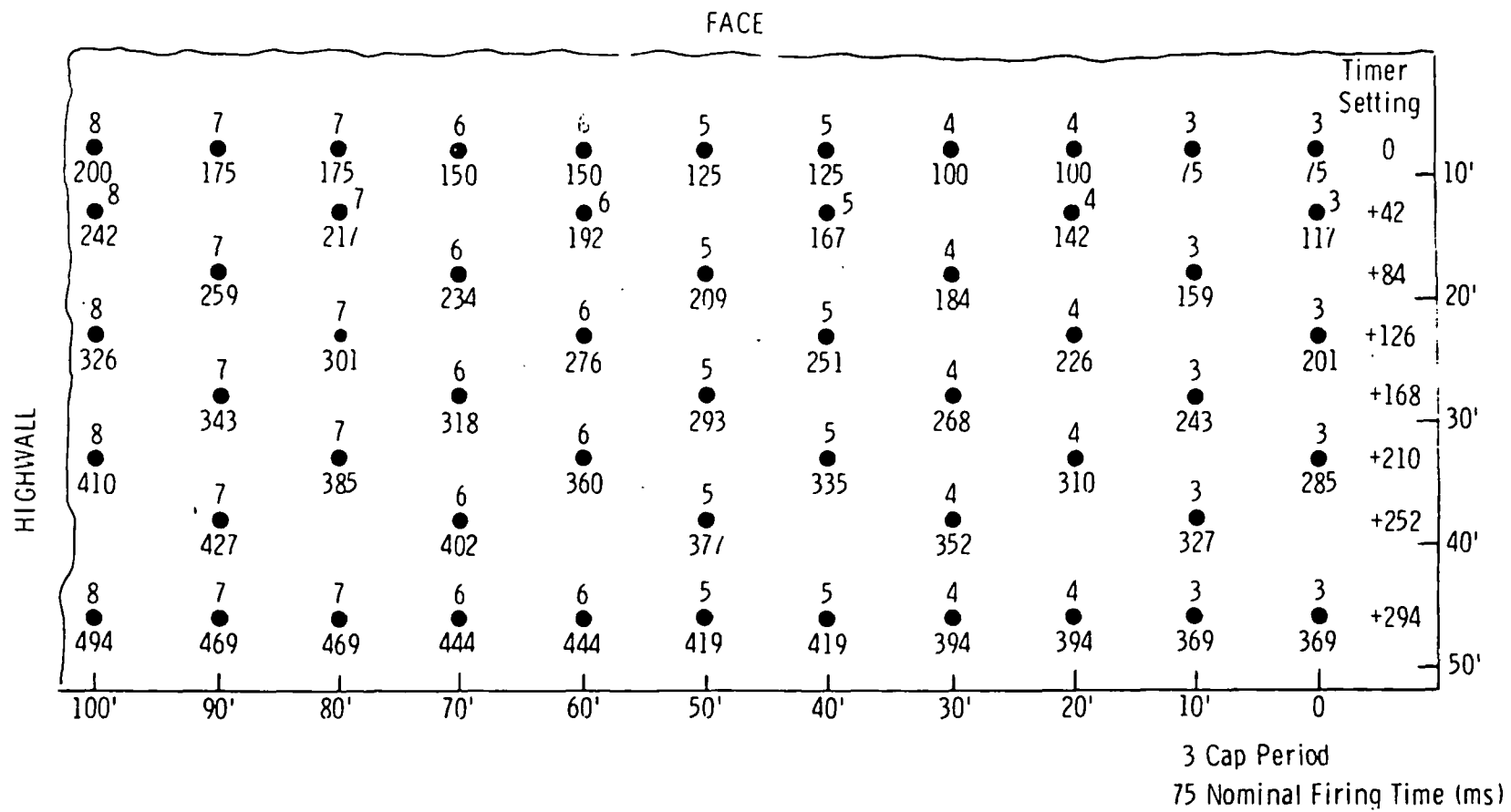


Figure 10. Widspace blasting pattern, Moline, Kansas.

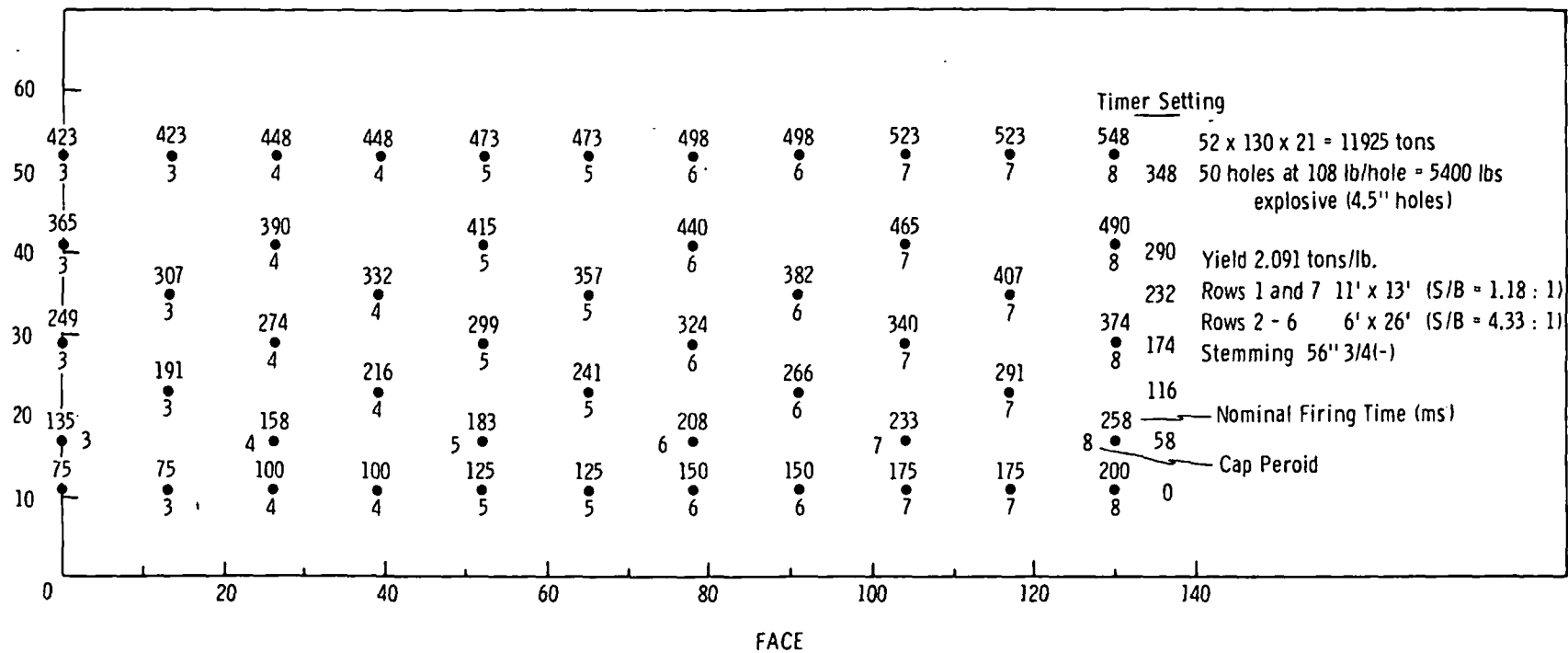


Figure 11. Wide space blasting pattern, Moline, Kansas. This pattern differs from that shown in Fig. 10 in that the relief measured on the echelon is 15.3 ms/ft rather than 14 ms/ft.



42 ms



58 ms

Figure 12. High-speed motion pictures of wide space blasting patterns, Moline, Kansas. Both photographs are taken about the same time in the event. The uppermost photo is of the shot using a 42 ms timer interval; the lower used a 58 ms interval. Note the reduction in vertical motion, especially along the rear rows of holes.

The regular convening of international Congresses (every two to three years) is a very important event for experts from all countries. Scientists mutually benefit each other and share their achievements in the region of scientific developments and in the practical aspects of the treatment of mineral raw material. Personal contacts between the delegates help to strengthen the friendship between nations.

200. Non-Ferrous
1979 v. 7 N 3

Articles

UDC 661.1

Technology of the tank method for microbiological leaching of complex copper-nickel materials

S I Pol'kin, E V Adamov, V V Panin, and S I Kazintseva (Moscow Institute of Steel and Alloys)

Zinc production in the USSR is realised mainly from difficult to concentrate copper-zinc and polymetallic ores from the Urals, Kazakhstan, and other deposits having a complex material composition, fine impregnation extending to emulsion-type impregnation of the minerals, and an increased content of secondary sulphides and oxidized copper minerals, which help to activate zinc blende and pyrite; this interferes with the selectivity in the flotation of copper-zinc ores. The most complex are the metacolloidal copper-zinc ores which hardly undergo selective flotation at all; the zinc is extracted to the extent of 80-85% into the copper concentrate, which contains up to 10-15% zinc, impairing the technological characteristics in the smelting of the concentrates with significant or complete loss of zinc, cadmium, and other accompanying metals.

Copper-zinc ores or collective concentrates having a complex material composition, containing copper sulphates and secondary sulphides, having a fine mutual impregnation of copper and zinc sulphides in the pyrite, and requiring extremely fine grinding (to 100% finer than 30µ) can be treated effectively by hydrometallurgical methods with the use of thio bacteria. In addition to the surface and underground leaching of copper and other metals the technology of the tank method for the microbiological leaching of metals from difficultly processed ores and various sulphide-containing materials is being vigorously developed. The microbiological method makes it possible to open up finely impregnated sulphide minerals and gold, effectively to remove harmful impurities such as arsenic, to extract metals selectively from complex ores and concentrates, and to dissolve and extract native gold.

The technological scheme which we proposed for the flotation-bacterial-hydrometallurgical treatment of stubborn metacolloidal ores involves collective copper-zinc flotation to produce a concentrate containing 9-11% Cu and 11-15% Zn, bacterial leaching, selective isolation of the metals from the bacterial solutions, and flotation of the copper concentrate from the cake after bacterial leaching (fig. 1).

During the development of the technology for the bacterial leaching of metals from stubborn copper-zinc products special attention was paid to the production of strains of micro-organisms active under the leaching conditions. The initial laboratory strain of the T ferrooxidans microorganism reduced its activity by 42-68% with increase in the copper content of the solution from 1.5 to 10 g/litre and by 42-68% with increase in the zinc content from 8 to 44 g/litre. The micro-organisms were adapted to the extremal conditions of bacterial oxidation of the metacolloidal copper-zinc products by preliminary continuous culture on the leached substrate with a gradual increase in the density of the pulp, with a copper concentration of up to 5 g/litre and a zinc concentration of up to 20 g/litre in the solution. In this way a production strain of T ferrooxidans was obtained which was active at copper and zinc concentrations two or more times exceeding those to which they were adapted. The main characteristics of the laboratory strain of the bacteria and the production strain after adaptation are given in table 1.

As seen from the presented data, the laboratory strain of the bacteria is significantly inferior in all its main technological parameters to the bacteria obtained after adaptation (the production strain), the use of which makes it possible to intensify the bacterial oxidation process and considerably reduce the length of the leaching process.

As we showed, the properties of the initial strain of bacteria are restored after culture of the adapted culture in a medium with ferrous iron not containing inhibiting metals. It is probable that the resistance of natural strains of micro-organisms to copper and zinc ions is determined genetically, i.e., only the potential characteristics of the organism are realised during the adaptation process without change in its genotype. We also found that the adsorption capacity of the microorganisms increased in the cultures of the bacteria which had been adapted to the concentrate leaching conditions. Whereas the equilibrium between cells adsorbed on the minerals and the free cells present in the solution during the bacterial oxidation of sulphide concentrates is established after 1-5h with the adapted strains of T ferrooxidans, with the unadapted strains this equilibrium is established only after 120-300h (from the moment of completion of the adaptation period to the moment of intensive oxidation of the substrate). This once again confirms the need and importance of adsorption of the adapted microorganisms on the minerals during the bacterial leaching process.

In order to study the relationships governing the adsorption of the microorganisms on the surface of the substrate we used direct (phase-contrast microscopy, fluorescence, and electron microscopy) and indirect (manometric and electrochemical) methods of investigation. The activity of the microorganisms was determined by a manometric method, since the bacterial oxidation of sulphides leads to the absorption of oxygen, the amount of which is directly proportional to the time and depends on the activity of the bacteria. The adsorption activity coefficient K_a represents the number of microlitres of oxygen adsorbed by 2 millilitres of the bacterial suspension per minute.

Investigation of the effect of the length of interaction between the microorganisms and the concentrate on the adsorption strength of the cells showed that the adsorption strength depends on the length of contact between the cells and the concentrate particles. With unprolonged contact (up to 1h) the bacteria are weakly adsorbed on the concentrate and are easily washed off. Here the activity coefficient of the initial bacterial-mineral suspension was 2.8 μ l/min, and that of the concentrate which had been washed from the bacteria was reduced to 0.67 μ l/min, i.e., by four times. As leaching proceeds and the cells develop, their stronger attachment to the sulphide minerals occurs. After 24h contact the activity coefficient of the bacterial-mineral suspension is 3.0 μ l/min, and that of the concentrate washed from the bacteria is reduced by only 1.8 times.

The "free" microorganisms, which during leaching amount to about 20% of their total number at a concentration of 10^5 cells/ml, consist of potentially physiologically active cells, the presence of which in the solution is due to exchange adsorption both enhanced (due to the action of mechanical factors and primarily intensive agitation) and essential (due to the physiological state of the bacteria). The obtained results show that the adsorption of the microorganisms on the surface of the minerals is a very important and essential stage in the development of the oxidation processes in sulphide minerals. Apart from the realisation of a production culture of bacteria, an essential condition for successful leaching is to maintain the microorganisms in the active state, and this is achieved by strict observance of the optimum parameters of the process.

Our investigations into the effect of the mineral composition of the product being treated, the acidity and density of the pulp, the particle size of the initial product, the aeration conditions, and other parameters on the technological characteristics of the leaching process and on the activity of the microorganisms made it possible to establish the following optimum technological parameters for the bacterial leaching of metals from stubborn copper-zinc material: 1) Particle size of initial material 88-100% of the -44 μ class, depending on the content of metacolloidal forms; 2) solid-liquid ratio of the pulp 1:5-1:3; 3) oxidation-reduction potential of the medium 600-700mV; 4) acidity of pulp 2.0-2.5pH units; 5) agitation and aeration of the pulp with air enriched to 0.1-1.0% with carbon dioxide; 6) the use of a culture of microorganisms adapted to the concentrate leaching conditions and having a high oxidizing activity under the extremal leaching conditions. With these parameters, as established by our investigations, there is no need to use special nutrient media or to add sulphuric acid and divalent iron from outside in order to develop active bacterial oxidation processes in the treatment of copper-zinc materials.

Owing to the large silver content of the investigated concentrate and to its high toxicity for the microorganisms we investigated the effect of this element on the activity of the bacteria and on the kinetics of the leaching of copper and zinc. It was established that with a content of up to 100 g/ton in the initial concentrate, silver passes partly into solution during bacterial leaching and at concentrations of 10-12 mg/litre not only does not suppress the bacterial oxidation

Table 1: Characteristics of the strains of the T. ferrooxidans bacteria

Parameters	Laboratory strain	Production strain
Number of cells in 1 ml	10^6	10^6
Activity in oxidation of Fe ²⁺ %	100	300
Activity coefficient of microorganisms in the oxidation of sulphides in concentrates μ l O ₂ /min	0.1	2.0-3.5
Concentration of copper suppressing the activity of cells by 30-40%	1.5	15.0
Concentration of zinc suppressing the activity of cells by 30-40%	8.0	100.0

of the sulphide minerals but even intensifies it. It is possible that the silver interacts with organic substances released by the microorganisms or with reduced sulphur compounds, which appear during the oxidation of sulphide minerals. By control and regulation of the above-mentioned technological parameters it was possible to extract up to 90-92% of the zinc and cadmium and up to 25% of copper into solution after 72h during the continuous leaching of copper-zinc materials. The variation in the composition of the bacterial solutions in the Pachuca tanks during direct-flow leaching (each Pachuca represents one leaching step) of copper-nickel materials is characterized by the data given in table 2. As seen from the presented data, selective leaching of zinc and copper is observed during the leaching of copper-zinc materials. This can be explained by the selective oxidation of the sulphide minerals present in the polymineral mixture, due to electrochemical processes which occur in the complex bacterial pulp.

It is known that the mechanism of the electrochemical oxidation of a mixture of sulphide minerals can be explained by the theory of microgalvanic cells or by the theory of local cells, according to which the specific potential difference which exists between the anodes and cathodes gives rise to the passage of electric currents, forcing the anode to dissolve. During the joint presence and contact of minerals with different oxidation potentials the oxidation of the mineral with the higher potential is retarded, and that of the mineral with the lower potential is accelerated.

The microbiological oxidation of polymineral mixtures goes in the same direction as electrochemical dissolution, but the process is greatly accelerated in the presence of bacteria. We showed that during the bacterial leaching of mixtures of sphalerite with chalcopyrite, sphalerite with pyrite, sphalerites with various degrees of isomorphous substitution, and collective copper-zinc concentrates there is a possibility of intensive electrochemical oxidation processes, due to the electrochemical characteristics of the sulphide minerals

Table 2: Characteristics of the bacterial solutions in the leaching of copper-zinc concentrates

Parameters	Leaching steps				
	1	2	3	4	5
pH	2.5	2.25	2.0	2.0	2.0
E, mV	300	620	670	690	720
Iron (III), g/l	1.7	3.9	4.75	6.2	7.7
Iron (II), g/l	0	0	0	0	0
Zinc g/l	5.4	8.68	12.3	16.9	22.8
Copper g/l	1.78	2.2	2.59	3.7	4.45
Cadmium g/l	-	-	-	-	0.12
Amount of bacteria, cells/ml	10 ⁶	10 ⁶	10 ⁶	10 ⁶	19 ⁶
Activity coefficient of micro-organisms, $\mu\text{l}/\text{min}$	3.2	3.06	3.13	3.03	3.06

present in the mixtures. The electrode potential of sphalerite in the bacterial solution varies from 430 mV at pH 1.5 to 230 mV at pH 2.3, whereas the potential of chalcopyrite amounts to 600 mV at pH 1.5 and 680 mV at pH 2.3. Over the whole investigated range of pH the electrode potential of chalcopyrite is thus 170-450 mV higher than the potential of sphalerite, and this shows that chalcopyrite is more resistant to oxidation than sphalerite in the given system. These results agree well with experimental data on the selective bacterial leaching of the collective copper-zinc concentrate. As seen from fig. 2, selective leaching of zinc occurs during the bacterial leaching of this concentrate, and up to 92% of the zinc passes into solution, whereas the extraction of copper into solution is not higher than 20-25%. During the bacterial oxidation of cleophane containing 2.72% of iron the extraction of zinc without replacement of the solution amounted to 27.5%, whereas the extraction of zinc from marmatite containing 10.1% of iron under the same conditions amounted to 52%. During the bacterial oxidation of mixtures of marmatite and chalcopyrite (1:1) and of marmatite and pyrite the extraction of zinc increased to 80 and 99% respectively.

Thermodynamic calculations of the stability of chalcopyrite, sphalerite, and their oxidation products in the region of the activity of the microorganisms showed that during bacterial oxidation sphalerite and chalcopyrite are thermodynamically unstable but are kinetically stable, i.e., their oxidation does not occur spontaneously in the absence of the microorganisms. The main thermodynamic relationships characteristic of the oxidation of sulphide minerals do not change during the geochemical activity of the microorganisms, and only affect the kinetics of these processes, although the main thermodynamic parameters (oxidation-reduction potential and the pH of the medium) vary

fairly wide range.

During bacterial leaching of the metal from copper-zinc products without control of the acidity the pH of the medium changes from 2.3-2.5 in the first Pachuca to 1.2-1.3 in the later ones, and the oxidation-reduction potential of the solution changes from 300-400 to 800-850 mV. Such sharp fluctuations in the oxidation-reduction characteristics of the solutions and their acidity leads to a reduction in the activity of the micro-organisms and the leaching rate by 2-10 times.

By our investigations it was shown that the highest activity in the micro-organisms in all the leaching steps (activity coefficient 3.05-3.2 $\mu\text{l}/\text{min}$) is observed when a pH value of 2.0-2.5 is maintained over the whole leaching period (fig. 3), and this corresponds to an oxidation-reduction potential of 600-700 mV. At higher potentials the decrease in the activity of the micro-organisms is probably due to interruption in the energy exchange of the micro-organisms.

The bacterial solutions after leaching of copper-zinc materials have a complex composition; up to 3-7 g/l of copper, 18-120 g/l of zinc, 5-10 g/l of iron, and 0.10-0.15 g/l of cadmium accumulate in the solution. After bacterial leaching, therefore, the metals must be extracted to produce standard commercial products. In spite of the fact that not more than 25% of copper is extracted into the solutions under the optimum leaching conditions, its use has industrial significance. In lump and underground leaching practice the removal of copper from the bacterial solutions is largely realised in cementation equipment with the production of cemented copper. The use of zinc dust for the separation of copper and cadmium from zinc sulphate solutions is also known. In our investigations the cementation of copper from the bacterial solutions is realised both with iron filings and with zinc dust as precipitant. The use of zinc dust as cementing agent gives better technological characteristics and makes it possible to eliminate the additional introduction of iron into the solution, which complicates its subsequent treatment. With the consumption of zinc dust in the stoichiometric ratio the extraction of copper from the solutions after 1-3 min amounts to 95% with a content of 88% in the cemented copper. In addition, cadmium is extracted into the cemented copper to the extent of 99%, and its content amounts to 3%. In order to eliminate the effect of trivalent iron ions on the cementation of copper it was precipitated in the form of the hydroxide at pH 3.0-3.1.

In order to separate the zinc from the bacterial solution we investigated the possibility of its precipitation as zinc hydroxide and zinc sulphide and also the concentration of the solution in zinc to concentrations suitable for electrolysis. During precipitation of the zinc in the form of the hydroxide by a 10% solution of calcium oxide at pH 7.5-8.5 after 1h we obtained gypsum hydrate precipitates containing 25% Zn, 0.1% Fe, and 0.01% Cu. Such material can be used as the raw material for zinc works and can be treated by the Waelz process, but it is a very low-grade material. During precipitation of the zinc with sodium hydroxide NaHS, which is a waste product from the chemical industry, zinc

sulphide containing 50-55%Zn is obtained with an extraction rate of 98-99%. The optimum consumption rate of sodium hydrosulphide at pH 2.0-2.5 amounts to 105-110% of the theoretical consumption on the precipitation of the zinc. As seen, a rich zinc product with almost complete extraction of the zinc is produced by this technique for the precipitation of zinc. However, a significant disadvantage of the method is the high consumption of sodium hydrosulphide, and this leads to the accumulation of sodium ions in the solution and complicates its subsequent utilisation.

We also investigated the possibility of producing bacterial solutions concentrated in zinc and containing more than 70 g/l of zinc suitable for treatment by electrolysis. This was achieved by recycling part of the solutions after cementation of the copper. Thus, after threefold recycling the concentration of zinc in the solution amounted to 71 g/l without a reduction in the activity of the microorganisms or deterioration in the leaching kinetics. With the attainment of the required minimum concentration of zinc for electrolysis the recycle was reduced, and the zinc concentration was kept constant. The maximum concentration of zinc which we obtained amounted to 120 g/l. The spent electrolyte after electrolysis can be used to reduce the pH during the cementation of copper and cadmium from 3.0 to 1.5, and the remainder can be returned to leaching after neutralization to pH 2.5.

During the bacterial leaching of collective copper-zinc concentrates the copper content of the leaching cake is increased by 1-2%, but this product is not up to standard with respect to copper content. In order to improve the quality of the copper concentrates obtained from the leaching cake we proposed a process for flotation of the copper sulphides under the following reagent conditions: 1.5 kg/ton sodium sulphide, 80 g/ton butyl aeroflot, 200 g/ton activated charcoal and 80 g/ton of pine oil on the initial material. The flotation is realized in an alkaline medium at pH 10-12 with lime as medium regulator. The use of such a flotation regime made it possible to obtain a copper concentrate containing 19.4%Cu from a leaching cake containing 9%Cu with an extraction rate of 89.4% (table 3).

The developed technological scheme was tested on a pilot plant scale in equipment consisting of a series of Pachucas with 3 litre capacity each. The technological characteristics (table 4) in the steady state were obtained with the optimum process parameters. Thus, in the developed scheme the overall extraction of copper, zinc, and cadmium into standard products amounts to 92.0, 90.0, and 89% respectively from the initial copper-zinc concentrate or 85.0, 88.5, and 85.8% from the initial ore. A technical and economic calculation demonstrated the high economic effectiveness of the method of bacterial leaching in a combined scheme for the treatment of metacolloidal copper-zinc ores and concentrates.

Table 3: Results from flotation of copper from cake after the leaching of copper-zinc concentrate

Products	Yield %	Content %		Extraction %	
		Copper	Zinc	Copper	Zinc
Copper concentrate	41.5	19.4	3.22	89.5	74.3
Tailings	58.5	1.64	0.79	10.5	25.7
Cake after leaching	100.0	9.0	1.8	100.0	100.0

Table 4: Technological characteristics of the combined scheme for treatment of stubborn metacolloidal copper-zinc ores

Products	Yield %	Content %			Extraction %		
		Copper	Zinc	Cadmium	Copper	Zinc	Cadmium
Copper-zinc concentrate	33.8	8.59	12.65	0.062	92.1	90.8	91.8
Cake after BL	20.3	10.59	2.1	0.01	68.2	9.1	10.2
Copper concentrate	8.4	23.0	3.76	-	61.1	6.8	4.2
Copper-cadmium cake	0.8	88.0	-	2.34	23.9	-	81.6
Cathode zinc	3.8	-	99.8	-	-	81.7	-
Tailings	66.2	0.78	1.3	0.006	15.0	11.5	14.2
Ore	100	3.15	4.7	0.022	100.0	100.0	100.0

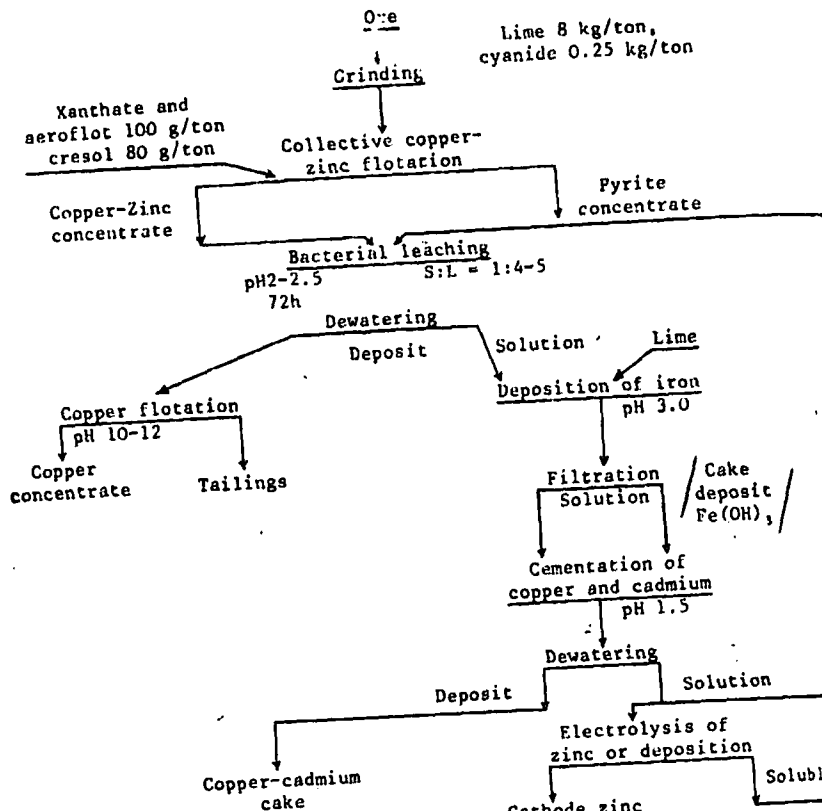


Fig. 1 Technological scheme for the treatment of stubborn metacolloidal copper-zinc concentrates with the use of bacterial leaching.

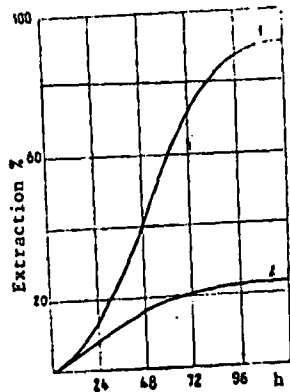


Fig. 2 The extraction of zinc (1) and copper (2) during the bacterial leaching of collective copper-zinc concentrate. Experimental conditions: Solid-liquid ratio 1:5, temperature 28°C, pH 1.75-1.1

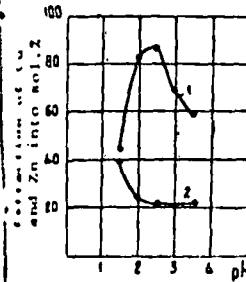


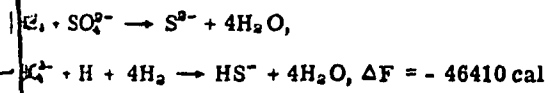
Fig. 3 Effect of the pH of the medium on the extraction of zinc (1) and copper (2) during bacterial leaching of collective copper-zinc concentrates.

UDC 622.7

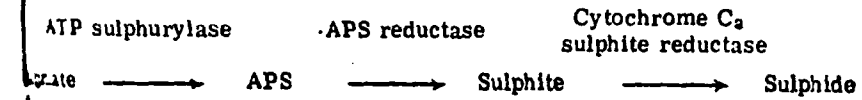
Reduction characteristics of sulphate-reducing bacteria in the treatment of ores

N. Solozhenkin, L. L. Lyubavina, L. F. Samokhvalova and V. S. Pupkov (Institute of Chemistry, Academy of Sciences of the Tadzhik SSR)

Microorganisms are being used more and more widely in various branches of technology. The thiobacteria *Thiobacillus ferrooxidans* are used for the leaching of copper, arsenic, uranium, and a series of other metals^{1,2}). Sulphate-reducing microorganisms are also widespread in nature. The *Desulfohalobio-desulfuricans* type is most representative of this class of bacteria³). The complete cells of sulphate-reducing bacteria rapidly reduce sulphate, liberating the molecular hydrogen:



enzymes (energy transfer agents - electron donors and acceptors) take part in the reaction). Peck proposed the following scheme for the reduction of sulphate⁴):



where ATP is adenosine triphosphate and APS is adenosine phosphosulphate.

The hydrogen sulphide formed on account of the reduction of gypsum, sulphates, and the organic substances of effluents by bacteria are used for the production of sulphur. Sulphate-reducing bacteria are used for the purification of effluents from heavy-metal cations by the formation of the corresponding metal sulphides⁵). However, investigators have paid little attention

to the use of sulphate-reducing bacteria as reagents in the flotation of ores. The present investigation was undertaken in order to fill the existing gap and to find methods for the wide utilisation of these bacteria in the treatment of ores.

The flotation was carried out in flotation machines of the mechanical type with a cell volume of 25 and 75 ml. The particle size of the mineral was $-125+63\mu$. In the experiments we used samples weighing between 1 and 3 g, while observing a solid-liquid ratio of 1:25 during flotation. Comparative flotation tests were carried out with sodium sulphide, a cumulative culture of bacteria (CCB), and hydrogen sulphide water both of natural origin (from wells) and obtained artificially by saturating water with hydrogen sulphide to a specific concentration. The cumulative culture of bacteria was isolated from the Tyrnyauz molybdenum-tungsten deposit. Postgate's medium was used for the culture of the CCB under laboratory conditions¹¹). When the CCB was diluted in a large volume we used an improved nutrient medium, in which linter dust [a waste product from the treatment of cotton seed⁷)] was used as source of carbon.

By direct counting it was established that the maximum number of bacteria in the cumulative culture of $220 \cdot 10^8$ cells/ml was reached on the fourth day. In this period up to 400 mg/litre of water-soluble hydrogen sulphide had formed which corresponded to a tenth of the solubility of hydrogen sulphide in water (0.1 M). After development for four days the CCB represented the finished working solution of the reagent and was used for flotation of the minerals and ores. As seen from table 1, there is a correlation between the number of bacterial cells and the amount of hydrogen sulphide released.

In the experiments we also used hydrogen sulphide water from wells No. 5 in the eastern part of the Dushanbe Basin Andigen, which has a hydrogen sulphide content of up to 100 mg/l⁸). Comparative tests on the flotation and investigation of the electrochemical potentials of the minerals with CCB, hydrogen sulphide water, and sodium sulphide were carried out with rigid control of the sulphide ion. The electrochemical potential of the minerals is shifted to the negative side more strongly with the use of the CCB than with the use of sodium sulphide. This is due to the fact that an insignificant layer of hydroxide is formed on the minerals when the CCB is used, and this improves the sulphidisation of the oxidized minerals compared with sodium sulphide.

Flotation characteristics of sulphate-reducing bacteria of various species are shown in Fig. 1. Fig. 1 shows the flotation of sulphide minerals as a function of the various concentrations of sulphide ion (sodium sulphide, natural hydrogen sulphide water, and CCB). The depression of galena, chalcopyrite, and antimonite is realized more effectively with the cumulative culture of bacteria, and this is due to the presence of hydrosulphide ions, which are released during the development of the CCB and retain their stability under the flotation conditions⁹⁻¹¹).

Experiments were carried out on the flotation of sulphide minerals with various concentrations of the CCB and butyl xanthate. On the basis of the relationships

Table 1: The relation between the number of bacterial cells and the amount of hydrogen sulphide released

Length of development of CCB (days)	1	2	3	4	5	6
Number of cells, 10^8 in 1 ml of solution	1.2	95	140	230	180	160
Amount of free H_2S mg/l	30	170	450	501	487	430

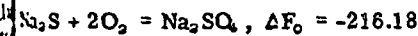
governing the flotation of sulphide minerals and with the use of the working equations^{1,2}) it was established that the ratio of $CCB S^{2-}$ ions present in the solution and the critical concentration has an effect on the floatability of galena, chalcopyrite, and pyrite. The results are shown in fig. 2. For all three investigated minerals $\log(S_{pr}^{2-}/S_{cr}^{2-})$ has a specific value, characteristic of the sulphide mineral, below which maximum flotation is observed. The critical concentration of the CCB sulphide ion is considerably lower than for sodium sulphide^{1,3}).

The depressing action of the CCB depends on the nature of the sulphide minerals. Initially, with short contact with the CCB, the flotation is improved on account of the sulphidisation of the slightly oxidized surface of the minerals, and with further treatment extensive depression of the sulphides begins. The same effect is observed in the flotation of oxidized minerals. With a CCB consumption rate of 15 mg/l (in S^{2-}) cerussite improves its floatability by 20-28%, while extensive depression is observed if the CCB consumption rate is increased to 20-25 mg/l. The floatability is reestablished after thorough washing of the depressed minerals with water.

On the basis of the high effectiveness of the reaction of the CCB sulphide ion with the surface of the sulphide minerals experiments were carried out on its use as a desorbent of xanthate coatings from the surface of minerals. By thermodynamic calculations it was shown that the oxidation of hydrogen sulphide by the reaction



occurs at a lower rate than oxidation of sodium sulphide by the reaction



The decrease in the concentration of S^{2-} and SH^- ions in the flotation pulp containing the CCB will be lower than in the pulp containing sodium sulphide. The desorption of xanthate from the surface of sulphide minerals by the CCB is therefore more effective than with solutions of sodium sulphide.

The obtained relationships were checked in the separation of an artificial mixture of minerals consisting of galena and sphalerite and also a mixture of molybenite and chalcopryrite (table 2). With the optimum reagent regime the extraction of galena into the lead concentrate after bacterial treatment with bacterial content of $23.7 \cdot 10^6$ cells in 1 ml of the CCB amounts to 83.63%, and the extraction of sphalerite under these conditions is 4.48%. In control tests selective separation of the lead-zinc concentrate was not observed ¹⁴).

The desorption of the xanthate from the surface of the minerals was realized by the following method. The mineral was floated with the optimum xanthate consumption rate. The froth product was collected in a test tube, treated with various amounts of CCB, and filtered. The solutions were analysed by spectrophotometry to determine the xanthate content. The mineral was then subjected to a secondary flotation (table 3). The CCB is an effective desorbent for the xanthate from the surface of the minerals.

The use of sulphate-reducing bacteria as sulphidiser for sulphide-oxide ore made it possible to improve the technological characteristics ¹⁵). At the State Institute of Nonferrous Metals senior scientific worker L A Glazunov undertook an investigation into the use of sulphate-reducing bacteria in the flotation of oxidized copper-molybdenum ore from the Almalyk deposit. The results showed that in the ore flotation cycle the CCB can totally replace sulphide without reducing the technological characteristics.

Investigation of the mechanism of the reaction of sulphide ions with the surface of minerals by means of spin-labelled reagents (Radicals) by the ESR Method. The investigation of radical-labelled sulphide minerals by electron spin resonance makes it possible to obtain information on the state of the free-radical fragment, which in turn depends on the structure and environment of the mineral in the region of the added label ¹⁶⁻¹⁷). The 4-(p-chloromercuribenzoate)-2,2,6,6-tetramethylpiperidin-1-oxyl radical, the spin-label analog of diethylaminophenylmercuracetate, the synthesis of which was realized in ¹⁶), was used in the work. The reagent exhibits specific sorption on the surface of sulphide minerals and stable compounds with the sulphur atoms of the mineral. The ESR spectra recorded on an RE 1306 radiospectrometer at liquid nitrogen temperature. Samples of the sulphide minerals spin-labelled with the radical were obtained after flotation or treatment of the natural and artificial minerals with water-alcohol solutions of the radical at various concentrations in distilled water. The minerals were separated from the water, washed thoroughly with water, placed after natural drying in a tube, and investigated by the ESR method. ESR spectra of the radicals are extremely sensitive to rotational mobility and the frequency of collision in the investigated systems.

The ESR spectrum of the radical in toluene represents a triplet (fig. 3a). With increase in temperature there is an increase in the intensity of the ESR signal, a narrowing of the lines, and gradual equalisation of the component intensities (fig. 3b). This is due to an increase in the frequency of rotation of the radicals. In the case of insignificant sorption of the radical on the surface of the mineral

Table 2: Dependence of the selective separation of a mixture of molybenite and chalcopryrite (1:1) on the length of bacterial treatment (chalcopryrite -125+63 μ , molybenite -63+0 μ)

Length of bacterial treatment min	Yield of mineral %		Experimental conditions
	Chalcopryrite	Molybenite	
0	88.7	91.5	Butyl xanthate 180 g/ton, pine oil 30.0 g/ton, CCB 6.5 mg/l Flotation time 3 min
10	74.4	89.9	
20	51.2	88.1	
30	32.7	87.7	
40	15.1	86.7	
60	8.0	87.1	

Table 3: The effect of the degree of desorption of xanthate from the surface of the minerals on their flotation with various CCB consumption rates

Concentration of CCB in S ²⁻ mg/l	Chalcopryrite		Galena		Pyrite		Antimonite	
	Extraction %	Desorption %	Extraction %	Desorption %	Extraction %	Desorption %	Extraction %	Desorption %
0	88	2	90	5	86	11	89	5
0.4	75	16	55	38	65	33	62	29
0.8	50	28	26	68	39	58	35	50
1.2	38	55	2	95	12	78	11	74
1.6	18	75	-	-	0	98	6	90
2.0	5	95	-	-	-	-	-	-

observed triplet ESR signal is observed (fig. 3b). With increase in the degree of sorption the local concentration of the radical increases, and this leads to a narrowing of the lines in the ESR spectrum, and a singlet spectrum is observed (fig. 3c). The amplitude of the ESR signal characterises the degree of sorption of the radical on the mineral.

The variation of the ESR spectrum as a function of temperature makes it possible to establish the various conformational transitions in the sorption layer. Fig. 4 shows the temperature dependence of the change in the rotation frequency of the radical sorbed on lead, bismuth, and mercury sulphides. The artificially obtained sulphides had a considerable active surface, and with a radical consumption rate of 50 mg/l a retarded triplet ESR spectrum was observed on their surface. The rotation parameters were calculated by the method given in the literature²⁰).

To study the effect of the structure of the microenvironment on the rotation diffusion of the radical we used the effective energy (ΔS_{eff}), which are related by the Arrhenius-Eyring equation:

$$\nu = \frac{kT}{h} \exp \frac{\Delta S_{eff}}{RT} \exp \frac{-\Delta E_{eff}}{RT}$$

The frequency of rotation of the radical does not depend on temperature over a wide range. The close to zero ΔE_{eff} and ΔS_{eff} values are an indication of the fact that the radical forms a stable sorption layer (matrix) not sensitive to fluctuations in temperature.

The character of sorption of the radical on the surface of cerussite was studied (Fig. 5). With increase in the concentration of sulphide ions the intensity of the ESR spectra increases, and this indicates an increase in the sorption of the radical. With further increase in the concentration of sulphide ions the intensity of the ESR spectra decreases a little, and the rotation frequency of the radical remains constant in the order of $\nu = 6 \cdot 10^7 \text{ sec}^{-1}$. The rotation frequency of the radical sorbed on the cerussite which had been treated with CCB was approximately five times less than the rotation frequency of the radical sorbed on cerussite which had been treated with sodium sulphide with equivalent concentrations of sulphide ions. This is convincing evidence for the fact that the sulphide film formed on the cerussite differs in nature and that the radical is attached more firmly in the case of the mineral treated with the relative bacterial culture.

The diffusion parameters and the local concentrations of the radical on the surface of the minerals depend largely on the concentration of the radical. The local concentration of the radical was determined by means of the formula: the variation of the width of the downfield line of the ESR spectrum in the case of the concentration of the radical $\Delta H = \Delta H_0 + AC$, where C is the concentration of the paramagnetic centres, ΔH_0 is the constant contribution to the width of the line due to the characteristics of the radical itself, and A is a coefficient equal to $42 \pm 2 \text{ Oe} \cdot \text{l/mole}$.

From data on the dependence of the average distances between the radicals on the local concentrations of the radical, given in the literature²¹), we obtained the average distances between the centres of the spin-labelled reagents in glassy solutions at 77°K.

The obtained data are shown in Fig. 6. With increase in the radical consumption

rate from 0 to 450 mg/l the local concentrations of the radical sorbed on the artificial bismuth and mercury sulphide increased from 0 to 0.15 mole/litre, and the average distances between them decreased to 20 Å. On galena a distance of 20 Å between the spin labels is reached even with a radical consumption rate of 100 mg/l, and this is due to the smaller specific surface area of the mineral compared with the artificial sulphides. With increase in the radical consumption rate the ESR spectrum changes from triplet to singlet, and this is due to the increase in the local concentration of the radical and to the possibility of spin-spin exchange between the closely situated labels (in the order of 7-10 Å).

The flotation and the sorption of the radical on the surface of pyrite were investigated as a function of pH (Fig. 7). The pyrite was first treated with sodium sulphide and CCB and thoroughly washed from unfixed S^{2-} ions. A sample was then treated with butyl xanthate (concentration 200 mg/l) and with the radical. Flotation was realised at specific pH values. Under the conditions of optimum floatability of the pyrite its surface is saturated by S^{2-} ions more rapidly during treatment with CCB than during treatment with sodium sulphide. This is evidently due to the fact that in the first case the sulphide ions are fixed more firmly and are more competitive with the hydrogen ions. In an alkaline medium the intensity of the ESR spectra of the radical decreases greatly, and this indicates a considerable increase in the sorption of hydroxide ions and displacement of the radical.

Conclusions

1. It was shown that sulphate-reducing bacteria are more effective sulphidisers for the oxidation of minerals than sodium sulphide. The technical and economic expediency of using a bacterial culture in the flotation of ores was demonstrated for the case of the flotation of oxidised lead and copper-molybdenum ores.
2. The high effectiveness of the bacterial culture as a sulphidiser and depressor is due to hydrolysis of hydrogen sulphide with the release of the hydrosulphide ion, which acts more effectively on the surface of the mineral.
3. The bacterial culture is an active desorbent of xanthate from the surface of the minerals. It is recommended as a selective reagent for the separation of collective sulphide concentrates and, in particular, for lead-zinc and copper-molybdenum concentrates.
4. A spin-labelled reagent, selectively attached to the surface of the minerals with the formation of stable compounds with the sulphur atoms, was used for the first time. It was shown that the nature of the sulphide film differs with treatment of the mineral by sodium sulphide and by the bacterial culture. It was established that the distance between the labels sorbed on the metal sulphides and minerals amounts to 7-20 Å. The distance between the labels varies, depending on the concentration of the radical sorbed on the surface.

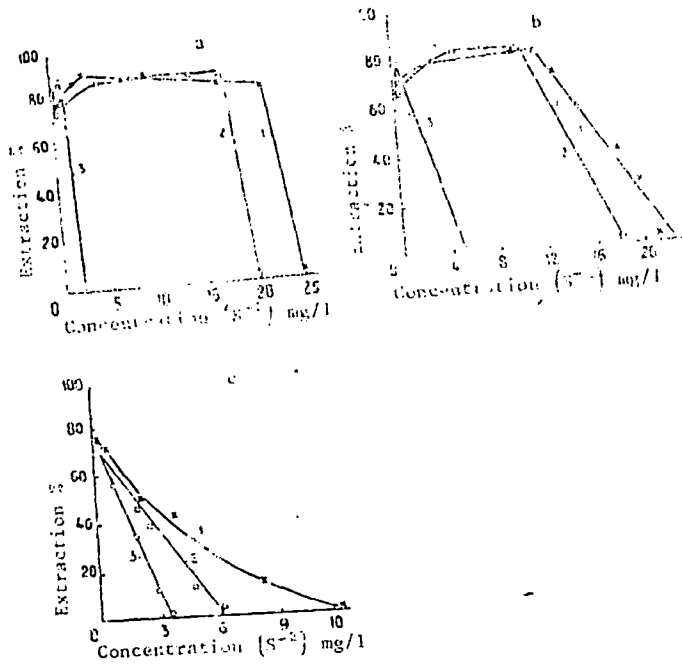


Fig. 1 Flotation of galena (a), chalcopyrite (b), and antimonite (c) as a function of the depressor consumption rate: 1) Sodium sulphide; 2) hydrogen sulphide water; 3) CCB.

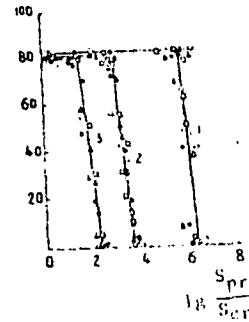


Fig. 2 The effect of the ratio of S^{2-} ions present in the solution and the ionic concentration on flotation: 1 - Galena; 2 - chalcopyrite; 3 - pyrite. Concentration of butyl xanthate (m/l): \circ - $6.65 \cdot 10^{-6}$, Δ - $1.33 \cdot 10^{-5}$, \square - $1.99 \cdot 10^{-5}$, \bullet - $2.66 \cdot 10^{-5}$, \blacktriangle - $5.32 \cdot 10^{-5}$.

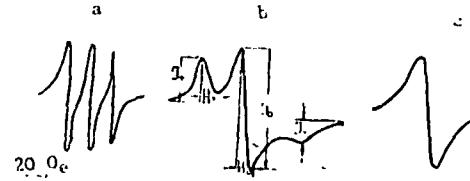


Fig. 3 The ESR spectra of the radical: a) dissolved in toluene (t 20°C), concentration of radical 10^{-5} mole/l; b) sorbed on the surface of the mineral, local concentration of radical $C < 0.15$ mole/l; c) sorbed on the surface of the mineral, local concentration of radical $C > 0.15$ mole/l.

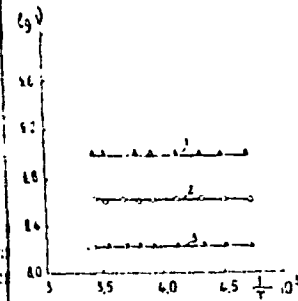


Fig. 4

The dependence of $\log v$ on $1/T$ for the radical (concentration 50 mg/l), sorbed on bismuth (1), lead (2), and mercury (3) sulphides.

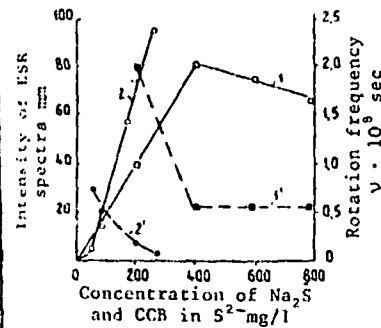


Fig. 5

The dependence of the intensity of the ESR spectra (1, 2) and the rotation frequency of the radicals (1', 2') sorbed on cerussite previously treated with sodium sulphide (1, 1') and CCB (2, 2'). Concentration of radical 50 mg/l.

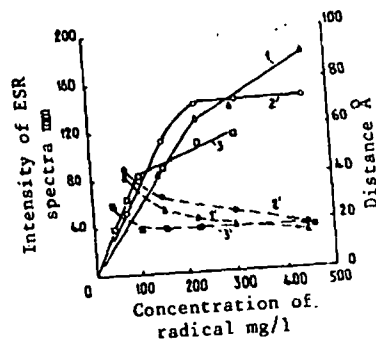


Fig. 6

The variation of the intensities of the ESR spectra of the radicals sorbed on the surface of bismuth (1) and mercury (2) sulphides and galena (3) and the distances between the labels respectively (1', 2', 3') on the concentration of the radical.

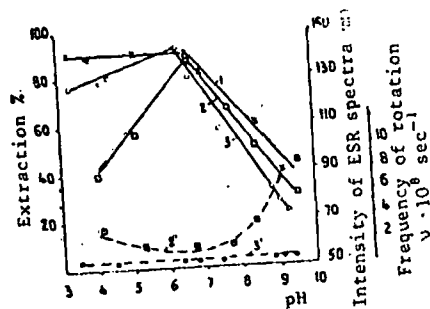


Fig. 7

The flotation of pyrite (1) and the variation in the intensities of the ESR signals (2, 3) and frequencies of rotation of the radical (2', 3'), sorbed on pyrite which had been previously treated with sodium sulphide (2, 2') and CCB (3, 3'), as a function of pH.

References

- 1) S I Pol'kin et alia: Proceedings of Ninth International Congress on the concentration of ores. Prague 1970.
- 2) G I Karavaiko et alia: The role of microorganisms in the leaching of metals. Nauka, Moscow 1972.
- 3) G A Sokolova et alia: Physiology and geochemical activity of thiobacteria. Nauka, Moscow 1964.
- 4) N D Reyc: Bacteriol. Rev., 1962, 26, 67.
- 5) A N Ilyaletdinov et alia: Methods for purification of industrial effluents. Tr. Kazmekhkhobra, Alma-Ata 1972, 8, p. 228.
- 6) I R Postgate et alia: Bacteriol. Rev., 1966, 30, 732.
- 7) L L Lyubavina et alia: Dokl. Akad. Nauk TadzhSSR, XIX, 1976, (6), 32.
- 8) N M Churshina: Dushanbe artesian basin and its mineral and thermal waters. Dushanbe. Donish 1972.
- 9) Yu N Knipovich et alia: Analysis of mineral raw material. Khimiya, Moscow 1956.
- 10) A A Abramov: Obogashchenie Rud, 1969, 7, (6).
- 11) K Jellinen et alia: Z. Physik Chem., 1922, 102, 438-479.

- 12) A A Abramov: Theoretical principles of the optimisation of selective flotation of sulphide ores. Nedra, Moscow 1978.
- 13) A M Goden: Flotation. Gosgortekhzdat, Moscow 1959, p. 342.
- 14) R D Kupeeva et alia: Obogashchenie Rud. Irkutsk 1977, (5), 158.
- 15) P M Solozhenkin et alia: Material composition and concentratability of mineral raw material. Moscow 1978, p. 29.
- 16) G I Likhtenshtein: Spin label method in molecular biology. Nauka 1974.
- 17) A N Kuznetsov: The spin probe method. Nauka, Moscow 1976.
- 18) A L Buchachenko et alia: Stable radicals. Khimiya, Moscow 1973.
- 19) D I Kogan et alia: Tsvetnye Metally 1978, (2), 70.
- 20) A N Kuznetsov et alia: Chem. Phys. Lett., 1971, (12), 103.
- 21) A I Kokorin et alia: Measurements of distances between iminoxyl spin labels as a method for studying the structure of macromolecules and solid solutions. Preprint of the Institute of Chemical Physics. Cheno-golovka, 1976.

UDC 622.7

Purification of water and aqueous solutions by flotoflocculation methods

N N Khavskii and V V Tokarev (Moscow Institute of Steel and Alloys)

Summary

Methods based on the flotation principle are used for the purification of effluents and solutions. The flotoflocculation method involves making the surface of suspensions water repellent by means of water-soluble high-molecular polymers containing various functional groups and subsequent flotation of the particles in counterflow equipment of the column type. Special devices are used to disperse the gas in the purified solution, and the froth product, in which the suspension is concentrated, is removed. The process makes it possible to remove solid and organic substances continuously from the solution.

Investigations showed that suitable high-molecular collector reagents are water-soluble polymers with a molecular weight higher than $(3-5) \cdot 10^4$, which reduce the surface tension of the water by not less than 1% at concentrations of 0.5 g/m^3 . Polyvinyl alcohol and its aldehyde derivatives, polyoxyethylene, and modified protein substances are effective and have been used successfully for the flotoflocculation purification of the suspensions of negatively charged particles in acidic and alkaline media. In media which are close to neutral cationic polyelectrolytes, which are adsorbed preferentially on the particles of the suspension, are effective. In the USSR the method has found industrial use in certain hydrometallurgical processes for the high purification of mineral suspensions instead of control filtration and for the purification of effluents from rolling processes. It has been tested on semi-industrial and industrial scales for the purification of aluminate solutions in the production of alumina, for the collection of precipitated copper, and also in water prepara-

USING ELECTRODES WITH EXTENDED SURFACES IN HYDROMETALLURGY

UDC 669.21/23.054.7

A. I. Maslii, A. P. Zamyatin, V. K. Varentsov, V. M. Krapivin,
and Yu. I. Frolov

The Institute of Physical Chemistry and the Machine Tool Institute of the Siberian Department of the USSR Academy of Sciences have developed multicell uniflow electrolytic cells with separated cathode and anode spaces and two versions of electrode with extended surfaces suitable for the extraction of gold and silver from sulfuric acid thiourea and alkaline cyanide solutions. The first version (Fig. 1a) uses plate cathode units made from titanium plates [1] placed perpendicular to the anode and separated by washers so that a gap is left between neighboring plates for the solution to pass through.

Experience in the use of plate cathode for gold extraction from thiourea solutions showed them to be highly efficient, even when the ratio of plate width to the distance between them is 80-100 [2]. The unit shown in Fig. 1a has an intrinsic volume of 3.4 dm^3 with a cathode surface of $\sim 5 \text{ m}^2$ and a weight of $\sim 7 \text{ kg}$. A cell (Technical Specification 48-22-33-74) with ten of these units takes up $< 1 \text{ m}^2$ of floor space and can process up to 5 m^3 of auriferous solutions per day at a current load of 500-700 A (with 99% gold extraction), i.e., 15-20 times more than a cell with flat electrodes. Cells of this type have been operating successfully since 1971 in the electrolysis section of the Lebedinskoe Gold-Extraction Plant [3].

An even higher degree of electrode surface extension can be achieved by using fibrous carbon-graphite materials as the electrode [4]. These materials are manufactured by heat treatment of viscous base and take the form of various kinds of felt, fabric, thread, and the like depending upon the nature of the base [5]. Carbon-graphite materials are stable in aggressive media, have a fair level of electrical conductivity, and have a very extensive surface.

The problem of evaluating the carbon-graphite material surface available for an effective electrolysis process has not yet been studied sufficiently, but as a first approximation it can be regarded as equal to the lateral surface of the threads. The surface will be $0.2 \text{ m}^2/\text{g}$ for threads to 10μ in diameter, which is several orders of magnitude higher than the figure for titanium plate cathodes and indicates the potential benefits of using carbon-graphite materials as electrodes with extended surfaces.

The cathode unit in which an extended surface is obtained by using carbon-graphite materials (Fig. 1b) consists of a central chamber with a layer of carbon-graphite material (the cathode proper) clamped to its perforated side walls. The solution to be processed is fed inside the cathode unit and is electrolyzed as it passes through the pores between the carbon fibers. Comparative operation of plate cathodes and of cathode units with carbon-graphite materials in the process of gold extraction from thiourea solutions showed that, with identical overall dimensions, the latter gives 3-4 times

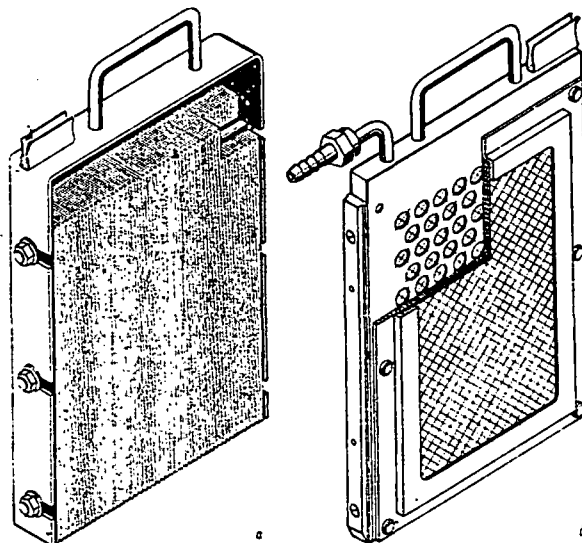


Fig. 1. Electrodes with extended surfaces: a - plate cathode unit; b - cathode unit using carbon-graphite material.

¹The work was directed by R. Yu. Bek and had the direct participation of T. A. Lavrovaya, A. G. Zelinskii, and G. N. Sorokin.

more output (and consequently have a working surface which is 3-4 times more effective). Electrolytic cells with 10 such units have been in operation since 1973 at one of the enterprises of the Yakutskoloto Group. When VVP-66-95 carbon fiber felt* (total weight of material per cell 0.6-0.8 kg) and a current load of 500 A are used, the capacity of the cell in terms of reclaimed solution reaches 15 m³/day. Improvements have now brought electrolytic cell capacity up to 20-25 m³/day without a substantial increase in overall dimensions. There are real possibilities of producing much more powerful cells based upon this design, with capacities of 100 and 1000 m³/day.

Another important feature of carbon-graphite material cathodes is that they can be used to deposit a much greater amount of metal per unit of electrode weight without the deposit peeling off or crumbling. In the process of electrolysis the carbon fibers, which are ~ 10 μ in diameter in the initial state, are gradually covered with metal (Fig. 2). In these circumstances 20-30 kg of gold are deposited on 1 kg of carbon-graphite material, i.e., the weight of the base itself accounts for 3-5%. It is also interesting to note that the speed of metal extraction from solution remains practically unchanged right up to the point of coalescence of the individual fibers into a monolithic deposit (Fig. 3). The only change is when the base is filled to a large extent with metal, when its hydrodynamic resistance to the flow of solution increases sharply and the capacity of the cell falls.

Thus using carbon-graphite materials as electrodes with extended surfaces for the electrolytic extraction of metals from dilute solutions permits considerable acceleration of the extraction process and also yields a concentrated finished product in the first stage. Various methods have been developed for removing the metal from carbon-graphite materials and regenerating the base, and it has been shown that the efficiency of carbon-graphite materials remains practically unchanged even after ten regenerations. As regards the extraction of precious metals, however, it is economically more advantageous to use the carbon-graphite materials once; this greatly simplifies the subsequent product-finishing operations. The industrial assimilation of this technology for gold extraction from production solutions at one of the enterprises has yielded annual savings of ~ 25000 rubles compared with chemical deposition. This technique will become feasible for the extraction of other metals as the industrial production of carbon-graphite materials increases and their cost is correspondingly reduced.

REFERENCES

1. R. Yu. Bek, A. I. Maslii, I. F. Baryshnikov, et al, Inventors' Cert. No. 349753, *Otkrytiya, Izobreteniya, Promyshlennye Obrazttsy, Tovarnaya Znaki*, 1972, No. 26, 69.
2. A. I. Maslii, N. P. Poddubnyi, R. Yu. Bek, and T. A. Lavrova, *Izvestiya Sibirsk. Otdeleniya Akad. Nauk SSSR, Seriya Khim. Nauk*, 1972, Issue 6, No. 14, 41.
3. A. I. Maslii, R. Yu. Bek, N. V. Makhnyr', V. M. Ganin, and V. A. Sheshin, *Tsvetnye Metall*, 1973, No. 8, 73-75.
4. R. Yu. Bek, A. I. Maslii, I. F. Baryshnikov, et al., Inventors' Cert. No. 395497, *Otkrytiya, Izobreteniya, Promyshlennye Obrazttsy, Tovarnye Znaki*, 1973, No. 35, 913.
5. A. A. Konkin, in: *Carbon and Other Oxidation-Resistant Fibrous Materials*, Moscow, *Khimiya*, 1974, 11-14.

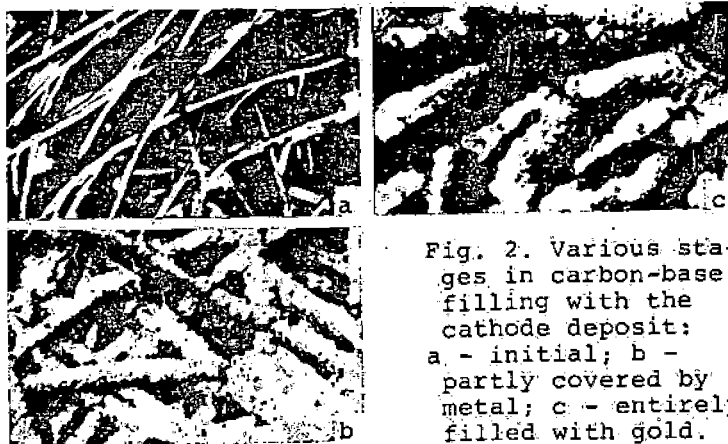


Fig. 2. Various stages in carbon-base filling with the cathode deposit: a - initial; b - partly covered by metal; c - entirely filled with gold.

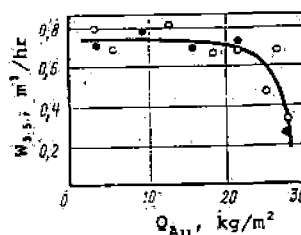


Fig. 3. Relationship of capacity of an electrolytic cell W with a 35-fold reduction in the gold concentration of the solution to the amount of deposited metal Q_{Au} per unit of visible electrode surface:

○, ● - various cells.

The material was developed at the All-Union Electrocarbon Component Research Institute under the direction of A. I. Bayer.

1976 v. 17 N1

TSVETNYE METALLY / NON-FERROUS METALS

USING ION EXCHANGERS TO REMOVE NICKEL FROM CADMIUM SULFATE SOLUTIONS

UDC 669.733:66.074..7

I. P. Tulenkov, E. I. Kazantsev, L. V. Bogatykh, and I. V. Samborskii

Finding a method of removing nickel from cadmium solutions is a matter of extreme urgency. A series of ion-exchangers containing aminocarboxylic and carboxylic groupings (ANKB-10, KB-2 x 7P), aminophosphoric groupings (ANKF-1B, ANKF-3G), and aminohydrazine groupings (No. 2, 3, 4, 308, 320, 324, 491) were tested, to extend the range of ion exchangers for nickel sorption. The latter resins were produced only in experimental batches; ANKB-1 and ANKB-7 were also tested for comparison.

Results of Nickel Sorption Experiments with Certain Resins (static conditions)

Starting solution, g/l			Resin	Ni content in solution, g/l	Sorption Ni, mg/l resin
Zn	Cd	Ni			
135,6	0,004	0,588	ANKB-1	0,382	10,3
			ANKB-7	0,367	11,05
			ANKB-10	0,529	3,0
			KB-2X7P	0,485	5,2
			308	0,264	16,2
			491	0,204	19,4
			491Gr	0,396	9,6
124,5	0,006	0,561	ANKF-1B	0,602	2,8
			ANKF-3G	0,620	2,0
			320	0,529	6,6
			324	0,455	10,2
			2	0,323	16,9
			3	0,459	10,2
			4	0,323	16,9
33,2	224,5	1,57	2	0,839	36,6
			3	1,12	22,5
			4	0,867	35,0
			308	1,03	27,0
			324	1,14	21,5
			491	0,96	30,5

The preliminary experiments on nickel sorption were under static conditions: 100 ml of the industrial solution used to produce zinc sulfate or for electrolysis of cadmium were brought into contact with 2 g of resin (converted to dry weight) and mixed with a mechanical mixer for 4 hours at 55°C and pH = 4. The results of these experiments (see Table) showed that the resins with aminohydrazine groupings had better sorption capacity for nickel ions than the other exchangers tested.

Experiments under dynamic conditions were conducted with 308, 4, 491, and 491Gr*, and ANKB-1 (see Fig). The initial solution was cadmium electrolyte with pH = 4. Sorption conditions were: resin weight 20 g., t = 55°C, rate of solution throughput 0.5-1.0 ml/(min·cm²). The resin was washed with distilled water (2 volumes to 1 volume of resin). Sulfuric acid at a concentration of 100 g/liter at 55-70°C and with a solution speed of 0.5 ml/(min·cm²) was used for desorption.

If 500 mg/liter is taken as the breakthrough,

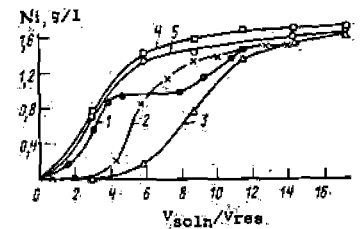
which guarantees production of metallic cadmium containing <0.0013% Ni, one volume of resin can purify three (resin 4) or seven (resin 491) volumes of solution, whereas ANKB-1 sorbs the same amount of nickel from only two volumes of solution. Capacity in these conditions was 26 mg Ni/g for resin 491 but only 7 mg Ni/g for ANKB-1. Resin 491 Gr has the same capacity as ANKB-1, but with greater mechanical and osmotic strength.

Three volumes of 2N H₂SO₄ per volume of resin are required to wash out the nickel from ANKB-1 and 491Gr, whereas 1.0-1.5 volumes are sufficient for the 4, 308, and 491 aminohydrazine resins. Consequently, the maximum nickel concentration in the rich batches of eluate from resin 491 was > 12 g/liter, as compared with about 5 g/liter from ANKB-1.

The investigations established the possibility of using resins containing aminohydrazine groupings for removal of nickel from cadmium-production solutions.

V. A. Leitsin participated in the work.

The resin is manufactured in "granulated" form (strong cylinders 3-4 mm long and 1.5-2 mm in diameter).



Output curves for nickel sorption from cadmium electrolyte containing (g/liter): 1.5 Ni, 190 1 - 4; 2 - 308; 3 - 491 Gr; 5 - ANKB-1 (1-5 ion exchangers).

UNDERGROUND LEACHING OF SULFIDE COPPER-NICKEL ORE

UDC [669.24+669.3]:66.061

V. A. Sedel'nikov, R. S. Voronova, A. K. Rozental', Yu. V. Koronelli,
and Ya. A. Vladimirov

Due to the need to expand the raw-material base for the copper-nickel industry, there is practical interest in studying process of leaching Lovnoozerskii copper-nickel ores. Melano-mesocratic norites were the technological ore sample. The ore was impregnated, and nodular veined. The sulfide minerals are pyrrhotite, pentlandite, and chalcopyrite. The content of basic components is: 0.9% Ni, 0.5% Cu, 18.45% Fe, 0.04% Co, 7.40% S, 39.18% SiO₂, 3.04% CaO, 15.12% MgO, and 5.82% Al₂O₃.

To perform the tests (flowsheet shown in Fig.) an ore batch (30 t) was separated into two parts. One part was crushed to -30 mm; the granulometric composition of the second part corresponded to the level achieved at the deposit after explosive crushing.

Ore samples 1 and 2 were leached at 50° and 20°C respectively. Total laboratory and enlarged test time was 5 years. The leaching method was developed in preliminary laboratory tests. The crushed-ore reactor was filled with a weak sulfuric-acid solution (12-15 g/l). After a 1-hour acid-ore contact, the solution was poured off and the ore was dried for 24 hours in two reactors at 20-50°C. All operations were then repeated until a solution was obtained with a concentration of 0.5 g/l Ni.

The drying period, when the ore was found in a moist-air state, was most suitable for decomposition of the metal sulfides by the combined effect of the air oxygen, the ions of oxide iron and sulfuric acid. The results of laboratory tests at 50°C showed that under these conditions one can extract up to 97% Ni and 80% Cu to the solution; with a continuous stable non-ferrous metals extraction to solution, one would obtain at least an up to 70% extraction level.

The degree of metal extraction to solution (Q, %), depending on the leaching time (τ, days), is described by the power function:

$$Q = a\tau^b;$$

on this curve there are several sections with different values for empirical coefficients a and b. As a rule, 3 were the maximum number of sections.

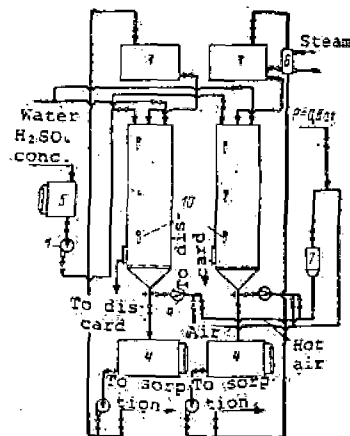
The presence of the first section can be explained by reagent interaction with the oxidized forms of the components and the sulfide inclusions located on surfaces of piece. The second intermediate section covers a conventionally small distance in time - of an order of several days. The third section is determined by the established leaching schedule and is of greatest interest since it permits extrapolation of the period needed for complete extraction. This section shows reagent interaction with sulfides inside ore pieces. Moreover, the process rate is determined by the diffusion properties of components. Using the formula to extrapolate up to 70% extraction shows that the following periods of time are required to attain this extraction level (in years): at 50°C, 2.4 for nickel and 1.9 for copper; at 20°C, 8.4 for nickel and 10.4 for copper.

It was established that leaching is possible for the pieces obtained following conventional explosive crushing; the process rate here however would be about 2.5 times less than for the most favorable size (<30 mm). Metal-leaching rate, determined as a time derivative:

$$\frac{dQ}{d\tau} = ab\tau^{b-1}$$

depends on the process duration; therefore, to obtain solutions with identical component contents at the end of all the leaching cycles, other conditions being equal, one would have to extend the cycles in proportion to the course of the process.

The original sulfuric-acid content determines three factors which are important for the process: the duration of the cycle, the metals concentration in the solution, and the reagent consumption per ton of nickel extracted to the solution. Each sulfuric acid concentration, no matter how long the cycle, corresponds to a specific maximum metal content in the solution which can be achieved in the leaching process in a given cycle. By altering the original sulfuric-acid concentration one can also regulate



Layout of a unit for leaching copper-nickel ore:

- 1, 2 - reactors, 1800 mm in diam., 8 m high; 3, 4 - pressure and collecting tanks, 4 m³ in capacity; 5 - 1 m³ tank for sulfuric acid; 6 - heat exchanger; 7 - electric air heater; 8 - pumps; 9 - flow meters; 10 - thermocouple sockets.

SUBJ
MNG
ULSCUNIVERSITY OF UTAH
RESEARCH INSTITUTE
EARTH SCIENCE LAB.

the iron content of a solution -- a very important factor for its subsequent treatment.

During the process of ore leaching at 50°C, about 90,000 liters of solution were obtained with average contents of 0.53 g/l Ni, 0.073 g/l Cu, 0.017 g/l Co, and 1.23 g/l Fe; at 20°C, 50,000 liters of solution were obtained with average contents of 0.48 g/l Ni, 0.015 g/l Co, 0.05 g/l Cu, and 3.4 g/l Fe. Following leaching, in most of the tests, the solution contained 1-5 g/l H₂SO₄.

When leaching ore at 50°C, the average acid consumption was 24 g per g of nickel extracted to solution; at 20°C, it was 28 g/l.

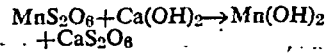
The obtained data can be used when planning the experimental system of underground leaching for the deposit. According to calculations made by the authors, using underground leaching to work the deposit can lead to considerable reductions in operating and capital costs as well as reductions in the cost of commercial nickel below the level obtained when using traditional technology.

SUBJ
MNG
UCSBP

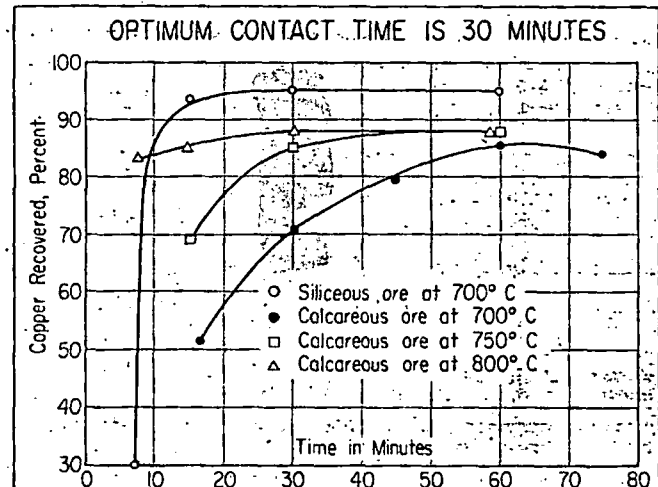
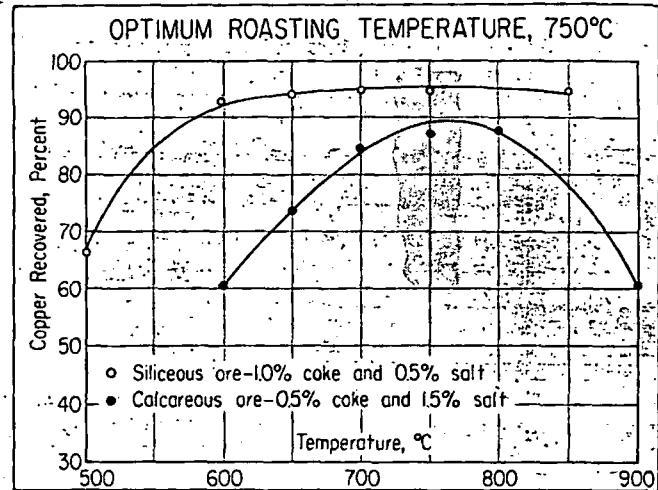
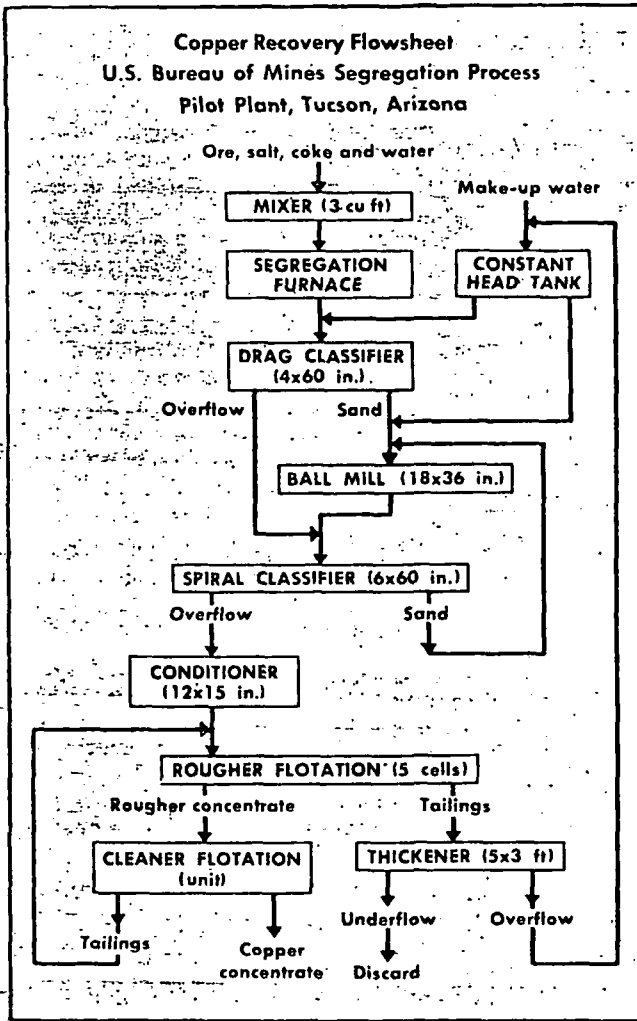
and sulphates that would interfere with the subsequent lime-purification step. Some additional acid is added by catalytic oxidation of SO₂ at the aeration step. The quantity of acid formed is usually adequate to dissolve any residual manganese oxide in the leach pulp by reaction.

After aeration, the pulp, which has a pH of 1.5 to 3.5, is neutralized to a pH of about 5.5 by adding a hydrated-lime slurry to precipitate alumina,

silica, iron, phosphorus, zinc, and other dissolved impurities. The partly neutralized pulp then is filtered, and the cake is washed to recover purified pregnant liquor. Quicklime then is added to the liquor to precipitate the manganese as the hydroxide, which regenerates the calcium dithionate according to the reaction:



The manganese hydroxide precipitate is filtered, washed, and dried and then is sintered or nodulized to give a ferrograde product assaying 63 to 66% Mn. The calcium dithionate is recycled for leaching additional ore, according to REPORT OF INVESTIGATION 5508, "Operation of a Dithionate-Process Pilot Plant for Leaching Manganese Ore from Maggie Canyon Deposit, Artillery Mountains Region, Mohave County, Arizona".



Redrawn from U.S.B.M. Report of Investigation 5501

UNIVERSITY OF UTAH
RESEARCH INSTITUTE
EARTH SCIENCE LABORATORY

USBM Charts Segregation Process

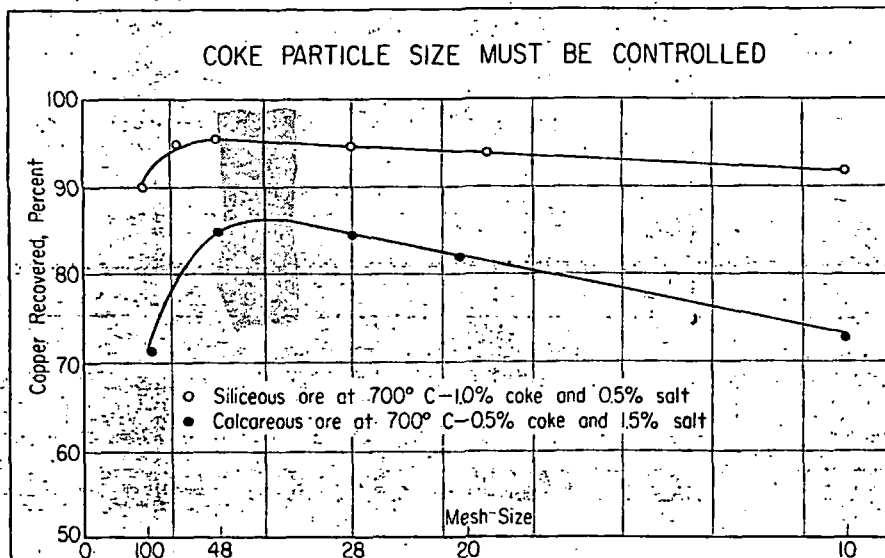
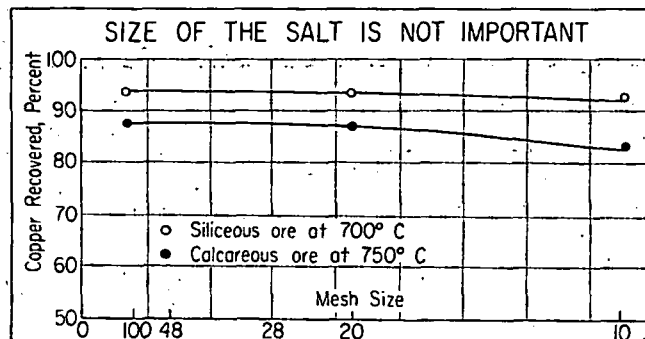
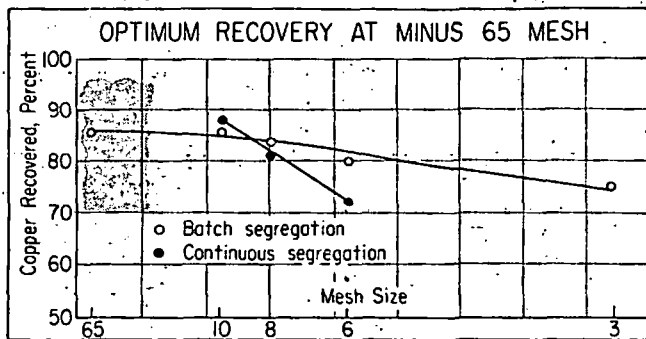
EXTENSIVE BENCH and pilot runs of the old Mineral Separations Ltd.'s Segregation Process show that domestic low-grade ores can be made to respond successfully. Scale-up by the Bureau of Mines researchers who did the work suggests that a 1,000-tpd furnacing and flotation operation could treat a mixed oxide-sulphide or a straight oxide ore for \$2.85 to \$3 a ton, depending on

whether coal (lower cost) or coke is used for the reduction.

On a 1% Cu ore at 88% recovery, the cost per pound would be about 16c in a concentrate containing about 26% Cu. This is too high, since straight oxide or sulphide can be floated and smelted for 5 to 7c per lb in a large-scale, 25,000-tpd plant (according to Arbiter in "Oxidized Copper, Part III", March

1957). However, on 5% Cu ores at the same recovery, the concentrate producing cost would drop to the 2- to 3-c per lb range.

The Bureau of Mines work was reported by Carl Rampecek, W. A. McKinney and P. T. Waddleton in REPORT OF INVESTIGATION 5501, "Treating Oxidized and Mixed Oxide-Sulphide Copper Ores by the Segregation Process". The authors, at the



Redrawn from U.S.B.M. Report of Investigation 5501

Bureau's Tucson center, have done an excellent job in recording and reporting the behavior of some of the more important process variables as shown in the diagrams presented here.

Estimating the Cost

The Bureau men estimate crushing, grinding and flotation costs at \$1.35 a ton and roasting or segregation costs at \$1.50 to \$1.65 per ton at 1,000-tpd. Depending on how the roast was ground, recoveries ranged from 70 to 92.4%. Process tailings ran from 0.28 to 0.77% Cu. The Bureau suggests 2.5-million Btu ton as a rough heat requirement figure. Salt content by weight is 1 to 2%; coke or coal needs are 1/2 to 1%. In the continuous pilot plant experiments, the ore samples were ground minus 100 mesh (76 to 83% minus 200 mesh). Two runs had feed assays of 1.52% and 2.4% Cu and produced 27.1% and 26.15% Cu concentrates respectively on 88.2% and 87% Cu recoveries after segregation and flotation. Flotation reagents were lime, K-amyl xanthate, Reagent 404 and methylisobutyl carbinol. Silver and gold recoveries in the second run were about 35%.

The copper segregation process involves heating oxide ore with a car-

bonaceous reducing agent and a chloride at 700 to 800° C to produce metallic copper which can be leached with ammonia-ammonium carbonate or floated with sulphide collectors. Such a concentrate must be refined by electrolysis and/or smelting—it is not a marketable product as such.

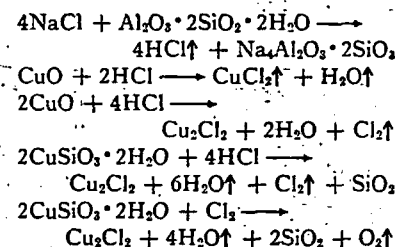
The first indications of such a process were uncovered at Sagasca, Chile in 1923-1924 when an ore was roasted at 700° C with coal, and the copper reduced and segregated rather than simply reduced in place. Examination of the ore led to the conclusion that halide in the ore was responsible for the peculiar behavior and the Segregation Process, better known as the Mineral Separations Process, was born.

Tried and Proved

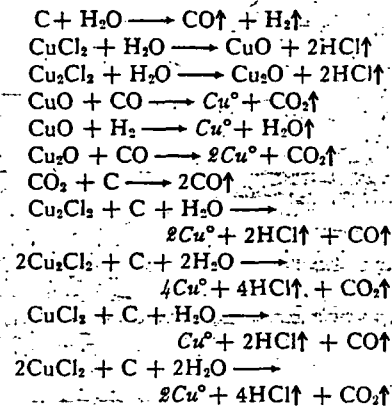
The process was tried twice in Africa in the 1920's. Mineral Separations built a plant in Southern Rhodesia. Union Miniere de Haut Katanga built one in the Congo. These two were successful, producing copper concentrates on better than 85% recovery. After short plant runs, the plants were closed due to a variety of reasons—mechanical problems, process irregularities and economics. Other methods were in vogue at the

time and segregation died out.

The process essentially is one involving the reaction of a chloride with water and clays in the ore at 700 to 800° C to produce HCl which then reacts with the oxides:



The chloride may also be provided as chlorine or hydrogen chloride gas with equal success. After the chloride is formed, the reducing atmosphere provided by the carbonaceous material at the 700 to 800° C reaction temperature completes the reaction, producing kidney-shaped globules of copper, carbon and gangue. Many reactions are involved:



Segregation is never complete and some copper is reduced in place as small particles which would require extra fine grinding to liberate for flotation. The globules are minus 65-mesh particles, fragile and easily broken on a vibrating screen. Flotation recovers the concentrate for smelting-refining. The Bureau is to be congratulated for their efforts, for the data presented here, for reviving interest in a process that may enjoy a revival in a time of high demand for copper buoyed by modern techniques and sound mechanical equipment.

Technology News

From the Bureau of Mines, United States Department of the Interior

Technology News provides information on results from the Bureau of Mines Mining Research Program. It is published to encourage the transfer of this information to the mining industry and its application in commercial practice. Mention of company or product names is for documentation only and does not imply government endorsement of a specific firm or product.

Bureau of Mines research is performed and reported under mandate of the United States Congress. To obtain a free subscription to Technology News, write to: Technology Transfer Group, Bureau of Mines, 2401 E St., NW, Washington, D.C. 20241.

SUBJ
MNG
UGVS



No. 63, March 1979

UNIVERSITY OF UTAH
RESEARCH INSTITUTE
EARTH SCIENCE LAB.

Underground Viewing System

Objective

Permit visual inspection of underground cavities from the surface.

Approach

A closed circuit TV camera and a 35mm still camera are lowered down a borehole, and remotely operated.

How It Works

A platform holding the cameras, and other equipment is lowered on a graduated cable until the depth of interest is reached. Then a quartz lamp and the TV camera are turned on. The television picture is monitored at the surface and recorded on video tape.

Areas of special interest are photographed with a 35mm still camera. These photographs contain more detail than TV images because photographic film is capable of higher resolution than a TV transmission.

The still camera is equipped with a shutter release/wind mechanism that is activated from the surface. A strobe light can be used with the still camera, but the illumination from the quartz lamp is usually bright enough to produce good results with 400 ASA film.



Cameras and auxiliary equipment suspended from tripod above a 12-inch ID borehole.

Illumination for the TV camera is provided by the single 650 watt quartz lamp. The TV camera used has a light correction range of over 10,000 to 1. As shown in the photograph, the quartz lamp is mounted on a platform above the still camera and the TV camera.

A hand operated winch mounted on a tripod is used to lower the platform into the borehole. The platform can be rotated horizontally in either direction through 360°, to stops. It is driven by a 3.3 rpm motor controlled from the surface.

A dry airstream is directed onto the camera lens to prevent fogging. The air is piped down to the camera through 3/16 ID plastic tubing connected to an air compressor tank on the surface.

In addition to the suspension cable and the air tubing connections there are two electrical cables connected to the platform mounted

components. Alternating current to power the platform rotation motor is transmitted to the system through a 18/8 SO neoprene cable. Both the d-c power supplied to the TV camera and the video output signals from the TV camera are transmitted through a single R6-59/u coaxial cable. All components of the system are available off-the-shelf.

Test Results

This underground viewing system was successfully field tested during borehole uranium mining and backfilling operations at Rocky Mountain Energy Company's Nine Mile Lake site in Natrona County, Wyoming. (At that site a cavity was excavated using the Bureau of Mines borehole mining system described in Technology News No. 56.)

Inspection using this viewing system, revealed that the borehole mined cavity was: saucer shaped, 50 feet wide at the maximum width, and 20 feet high at the center.

Inspection also revealed that the roof of the cavity remained stable over a 50 foot span. Distances were estimated by noting the position of pipes that were lowered into vertical holes drilled down to the cavity. Pictures, taken later during backfilling of the cavity, demonstrated that a slurry jet effectively emplaced fill, both through air and under water.

An underground survey system having self contained range finding and similar, more flexible viewing is now being developed. This work and development of underground viewing systems is done at the

Bureau of Mines Twin Cities Mining Research Center. Mr. Walter G. Krawza built the viewing system.

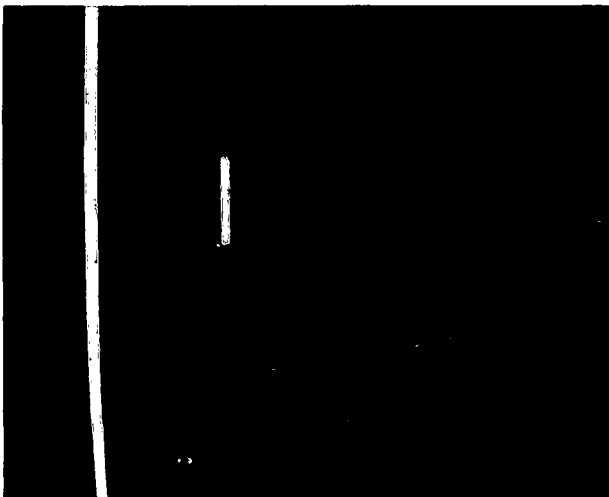
Patent Status

The United States Department of the Interior is not applying for a patent on this development.

For More Information

A bill of material, drawings, and application notes are available for persons having a possible use. To receive this material and answers to questions write to:

Technology Transfer
Officer
Twin Cities Mining
Research Ctr.
Bureau of Mines
P.O. Box 1660
Twin Cities, MN 55111



Size of cavity is estimated by reference to white pipes lowered through boreholes.



After partial backfilling, light colored sand fills the cavity almost up to the shelf that runs around the rim.

THE USE OF FLUORIDES IN HYDROMETALLURGICAL PROCESSING OF SCHEELITE CONCENTRATES

UDC 669.27

N. N. Rakova

UNIVERSITY OF UTAH
RESEARCH INSTITUTE
EARTH SCIENCE LAB.

Improvements to flowcharts have assumed greater urgency because of the increased scales of hydrometallurgical processing of tungsten and tungsten-molybdenum material with various compositions.

The autoclave-soda process of breaking down both standard scheelite concentrates and various low-grade tungsten intermediate products has now become widespread in industrial practice.

The process has a number of disadvantages (high reagent consumption, large quantities of waste solutions, many stages, large amounts of recirculating products, and so on); this leads to the necessity for improvements within the framework of the existing process (seeking new reagents, using solvent-extraction and sorption processes, and new equipment) or for the development of essentially new process versions (acid and acid-solvent extraction processes, chlorination, etc.).

An examination is made in the present review article of the possible ways of processing scheelite concentrates using fluorides¹ (ammonium and sodium fluoride), and of the effect of fluorine upon the processing of sodium tungstate solutions.

Utilization of Fluorides in Breaking Down Scheelite Concentrates. The process of scheelite decomposition by fluorides is based upon an exchange reaction, resulting in the production of sodium (ammonium) tungstate solutions and calcium fluoride precipitates:



where Me is Na or NH₄.

Using ammonium fluoride to break down scheelite concentrates substantially reduces the extent of the flowchart (See Fig.). The autoclave decomposition yields ammonium tungstate solutions, from which crystals of ammonium paratungstate can be isolated by the accepted routines. This excludes the operations of sodium tungstate solution processing, precipitation of artificial scheelite, production of tungstic acid, and a number of others. The calcium fluoride precipitates which form are a valuable by-product which can be used to produce hydrofluoric acid and fluorides, and also as a flux in the metallurgical industry.

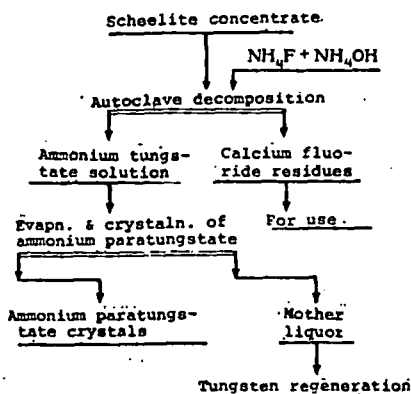
Scheelite concentrates are completely (98-99%) decomposed by solutions of ammonium fluoride in an ammonia agent at ~200° C and with a reagent consumption of 175-200% of that theoretically necessary for reaction (1). The speed of concentrate decomposition depends upon many factors, including the origin of the concentrate. Tyrgyz molybdenum-bearing scheelite concentrates decompose completely in 2-3 hr, in contrast to concentrates which do not contain molybdenum which require 5-6 hr of treatment.

The decomposition of scheelite concentrates with ammonium fluoride solutions is limited to concentrates with a low molybdenum content, because methods for separating tungsten and molybdenum in ammonia agents have not been worked out [1].

The use of sodium fluoride for breaking down scheelite concentrates has a number of advantages over the use of soda. Sodium fluoride is a more effective reagent; the equilibrium constant of the scheelite-sodium fluoride reaction at 225° C is 24.5, as against 1.56 for the scheelite-soda reaction under the same conditions [2].

This was subsequently confirmed by comparative laboratory studies of the conditions of scheelite concentrate decomposition by solutions of sodium fluoride and soda. At 225° C (τ = 2 hr) the extent of tungstate extraction into solution is 99.5% when the concentrate is treated with sodium fluoride solutions and 81.9% when treated with soda; reagent consumption is 180% of that theoretically necessary for the reaction. It should be noted that raising the temperature to 280-300° C intensifies the process of decomposition and makes it possible to cut the treatment time to 5 min; tungstate extraction into solution is 99.8% [3].

¹The work is being directed by A. N. Zelikman.



Flowchart for processing scheelite concentrates using ammonium fluoride.

TSVETNYE METALLY / NON-FERROUS METALS

Fluoride decomposition yields sodium tungstate solutions containing sodium fluoride; it was therefore necessary to keep track of the mutual effect of the constituents upon their solubility in the sodium tungstate-sodium fluoride-water ternary system at $T = 225^{\circ} \text{C}$ [4]. This system is of interest in explaining the chemical mechanism of the processes in the autoclave-soda decomposition of scheelite, because it was observed in [5,6] that changes in the leaching conditions for scheelite concentrates containing fluorite (temperature, treatment time, soda equivalent) do not substantially affect the fluoride ion content (4-6 g/liter) of sodium tungstate solutions. It has been established that the solubility of sodium fluoride in the ternary system at 225°C decreases when the sodium tungstate content increases [4], % (by mass):

Na_2WO_4	3.2	11.2	22.1	22.3
NaF	32.7	2.3	1.7	1.7
Na_2WO_4	1.3	33.0	43.8	44.1
NaF		1.2	0.96	0.90
Eutectic	47.0	46.9	47.0	47.4
Na_2WO_4 crystallization side	0.73	0.77	0.76	0.86
Na_2WO_4 crystallization side	47.0	47.1	46.7	46.4
NaF	0.60	0.41	0.54	-

The amount of NaF (by mass) which corresponds to a solution Na_2WO_4 content of 47% (by mass) is 0.7%, i.e., production solutions should not contain > 6-7 g/liter F^- . Laboratory investigations have established an optimum routine for leaching Tyrnyaur concentrates with commercial sodium fluoride solutions. Tungsten extraction into solution is 99.3-99.5% in two-stage leaching at 225°C with a reagent consumption of 175% the amount theoretically necessary. The adverse effect of the silica gel precipitation (-10% of concentrate weight) to the pulp, which leads to formation of a sodium aluminosilicate precipitate. The optimum conditions for leaching Tyrnyaur subsequent stages in the solution processing scheme as far as the finished product were checked in pilot-plant tests on the sodium-fluoride technology [2]. Thus the process can be carried out at high speed and with a reduced reagent consumption when sodium fluoride is used. The decomposition solutions have a weakly alkaline reaction to remove silicon from the solution. The reduction in acid consumption, using sodium fluoride makes fuller use of the raw material, by utilizing purification to remove silicon, phosphorus, and arsenic from the solution. The decomposition solutions have a weakly alkaline reaction to remove silicon from the solution. The reduction in acid consumption, using sodium fluoride makes fuller use of the raw material, by utilizing purification to remove silicon, phosphorus, and arsenic from the solution.

Effect of Fluorine upon the Processing of Sodium Tungstate Solution
 the principal operations in producing tungsten compounds from sodium tungstate solutions are: solution purification to remove silicon, phosphorus, and arsenic with ammonia, with subsequent crystallization of ammonium paratungstate precipitates. The reduction in acid consumption, using sodium fluoride makes fuller use of the raw material, by utilizing purification to remove silicon, phosphorus, and arsenic from the solution.

As has been observed, the solutions after autoclave decomposition of $\text{Me}_2\text{WO}_2\text{F}_6$, $\text{Me}_2\text{WO}_3\text{F}_6$, and $\text{Me}_2\text{WO}_4\text{F}_6$ solutions, according to the tungsten and fluorine content, are characterized by a high fluoride ion content. When the solutions are concentrated, the fluoride ion content increases, and the quality of the product. When the solutions are concentrated, the fluoride ion content increases, and the quality of the product. When the solutions are concentrated, the fluoride ion content increases, and the quality of the product. When the solutions are concentrated, the fluoride ion content increases, and the quality of the product.

Rela
and
Init
cont
97
wo.
49.1
49.1
49.1
0
Note:
Oxyl
is the

twee
an
the
rec
wh
n

In view of the adoption of solvent-extraction of tungsten from sodium tungstate solutions, the effect of fluorine upon the course of the process is of some interest.

It has been established (see Table) that the presence of fluorine in the solution leads to a sharp drop in the tungsten distribution ratio, from 420 in solutions which do not contain fluorine to 8.6 with an initial fluorine content of 5 g/liter.

Relationship of Tungsten and Fluorine Extraction (ϵ) and Distribution Ratios (D) to Solution Composition

Initial content, g/liter		(F:W) _{init}	Equilibrium content, g/liter				ϵ_W , %	ϵ_F , %	D_W	D_F	
WO ₃	F		aq. phase		organic phase						
WO ₃	F		WO ₃	F	WO ₃	(F:W) _{o.p.}					
49,1	0	0	0,12	—	49,0	—	—	99,8	—	400	—
49,1	5	1,25	5,1	0,46	44,0	4,54	1,26	89,6	90,8	8,6	9,9
49,1	10	2,5	9,5	0,66	39,6	9,34	2,88	80,7	93,4	4,2	14,2
0	10	—	—	5,9	—	4,1	—	—	41,0	—	0,69

Note: Organic phase (o.p.): 10% (vol.) TAA (70% basic substance) and 2% octyl alcohol in kerosene. Phase volume ratio org:aq = 1:1, $pH_{eq} = 3$. F:W is the molar ratio.

At the same time the fluorine distribution ratio increases substantially in the presence of tungsten; the mutual influence of fluorine and tungsten can be explained by the formation of $WO_2F_4^{-2}$ or $WO_3F_3^{-3}$ type compounds in the aqueous medium.

The presence of fluorine in the solutions also has an adverse effect upon the reextraction of tungsten. Whereas > 92.6% W passes into the reextract in the absence of fluorine after two contacts be-

tween the extract and 10% NH_3 (org : aq = 2 : 1), after extraction from solution with an initial fluorine content of 5, 10, and 15 g/liter the extraction of tungsten from the organic phase into the reextract falls to 88, 80, and 75% respectively. Thus the reduction in tungsten extraction in solvent extraction-reextraction processes, even when the solution fluorine content is comparatively low (5 g/liter), makes preliminary purification of the solution to remove fluoride ions essential.

REFERENCES

1. A. N. Zelikman and N. N. Rakova, *Tsvetnye Metally*, 1975, No. 9, 47-49.
2. A. N. Zelikman, T. T. Agnokov, and N. N. Rakova, in: *Hydrometallurgical and Chlorine Processes in Rare Metal Production*, Moscow, *Metallurgiya*, 1972, 8-14.
3. P. M. Perlov, *Obogashchenie Rud*, 1974, No. 2, 42-44.
4. A. N. Zelikman, N. N. Rakova, T. T. Agnokov, et al., *Second All-Union Conference on Molybdenum and Tungsten Chemistry and Technology (Summaries of Papers)*, Nal'chik, *Kabardino-Balkarsk State University*, 1974, p. 174.
5. I. A. Khar'kovskii, *Tsvetnye Metally*, 1972, No. 2, 46-48.
6. I. A. Khar'kovskii, in: *Molybdenum and Tungsten Chemistry and Technology*, Nal'chik, *Kabardino-Balkarsk State University*, 1971, pp. 71-73.